ANNUAL REPORTS ON

NMR SPECTROSCOPY

Edited by

G. A. WEBB

Department of Chemistry, University of Surrey, Guildford, Surrey, England

VOLUME 33

ACADEMIC PRESS

San Diego • London • Boston
New York • Sydney • Tokyo • Toronto

This book is printed on acid-free paper.

Academic Press, Inc.
525 B Street, Suite 1900, San Diego, California 92101-4495, USA
http://www.apnet.com

Academic Press Limited
24–28 Oval Road, London NW1 7DX, UK
http://www.hbuk.co.uk/ap/

ISBN 0-12-505333-9

A catalogue record for this book is available from the British Library

Typeset by Keyset Composition, Colchester, Essex
Printed in Great Britain by Hartnolls Ltd, Bodmin, Cornwall

96 97 98 99 00 01 02 EB 9 8 7 6 5 4 3 2 1

List of Contributors

Lance Ballard, *Department of Chemistry, School of Chemical Sciences, University of Illinois, Urbana, Illinois 61801, USA.*

St. Becker, *Physikalisches Institut der Universität Stuttgart, 70550 Stuttgart, Pfaffenwaldring 57, Germany.*

Shangwu Ding, *Department of Chemistry, University of British Columbia, 2036 Main Mall, Vancouver, B.C., Canada V6T 1Z1.*

Jiri Jonas, *Beekman Institute for Advanced Science and Technology, University of Illinois, Urbana, Illinois 61801, USA.*

John Malito, *Department of Chemistry, Cork Regional Technical College, Rossa Avenue, Bishopstown, Cork, Ireland.*

Francis P. Miknis, *Western Research Institute, 365 North Ninth Street, Laramie, WY 82070, USA.*

F. Noack, *Physikalisches Institut der Universität Stuttgart, 70550 Stuttgart, Pfaffenwaldring 57, Germany.*

J. Struppe, *Physikalisches Institut der Universität Stuttgart, 70550 Stuttgart, Pfaffenwaldring 57, Germany.*

Chaohui Ye, *Laboratory of Magnetic Resonance and Atomic and Molecular Physics, Wuhan Institute of Physics, The Chinese Academy of Sciences, PO Box 71010, Wuhan 430071, China.*

Jinyuan Zhou, *Laboratory of Magnetic Resonance and Atomic and Molecular Physics, Wuhan Institute of Physics, The Chinese Academy of Sciences, PO Box 71010, Wuhan 430071, China.*

Preface

In comparison with other methods currently available for investigating the structure and dynamics of molecules NMR is egregious. The widespread applicability of the series of NMR techniques now commonly available is exemplified in the topics appearing in the present Volume of *Annual Reports on NMR Spectroscopy*. It is a very great pleasure for me to express my gratitude to all of the contributors for the insights which they have provided into the five areas of science which they have reported on. Professor F. Noack, Dr St. Becker and Dr J. Struppe cover Applications of Field-Cycling NMR, Professor C. Ye, Dr S. Ding and Dr J. Zhou report on Progress in High-Resolution NMR in Solids. High-Pressure NMR is the subject of the report by Professor J. Jonas and Dr L. Ballard, Dr J. Malito writes on Molybdenum NMR Spectroscopy and the final report by Dr F. P. Miknis is on Applications of NMR in Oil Shale Research.

My gratitude is extended to the production staff at Academic Press (London) for their kind cooperation and patience shown in the evolution of this volume.

University of Surrey
Guildford, Surrey
England

G. A. Webb
May 1996

Applications of Field-Cycling NMR

F. NOACK, St. BECKER, and J. STRUPPE

Physikalisches Institut der Universität Stuttgart, 70550 Stuttgart, Pfaffenwaldring 57, Germany

1. INTRODUCTION

Since the beginning of NMR spectroscopy in the early 1940s, many special techniques have been developed to facilitate or improve the analysis of structural or dynamical problems, where the conventional method does not give satisfactory results. One such technique not discussed previously in this series is *field-cycling* NMR, which is primarily concerned with a more systematic approach to analysing molecular reorientations, i.e. to measure dynamic properties of molecules in solid or liquid environments in greater detail than is possible with standard instruments. In conventional NMR experiments the spin resonance signal is observed by irradiating selected nuclear magnetic dipoles of the sample material, which is exposed to a *fixed* high magnetic flux density B_0 (Zeeman field), with appropriate time-dependent radiofrequency fields $B_1(t)$ tuned in resonance with the Larmor frequency $\nu \equiv \omega/2\pi$ of the considered nuclei. This resonance frequency ν normally varies linearly with the strength of the Zeeman field, B_0, according to the Larmor condition $\nu = \gamma B_0/2\pi$, where γ is the characteristic magnetogyric ratio of the nuclear spin species; therefore, with decreasing strength of B_0 the standard procedure becomes more and more impracticable or even impossible for several reasons. The main difficulties result from the related well-known weakening of the NMR signal, which for a constant number of

ANNUAL REPORTS ON NMR SPECTROSCOPY
VOLUME 33 ISBN 0-12-505333-9

spins and equivalent signal processing approximately falls as $B_0^{3/2}$. Commercially available and also most home-made spectrometers work under the *high-field* condition, where ν is large compared with the line width $\Delta\nu$ of the resonance; for protons this is in the frequency range between about 4 up to 800 MHz, and up to 100 MHz for several spins with smaller γ-values such as deuterons. The upper limits correspond to maximum Zeeman fields of nearly 20 T, provided by powerful modern cryomagnets.

The rather narrow ν-range implies a strong restriction to almost any spin relaxation study because a clear interpretation usually requires data that are frequency or field dependent, i.e. the *relaxation dispersion*, over many decades. In addition it unfortunately also prevents direct experiments under the *low-field* condition, which are desirable in order to better separate relaxation mechanisms of different spin order, such as that of the Zeeman, dipolar or quadrupolar energies. Hence, several procedures have been considered and realized successfully to circumvent the problems of magnetic resonance below the MHz regime, ranging from simple sample enlargement to sophisticated polarization transfer. Field-cycling (FC) or more correctly *fast field-cycling* NMR, where the name refers to the basic requirement of periodically switching (cycling) the Zeeman field, B_0, between several distinct adjustable levels instead of keeping it fixed, is certainly the most obvious and general technique.

FC is not a new method, but it is still relatively rarely applied because commercial instruments are still being developed and are not yet available. Its origins go back to the early 1950s, when several research groups started low-field work and looked for adequate means to improve the weak NMR signal. A simple, slow *mechanical* field switch was first reported in 1951 by Pound.[1] However, it took many years to develop spectrometers with fast *electronic* switches which made it possible to use FC in other than the most convenient cases. Essentially based on the pioneering work of Redfield *et al.*[2] about energy storage and cycling, efforts by a few university laboratories succeeded to develop versatile, i.e. sufficiently fast field-cycling devices for measurements of the spin dynamics of protons or other nuclei in liquids or solids, without significant restrictions resulting from the often typically short relaxation times in the millisecond range. Several powerful machines and their utilization have been described in the literature, and detailed reviews on different aspects of the subject are available.[3–7] The following text will therefore only briefly sketch some basic physical and technical ideas and then concentrate on selected recent applications, where advanced instrumentation is needed. In particular we illustrate such new developments as combined frequency- and angular-dependent Zeeman relaxation (T_{1Z}) studies of liquid crystals aligned by selectable angles relative to the Zeeman field, frequency-dependent Jeener relaxation (T_{1D}) measurements of dipolar ordered liquids, and experiments to determine self-diffusion constants (D) and viscosities (η) of low-viscosity nematic liquids.

2. BASIC FIELD-CYCLING CONCEPTS

2.1. Operating principles

FC NMR requires the sample material to be in different external Zeeman fields, B_0 (two or more), at different times.[4,5] In the simplest case of frequency-dependent measurements of the longitudinal Zeeman relaxation time, T_1, the sample spins are polarized and detected as usual in a B_0 field that is sufficiently high to obtain a satisfactory signal quality. But unlike standard high-field NMR, between the periods of *polarization* and *detection* one inserts a period of *relaxation* or *evolution*, during which the external magnetic field is changed to the desired lower level, and by such a field-cycle the Larmor frequency ν can be conveniently tuned for a selectable time over a very broad range $\nu_{min} < \nu < \nu_{max}$, where the limits are determined mainly by the properties of the available magnet system and the exactness of the earth's field compensation. Consequently, FC, either with the simple relaxation (Fig. 1) or with more sophisticated multilevel evolution periods, allows one to study, in rather small samples of about 1 cm^3, many features characteristic of spin signals for Larmor frequencies in the range between almost zero and an upper limit ν_{max}, at present typically 10 MHz to 50 MHz for protons. It is important that this may be achieved by well-established NMR detection methods at a single fixed receiver frequency, i.e. there is no need to retune the resonance circuits, provided that the B_0 magnet and the additionally required B_0 switch device fulfil several conditions with respect to speed and stability. Sometimes, to make use of available transmitter and signal amplifier networks, it has been found advantageous to use the highest accessible B_0 flux not for spin polarization and detection, but for the evolution period; FC can therefore be a technique for both lowering and increasing the Larmor frequency, ν, relative to the fixed detection channel.

To make such experiments as clear as possible (i.e. to avoid uncontrolled polarization and relaxation effects), as a rule the cycle transits should be shorter than or at least not significantly exceed the considered relaxation time, T_i, of the studied spins, which means that $B_0/(dB_0/dt) < T_i$. For relaxation times longer than about 0.1 s, this condition has been achieved[1] by moving or shooting the sample in a shuttle between the different field levels of the cycle, which at moderate velocities is relatively easy to do. Studies of shorter time constants need the more powerful, faster and hence more difficult to handle alternative,[2] where the transits are obtained by quickly turning on or off parts of the electric current through a magnet coil by means of a switchable power supply. At present, electronic switches allow one to measure relaxation processes with time constants as short as about 0.5 ms at low Zeeman fields. A combination of both methods has been used to produce even faster measurements, with very small field steps of a few

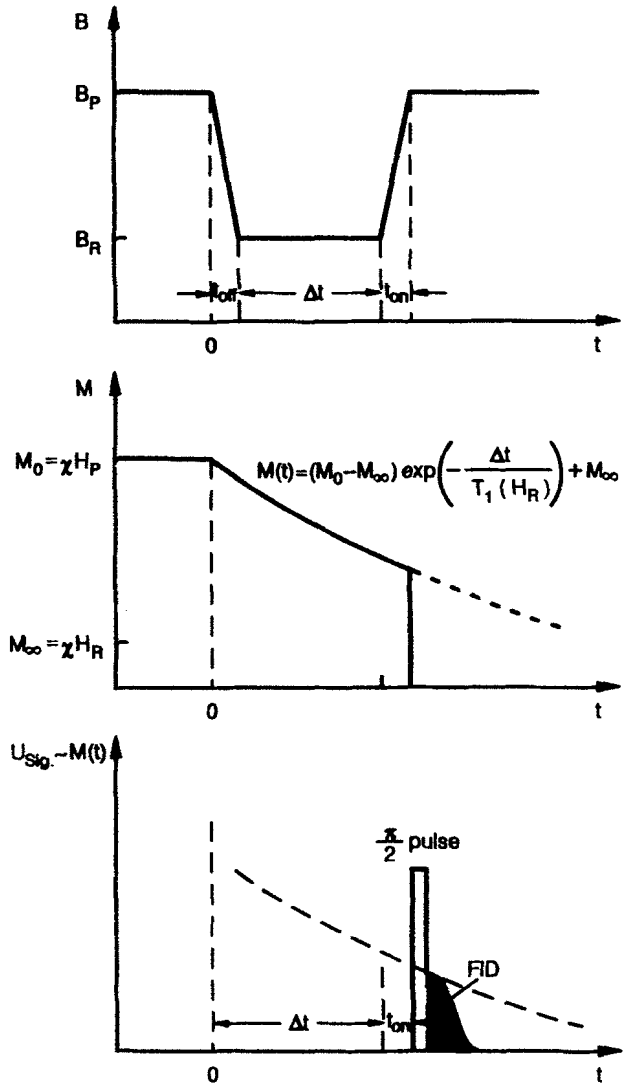

Fig. 1. The FC principle for measurements of the longitudinal spin relaxation time T_1 at different Larmor frequencies (ν) or Zeeman fields (B_0), i.e. of the relaxation dispersion $T_1(\nu)$ or $T_1(B_0)$. The upper diagram illustrates the $B_0(t)$ cycle with finite transit times between the polarization, relaxation (evolution) and detection period, the diagrams below show the related magnetization decay $M(\Delta t)$ from M_0 to M_∞. and the FID signal $U_{Sig}(t)$ with exponentially decreasing amplitude $U_0(\Delta t)$ after a $\pi/2$ $B_1(t)$ r.f. pulse perpendicular to B_0. Magnetic flux densities are denoted by B, magnetic fields by H, and χ is the nuclear magnetic susceptibility.

microseconds superimposed on rather slow, but large field transits.[8] If the field changes involve not only the strength but also the orientation of B_0 relative to a symmetry axis of the sample material, one must also observe an upper limit for the speed, above which the field transits $B_0(t)$, similar to the radio-frequency pulses $B_1(t)$, may eventually alter the spin order and magnetization. This "adiabatic condition" sets a limit relative to the time-scale of the Larmor periods involved and thus often becomes difficult to accomplish at low values of ν.[4,5] Therefore, both the construction of the electronic network needed and the optimal adjustment of the cycle transit characteristics are still delicate technical and physical tasks.

2.2. Technical problems

Magnets and current regulators for fast field-cycling NMR should provide from a given electric power, P, a flux density, B_0, as high as possible, the fast flux variation dB_0/dt needed for the cycle, and a sufficient field homogeneity and stability $B_0/\Delta B$ over the sample volume.[4,5] These requirements are strongly correlated, so that the problems involved in producing the most favourable switching network and coil geometry are still not completely solved. For example the maximization of both B_0 and dB_0/dt for a selected value of P involves conflicting conditions on the magnet geometry. Several efficient approaches have been described in the more recent literature,[9–12] which make use of suitable compromises between producing either maximum field strength or minimum transit time, frequently by combination of a mechanical and an electronic switch. In order to allow fast transits, the inductance of the magnet has to be small and the driving voltage must be very large. This implies that relatively small, high-current air-bored coils replace the common large iron-core magnets; because of the small coil dimensions both the field homogenization and all temperature controls are more difficult than with standard NMR apparatus. Cryomagnets are not (yet) a satisfactory solution,[9] primarily because they do not accept currents as high as normal conductors. Conversely, the high-voltage (up to 2 kV) switching of such high currents (up to 500 A) demands very powerful electric supplies, at least over the short transit intervals, and these two aspects are responsible for the main technical problems of FC NMR spectrometers.

Three novel possibilities have greatly facilitated the progress achieved in recent years. (1) Improved methods of calculating the optimal current geometry of compact, low-inductance homogeneous coils,[10] (2) computer controlled cutting of the calculated complex conductor arrangements, with variable cross-section, from cylindrical copper or aluminium tubes[10,11] which replace traditional constant diameter copper wires; and finally (3) the availability of reliable low-cost, high-voltage semiconductor devices[13] such as bipolar power Darlington transistors, GTOs, MOSFETs or IGBTs to

utilize Redfield's[2] energy storage principle for the very high transient electric switching power of up to nearly 1 megawatt presently required. Fast FC spectrometers have been built for many types of NMR studies and problems.[9–12] Known instruments presently allow one to measure the dispersion of all familiar relaxation processes over rather broad frequency ranges, i.e. not only of the longitudinal and transverse Zeeman relaxation times, T_1 and T_2, but also of the dipolar and of the rotating frame relaxation times, T_{1d} and $T_{1\rho}$. The apparatus could be used to observe various cross-relaxation resonances, where the adjustable Zeeman levels cross other energy states of the spins or molecules, and to perform zero-field and double-resonance experiments, where special spin resonances are sampled under the low-field condition. Some of the devices enable one to investigate simultaneously angular and frequency dependences by switching both the strength and the direction of the Zeeman field. In favourable cases the method has been combined with standard fast Fourier-transform signal processing for spectrally selective relaxation measurements. Last but not least, FC spectrometers significantly extend the pulsed field-gradient method for diffusion or flow studies by making use of a magic-angle field rotation. Most of this work has been done on proton spins (^{1}H), but some results are also reported for other nuclei such as ^{2}H, ^{6}Li, ^{7}Li, ^{27}Al, ^{31}P, ^{63}Cu and ^{65}Cu. The following Sections illustrate and summarize some recent FC applications mainly from Stuttgart's NMR groups. For experimental details and other developments refer to the original literature and the related reviews.[3–12]

3. APPLICATIONS

3.1. Frequency- and angular-dependent longitudinal Zeeman relaxation in liquid crystals

Proton, deuteron and carbon spin relaxation measurements of liquid crystals have provided detailed information about the molecular motions of such anisotropic liquids (anisotropic rotation and translation diffusion of individual molecules), and about a peculiar feature of liquid crystalline phases, namely collective molecular reorientations or order fluctuations.[14,15] Spin relaxation in liquid crystalline mesophases has challenged NMR groups since the early 1970s, shortly after the publication of theoretical predictions that order fluctuations of the director (OFD, OF), i.e. thermal excitations of the long-range orientational molecular alignment (director), may play an important unusual role in nuclear spin relaxation of ordered liquids. Unique to these materials, which are composed of rod-like or disc-like (i.e. strongly anisotropic molecules), it was predicted that such thermal fluctuations of the director should, at the frequencies of these fluctuation modes, produce rather peculiar $T_1(\nu)$ dispersion profiles. For example in the case of uniaxial nematic

order, they should produce a square-root law frequency dependence[16,17] $T_1 \sim \nu^{1/2}$, and in the case of the most common layered smectic order (sm-A) the theory expects a broad linear increase[18,19] $T_1 \sim \nu$; moreover, manifold variants of T_1 dispersion laws were suggested for more complex structured mesophases. All these relations describe a rather unusual relaxation behaviour of liquids, where as a rule for systems with a normal viscosity at low frequencies any relaxation dispersion vanishes.[20,21]

3.1.1. The problem

Because the collective motions are superimposed on simultaneous noncollective rotation and translation reorientations of individual molecules, and the range of Larmor frequencies accessible to conventional spectrometers is restricted, for a long time a clear distinction of the different relaxation processes was virtually impossible. With the development of sufficiently fast FC instruments,[22] capable of extending $T_1(\nu)$ measurements from the megahertz to the kilohertz and hertz regimes, where the OF contributions to the overall spin relaxation rate $1/T_1$ should dominate over other competing terms, a more reliable and unambiguous separation of the significant reorientation processes emerged. By fast FC, some peculiar OF dispersion profiles became directly observable in many thermotropic and lyotropic mesophases,[22,23] and the results leave no doubt that at low Larmor frequencies the theoretical concept of spin relaxation by collective molecular motions is basically correct; in contrast to this finding, at conventional frequencies, $T_1(\nu)$ is clearly governed by motions of individual molecules or molecular groups. However, despite the better understanding achieved by extensive $T_1(\nu)$ studies and the merits of numerous high-field NMR works,[14,15] many details of the underlying models are still open to controversy, essentially because of insufficient experimental data which does not allow one to decide reliably between the suggested alternative refinements. In particular, controversies exist about the magnitude of the low or high cut-off frequencies of the director mode spectra,[15–19] and above all with respect to the clear choice of the most appropriate of the various rotational diffusion models. Anisotropic rotations in an ordering potential have been treated in the literature in many ways[14,15,21,24–26] by stochastic *small-step diffusion* (weak collision) and *jump diffusion* (strong collision) processes, and countless variants were suggested on the basis of the first more "liquid-like" than "solid-like" concept. In particular, many workers attempted to find out whether Nordio *et al.*'s small-step[24] approach or Vold and Vold's "third rate approach"[25] is closer to reality. In the first case the rotational diffusion tensor is determined by the components along and perpendicular to the molecular symmetry axis, whereas in the third-rate[25] approach, based on the anisotropic viscosity model developed by Polnaszek and Freed,[26] the rotational diffusion is described by the motions about the director axis, about an axis

perpendicular to the director, and also by fast rotations of the molecule about its long axis. No systematic comparison of these ideas using proton spin relaxation has yet been reported, because, unlike deuteron spin relaxation, in protons even the rotation and translation processes are generally difficult to distinguish. This implies that similar open questions exist about the quality and usefulness of anisotropic translational diffusion models,[27–29] where extensions of the original simple relaxation theory of isotropic liquids[21] are still harder to analyse than for the molecular rotations.

3.1.2. *Angular-dependent* $T_1(\nu)$ *measurements*

To improve the relaxation analysis we have recently started to study, with improved FC facilities, both the dependence of the proton spin relaxation time, T_1, on the frequency ν and on the angle Δ between the Zeeman field, $\vec{B}$, and the director axis, $\vec{n}$, for typical thermotropic nematogen liquid crystals. As pointed out and discussed in detail by Morrison and Bloom,[30] such a step considerably enriches the amount of experimental data in order to better discriminate alternative concepts. Angular-dependent NMR studies in low-viscosity nematic liquid crystals are difficult, because normally the director $\vec{n}$ realigns rather rapidly in the parallel direction relative to the external Zeeman field $\vec{B}_0$, and hence the mechanical rotation of the sample by the desired angle is generally too slow to obtain a well-defined quasi-stationary state with $\vec{n}$ oblique to $\vec{B}_0$. FC allows one to adjust any angle Δ fast enough to observe the related signal by rotating $\vec{B}_0 \equiv \vec{B}_z$ to $\vec{B}_\Delta \equiv \vec{B}_z + \vec{B}_x$, using two simultaneously switched magnet coils with their axes (x,z) perpendicular to each other.[5]

Figure 2 illustrates some selected proton relaxation results for two typical low-temperature nematics, namely the *n*-alkyl-cyano-biphenyls 5CB and 8CB,[31,32] which distinguish between the lengths of the flexible side groups. The upper diagram shows $T_1(\nu)$ at different director orientations Δ, and the data at the bottom show $T_1(\Delta)$ at different frequencies ν. The measurements were taken in the middle of the nematic temperature ranges at 30°C and 37°C, respectively, and exhibit characteristic features that are qualitatively very similar for other nematic mesogens. The FC method up to about 10 MHz was extended by conventional techniques to the high-field regime.[31] In contrast to results for isotropic liquids of comparable viscosity, in nematic samples there exists a strong variation of T_1 with increasing ν by more than one order of magnitude, which roughly can be separated into four regimes. At $\Delta = 0$ we see (1) a plateau below 5×10^3 Hz, then (2) a square-root range up to about 10^6 Hz, followed (3) by a decreasing slope up to approximately 10^7 Hz with the tendency to level to another plateau (which is often better pronounced for high-temperature nematics), and finally (4) the beginning of a new shallow dispersion step above 10^7 Hz. At $\Delta = 90°$, the relaxation times are always shorter, but the behaviour in ranges (2), (3) and (4) is qualitatively

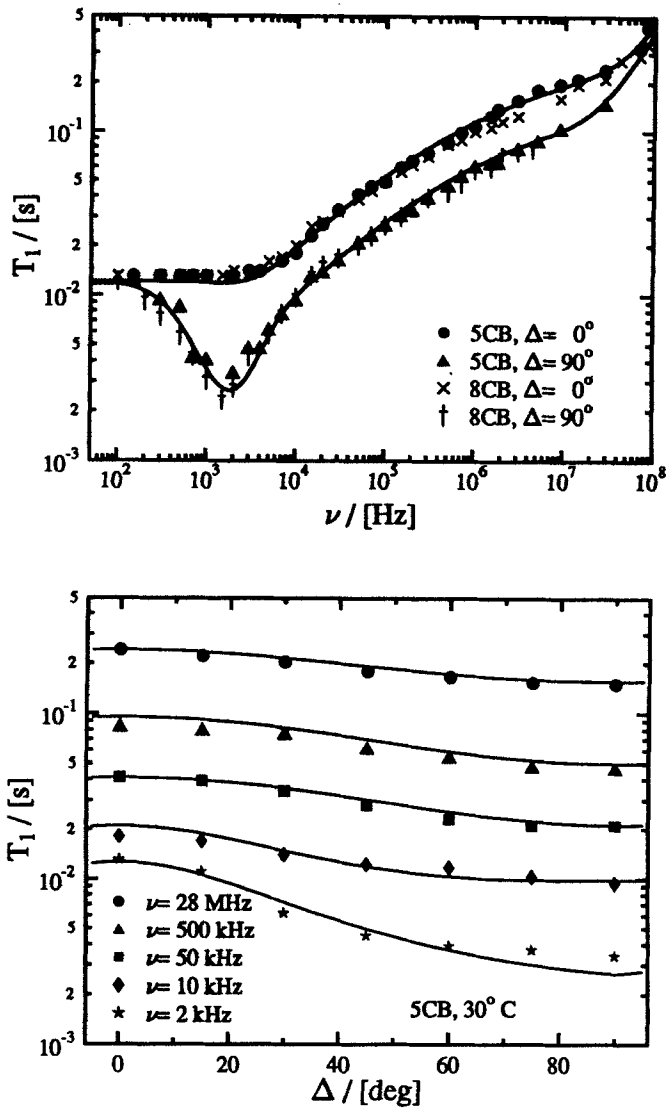

Fig. 2. Larmor frequency and angular dependences of the longitudinal proton spin relaxation time T_1 for the two *n*-alkyl-cyano-biphenyls 5CB and 8CB, respectively, at temperatures in the middle of the nematic mesophases. The upper diagram shows the dispersion profiles $T_1(\nu)$ with the director $\vec{n}$ aligned parallel ($\Delta = 0$) and perpendicular ($\Delta = 90^0$) to the external Zeeman field, $\vec{B}_0$, and suggests to distinguish at least four relaxation regimes. The lower diagram shows $T_1(\Delta)$ in different frequency ranges of the dispersion profile. The solid lines are model fits of equation (3a) to the experimental 5CB data points as discussed in the text.

very similar for both orientations; only range (1) significantly changes and reveals a deep $T_1(\nu)$ minimum near 2×10^3 Hz. The angular dependence decreases slightly from a factor of about 2 in range (2) to a factor of 1.3 in range (4). The molecular side groups have only a minor effect on the relaxation dispersion. For $\nu \leq 20$ kHz, where the $T_1(\nu)$ minimum occurs, the ratio $T_1(\Delta = 0)/T_1(\Delta = 90°)$ becomes rather large (approximately 5), but no anomaly is seen in the $T_1(\Delta)$ plots. Qualitatively comparable data have been obtained for a variety of nematic liquid crystalline molecules,[22,23] where essentially owing to the unlike mesophase temperatures the four denoted ranges shift in width and clearness. Such extensive data sets at fixed temperatures should be contrasted with the restricted information obtainable by standard spectrometers in the high-frequency range. The FC results enable a more critical model analysis, which will be briefly described below.

Nematic liquid crystals are systems which usually exhibit cylindrical symmetry about the nematic director $\vec{n}$. According to well-established theoretical formalisms,[14,15,20,21] spin relaxation of such materials reflect both the orientation and fluctuations of this axis relative to the Zeeman field, and also the various inter- and intra-molecular movements of the interacting spins considered; this is usually expressed in terms of *spectral densities* $J(\nu)$ of the underlying processes and interactions. Most of the explicit calculations of spectral densities reported both in older and in more recent literature are primarily concerned with the relaxation of deuteron (^{2}H) spins, because the quadrupolar relaxing deuterons allow one to separate individual spin positions on the molecules more easily than the dipolar coupled proton (^{1}H) spins. This means that in order to use relaxation models for protons, the calculated relaxation rates have to be averaged over many sites for a quantitative analysis of the experimental data, whereas this averaging is not necessary for deuteron studies. Conversely, because of existing instrumental limitations, angular-dependent FC studies with deuterons[33] are not yet possible as with protons. Therefore it was challenging to investigate if, and to what degree, presently feasible proton FC measurements can support, improve or eventually modify the more familiar results of high-field deuteron NMR.

3.1.3. Discussion

To test the quality of both the established and the disputed relaxation models in the light of the new angular-dependent results, we performed simulations and tried model fits of the pertinent theories for proton spin relaxation by reorientations of dipolar coupled inter- and intra-molecular proton pairs. Assuming fast magnetization transfer between unlike spin pairs and a superposition of the three independent reorientations (M) known to be important mechanisms for common nematic liquid crystals,[15] namely nematic

order fluctuations (OF),[16,17] anisotropic small-step rotations in a uniaxial ordering potential (Rot),[24,25] and slightly anisotropic molecular self-diffusion (SD),[28] the total Zeeman relaxation rate parallel to the external field B_0 should follow the familiar standard expression[15,20]

$$1/T_{1Z}(\nu,\Delta) \equiv R_{1Z} = \Sigma_M R_{1ZM} = 1/T_{1ZOF} + 1/T_{1ZRot} + 1/T_{1ZSD} \quad (1a)$$

provided that B_0 is large compared with the internal local field B_{loc} at the site of the spins. For dipolar interacting $I = 1/2$ spins like protons, the rate R_{1ZM} of every individual kind of motion depends on two characteristic, angular-dependent spectral densities $J_M^{(p)}(p\nu,\Delta)$ with $p = 1$ and 2, in Abragam's notation[20] by

$$R_{1ZM}(\nu,\Delta) = \frac{9}{8}\frac{(\mu_0\gamma^2 h)^2}{(8\pi^2)^2}[J_M^{(1)}(\nu,\Delta) + J_M^{(2)}(2\nu,\Delta)] \quad (1b)$$

where $\nu = \gamma B_0/2\pi$, and μ_0, γ, h denote the vacuum magnetic permeability, the gyromagnetic ratio of protons, and Planck's constant, respectively. The two bi-dimensional spectral densities $J_M^{(p)}(p\nu, \Delta)$ which, as a rule in mathematically complex forms, determine the frequency dependence of T_1, were reduced in numerous works, particularly by Freed,[34] to three one-dimensional spectral densities $J_M^{(q)}(\nu, \Delta = 0)$ with $q = 0,1,2$ at the specific orientation $\Delta = 0$ through a Wigner rotation matrix $F_{pq}(\Delta)$[15,34] for second-order spherical harmonics. This step separates angular from frequency dependence and leads to more tractable results

$$\begin{aligned} J_M^{(1)}(\nu/\Delta) = {} & (1/4)[\cos^2(\Delta)\sin^2(\Delta)]J_M^{(0)}(\nu) \\ & + (1/2)[1 - 3\cos^2(\Delta) + 4\cos^4(\Delta)]J_M^{(1)}(\nu) \\ & + (1/8)[1 - \cos^4(\Delta)]J_M^{(2)}(\nu) \end{aligned} \quad (2a)$$

$$\begin{aligned} J_M^{(2)}(2\nu,\Delta) = {} & (1/4)[\sin^4(\Delta)]J_M^{(0)}(2\nu) + 2[1 - \cos^4(\Delta)]J_M^{(1)}(2\nu) \\ & + (1/8)[1 + 6\cos^2(\Delta) + \cos^4(\Delta)]J_M^{(2)}(2\nu) \end{aligned} \quad (2b)$$

and thus to theoretical model expressions explicitly available in the literature, since the $J_M^{(q)}(\nu)$ values have been calculated and reported for the OF, Rot and SD processes considered in Fig. 1. As can be seen from equations (2a) and (2b), $T_1(\Delta)$ differs for unlike motions M if the ratios $J_M^{(0)}:J_M^{(1)}:J_M^{(2)}$ are not the same for the reorientations involved and this behaviour greatly helps one to disentangle the mechanisms. As a rule, T_1 decreases for larger angles Δ, but both positive and negative variations are expected for SD models. The special forms of such spectral densities $J_M^{(q)}(\nu)$ used to obtain the model curves shown were taken from the original papers[17,24,25,28] with some minor numerical modifications.[31,32]

In FC experiments, where the external Zeeman field, $\vec{B}_0$ (with selectable

components B_x and B_z), can fall to values of similar magnitude as the internal local field $\vec{B}_{loc}$ of the magnetic dipoles, and where the detection B_1 pulses sample the total spin order, equation (1) no longer describes the full spin relaxation at low frequencies.[20,35,36] The observable overall relaxation rate $1/T_1$ of the changing spin order in this case becomes, in an extension of equation (1), a mixture of the relaxing Zeeman magnetization (time constant T_{1Z}), and the relaxing dipolar order (time constant T_{1D}), which according to Goldman[35] should be given by the weighted average

$$1/T_1(\nu^*, \Delta^*) \equiv R_1 = \frac{B_0^2/T_{1Z} + B_{loc}^2/T_{1D}}{B_0^2 + B_{loc}^2} \tag{3a}$$

with the effective Larmor frequency

$$\nu^* = \gamma B_{eff}/2\pi, \; B_{eff} \equiv (B_\Delta^2 + B_{loc}^2)^{1/2} \tag{3b}$$

and the locally effective field inclination angle relative to the director $\vec{n}$

$$\Delta^* \cong \text{arctg}(B_x/(B_z + B_{loc})). \tag{3c}$$

For simplicity, in equation (3c) $\vec{B}_{loc}$ is assumed to be mainly along the director axis $\vec{n}$,[37] and $\vec{n}$ is aligned parallel to $\vec{z}$. For $B_{loc} \ll B_0$, the total T_1 is equal to T_{1Z}, whereas in the opposite case $B_{loc} \gg B_0$ one has $T_1 = T_{1D}$. Evidently, the finite local field contribution complicates the control of the angle adjustment without an exact knowledge of $\vec{B}_{loc}$, and because of equation (3c) the inclinations of 90° become impossible by external field switches. Furthermore, the spectral densities for T_{1D} are not discussed in the literature to the same extent as for T_{1Z}, nor does there exist a critical experimental examination of the validity of the basic expression equation (3a). Approximate predictions about T_{1D} with the Redfield formalism[20,21] give, for the completely isolated, i.e., uncoupled proton spin-pair ($I = 1$) and high spin-temperature approach[15,38]

$$1/T_{1D}(\nu^*, \Delta^*) \equiv R_{1D} = \sum_M R_{1DM} = \frac{27}{8} \frac{(\mu_0 \gamma^2 h)^2}{(8\pi^2)^2} \sum_M J_M^{(1)}(\nu^*, \Delta^*), \tag{4a}$$

which produces a maximum ratio of $T_{1Z}/T_{1D} = 3$, that is if the $J_M^{(2)}$ contributions to T_{1Z} in equation (1b) are negligible. In contrast to equation (4a), the mean-field or *one-spin* approach[35] allows a much larger, frequency-dependent ratio from 2 to infinity, where the details are determined by the degrees of correlation and coherence between the spins; unfortunately the angular dependence has not been treated quantitatively as in the Redfield formalism by equations (2a) and (2b). To generalize equation (4a), Morrison

and Bloom[30] suggest an alternative with adaptable model constants in the form

$$1/T_{1D}(\nu^*, \Delta^*) = a_0 + a_1 P_2[(\cos(\Delta^*)] + a_2 P_4[\cos(\Delta^*)] \qquad (4b)$$

where a_0, a_1 and a_2 are functions of the nematic order parameter and normalized spectral densities, and P_2 and P_4 are the Legendre polynomials of second and fourth order. Although no explicit calculations of the quantities a_i have been reported, T_{1D}, as shown in equation (4b) may involve, at any angle Δ^*, all three spectral densities, $J_M^{(q)}$, in particular $J_M^{(0)}$, which obviously diminishes T_{1D} without affecting T_{1Z}, and thus one can interpret T_{1Z}/T_{1D} ratios much larger than 3. Related arguments for the deficiency of equation (4a) as a result of the common infinite spin temperature approximation in Redfield's approach have recently been discussed by Jeener *et al.*[39]

Using equations (1a), (1b), (2a), (2b), (3b), (3c), and (4a) or (4b), together with the special spectral densities $J_M^{(q)}(\nu)$ for the three processes M = OF, Rot and SD described in the literature,[15,17,24,25,28] $1/T_1$ of expression (3a) can be written as a combination of three characteristic model functions f_{OF}, f_{Rot} and f_{SD}, which depend on the two experimentally selectable variables (ν^*, Δ^*) and up to 11 adjustable model parameters of the superimposed relaxation mechanisms, namely

$$\begin{aligned} 1/T_1 = {} & f_{OF}(A_1, \nu_{CL}, \nu_{CH}, B_{loc}) \\ & + f_{Rot}(A_2, \tau_{Rot}, \sigma, B_{loc}) + f_{SD}(A_3, \tau_{SD}, \varepsilon, \alpha, B_{loc}) \end{aligned} \qquad (5)$$

where A_1, A_2 and A_3 denote the strengths of the three individual contributions and hence the relaxation rates in the limit $\nu \rightarrow 0$, whereas the other eight parameters determine both the position and the profile of the usually overlapping dispersion ranges: ν_{CL} and ν_{CH} are the low and high cut-off frequencies of the OF mode spectrum; τ_{Rot} and σ are the correlation time for rotations of individual molecules about their short axis and the related rotational anisotropy ratio; τ_{SD}, ε, α designate the correlation time for translational diffusion perpendicular to the long molecular axis, the translational anisotropy ratio, and the jump length in units of molecular diameters, respectively. Finally, B_{loc} is the z-component of the internal dipolar field. The explicit form of equation (5) for various disputed alternatives, on the one side using the distinct T_{1D} terms of equations (4a) and (4b) by Morrison and Bloom[30] and Vold and Vold,[38] and on the other, using in equations (1a) and (1b) $J_{Rot}^{(q)}(\nu)$ spectra of Nordio *et al.*[24] and Vold and Vold[25] respectively, is described by Struppe and Noack.[31,32] Such model functions are fitted to the experimental $T_1(\nu, \Delta)$ profiles by a standard Levenberg–Marquardt nonlinear least-squares optimization procedure (Micromath) for those parameters that permit a critical minimization of the least-squares deviation Σ between the data points and the model plot. One should note that a typical

Table 1. Relaxation model parameters obtained by a Levenberg–Marquardt fit optimization of equation (5) of the experimental $T_1(\nu,\Delta)$ data for 5CB and 8CB, shown in Fig. 2. Both data sets are rather similar, which on one hand demonstrates that the fitting is reproducible, and on the other shows the minor importance of the chain length variations on the T_1 dispersion. The model constants denoted by (*) could not be determined reliably and were estimated theoretically.[31,32] $D_{R\|}$,$D_{R\perp}$ are the rotational diffusion constants parallel and perpendicular to the long molecule axis, and $D_{\|}$,$D_{\perp}$ the translational diffusion constants parallel and perpendicular to the nematic director; $<r_{\perp}^2>$ is the mean translational jump width perpendicular to the molecular long axis and d the molecular diameter.

Parameter	5CB (30°C)	8CB (37°C)	Ref.
A_1 (s)	0.41	0.39	15,17,61
ν_{CL} (Hz)	<2400	<2100	
ν_{CH} (Hz)	$>10^8$	$>10^8$	
A_2 (s)	0.42	0.40	15,25,26
τ_{Rot} (ns, Vold)	3.3	2.8	
$\sigma \cong D_{R\|}/D_{R\perp}$ (*)	2.9	2.9	
τ_{Rot} (ns, Nordio)	2.2	1.9	
$\sigma \cong D_{R\|}/D_{R\perp}$ (*)	30	30	
A_3 (s)	0.59	0.54	15,27,28
τ_{SD} (ns)	37	57	
$\epsilon \equiv D_{\|} / D_{\perp}$ (*)	2.0	2.0	
$\alpha \equiv <r_{\perp}^2>/d^2$ (*)	0.2	0.2	
B_{loc} (μT)	60	50	30,35,38
a_0 (s)	383	383	
a_1 (s)	428	121	
a_2 (s)	−417	−431	

FC data set at 30 Larmor frequencies and two director orientations makes use of more than 50 $T_1 - \nu$ pairs at one constant temperature to find, by iterative steps, up to 11–14 unknown quantities. It is evident that not all the model characteristics could be evaluated reliably because of very strong correlations in the fitting process. In particular the fitting of both OF-mode cut-off frequencies ν_c, of the anisotropy ratios σ and ε, and of the jump length parameter α, proved rather insensitive near physically plausible constraints. Some results obtained in this way are listed in Table 1 to illustrate differences between 5CB and 8CB. These data have been interpreted[31,32] with astonishing success by means of the molecular geometry, i.e. by spin-pair orientations and separations, and available visco-elastic material constants, i.e.

by viscosities and elastic curvature modili, of the *n*-alkyl-cyano-biphenyl series.

The diagrams demonstrate clearly that the final curve fits with the selected preferences, namely Morrison's Ansatz[30] equation (4b) for the dipolar relaxation rate, and Vold's third-rate concept[25] in equation (1b) for the anisotropic molecular rotations, prove to be very satisfyingly within the experimental error limits of typically 5%, even in the problematic kHz range. Whereas the alternative equation (4a) leads to dramatic discrepancies in the low-frequency regime, Nordio's small-step concept in equation (1b) entails only minor, yet clearly not negligible, deviations in the high-frequency regime. Details are represented by Fig. 3, which, in addition to the overall $T_1(\nu)$ curve fits, also includes the individual $T_{1ZM}(\nu)$ contributions for both the Nordio and Vold models. The esssential findings of the analysis can be summarized as follows: the angular dependence of $T_1(\nu)$ supports and extends previous conclusions about the significance of the order of fluctuation relaxation process at kHz frequencies up to the low MHz regime, and the parameters obtained are compatible with theoretical estimations from the molecular geometry and material constants. $T_1(\nu, \Delta)$ also reveals that the common treatment of the dipolar relaxation spectral density only by $J_M^{(1)}(\nu)$ terms in equation (4a) is inadequate at low frequencies, at least for protons. Furthermore the results provide a basis for an improved disentanglement and discrimination of sophisticated rotation relaxation models, although more and more accurate FC data are still needed to decide between all of the suggested concepts.[15] In the system studied the Vold third-rate concept gives a better description of the measurements than the Nordio small-step model. This result supports and extends conclusions from high-field deuteron studies from the literature[15] at conventional Larmor frequencies.

3.2. Flow and viscosity studies in nematic liquid crystals

The NMR FC technique has most often been applied to determine the frequency dependence of nuclear relaxation times[4–7] as discussed in the previous chapter. In anisotropic liquids, where the individual molecules and the axes of the molecular order align in an external magnetic field, the FC principle can also be used in a different way for a quite different aim, namely to study anisotropic flow processes related to the alignment. Because of the anisotropy, systematic flow or viscosity measurements in distinct, well-defined geometries by known methods are difficult, hence rare and often inconsistent.[40] The new FC procedure[41,42] measures, by observing NMR signal changes in the course of the flow, at least some of the underlying visco-elastic material constants more reliably than the rather indirect relaxation analysis of molecular reorientations described before, and competes with other direct techniques to determine anisotropic viscosities.

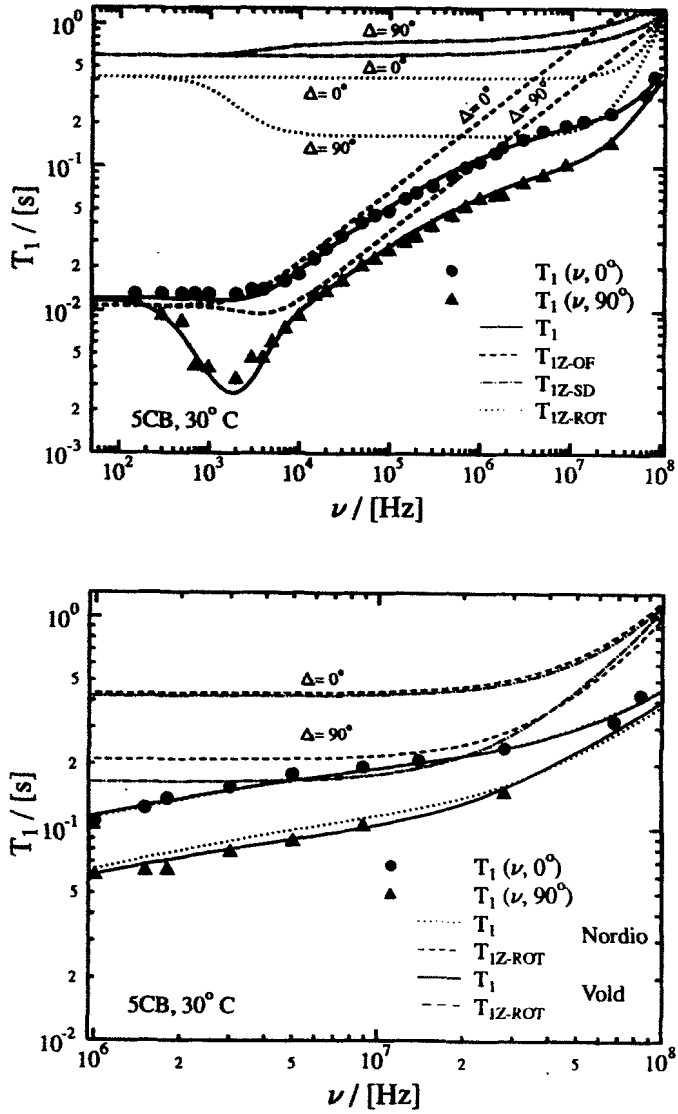

Fig. 3. Details of the model analysis of Fig. 2. The upper diagram shows, in addition to the overall T_1 fit for 5CB, the three T_{1ZM} contributions (M = OF, Rot and SD) according to equations (1a) and (1b) and indicates that, with a maximum T_{1Z}:T_{1D} ratio of 3, the T_{1D} contribution by equation (4a) cannot describe the angular dependent results in the kHz regime. The lower diagram illustrates the differences between the Nordio small-step and the Vold third-rate rotational model and the preference of the second concept, which becomes visible mainly by the $\Delta = 90°$ data in the MHz regime. In the first case (Nordic model), the experimental error limits of ±7% are smaller than the standard deviation of 17% between the calculated and the observed relaxation times. In the second case (Vold model), both limits are of comparable magnitude.

Originally, the basic idea was realized without an FC switch by a continuous or one-turn rotation of the sample perpendicular to the external magnetic field direction, in order to induce a flow;[43,44] but such a mechanical rotation is, similar to a mechanical FC switch, much too slow to establish reproducible states of motions in common, low-viscosity anisotropic liquids; such measurements were therefore restricted to high-viscosity liquid crystalline polymers.[43,44] Fast electronic FC eliminates these restrictions, but to date the new technique has only been used with proton spin signals owing to instrumental limitations.[5,41]

3.2.1. The method

The principle of a field-cycle to measure the flow and the underlying material constants in a liquid crystal by the changes of the proton line splitting, or more generally by changes of the full line profile of the proton spectrum, is illustrated by Fig. 4. Similar to Fig. 1, the cycle is separated into three periods, which, however, have tasks that differ from those in the relaxation experiment. The first polarization period, I, creates a thermodynamic equilibrium of both the magnetization $\vec{M}$ and the director field $\vec{n}$, which means that for liquid crystals with positive magnetic anisotropy $\vec{n}$ becomes parallel to the external Zeeman field $\vec{B}_P$ aligned along the z-axis. At a time $t = \tau_0$, the second evolution or flow period II starts. The field in the z-direction is then switched to a lower value, B_z, while at the same time a field in the x-direction with strength B_x is turned on to produce an inclination of the total field B_Δ

$$B_\Delta = (B_x^2 + B_z^2)^{1/2} \tag{6a}$$

by an angle

$$\Delta = \text{arctg}(B_x/B_z) \tag{6b}$$

relative to the z-axis, i.e. also to the director $\vec{n}_0$ at time τ_0. This is a non-equilibrium configuration, and a reorientation process $\vec{n}(t)$ of the director will start, where the angle between $\vec{n}(t)$ and B_Δ will decrease from Δ to zero, i.e. the inclination $\theta_n(t)$ of $\vec{n}(t)$ relative to the z-axis will increase from zero to $\theta_0 = \Delta$. It is measured by the signal following a detection, B_1, pulse in the third detection period III, which begins at time $t = \tau_R$ after the field B_x is turned off and B_z is switched back to the high B_P value for a satisfactory signal amplitude. After a short delay time δt, which is necessary to improve the field stability, the free induction decay (FID) signal is produced, as usual, by a $\pi/2$ $B_1(t)$ r.f.-pulse and then processed by a fast Fourier transform (FFT) to give a spectrum of the spins. In this way the director flow and all viscosities become observable through the separations, widths, and relative amplitudes of the individual lines. The lowering of B_z

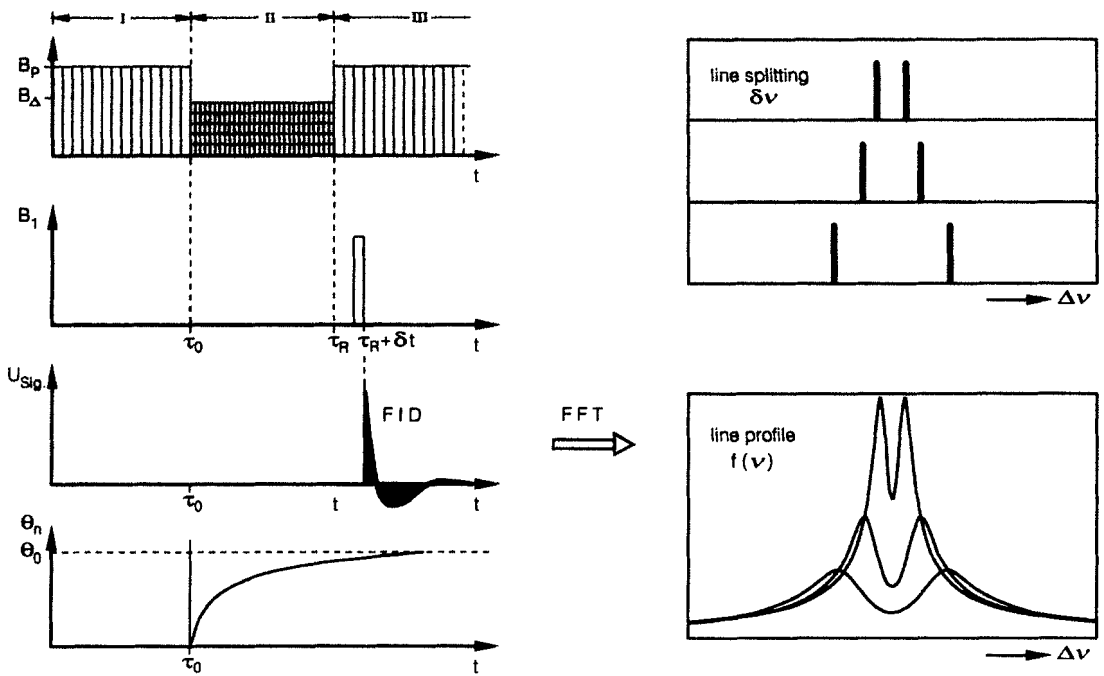

Fig. 4. Polarization, flow (evolution) and detection periods (I, II, III) for flow measurements in liquid crystals by angular dependent fast field-cycling. The left diagram illustrates schematically the $B_0(t)$-cycle with a z- and x-component at the limit of zero transit times, the FID signal $U_{Sig}(t)$ following a $\pi/2$ $B_1(t)$ r.f. pulse perpendicular to B_z, and the increasing nematic director inclination $\theta_n(t)$ relative to the z-axis from zero to θ_0. The right diagram shows that fast Fourier transformation of the FIDs yields changing line profiles $f(\nu) \equiv f(\nu_0 \pm \Delta\nu)$ around the central Larmor frequency, ν_0; the changing line splits $\delta\nu$ are directly related to $\theta_n(t)$. A more detailed analysis of the flow must take into account the complete spectrum, which however reflects $\theta_n(t)$ with greater complexity.

is required for two reasons: an instrumental and a physical one. First, to adjust an angle of 90° by a field switch, according to equation (6b) one must have $B_x \gg B_z$. Second, according to equation (6a) the lowering of B_z reduces the total field strength B_Δ over the flow period and thus allows one to diminish the speed, $d\theta_n/dt$, and consequently increase the available time τ_R of the flow, which is helpful for low-viscosity liquids. Because the director reorientation towards the new equilibrium $\vec{n} \| \vec{B}_\Delta$ is not necessarily a homogeneous motion with the same director inclination $\theta_n(t)$ over the whole sample, for the more general inhomogeneous process this angle must be understood locally as $\theta_n(\vec{r},t)$, and NMR observes a properly weighted average over all positions $\vec{r}$.

By varying the length τ_R of the flow period II from, typically, zero to 100 s, the form of the spectrum changes owing to the increasing angle $\theta_n(t)$ between the local director $\vec{n}(r)$ and the magnetic detection field B_z, and this development is recorded. Both the observed dependence of the line splitting Δ and of the full line profile $f(\nu)$ on the flow time τ_R reflect the flow state of the molecules, and in principle both the splitting and the full spectrum allow one to distinguish a homogeneous from an inhomogeneous flow. However, the information and the data handling are more exact when considering details of the line profile, in particular when the splittings approach zero or completely disappear owing to a director inclination near the magic angle.

In the simple case where the sample material contains only one type of proton spin pair with a separation r_{12} and a fixed (i.e. over the time of the measurement not motionally averaged) orientation β_{12} relative to the external detection field B_z, the spectrum consists of two lines (Pake doublet) with splitting Δ[46]

$$\Delta = \frac{3\gamma^2 h}{4\pi r_{12}^3}(3\cos\beta_{12}^2 - 1) \tag{7a}$$

as illustrated by Fig. 4, where γ is the gyromagnetic ratio of the protons. The preferred axis of the nematic liquid crystalline order now is the director $\vec{n}$, and hence the angle β_{12} can be expressed by the angle θ_n between the field B_z and the director, by the angle ϑ between the director and the average long molecular axis $\vec{m}$) and by the average angle α_{12} between $\vec{m}$ and the spin pair axis $\vec{r}_{12}$. According to Schmiedel *et al.*[47] this separation of β_{12} gives approximately (under the realistic assumption of fast molecular rotation about the long molecule axis) the splitting as a function of the flow angle

$$\begin{aligned}\Delta(\theta_n) &= \frac{3\gamma^2 h}{4\pi r_{12}^3}(3\cos^2\theta_n - 1)/2 * \langle(3\cos^2\vartheta - 1)/2\rangle * \langle(3\cos^2\alpha_{12} - 1)/2\rangle \\ &\equiv \text{const}\, S_n(\cos\theta_n) S(\cos\vartheta) \\ &\equiv \Delta_0 S_n(\cos\theta_n);\end{aligned} \tag{7b}$$

this is a quantity which by $S_n = 1/2\langle 3\cos^2\theta_n - 1\rangle$ implicitly depends on the searched director inclination relative to the detection field B_z. Averages over the sample volume are denoted by the brackets $\langle \ldots \rangle$. In a homogeneous director flow the angle θ_n is the same for all molecules, but in the general case averages $\langle\cos^2\theta_n\rangle$ must also be considered. The maximum splitting Δ_0 is observed when $\vec{n}$ is parallel to B_z so that $S_n = 1$. It reflects the spin pair separation and the nematic order parameter $S = 1/2\langle(3\cos^2\vartheta - 1)\rangle$, and thus the decreasing anisotropy at higher temperatures.

Because the real sample contains unlike spin pairs, and the orientation process of the director is not necessarily homogeneous over the whole sample, $\Delta(\theta_n)$ is generally not sufficient to describe the flow. More detailed information than that given by equation (7b) can be obtained from the full line spectrum $f(\nu)$, which is also illustrated by Fig. 4. To analyse the flow by this means it is not necessary to calculate the spectrum of a complex molecule from first principles, if one measures it precisely at the angle $\theta_n = 0$. The spectrum for finite angles $\theta_n > 0$ then follows from the spectrum $f_0(\nu)$ at $\theta_n = 0$ by scaling it with the orientation parameter S_n (as implied by equation (7b)) and weighting it over all contributing values of θ_n (to extend equation (7b)),[48] which gives

$$f(\nu) = \int_0^{\theta_{max}} P(\theta_n) S_n^{-1} f_0(\nu/S_n)\,\mathrm{d}\theta_n, \tag{8a}$$

where $P(\theta_n)$ denotes a model dependent probability density function of the director field orientations over the sample volume. It must be calculated from adequate solutions of the equations of motion for anisotropic liquids, the Leslie–Ericksen equations.[40,43,44] For a homogeneous director flow $\vec{n}(t)$ or $\theta_n(t)$ this distribution simplifies to a δ-function around the preferred angle θ_n^*, and with $P(\theta_n) = \delta(\theta_n^* - \theta_n)$ the general spectrum of equation (8a) becomes simply the scaled line profile

$$f(\nu) = S_n^{-1}\, f_0(\nu/S_n) \tag{8b}$$

of the spectrum before the flow begins. In this case the data handling by either equation (7b) or (8b) is completely equivalent. According to the Leslie–Ericksen theory the homogeneous rotational flow only involves one single viscosity of the anisotropic liquid,[40,43] "rotational viscosity" γ_1, whereas inhomogeneous motion brings into play five of the six nematic Leslie viscosities, α_i, with i = 1–6.[40,43] In order to measure all of these material constants, the experiment must provide suitable conditions for this type of motion, and complex calculations of the director distributions must be performed. At present, it is assumed that the conditions needed to change the flow character can be realized by variations of the maximum rotation angle $\theta_{n\,max} = \theta_0 = \Delta$.[43,44,45] For $\theta_{n\,max} < 45°$ it has been found that the flow

stays homogeneous over the whole evolution, whereas above a critical angle $\theta_{n\,\max} > \theta_c$ with $45° \geq \theta_c \leq 90°$, optically verified one- and two-dimensional pattern formations indicate a transition to a different, complex flow profile. The details of this dynamic transition are still disputed, in particular the exact value of the critical angle θ_c, as are the results of viscosity measurements by NMR methods under inhomogeneous flow conditions.[42,49]

3.2.2. Results and discussion

Using the FC technique described earlier, the line splittings and full spectra of several *n*-alkyl-cyano-biphenyls (*n*CBs, $n = 5, 6, 7, 8$) and *n*-alkoxy-cyano-biphenyls (*n*OCBs, $n = 5, 6, 7, 8$) were determined for different temperatures and starting angles θ_0 of the orientation process $\vec{n}(t)$ towards the new equilibrium along B_Δ. The original equilibrium spectra $f_0(\nu)$ with $\vec{n}$ along B_z typically show two poorly resolved doublets, i.e. two line pairs with similar splits of about 20 kHz, which of course both measure the flow. Because of the scaling with S_n the outer lines allow a more accurate signal analysis by equation (7b) than the inner ones, and near the magic angle of 54.7°, where all the lines collapse, only the full line profile still manifests the rotation of the director. Up to starting angles, θ_0, of about 85° the observed spectra as shown by equation (8b) clearly demonstrate the absence of a significant flow inhomogeneity. For such simple homogeneous geometry the Leslie–Ericksen differential equation of the director reorientation in the flow period of the field-cycle (see Fig. 4) simplifies to[50]

$$\gamma_1 \, \mathrm{d}\theta_n/\mathrm{d}t = \frac{(\chi_\parallel - \chi_\perp)}{2\mu_0} B_\Delta^2 \sin 2(\theta_0 - \theta_n) \tag{9a}$$

with the solution[50]

$$\theta_n(t) = \theta_0 - \arctan[\tan\theta_0 \times \exp((t - \tau_0)/T_R)], \tag{9b}$$

where $\chi_\parallel$ and $\chi_\perp$ denote the diamagnetic susceptibilities parallel and perpendicular to $\vec{n}$, respectively, and T_R is a characteristic time constant of equation (9a). This time constant involves the balance between the magnetic and the frictional torque on the director and enables a precise measurement of the rotational viscosity γ_1 by the relation

$$\gamma_1 = \frac{(\chi_\parallel - \chi_\perp)}{\mu_0} T_R B_\Delta^2, \tag{9c}$$

provided that the diamagnetic anisotropy $(\chi_\parallel - \chi_\perp)$ is available,[40,41] and the magnetic flux density B_Δ is determined accurately; μ_0 denotes the vacuum permeability. Some values of γ_1 obtained by equation (9c) from T_R

measurements[41,42] for the *n*-CB series are listed in Table 1. Within the error limits and with the exception of 7CB the results essentially support γ_1 data studied in the literature by more conventional flow techniques.[40,50–53] The essential advantage of the NMR FC procedure in comparison with known alternatives is that it controls the underlying homogeneous flow pattern which, in view of the open questions related to the value of θ_c, is an important aspect.

For angles of θ_0 near to 90° the evolution of the spectra $f(\nu)$ could no longer be interpreted by equation (8b), because the behaviour is different from that of a homogeneous director rotation. In the early phase of the flow period where $\tau_R < T_R$, the inconsistency remains rather small or even negligible, but with increasing time τ_R one obtains, in addition to the narrowing doublet (or doublet pairs), a central line and this triplet (multiplet) finally ends in a broad, structured and nearly time-independent line profile.[41,42] Following equation (8b) the final state should have the same form as $f_0(\nu)$, but the line splits should be reduced by a factor of 2 ($S_n = 1$ for $\theta_n = 0$, $S_n = -0.5$ for $\theta_n = 90°$). All our experiments with $\theta_0 \approx 90°$ did not reveal this final state expected for $\theta_0 < \theta_c$, and we had to consider spectral simulations for more general $P(\theta_n)$ distributions than the δ-function.

In a pioneering viscosity study of polymeric (high-viscosity) liquid crystals Martins *et al.*[43] considered an extension of equation (9a), a planar Leslie–Ericksen approximation for director motions in a plane (x, z) with an elastic inhomogeneity term periodic in one dimension (z). This approach,

$$[\gamma_1 - F(\theta_n)]\partial\theta_n/\partial t = \frac{(\chi_\parallel - \chi_\perp)}{2\mu_0} B_\Delta^2 \sin 2(\theta_0 - \theta_n) - \langle K\rangle \partial^2 \theta_n/\partial z^2, \tag{10a}$$

unlike equation (9a), is a partial differential equation that brings into play, by the coefficient of $\partial\theta_n/\partial t$ (effective viscosity) and by its dependence on z, in addition to the viscosity $\gamma_1 \equiv \alpha_3 - \alpha_2$, four more Leslie viscosities α_1, α_2, $\alpha_4 + \alpha_5$, and the average Frank elastic constant, $\langle K\rangle$. It allows special periodic solutions for inhomogeneous flow patterns of the form

$$\theta_n(z,t) = \theta_{\max}(t) \cos^{\varepsilon(t)}(q_z z) \tag{10b}$$

with maximum distortion angle $\theta_{\max}$, wave vector q_z of the periodicity along z, and anharmonicity exponent ε. The one-dimensional director distribution density is related to equation (10b) by $P(\theta_n) = \text{const}\ (\partial\theta_n/\partial t)^{-1}$. In this way we were able to describe, at least approximately, the evolution of the measured spectra by iterative model simulations.[42] However, the complex integrand of equation (8a) did not allow a unique model fit of the spectrum with unambiguous values of $\theta_{\max}$, ε and the α_i. Table 2 summarizes the best α_i results for 5CB compared with Leslie viscosities reported in the literature.[51–53] Within the large error limits of 10% for α_2 and up to 400%

Table 2. Selected rotational viscosities γ_1 and Leslie viscosities α_i of the liquid crystalline *n*-alkyl-cyanobiphenyl series (*n*CB, $n = 5$–8) obtained by FC flow experiments at different temperatures $\Delta T \equiv T_C - T$ relative to the nematic-to-isotropic transition temperature T_C (clearing point). Within the large error estimations of 10% for γ_1 and α_2, 100% for $(\alpha_4 + \alpha_5)$, 300% for α_3, and 400% for α_1, the results are essentially consistent with data reported in the literature.[41,42, 51–53]

	ΔT/°C	5CB	6CB	7CB	8CB
T_C (°C)		35.2	28.6	39.5	40.3
γ_1 (Pa s)	2	0.033	0.058	0.042	0.043
	4	0.042	0.08	0.052	0.056
	6	0.054	0.11	0.061	0.084
α_1 (Pa s)	2	−0.008	−0.013	−0.01	−0.02
	6	−0.014	−0.020	−0.015	–
α_2 (Pa s)	2	−0.036	−0.063	−0.046	−0.046
	6	−0.059	−0.111	−0.067	–
α_3 (Pa s)	2	−0.003	−0.005	−0.004	−0.003
	6	−0.005	−0.009	−0.006	–
$\alpha_4 + \alpha_5$ (Pa s)	2	0.08	0.12	0.085	0.088
	6	0.111	0.21	0.12	–

for α_1 the findings are consistent, but further methodical refinements are needed to allow a critical discussion of different theoretical concepts.[54–56]

3.3. Frequency-dependent dipolar relaxation in ordered systems

Jeener and Broekaert[57] introduced, in 1967, a three-pulse $B_1(t)$ sequence to measure the relaxation time T_{1D} of the dipolar order of $I = 1/2$ spin systems in the presence of a conventional high Zeeman field, B_0, which is based on the decay time of the so-called "Jeener echo". It was later extended by Spiess[58] and Kemp-Harper and Wimperis[59] to study in a similar way the quadrupolar order in $I \geq 1$ systems. The appearance of a Jeener echo depends upon the existence of interactions that are not averaged out by molecular motions on the considered time scale. The method has become of great importance in recent relaxation studies, in particular of liquid crystals[14,15] because, in standard spin relaxation theories, it provides a powerful means to separate and analyse the spectral densities $J^{(1)}(\nu)$ and $J^{(2)}(\nu)$:[14,15,20,25] see

for example equations (1b) and (4a) in Section 3.1.3. However, the theoretical conclusion that, unlike the Zeeman relaxation time T_{1Z}, the dipolar and quadrupolar relaxation times T_{1D}, T_{1Q} depend only on the spectral density $J^{(1)}(\nu)$, has never been examined experimentally in sufficient detail, because conventional spectrometers cannot achieve the low-frequency conditions where the T_1/T_{1D} ratio should accept well-defined limiting values. To date, Jeener measurements in the literature for protons and deuterons are restricted to the MHz regime,[14,15] where the standard technique yields a satisfactory NMR signal. Suitably modified field-cycles in combination with the Jeener technique provide a means to extend these experiments by adjusting the Larmor frequency in the T_{1D} relaxation state over a similar broad range as in a T_1 cycle, although for T_{1D} some instrumental requirements are harder to fulfil.

3.3.1. The method

In the original Jeener procedure the Zeeman order of the considered spins is transformed to a local-field order by a pair of r.f. pulses with special pulse lengths and phases. The two pulses are separated by a brief delay time τ_1, which must be shorter than the FID after the first pulse, and phase shifted by an r.f. phase of 90°. The decay of the dipolar or quadrupolar order generated in this way is then sampled after a variable time, τ_2, by a third detection pulse in phase with the second one, which retransforms the remaining dipolar order to a Zeeman magnetization. This is observed by the amplitude of the Jeener echo that develops immediately after the third detection pulse. Although this order transformation has an efficiency[57] considerably smaller than 100% (the theoretical optimum is 56%), it implicates two advantages over the alternative transformation by the more direct and less sophisticated adiabatic B_0 field switch:[4,5] it operates faster, and above all the technique can be performed using conventional pulsed spectrometers. However, the utilization of standard apparatus makes it impossible to study T_{1D} critically, i.e. frequency-dependent data are required. Jeener's $B_1(t)$ pulse sequence is usually abbreviated in the form

$$(\pi/2)_0 - \tau_1 - (\pi/4)_{90} - \tau_2 - (\pi/4)_{90} - \mathrm{Echo}(\tau_2) \qquad (11a)$$

where the numbers denote the pulse lengths (spin rotation angles) and r.f. phases (relative to the x-axis), respectively. Following the detection pulse, the echo amplitude U_{echo} versus the time τ_2 spent in the state of dipolar order normally decays exponentially with time constant $T_{1D}(\nu)$ which, like any relaxation process, depends on the applied magnetic field and thus on the related Larmor frequency, ν, of the spins:[15,20]

$$U_{\mathrm{echo}} = U_0 \exp(-\tau_2/T_{1D}(\nu)). \qquad (11b)$$

In order to measure T_{1D} of equation (11b) frequency or field dependent for frequencies greater than 5 MHz, where the standard technique no longer works, B_0 must be varied over the relaxation period; the generation and detection of the local spin order can be achieved under any suitable high-field condition. We realized this possibility with two of our FC spectrometers by a B_0 cycle with a fast field switch $|B_P \downarrow B_R|$ from the polarization to the relaxation field at the beginning of the relaxation period (τ_2 interval), and the inverse switch $|B_R \uparrow B_P|$ from the relaxation to the detection field $B_D = B_P$ at the end of the τ_2 interval. The extended Jeener sequence

$$(\pi/2)_0 - \tau_1 - (\pi/4)_{90}|B_P \downarrow B_R| - \tau_2 - |B_R \uparrow B_D|(\pi/4)_{90} - \text{Echo}(\tau_2) \quad (12)$$

allowed us to perform T_{1D} studies on ordered proton spin systems in the range between about 2 kHz and 40 MHz. As in the standard experiment, special care must be taken to position the second pulse correctly to ensure maximal transfer to dipolar order,[57,58] and to control adjustments with nonexponential echo decay; in addition to these known difficulties the unavoidable field instabilities due to the fast field switches make the T_{1D} cycle more sensitive to disturbances than the T_1 cycle, and so the error limits of T_{1D} are somewhat greater. Experimental details have been described by Becker.[60]

3.3.2. Results and discussion

As emphasized previously, FC $T_1(\nu)$ measurements can reveal the transition from Zeeman order to dipolar order, and hence the underlying relaxation processes with respective time constants T_{1Z} and T_{1D} if the external Zeeman field B_0 becomes comparable to the internal dipolar field B_{loc}. However, the separation of the relaxation time T_{1Z} from T_{1D} by the Goldman formula[35] is rather inaccurate and only possible in the low-field limit. The new Jeener FC sequence (12) allows one to improve the T_{1D} analysis and related studies independently of the strength of B_0. Again, liquid crystals were selected as suitable candidates for this type of investigation, because of the peculiar spectral density $J^{(1)}(\nu)$ originating from order fluctuations. Figures 5 and 6 compare typical FC results of proton T_1 and T_{1D} measurements on two standard nematogens, namely *p*-methoxybenzylidene-*p*-butylaniline (MBBA)[40,50] and selectively, methyl-deuterated *p*-azoxyanisole (PAA-d_6).[40,50] The deuteration was introduced to eliminate such protons which could violate the spin pair ($I = 1$) approximation; the nearest proton neighbours on the central rings of the molecules represent an ideal $I = 1$ system. Both data show that T_{1D} increases with increasing frequency almost parallel to the well-known T_1 dispersion,[5,22,23] but the ratio T_1:T_{1Z}, is not constant and near $\nu \approx 5 \times 10^5$ Hz significantly exceeds a value of 3. At low frequencies the two time constants approach each other, which is clearer in Fig. 5 than in Fig. 6 because of insufficient signal sensitivity at

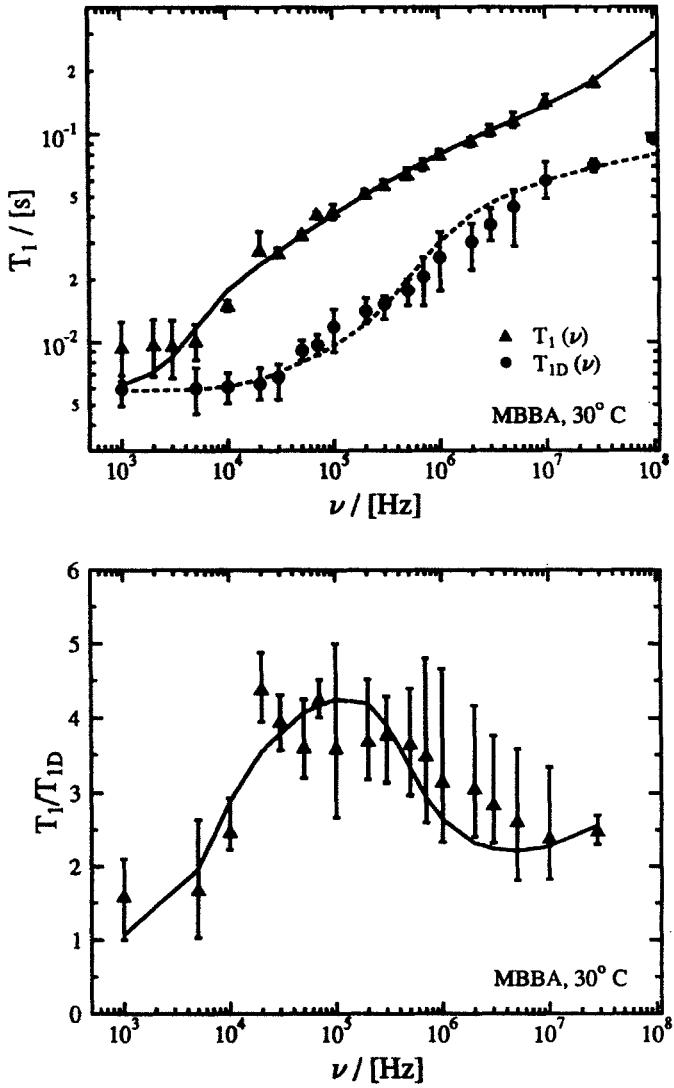

Fig. 5. Comparison of the frequency dependence of the total longitudinal proton relaxation time T_1 and of the dipolar proton relaxation time T_{1D} in the low-temperature nematic liquid crystal MBBA. $T_1(\nu)$ was measured by the usual T_1 field-cycle with one B_1 r.f. pulse, shown by Fig. 1. T_{1D} was measured by the usual Jeener–Broekaert sequence of three B_1 r.f. pulses, in combination with a B_0 field-cycle, which introduced an adjustable relaxation period between the second and third B_1 pulse to give $T_{1D}(\nu)$. The plots in the upper diagram show model fits according to equations (13a)–(13d) with extensions described in the text. From the details at bottom about the experimental errors it can be clearly seen that the ratio T_1/T_{1D} significantly exceeds a value of 3 at medium frequencies, and in accordance with the model plot (full line) approaches 1 in the low-frequency limit, where B_0 is smaller than B_{loc}.

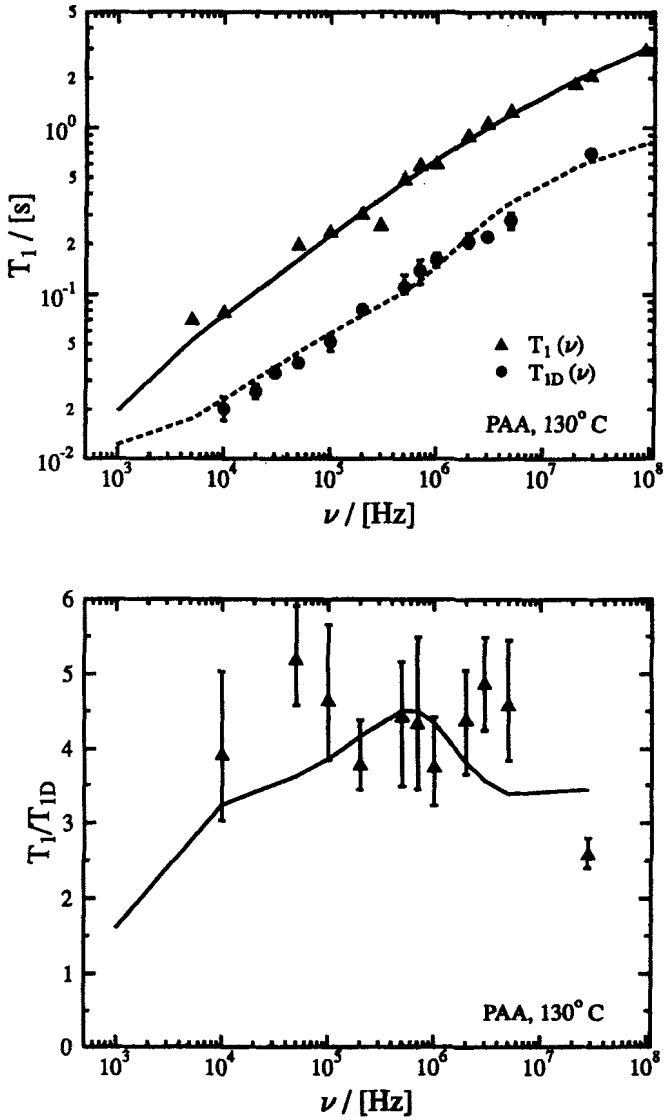

Fig. 6. Comparison of the frequency dependence of the total longitudinal proton relaxation time T_1 and the dipolar proton relaxation time T_{1D} in the selectively methyl-deuterated high-temperature nematic liquid crystal PAA-d_6 (upper diagram). The characteristic features are qualitatively similar to the results of Fig. 5. However, because of the higher temperature both relaxation times are longer and the local field is smaller; therefore the limit $B_0 < B_{loc}$ is shifted to lower ν values and the regime with $T_1/T_{1D} \cong 1$ is not fully seen (lower diagram) for experimental reasons.

low frequencies in the deuterated PAA-d_6 sample. The ratio varies from approximately 1 for $\nu < 10$ kHz to about 4 at medium frequencies and then slightly decreases at high frequencies to about 2 for MBBA and to about 3 for PAA-d_6. Qualitatively similar dispersion profiles have been observed for numerous other liquid crystals.[60]

These FC T_{1D} results lead to two important conclusions by contrasting the data with pertinent theoretical expressions.[15] Making use of the well-established finding[22,23] that order fluctuations (OF) of the nematic director dominate the Zeeman relaxation time, T_{1Z}, in the kHz region up to typically 1 MHz, one can simplify equations (1b), (3a) and (4a) for frequencies $<10^3$ kHz to the special forms[15,17]

$$1/T_{1Z} \approx 1/T_{1ZOF} = \frac{9}{8}\frac{(\mu_0\gamma^2\hbar)^2}{(8\pi^2)^2} J^{(1)}_{OF}(\nu). \tag{13a}$$

$$1/T_{1D} \approx 1/T_{1DOF} = \frac{27}{8}\frac{(\mu_0\gamma^2\hbar)^2}{(8\pi^2)^2} J^{(1)}_{OF}(\nu), \tag{13b}$$

$$1/T_1 \approx \frac{B_0^2/T_{1ZOF} + B_{loc}^2/T_{1DOF}}{B_0^2 + B_{loc}^2} \tag{13c}$$

with the OF spectral density[61,62]

$$J^{(1)}_{OF}(\nu) = \frac{A}{\nu^{1/2}}\left\{1 - \pi^{-1}\left[\operatorname{artg}\left\{\frac{(2\nu/\nu_{CL})^{1/2}}{(\nu/\nu_{CL}-1)}\right\} - \operatorname{artgh}\left\{\frac{(2\nu/\nu_{CL})^{1/2}}{(\nu/\nu_{CL}+1)}\right\}\right]\right\}$$
$$+ \theta(\nu/\nu_{CL} - 1), \tag{13d}$$

which above the low-frequency mode cut-off ν_{CL} is a square-root law and for $\nu < \nu_{CL}$ approaches a constant. The factor A denotes a material parameter and $\theta(\nu/\nu_{CL} - 1)$ is the unit step function at $\nu = \nu_{CL}$. The new measurements show that the transition $T_1 \approx T_{1Z}$ to $T_1 \approx T_{1D}$, expected from equation (13c) at $B_0 \approx B_{loc}$, is indeed seen; however, the $T_1/T_{1D} \approx T_{1Z}/T_{1D}$ ratio of 3, predicted by equations (13a) and (13b) for $B_0 > B_{loc}$ in the fully developed square-root range, is not observed within the error limits — in the illustrated and many other examples it approaches significantly higher values near 4. This cannot be ascribed to neglect of relaxation mechanisms other than OF, which all shorten T_1 more than T_{1D} owing to the presence of $J^{(2)}(\nu)$ spectral densities.[15,20,21] This trend is clearly indicated by the data at the highest frequencies where the relative importance of individual molecular reorientations (rotations, translations) increases.[31] The ratio > 3 implies that equation (13b) is incomplete and most likely suggests that T_{1D} involves additional terms that differ from $J^{(1)}(\nu)$. Such a necessity has been discussed many times in the literature,[35,39] and it appears essentially to be based on the incorrect

treatment of slow quantum correlations and coherences in the familiar semiclassical, i.e. high spin-temperature formalisms.[20,38] However, this has never been examined quantitatively by critical T_{1D} experiments. Our finding confirms a similar previous conclusion from angular-dependent FC T_1 studies.[31] The observed discrepancies at medium frequencies could be removed by including in equation (13b) a small additional Debye-type spectral density (≈30–50%), as discussed by Goldman[30] for the case of completely absent motional correlations. Both the $T_{1D}(\nu)$ plots and the related T_1/T_{1D} ratios in Figs 5 and 6 illustrate that the extended spectral densities in equations (13a)–(13d), modified by a Debye-term to allow $T_1{:}T_{1D}$ ratios greater than 3, and without the restriction to OF at high frequencies, can provide satisfactory model fits to the data. Note that the maximum of the ratio is related to the correlation time ($\approx 5 \times 10^{-7} - 5 \times 10^{-8}$ s) of the additional T_{1D} process. Details of the calculations are explained by Becker.[60]

3.4. Fast magic-angle field rotation for diffusion studies

Field-cycling the orientation of the Zeeman field relative to special symmetry axis opens up numerous new NMR procedures, where the simpler alternative, namely the mechanical rotation of the sample, is too slow. Peculiar features arise if the selected angle Δ is near the magic angle of 54.7°, because all interactions which scale with the second-order Legendre polynomial $P_2 = (3\cos^2\Delta - 1)/2$ then vanish, or at least are strongly diminished.[20] Because the inhomogeneity of the best FC magnets[5,10] is by a factor of typically 100 times worse than the resolution of steady-state iron or cryomagnets, the power of magic-angle switching cannot be exploited to the same extent as, for example, magic-angle-spinning techniques in conventional NMR.[36] However it has proved extremely useful to improve broad solid-state signals, and has successfully been applied in combination with pulsed field-gradient diffusion measurements.[63–66]

3.4.1. The method

Magnetic resonance with nuclear or electronic spins provides a broad spectrum of direct or indirect techniques for the measurement of self- and binary diffusion.[20,36,63] The most reliable are based on special spin-echo signals, which allow one to observe directly the magnetization decay $\vec{M}(\vec{r},t)$ caused by diffusion by applying strong magnetic field-gradients (FG), either stationary (SFG) or pulsed (PFG), superimposed on the usually homogeneous Zeeman field, B_0. This requires creation of suitably inhomogeneous conditions and analysis of Fick's law diffusion term for the spin

magnetization $M_\perp$ transverse to the field B_0, according to the generalized Bloch equations[20]

$$\frac{\partial M_\perp}{\partial t} = -\frac{M_\perp}{T_2} + D\frac{\partial^2 M_\perp}{\partial \vec{r}^2}, \tag{14a}$$

where T_2 is the transverse relaxation time of the considered spins, and D is the diffusion tensor. In order to determine the components of D, the field gradient $\vec{G} \equiv \partial B/\partial \vec{r}$, which results in the last term in equation (14) by diffusion along $\vec{G}$, must be oriented parallel to any desired direction by suitable gradient coils, and the diffusion damping by D must dominate the relaxation damping by T_2. For a Hahn $\pi/2 - \pi$ two-pulse, field-gradient spin-echo experiment with adjustable pulse separation τ and a constant, i.e. time- and space-independent gradient for equal intervals τ after both pulses, equation (14) gives, in response to the sequence, the echo-amplitude at time $t = 2\tau$[20]

$$M(2\tau) = M(0)\exp[-2\tau/T_2]\exp[-2D_G^2\gamma^2 G^2\tau^3/3], \tag{14b}$$

which evidently sets a lower limit to the range of accessible diffusion constants D_G along G to about $D_{G\,\min} \geq 10/(T_3^2\,\gamma^2\,G^2)$; in the case of short, solid-like T_2s ($<50\,\mu$s) and small, solid-like Ds ($<< 10^{-10}\,\mathrm{m^2\,s^{-1}}$) this condition requires extremely strong gradients ($>10\text{–}2 \times 10^2\,\mathrm{T\,m^{-1}}$). It is still extremely difficult to realize diffusion-controlled echo signals in crystalline systems satisfactorily, and the best ways to achieve the aim are unclear. For a long time it was believed that pulsed rather than constant gradients in the FG echo sequence provided a more effective means to observe slow diffusion decays because of the absence of G during the signal detection. However, brute-force methods with constant gradients in the fringe field of cryomagnets[67] could reduce the lower limit of observable diffusivities considerably to less than $10^{-16}\,\mathrm{m^2\,s^{-1}}$. Because the required means are generally not available in standard spectrometers and such high gradients imply many conflicts with the signal processing of the badly broadened resonance lines, FC may be a more convenient alternative to extend the FG method to smaller Ds with customary pulsed field gradients, by diminishing the effective relaxation term in equation (14) rather than by strengthening the diffusion signal decay. Again, nematic liquid crystals, where the usual PFG technique cannot create the experimental conditions[68] required for diffusion studies, are considered as examples[64–66] to demonstrate the method. Results discussed in the literature using other techniques[64,68] are highly contradictory.

In liquid crystals the proton resonance line width and the related effective transverse spin relaxation time T_2 depend on the angle θ between the magnetic field $\vec{B}$ and the director $\vec{n}$, which is described approximately by[15,46,47]

$$T_2 = T_2(\theta = 0)/P_2(\cos\theta) \equiv 2T_2(\theta = 0)/(3\cos^2\theta - 1) \tag{15}$$

so that a rotation of the field to the magic angle lengthens the relaxation term in equation (14b) within the instrumental limits dramatically, in nematic liquid crystals typically from 50 μs to 5 ms. Because of the positive magnetic anisotropy of most nematic molecules[40] the equilibrium orientation of $\vec{n}$ is parallel to $\vec{B}$. One can take advantage of equation (15) for diffusion studies by aligning the director over the full $B_1(t)$ r.f. pulse and $G(t)$ pulsed field-gradient sequence which generates and samples the spin-echo decay. This is achieved by first preceding the sequence by a field switch $|B_P \Rightarrow B_\Delta|$ to the magic angle $\Delta = 54.7°$ and maintaining B_Δ for a sufficient orientation time τ_0 until $\vec{n}$ is parallel to $\vec{B}_\Delta$ (polarization period), the switch $|B_\Delta \Rightarrow B_P|$ back to B_P, where the $\pi/2 - \pi$ pulse pair and the gradient are applied (evolution or diffusion period) then creates the desired director inclination. Because this is a nonequilibrium state of $\vec{n}$, and flow tries to reorient the director along B_P, as discussed in section 3.2, the B_0 changes have to be fast and the PFG sequence must be turned on at $t = t_0 = 0$ immediately following the beginning of the non-equilibrium state in order to measure diffusion in the oriented system and not flow. At $t = 2\tau$, the gradient is turned off and the echo signal detected as usual (detection period). Similar to equation (12) we abbreviate individual steps of the combined FC-PFG cycle in the short form

$$|B_P \Rightarrow B_\Delta| - \tau_0 - |B_\Delta \Rightarrow B_P|(\pi/2)_0 G(\tau)(\pi)_0 G(\tau)\,\mathrm{Echo}(2\tau), \qquad (16)$$

where the longest interval is the orientation time τ_0.

In a typical experiment with nematic liquids,[66] τ_0 is of the order of 10–100 s, τ of the order of 5–50 ms; to find a compromise between good signal sensitivity and negligible flow in the diffusion–detection B_P state, the strength of B_P must be varied in the range between 0.1 T and 0.25 T. Although flow, which becomes faster at stronger B_P fields can, in principle, be separated from diffusion by different signal forms,[63] it disturbs the exact maintenance of the magic-angle alignment and makes the effective T_2 slightly time dependent. The amplitude of the gradient G can be adjusted by quadrupole coils in any direction up to 10 $T\,\mathrm{m}^{-1}$,[65] which is sufficient for all considered diffusion constants. Details of the procedure and refinements of the basic pulse programme to reduce effects of both flow and field inhomogeneity on the exact magic angle rotation are described by Mager.[66]

3.4.2. Results and discussion

The new FC technique made possible extensive measurements of the self-diffusion constans $D_\parallel$ and $D_\perp$ of liquid crystals, parallel ($\parallel$) and perpendicular ($\perp$) to the director axis, with values as low as $10^{-11}\,\mathrm{m}^2\,\mathrm{s}^{-1}$. The most challenging requirements exist for nematic mesophases because their low viscosity facilitates flow in the nonequilibrium state and so necessitates the fast FC procedure to establish the magic angle rotation of the director

alignment.[63,64,66] Without this, previous PFG studies succeeded only in determining the diffusivity, D_{iso}, in the isotropic phase of nematogen materials, where T_2 is much longer as in normal liquids.[63] Diffusion constants of nematics reported in the literature[68] scatter widely[64,69] and thus reflect the considerable difficulties of the generally rather indirect experimental concepts used. As a rule, the FC PFG results strongly deviate from findings by the indirect optical and neutron spectroscopies and by NMR relaxation analysis, but are roughly in accordance with the rare data obtained by direct tracer techniques. They clearly show several characteristics that have not been observed previously and are not in agreement with available theoretical models.[70,71] A summary of typical diffusivities, a comparison of FC with other experimental methods, and an overview of some standard theoretical concepts has recently been given in the literature[68,69], therefore only some brief remarks shall illustrate the main problems here.

The FC PFG studies of numerous nematic mesophases, such as those of *n*-alkyl and *n*-alkyloxy-cyano-biphenyls (*n*CBs, *n*OCBs), surprisingly exhibit, within the experimental error limits, always a simple Arrhenius-type behaviour

$$D_i(T) = D_{0i} \exp(-E_i/kT),\ i = \parallel \text{ or } \perp, \tag{17}$$

of D_{iso}, $D_\parallel$ and $D_\perp$; i.e. molecular jumps are controlled as in common classical liquids by activation energies (barriers) E_i scaled with the thermal energy kT, where k is Boltzmann's constant. This dependence of the D_i values on the absolute temperature T with similar magnitudes of the pre-exponential factors D_{0i} and of the activation energies E_i for all three mechanisms is illustrated for 5CB and 5OCB in Fig. 7. An important and long-disputed aspect is[68] that the anisotropy ratio $D_\perp/D_\parallel$ in nematics is rather small, near 0.5 to 0.7, and only slightly temperature dependent owing to the similar activation energies of the molecular motion in both directions. As seen in Table 3, values of E_i range between typically 20 to 70 kJ mol^{-1}. At the transition temperature from the nematic to the isotropic phase, the clearing point T_C of the fluid, D changes discontinuously. In the diagrams shown one has $D_\perp < D_{iso} < D_\parallel$, but not exactly in the way expected by theoretical models, which predict $D_{iso} = 1/3(D_\parallel + 2D_\perp)$. This finding and many other details are in remarkable disagreement with theoretical concepts,[70,71] where a more visible non-Arrhenius like influence of the liquid crystal order parameter and of the involved Leslie viscosities is suggested. By variation of the chain length the diffusivities show odd–even alternations which, except for 8OCB, parallel the alternation of the clearing temperature. Comparable effects are observed in the activation energies. Table 3 summarizes some selected data[66] to demonstrate that the FC technique allows fast systematic routine studies, which should give a basis to improve the presently unsatisfactory theoretical models of self-diffusion in liquid crystals.[69–70]

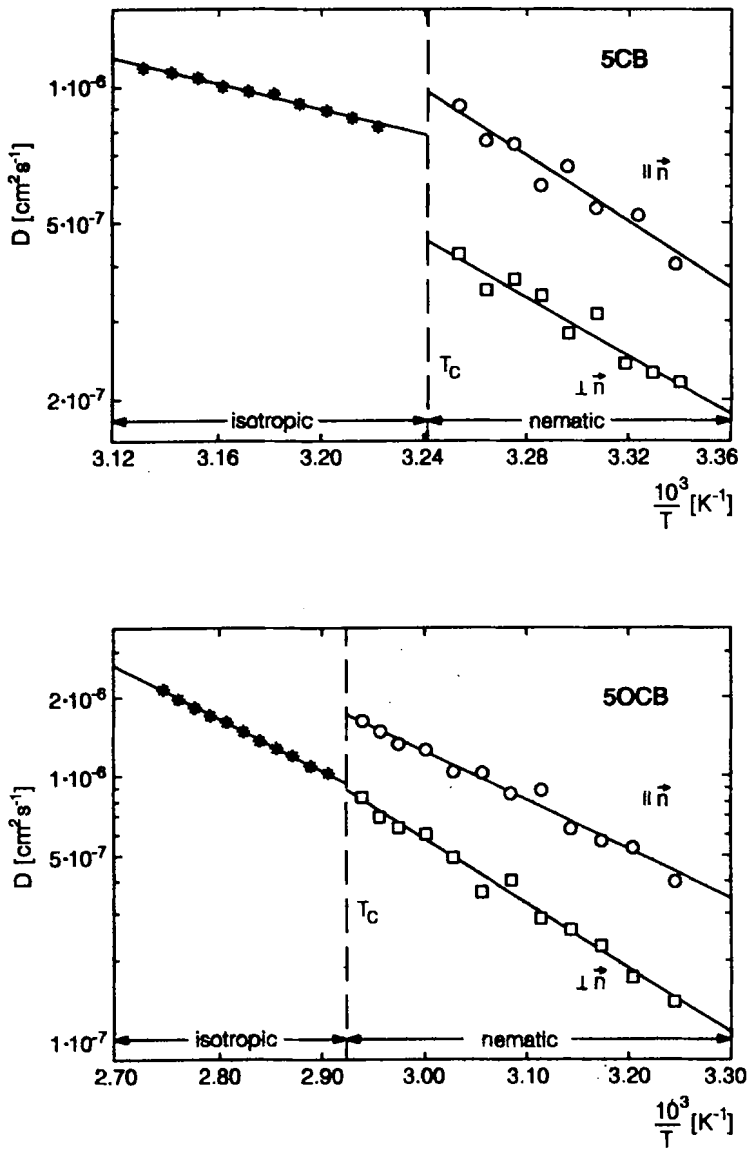

Fig. 7. Arrhenius plots of diffusion constants of nematic and isotropic pentyl-alkyl-cyano-biphenyl 5CB (upper) and pentyl-alkyloxy-cyano-biphenyl 5OCB (lower) to illustrate the quality of the Arrhenius law, the anisotropy ratio and the changes due to the slightly different side-groups of the two cyano-biphenyls. The data cannot be interpreted with existing theories.[66]

Table 3. Selected self-diffusion constants D_{iso}, $D_{\parallel}$, $D_{\perp}$ and related activation energies E of some homologues of the liquid crystalline *n*-alkyl-cyano-biphenyl (*n*CB, $n = 5$) and *n*-alkyloxy-cyano-biphenyl (*n*OCB, $n = 5$–8) series obtained at different temperatures $\Delta T \equiv T_C - T$ relative to the clearing point T_C by FC-PFG diffusion experiments. The error limit estimated from the experimental standard deviation is ± 10%.

	ΔT(°C)	5CB	5OCB	6OCB	7OCB	8OCB
T_C (C°)		36.2	68.9	77.5	76.1	80.6
D_{iso} (10^{-11} m^2 s^{-1})	−5	9.64	11.4	14.0	12.6	14.1
$D_{\parallel}$ (10^{-11} m^2 s^{-1})	+5	5.99	14.1	19.4	18.5	11.6
$D_{\perp}$ (10^{-11} m^2 s^{-1})	+5	3.43	6.71	7.89	6.47	7.02
E_{iso} (kJ mol^{-1})		29.6	38.3	30.9	35.7	36.4
$E_{\parallel}$ (kJ mol^{-1})		69.7	34.8	36.1	29.0	43.1
$E_{\perp}$ (kJ mol^{-1})		60.4	46.4	24.8	26.6	36.3

4. OTHER DEVELOPMENTS AND OUTLOOK

The preceding sections have shown that fast field-cycling NMR is not restricted to frequency dependent relaxation studies, as often believed. Although the four new kinds of applications illustrated are typical for the basic procedures, it should be pointed out that the method has already been applied in other directions, and so resulted in new growing fields of research in the recent NMR literature. Readers may encounter various headlines intimately related to FC techniques, which however is not always clearly seen or described, for instance: zero-field NMR,[5,7,8], cross-relaxation spectroscopy,[4,5,7] nuclear quadrupole double-resonance (NQDR)[3,5,12] and NMR imaging in low fields.[7,72] In all these topics field switches are essential to observe, or to significantly facilitate, the analysis of special spin dynamics and material parameters, which are not, or not easily, accessible without the FC method.

One major problem of FC derives from the circumstance that commercial instruments are not (yet) available, so that to exploit its full flexibility and power, the few laboratories involved could spend almost all their time in the construction of alternatives and extensions for new promising topics. To the experience of the authors major changes, such as the development of apparatus for performing experiments with deuterons or other nuclei in the solid state, required so much time that any use of the existing capabilities was unduly neglected. However, with the increasing number of laboratories working in the field this situation will probably greatly improve in the (near) future, and hopefully many current problems will be addressed.

After finishing this review, Job *et al.* announced the development of a

computer-based fast field-cycling spectrometer operating at magnetic fields up to 2T.[73]

ACKNOWLEDGEMENTS

The authors thank the Deutsche Forschungsgemeinschaft for the financial support over many years and gratefully acknowledge the contributions of the numerous students involved in both the technical and theoretical developments.

REFERENCES

1. R. V. Pound, *Phys. Rev.*, 1951, **81**, 156.
2. A. G. Redfield, W. Fite and H. E. Bleich, *Rev. Sci. Instr.*, 1968, **39**, 710.
3. D. T. Edmonds, *Phys. Rep.*, 1977, **29**, 233.
4. R. Kimmich, *Bull. Magn. Res.*, 1980, **1**, 195 (and refs therein).
5. F. Noack, *Progr. Nucl. Magn. Res. Spectrosc.*, 1986, **18**, 171 (and refs therein).
6. S. H. Koenig and R. D. Brown, *Progr. Nucl. Magn. Res. Spectrosc.*, 1990, **22**, 487 (and refs therein).
7. F. Noack in *Encyclopedia of Nuclear Magnetic Resonance* (eds D. M. Grant and R. K. Harris), p. 1980. Wiley, London, 1996.
8. D. B. Zax, A. Bielecki, K. W. Zilm, A. Pines and D. P. Weitekamp, *J. Chem. Phys.*, 1985, **83**, 4877.
9. G. Schauer, W. Nusser, M. Blanz and R. Kimmich, *J. Phys. E.*, 1987, **20**, 43.
10. K. H. Schweikert, R. Krieg and F. Noack, *J. Magn. Res.*, 1988, **78**, 77.
11. M. Blanz, T. J. Rayner and J. A. S. Smith, *Meas. Sci. Technol.*, 1993, **4**, 48.
12. M. Notter, K. Konzelmann, G. Majer and A. Seeger, *Z. Naturforsch.*, 1994, **49a**, 47.
13. *Product Selection Guide* (ed. Harris Semiconductor Literature Dept.), Harris Corp., Melbourne, USA, 1992.
14. *The Molecular Dynamics of Liquid Crystals* (eds G. R. Luckhurst and C. A. Veracini). Kluwer, Dordrecht, 1994.
15. R. Y. Dong, *Nuclear Magnetic Resonance of Liquid Crystals*. Springer, Heidelberg, 1994.
16. P. Pincus, *Solid State Commun.*, 1969, **7**, 415.
17. R. Blinc, D. L. Hogenboom, D. E. O'Reilly and E. M. Perterson, *Phys. Rev. Lett.*, 1969, **23**, 969.
18. R. Blinc, M. Luzar, M. Vilfan and M. Burgar, *J. Chem. Phys.*, 1975, **63**, 3445.
19. J. A. Marqusee, M. Warner and K. A. Dill, *J. Chem. Phys.*, 1984, **81**, 6404.
20. A. Abragam, *The Principles of Nuclear Magnetism*, Clarendon Press, Oxford, 1962.
21. J. McConnell, *The Theory of Nuclear Magnetic Relaxation in Liquids*. Cambridge University Press, Cambridge, 1987.
22. W. Wölfel, F. Noack and M. Stohrer, *Z. Naturforsch.*, 1975, **30a**, 437.
23. F. Noack, M. Notter and W. Weiß, *Liq. Cryst.*, 1988, **3**, 907.
24. P. L. Nordio, G. Rigatti and U. Segre, *J. Chem. Phys.*, 1972, **56**, 2117.
25. R. R. Vold and R. L. Vold, *J. Chem. Phys.*, 1988, **88**, 1443.
26. C. F. Polnaszek and J. H. Freed, *J. Phys. Chem.*, 1975, **79**, 2283.
27. H. C. Torrey, *Phys. Rev.*, 1953, **92**, 962.
28. S. Žumer and M. Vilfan, *Phys. Rev. A*, 1978, **17**, 424.
29. M. Vilfan and S. Žumer, *Phys. Rev. A*, 1980, **21**, 672.
30. C. Morrison and M. Bloom, *J. Magn. Res. A*, 1993, **103**, 1.

31. J. Struppe and F. Noack, *Liq. Cryst.*, 1996, **33**, 595.
32. J. Struppe. Thesis. Universität Stuttgart, 1996.
33. R. Köllner, K. H. Schweikert and F. Noack, *Liq. Cryst.*, 1993, **13**, 483.
34. J. H. Freed, *J. Chem. Phys.*, 1977, **66**, 4183.
35. M. Goldman, *Spin Temperature and Nuclear Magnetic Resonance in Solids*. Clarendon Press, Oxford, 1970.
36. E. Fukushima and S. B. W. Roeder, *Experimental Pulse NMR, A Nuts and Bolts Approach*. Addison-Wesley, Reading, 1981.
37. A. M. Thayer, M. Luzar and A. Pines, *J. Phy. Chem.*, 1987, **91**, 2194.
38. R. R. Vold and R. L. Vold, *J. Chem. Phys.*, 1988, **88**, 4655 (and refs therein).
39. J. Jeener, A. Vlassenbroek and P. Broekaert, *J. Chem. Phys.*, 1995, **103**, 1309.
40. G. Vertogen and W. H. de Jeu, *Thermodynamic Liquid Crystals, Fundamentals*. Springer, Heidelberg, 1988.
41. H. Gotzig, S. Grunenberg-Hassanein and F. Noack, *Z. Naturforsch.*, 1994, **49a**, 1179 (and refs therein).
42. H. Gotzig. Thesis. Universität Stuttgart, 1995.
43. A. F. Martins, P. Esnault and V. Volino, *Phys. Rev. Lett.*, 1986, **57**, 1745.
44. N. Schwenk and H. W. Spiess, *J. Phys. II France*, 1993, **3**, 865.
45. J. P. Casquilho, P. Esnault and F. Volino, *Mol. Cryst. Liq. Cryst.*, 1990, **180B**, 2632.
46. G. E. Pake, *J. Chem. Phys.*, 1948, **16**, 327.
47. H. Schmiedel, B. Hillner, S. Grande, A. Lösche and S. Limmer, *J. Magn. Res.*, 1980, **40**, 369.
48. A. Frieser, H. Schmiedel, B. Hillner and A. Lösche, *Mol. Cryst. Liq. Cryst.*, 1984, **109**, 245.
49. J. P. Casquilho. Thesis. Universidade de Lisboa, 1989.
50. P. G. de Gennes, *The Physics of Liquid Crystals*, Clarendon Press, Oxford, 1975.
51. A. G. Chmielewski, *Mol. Cryst. Liq. Cryst.*, 1986, **132**, 339.
52. H. Kneppe, F. Schneider and N. K. Sharma, *J. Chem. Phys.*, 1982, **77**, 3203.
53. P. Chattopadhyay and S. K. Roy, *Mol. Cryst. Liq. Cryst.*, 1993, **237**, 1.
54. G. Marrucci, *Mol. Cryst. Liq. Cryst.*, 1982, **72**, 153.
55. D. Baalss and S. Hess, *Z. Naturforsch.*, 1988, **43a**, 662.
56. R. G. Larson and L. A. Archer, *Liq. Cryst.*, 1995, **19**, 883.
57. J. Jeener and P. Broekaert, *Phys. Rev.*, 1967, **157**, 232.
58. H. W. Spiess, *J. Chem. Phys.*, 1980, **72**, 6755.
59. R. Kemp-Harper and St. Wimperis, *J. Magn. Res. B*, 1993, **102**, 326.
60. St. Becker. Thesis, Universität Stuttgart, 1996.
61. I. Zupančič, V. Žagar, M. Rožmarin, I. Levstik, F. Kogovšek and R. Blinc, *Solid State Commun.*, 1976, **18**, 1591.
62. V. Graf. Thesis. Universität Stuttgart, 1980.
63. J. Kärger, H. Pfeifer and W. Heink, *Adv. Magn. Res.*, 1988, **12**, 1.
64. F. Noack, *Mol. Cryst. Liq. Cryst.*, 1984, **113**, 247.
65. G. Rollmann. Thesis. Universität Stuttgart, 1984.
66. J. Mager. Thesis. Universität Stuttgart, 1993.
67. I. Chang, F. Fujara, B. Geil, G. Hinze, H. Sillescu and A. Tölle, *J. Non-Cryst. Sol.*, 1994, **172**, 674.
68. G. J. Krüger, *Phys. Rep.*, 1982, **82**, 229.
69. F. Noack in *Handbook of Liquid Crystals* (eds D. Demus, J. W. Goodby, G. W. Gray and H. W. Spiess). VCH-Verlag, Weinheim, 1996 (in press).
70. K. S. Chu and D. S. Moroi, *J. Phys. Colloq.*, 1975, **36**, C1-99.
71. S. Hess, D. Frenkel and M. Allen, *Mol. Phys.*, 1991, **74**, 765.
72. S. D. Swanson and S. D. Kennedy, *J. Magn. Res., A*, 1993, **102**, 375.
73. C. Job, J. Zajicek and M. F. Brown, *Rev. Sci. Instrum.*, 1996, **67**, 2113.

Progress in High-resolution NMR in Solids

CHAOHUI YE, SHANGWU DING AND JINYUAN ZHOU

Laboratory of Magnetic Resonance and Atomic and Molecular Physics, Wuhan Institute of Physics, The Chinese Academy of Sciences, PO Box 71010, Wuhan 430071, China

1. INTRODUCTION

The last two decades have witnessed a large number of important advancements in solid-state NMR spectroscopy. The intimate interaction and mutual promotion between theory and experiment continually broaden and deepen this field of research. Among the most important areas

ANNUAL REPORTS ON NMR SPECTROSCOPY
VOLUME 33 ISBN 0-12-505333-9

of progress are the combination of magic-angle spinning[1-3] and cross-polarization[4-7] (CPMAS) and high-power heteronuclear decoupling,[8,9] the multi-pulse (MP)[10-12] technique and its incorporation with magic-angle spinning to remove interactions (e.g., CRAMPS[13]) or to recover couplings (e.g., SEDOR,[14,15] REDOR[16]), time-domain multi-quantum coherence (MQC)[17-21] spectroscopy, zero-field NMR,[22,23] high-resolution quadrupole NMR,[24-26] low-temperature NMR,[27,28] optical detection,[29,30] dynamic nuclear polarization,[31,32] and their multi-dimensional versions.[33,34] These have enriched enormously the theoretical aspects of magnetic resonance spectroscopy, and provide new vistas on future research activities by providing better tools for material studies. With the continuing refinement of spectrometer technologies and of theoretical descriptions, solid-state NMR will undoubtedly undergo further developments.

As with spectroscopy techniques, the most important problem in solid-state NMR has been, and still is, how to obtain the highest possible sensitivity and best resolution. In NMR, these goals are achieved mainly by raising the applied magnetic field, by suppressing internal interactions and by using multidimensional techniques. In addition to the technological factors, e.g., state-of-the-art electronics, computer soft/hardware, every step in the progress of solid-state NMR rests on the better understanding of the properties of the interactions involving nuclear spin systems in solids. While solid-state NMR shares very much with its liquid counterpart, it differs from the latter in many aspects which will be emphasized in this review. Generally, a nuclear spin system in solids shows more complexity than in liquids because of the following reasons. First, the interaction Hamiltonians are complicated because almost all types of interactions are present simultaneously and in many cases none of them is negligible. For certain interactions, higher-order terms should be taken into consideration. Second, all interactions are anisotropic, which produces broad spectra for powder samples on the one hand, and brings about anisotropic dynamic effects such as spin relaxation and diffusion on the other. Third, the Hamiltonian may become insoluble, e.g., for a system with strong homonuclear dipolar interactions which renders the spins into an infinite network. Fourth, for samples under rotation and/or multi-pulse irradiations, the Hamiltonian becomes time dependent and approximations should be invoked on a case-by-case basis. Fifth, the motion of nuclear spins in a solid, or the fluctuation of interactions, occurs in a broad range with correlation times varying from 10^{-12} to 10^{2} s. The richness and complexity of solid-state NMR are further increased by the variations of external parameters such as the static magnetic field, radio-frequency (r.f.) irradiation field power, spinning rate, spinning axis direction, temperature, pressure, etc. It is because of these characteristics of solid-state NMR that new effects and phenomena are continually discovered which give rise to new developments both in theory and in experiment. Conversely, these unique characteristics supply inexhaustible flexibility and selectivity in the extraction

of structural and dynamical information in solids, allowing solid-state NMR to play a more and more important role in the investigation of solid-state materials.

A large number of review papers on solid-state NMR have appeared. The progress in this field of research is summarized and reviewed promptly, on a regular basis, in *Annual Reports of NMR Spectroscopy*, *Advances in Magnetic Resonance and Optic Resonance*, *Progress in NMR spectroscopy*, and *NMR: Basic Principles and Progress*. In this Chapter, we present a systematic summary of the progress in solid-state NMR over the last two decades, with emphasis placed on the latest advancements of theory and methodology in recent years. We attempt to provide a different perspective on this prosperous and rapidly growing field, which is generally indicated by the layout of the text and the organization of the contents. The description of the applications is therefore far from complete. For the same reason, imaging is not included in this Chapter, instead the interested readers are referred to some recent excellent reviews.[35–38]

The review begins from Section 2, where a general account of the internal interactions important to solid-state NMR is given, with a brief summary of the theories describing these interactions. General aspects of polarization transfer and irreversible processes are discussed in Section 3 where cross-polarization and spin diffusion in solids are emphasized. Section 4 reviews the suppression of the interactions by sample rotation and/or r.f. pulse irradiation, followed by Section 5 which discusses the recovery and evaluation of the interactions which are averaged by magic-angle spinning or multi-pulse sequences. Multi-quantum coherence in solids is covered in Section 6 with emphasis placed on spin-1/2 systems. The last part, Section 7, deals with zero-field NMR.

2. INTERACTIONS

2.1. General properties

Because the temperature of a realistic nuclear spin system is not at zero degrees absolute, the internal interaction Hamiltonians always contain two parts: one is stationary or coherent, the other fluctuating or incoherent, or random. The former part usually determines the positions of the peaks in a spectrum, the latter part governs the dynamics of the system. However, they may become entangled under certain conditions. For spin-1/2 systems, r.f. interactions can be made larger than the internal interactions in most cases, thus the manipulation of the interactions with r.f. pulses is realizable. This is an advantage of NMR over many other spectroscopies. In fact, most experimental methods in NMR spectroscopy correspond to certain manipulations of the internal interactions. For quadrupolar spin systems, the internal

interaction can exceed r.f. interactions and its manipulation is more complicated than in spin-1/2 systems.

Because NMR deals with radio frequencies where the spontaneous radiation is rather weak, the interaction Hamiltonians can be written in semiclassical form, i.e., the r.f. field can be described by classical quantities such as magnetic field, B_1. In solid-state NMR, the most important interactions are chemical shift, dipolar, and electric quadrupolar interactions.[14,33,39,40] Dipolar interactions can also be divided into direct and indirect parts according to their origins, or into heteronuclear and homonuclear interactions according to the species of the coupling nuclei. The Hamiltonians corresponding to these internal interactions can be expanded in terms of the tensor product of two rank-2 irreducible tensors.[39,40] One tensor is related to the spin angular momentum operators and the other to the spatial positions or orientations which bear the geometric and electronic information. An internal interaction Hamiltonian can itself be regarded as a scalar but the presence of a strong static magnetic field which specifies a privileged direction renders more important the terms that are exchangeable with the Zeeman interaction than the others. The dominant terms of the tensorial form are anisotropic and in general produce broad spectra. However, the scalar feature can be restored even in high magnetic field[23] (see Section 7). Because the interaction Hamiltonian in high magnetic fields consists of the products of two elements of rank-2 tensors, the manipulation of the interaction Hamiltonians falls naturally into two categories: manipulating the geometric element, e.g., by sample rotation, or manipulating the element relating to spin operators, e.g., by multi-pulse. In practice, both methods may be used simultaneously.

Although internal interaction Hamiltonians are generally rank-2 tensor, there is some simplified case for a specific interaction. For example, chemical shift interaction only includes linear terms of angular momentum operators; both chemical shift and quadrupole interactions only involve the spin operators at the same site, therefore, their exact analytical solutions can be obtained in certain cases[40] and can always be exactly solved numerically. For dipolar interactions, the Hamiltonian contains spin operators from different sites, so any processes related to energy transfer (coherence or polarization transfer) are mediated by them alone. Moreover, exact and analytical solutions for dipolar interactions are generally unattainable except for special cases such as isolated heteronuclear spin pairs.

2.2. Decomposition of Hamiltonians

For a practical spin system, the total Hamiltonian frequently must be decomposed and recombined in a way that the object of the problem is clear and straightforward. The decomposition is of course based on the physical processes involved in the problem.

2.2.1. From commutation relations

In high-field NMR, the Zeeman interaction with the static magnetic field is much stronger than internal interactions. Therefore, the total Hamiltonian is divided into terms commutable with the Zeeman term, i.e., the secular terms, and terms uncommutable with the Zeeman term, i.e., nonsecular terms. When the lineshape is calculated, usually only secular terms are important except for cases where the secular terms are negligible such as the central transitions of quadrupole spin systems with a strong internal electric field gradient (EFG). In dynamic investigations, however, nonsecular terms may play a more important role. The secular terms are always exchangeable with the total Hamiltonian for a static sample but for a rotating sample, they may become unexchangeable. For chemical shift, heteronuclear dipolar and quadrupolar interactions, this exchangeability is maintained and they are called inhomogeneous.[3] For homonuclear dipolar and indirect dipolar (J coupling) interactions, this exchangeability is lost and they are called homogeneous.[3] When both inhomogeneous and homogeneous interactions exist simultaneously, the summation is homogeneous. Note that here we are talking about secular terms because nonsecular terms cannot be exchanged with the total Hamiltonian. Homogeneous and inhomogeneous interactions differ greatly in many aspects ranging from lineshape to dynamics.

2.2.2. From spin species

When a system of interest contains more than one spin species, the total Hamiltonian is usually divided into the Hamiltonian of each spin species and the interaction Hamiltonians between them. This division relies on the fact that the Zeeman frequencies of different spin species are much larger than the internal interactions and each spin species forms a relatively independent subsystem.

2.2.3. From the objects of the research

As mentioned above, the total Hamiltonian of a spin system can be divided into coherent and random parts which describe lineshape and dynamics, respectively. This is the most fundamental classification. For a specific problem, a more detailed classification might be necessary, based on the goals of the research. For example, in the study of polarization transfer, the Hamiltonian of the entire system is frequently divided into that of several fictitious systems.

The classification *2.2.1* is mathematically natural and it is generally the first step in solving a concrete problem. The classifications *2.2.2* and *2.2.3* are more or less artificial but are closely dependent on the physical insight; they are frequently essential in rendering a seemingly complicated problem more amenable to solution.

2.3. Lineshape calculations

There are a number of formalisms available for calculating the lineshape of a Hamiltonian, each of which has its strong points and drawbacks. In solid-state NMR, few problems can be solved exactly, and approximations should be employed in many cases.

2.3.1. Exact and analytical

When only inhomogeneous interactions are involved and the dynamic effects are neglected, the Hamiltonian becomes exactly solvable and frequently in analytical forms. For example, the lineshapes of the chemical shift, heteronuclear dipolar and quadrupolar interactions can be calculated exactly and analytically, either for static or for rotating samples.[39,40]

2.3.2. Average Hamiltonian theory[3,12,39–42]

In a solid, all types of interactions coexist and the spectrum of a static sample with single-pulse excitation is generally broad and featureless. It is therefore necessary to suppress certain interactions while keeping other(s). However, to date, all methods proposed which suppress internal interactions also introduce time dependence of interactions and the evolution of the density operator involves a time-ordering operator which usually prevents the acquisition of analytical and exact solutions. For an analytical solution, some approximation should be employed. For a general time-dependent Hamiltonian, a Magnus expansion can be utilized. In solid-state NMR, the time-dependent Hamiltonian is usually periodical so the coherent averaging Hamiltonian theory can be used.[12,39] Different orders of average interactions can then be calculated with a time average over only one period. For inhomogeneous interactions, all orders rather than the 0th order of the coherent average Hamiltonian vanish so the Magnus expansion is always convergent. For homogeneous interactions, however, the convergence condition might be quite stringent, which requires that the phase accumulated by the interaction over a period be less than 360°. By means of average Hamiltonian theory, the lineshape calculation of a time-dependent system is reduced to that of a static system. The application of average Hamiltonian theory to lineshape calculations is well demonstrated with rotating homonuclear spin–pair systems with higher-order terms included.[43–52] It also plays an important role in the initiation and understanding of, for example, multi-pulse decoupling techniques. The problem with using this theory is that the detailed information within one period is lost because the averaging procedure is actually a "stroboscopic" observation of the evolving system with a time-step of one period.[3,39] Therefore, whenever the sidebands are involved, average Hamiltonian theory is insufficient. Other drawbacks of

average Hamiltonian theory are discussed by Goldman *et al.*[53] They propose the use of stationary perturbation theory when higher orders are considered or when the system is highly degenerate.

2.3.3. *Floquet theory*[54–66]

This method circumvents the difficulty of calculating a time-ordering operator while keeping its time dependence as a remedy to average Hamiltonian theory. In this theory, the time-ordering calculation is transformed into an infinite summation over Floquet states.[54,56,62,63] Proper approximations should be used in practice because of the infinite summation. Two different calculation approaches, which are equivalent physically, have been proposed. One diagonalizes an approximate Floquet matrix by using a transformation matrix[55–59,61,63,65,66] while the other calculates the eigenvalues and eigenstates by perturbation iterations.[62,64] In addition to application to lineshape calculations, the Floquet formalism has also been found to be powerful in the processing of a variety of problems ranging from calculation of spin exchange,[57,58] design of optimum excitation or mixing sequences,[59,67] and the calculation of field-dependent chemical shift,[68] among others.

2.3.4. *Projection operator formalism*[40,69–76]

In NMR, it is possible, although not common, to find the lineshape closely related to the detail of the spin relaxation. In those cases, the linewidth cannot be described simply by a transverse relaxation constant. In other words, nonequilibrium characteristics should be considered in the calculation of the lineshape. An example of this situation is the lineshape of an abundant spin system with strong homonuclear dipolar interactions. Exact calculation, even numerically, is usually formidable in practice because the relevant system would become infinitely large. In principle, the aforementioned methods can be applied if the whole system is brought into consideration. Borckmans and Walgraef[77,78] calculated the lineshape of CaF_2 using graph techniques;[79] however, the long-term features are not reproduced satisfactorily. Other methods involving extensive calculation of moments, up to the fourteenth, were also proposed.[80–83] The moment method can give satisfactory lineshapes but it is tiresome in calculation. Moreover, the moment expansion may be divergent. A framework for calculating NMR lineshape based on Mori's memory function approach and the projection operator technique has been established.[72–74] In this formalism, the calculation of the lineshape is eventually reduced to the assumption of a memory function. This substantially simplifies the calculation while reproducing the lineshape on different time scales. The other strong point of this formalism is that both lineshape and relaxation are treated simultaneously. A recent intriguing phenomenon observed in strongly coupled proton systems, in which high-

resolution proton spectra can be observed simply by single pulse excitation and delayed acquisition, may be explained by numerical simulation based on the memory function approach.[84–86] Goldman cautions that, when using Mori's formalism, care should be exercised in the selection of the relevant operators,[87] although this is not a difficulty when the goal of the problem is clear.

2.3.5. Wei–Norman approach

A new approach to calculating the lineshape of spin systems has been proposed which invokes Wei–Norman Lie algebra.[88,89] A Hamiltonian is decomposed in terms of the generators of a Lie algebra and the evolution of the generators is then calculated. This method is useful when the time dependence of the Hamiltonian is not cyclic.[90–93] Analytical solutions can be obtained in certain cases.

2.3.6 Numerical

Whenever it is difficult to obtain an analytical solution or in cases where the analytical solution is unnecessary, for a practical problem in finite Liouville space, the exact evolution of a density operator can always be obtained numerically. This can be achieved either by direct computation of the time-ordering evolution operator, or by iteration of the Liouville equation. A general physical picture or universal conclusions cannot be drawn from the numerical technique alone, but it is helpful for providing a better understanding of a complicated problem and indicates the direction for general conclusions. Moreover, even for a problem where the analytical solution is available, numerical calculation helps to provide a visual account.

For a powder sample, the average over the three Euler angles can usually be obtained only by numerical procedures. The lineshapes of some typical interactions, both in static and rotating samples, are shown in Fig. 1 and Fig. 2, respectively.

3. POLARIZATION TRANSFER AND IRREVERSIBLE PROCESSES

Before proceeding further with this section, we will emphasize some important points closely associated with the dynamic processes encountered in solid-state NMR. In the most general sense, relaxation, spin diffusion/exchange and polarization transfer can be regarded as different aspects of coherence transfer. They all involve mutual transformation among

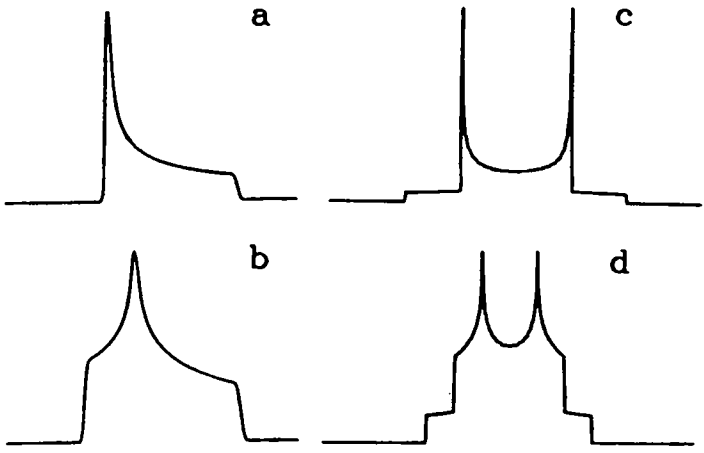

Fig. 1. The single quantum static lineshapes of several typical internal (first-order) interactions in solid-state NMR. (a) Symmetric chemical shift interaction; (b) asymmetric chemical shift interaction ($\eta_{CS} = 0.75$); (c) symmetric quadrupolar interaction and (d) asymmetric chemical shift interaction ($\eta_Q = 0.5$). The dipolar interaction (for a spin pair) has the same lineshape as (c).

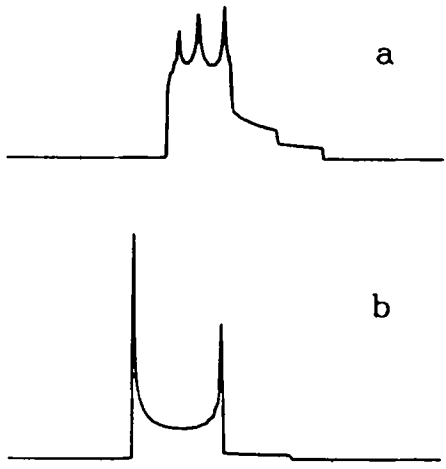

Fig. 2. The second-order central transition (1/2 – – 1/2) spectra of the (a) asymmetric ($\eta_Q = 1.0$) and (b) symmetric quadrupolar interaction of a half-integer quadrupole spin system.

the density matrix elements. The distinction between coherent and incoherent is only technically meaningful in given temporal and spatial scales. When a reduced density matrix is used, incoherent terms arise and irreversible processes emerge. However, in practice, distinction between these two types of process is necessary before the problem can be solved.

For example, the system might become too large and there would be too many interactions to deal with effectively. How to define a system is somewhat artificial and arbitrary, but in most cases, it is clear enough from physical considerations how to choose a system and its environment. Because the modern NMR technique can deal with interactions almost at will, time intervals as short as a few microseconds and spatial ranges as small as the typical distance between two atoms in a molecule can be "resolved" by NMR spectroscopy. The local and instant processes can easily be observed. A process which is irreversible and incoherent on a large temporal and spatial scale may behave reversibly and coherently if the observation is undertaken during a short time period. During this time, the system is well isolated from its environment and can be treated according to coherent NMR methods. More and more examples have recently emerged, from cross-polarization (CP) to spin diffusion (SD) which will be reviewed below. However, the final result is always approaching equilibrium and the process is irreversible as a whole.

3.1. Polarization transfer

In liquid-state NMR, coherence transfer is the most important topic because of the following important facts: (1) All anisotropic interactions are removed by random and fast molecular tumbling. Only the isotropic chemical shift and J coupling survive; the spectral lines are sharp. (2) Relaxation times (T_1, T_2, T_{SI}, etc.) are long in liquids, thus many r.f. pulse manipulations can be carried out before a coherence dies out. (1) and (2) make it possible for a coherence to be refocused. In liquids, the coherence transfer is usually carried out by timing pulses in terms of coupling constants such as in DEPT, INEPT, INADAQUATE.[33] In solids, the coexistence of multi-interactions and their anisotropies make these impossible in most cases unless special techniques are employed. Refocusing can be realized only in special situations. At short time regimes, with weak interactions, and small anisotropy systems, solid-state NMR can be regarded approximately as solution NMR. Coherence transfer techniques can be translated from solution NMR to solid NMR, such as COSY[94–98] and INADAQUATE.[99,100] Generally, this is not the case. A large number of works have been devoted to the establishment and transfer of coherence transfer in solids, including those elaborated in Sections 5 and 6. The central point is how to remove anisotropies while keeping certain dipolar interactions which are used to mediate coherence transfer processes. Longitudinal coherence transfer, i.e., polarization transfer, which involves Zeeman energy exchange, is more easily realized in solids with high resolution intact. Two important polarization transfers can be carried out: CP and SD, which are reviewed below. They are basically the same, except that they occur in different reference frames. CP corresponds to Zeeman

energy exchange in a tilted double-rotating frame while SD involves Zeeman energy exchange in a laboratory frame.

3.1.1. Cross-polarization

This technique, invented by Hartman and Hahn (HH),[5] has been widely used for the sensitivity enhancement of rare nuclei. By applying it to dipolar coupled spins with two equal-amplitude r.f. fields that are much larger than local interactions, the resonance condition (HH matching) can be satisfied and the prepared polarization of the abundant nuclei can be transferred to the rare ones, thus increasing the sensitivity of the latter. This method became powerful for dilute spin systems after it was revised to incorporate direct detection and MAS by Pines *et al.*[6,7] so that the resolution is greatly improved. Further improvement was made by means of high-power heteronuclear decoupling.[8,9] Much attention has been paid to the calculation of cross-relaxation times. Based on spin temperature theory, Hartman and Hahn *et al.*[5,101–103] and Lang and Moran[104] gave a systematic description of the evolution of magnetization in this double-resonance experiment. Expressions of cross-relaxation time have been obtained.[5,75,102,103] Although, as pointed out by Stokes and Allion,[105] the memory effect in the cross-relaxation does not play an essential role and the simple exponential decay derived by McArthur *et al.*[103] proves sufficient. A more exact treatment based on projection operator formalism and memory function approach has been given by Demco *et al.*[75] Both the long- and short-term behaviours of the cross-relaxation were investigated.[40,75] Chueng and Yaris[106] considered the situations when the molecular motion is implicitly included. The possible effect of the nonsecular terms of heteronuclear dipolar interaction on cross-relaxation has been discussed by Ding and Ye.[107] CP is mediated by dipolar coupling which decays rapidly with the distance between the coupling partners; therefore, the cross-polarization process is quite localized,[108] especially at the first stage, as shown by Wu and coworkers[109–116] who demonstrated that there are usually two stages in a CP process. A direct result of this locality is the lack of quantitativeness of a CP spectrum. Polarization–depolarization[115–118] and the multicontact method[119,120] were proposed to overcome this problem. However, as shown by Wu and Zilm[109,121–124] and Sangill *et al.*,[125] this phenomenon, incorporated with long contact, short contact and phase-inversion, can be used to develop a spectral editing technique. An example of ^{13}C spectral editing based on CP dynamics and thermodynamics is shown in Fig. 3. The locality of the CP process brings a more theoretically interesting problem: i.e., the discrepancy between the thermodynamic description (more or less based on a spin temperature assumption) and the quantum mechanical description (based on the Liouville equation). This was conspicuously revealed by numerous authors.[126–135] A universal bound shown by Sørensen says that the CP efficiency given by a

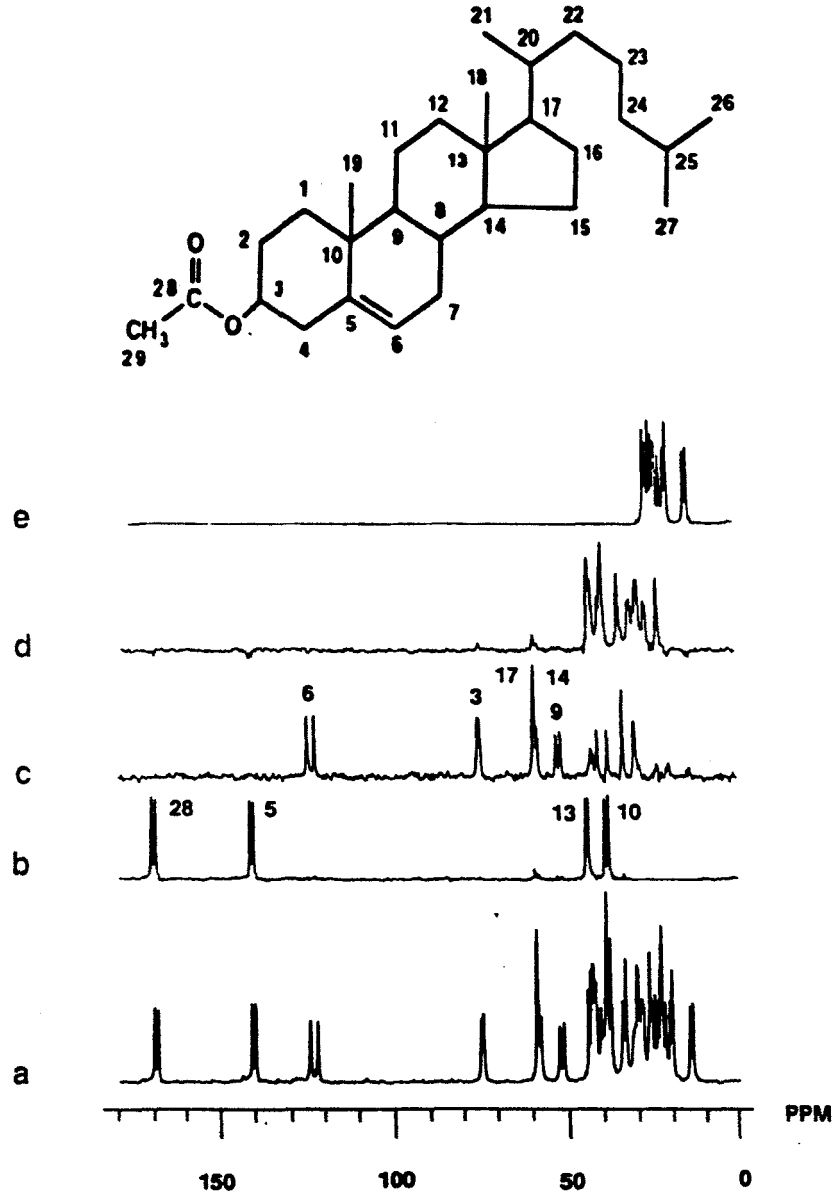

Fig. 3. The CPMAS spectrum and four subspectra of cholesteryl acetate. (a) Standard CPMAS; (b) nonprotonated ^{13}C-dominated subspectrum; (c) ^{13}CH subspectrum; (d) $^{13}CH_2$ subspectrum; (e) $^{13}CH_3$-dominated subspectrum. The numbers indicated in the spectra represent the assignment of the resonance. (Reproduced from Wu *et al.*[124] with permission.)

quantum mechanical description is unanimously less than that by a thermodynamic description.[126,127,130] For example, when one rare spin is coupled to an infinite number of abundant spins, strikingly, the CP efficiency is only about 0.8,[126] in contrast to the thermodynamic value of 1.[5,40] As shown in Fig. 4, for CP in $I_M S_N$, only when both M and N are infinite can the thermodynamic value of transfer efficiency be reached.

The CP dynamics at mismatching have been investigated by several authors.[111–115,136–138] For a static sample, mismatching can be compensated by synchronous phase reversal of locking fields (MOIST[136,137] or its variant W-MOIST[138]). As a result of mechanical improvements, sample spinning speed has been increasing. High-speed MAS is useful for better resolution but causes the HH matching condition to become unstable. As shown by Stejskal *et al.*[139] and Maciel and coworkers,[140–142] when the spinning speed is greater than the static proton line width, the broad HH condition is split into five narrow matching bands. The higher the spinning speed, the narrower the matching bands, resulting in fragile matching. A series of new dynamic and thermodynamic characteristics has emerged.[143–146] Many authors have proposed a variety of methods to restore efficient CP under high-speed MAS conditions. However, the solution to this problem corresponds to the reintroduction of the heteronuclear dipolar interaction between abundant and dilute nuclei at high-speed MAS. Because CP is undertaken in a tilted double-rotating frame, most of the recoupling schemes introduced in Section 5 cannot be directly applied to this case. A number of techniques have been proposed, including phase inversion in one and both channels,[121–123,136–138,147] amplitude modulation without[148–155] and with[156,157] rotor synchronization, frequency sweeping[158] and multi-pulse contact.[159] Mechanical solutions have also been suggested, such as making contact at off-magic angle by switching the angle sample spinning (SASS[142]), stopping[140] or slowing[160] the sample spinning during contact.

CP between spin-1/2 and quadrupole spin systems has been investigated in recent years. Most studies focus on CP between the spin-1/2 (mostly protons) and the central transition of half-integer quadrupole nuclei including ^{27}Al,[161–169] ^{11}B,[170] ^{43}Ca,[171] ^{17}O,[172,173] ^{23}Na,[169,172–178] and ^{95}Mo.[179] A few publications have been devoted to CP between proton and ^{14}N,[180] ^{2}H.[181] Sensitivity enhancement is not the major purpose in these quadrupole systems because they can be considered abundant. Instead, the selection characteristic of CP due to its locality is mostly used to estimate the distance between the spin-1/2 and the quadrupole nuclei at different sites.[167] The presence of the strong quadrupole interaction causes evident spectral distortion. Vega[175,176] introduced a parameter to characterize this distortion. The theoretical simulation of CPMAS lineshapes involving half-integer quadrupole spins has been given by Ding and McDowell.[169] One example of this calculation is shown in Fig. 5.

CP with three spin species has been explored by Schaefer *et al.*[182] CP

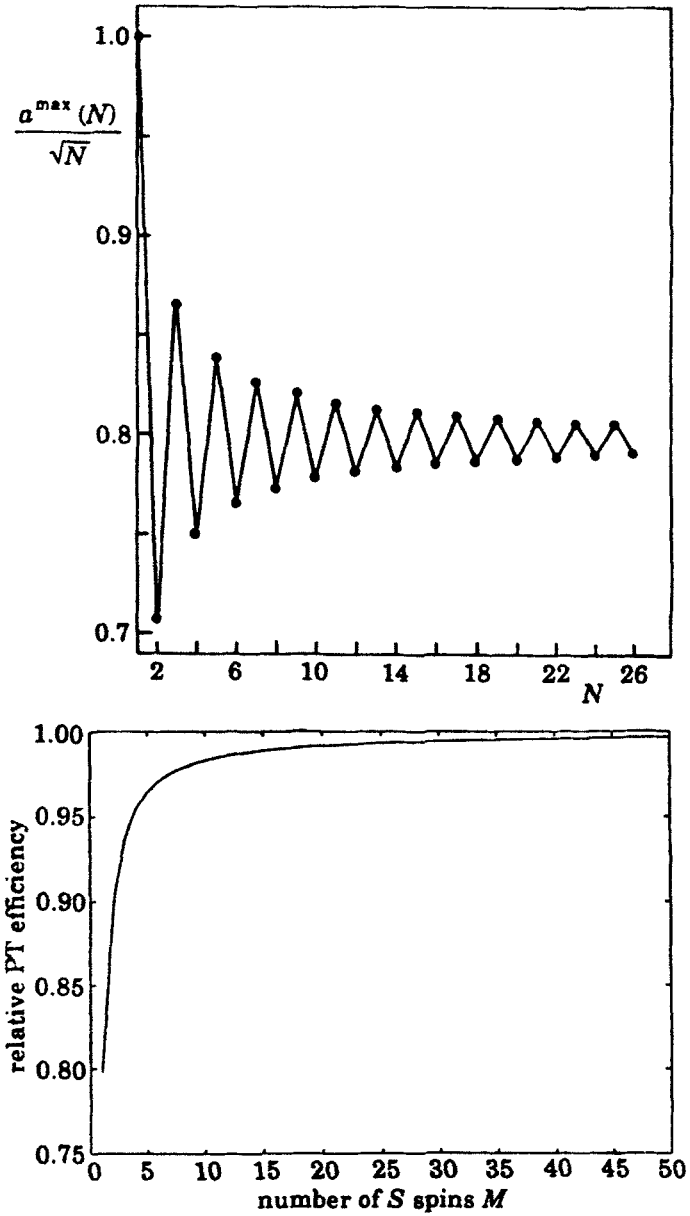

Fig. 4. Illustrations of the maximum possible transfer efficiency relative to the efficiency predicted by entropy bound, $a^{max}(N)/\sqrt{N}$, for the polarization transfer from I-spins to S-spins in $I_N S$ systems (top, adapted from Sørensen[126] with permission) and $I_N S_M$ systems (bottom, adapted from Levitt[129] with permission).

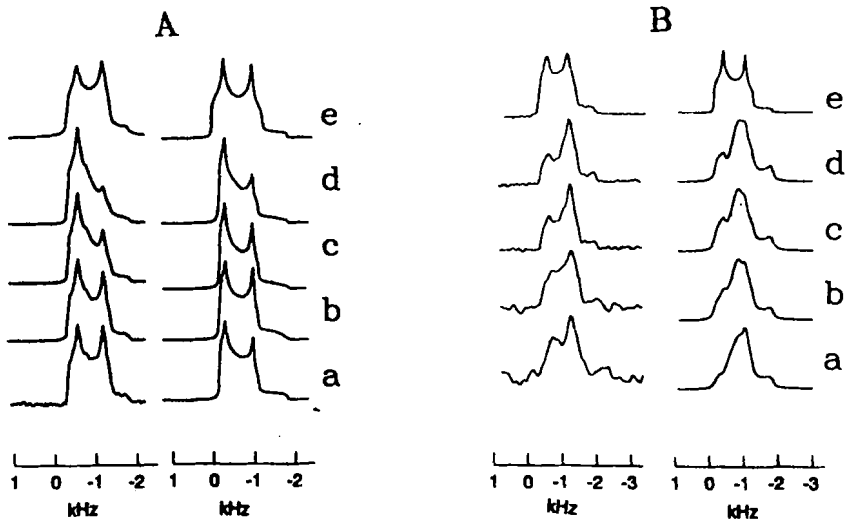

Fig. 5. The theoretical (right) and experimental (left) $^{1}H \rightarrow {}^{23}Na$ CPMAS spectra of $NaH_2PO_4.H_2O$ with $\omega_{1I} = 60.0$ kHz, $\omega_r = 3.5$ kHz for different matching conditions (A) $\omega_{1S} = 31.0$ kHz, (B) $\omega_{1S} = 58.0$ kHz with different contact times (all less than one spinning period) (a) $t_{cp} = 10\ \mu s$; (b) $t_{cp} = 20\ \mu s$; (c) $t_{cp} = 90\ \mu s$; (d) $t_{cp} = 160\ \mu s$; (e) single pulse spectra (from Ding and McDowell[169] with permission).

involving free radicals, i.e., dynamic nuclear polarization, has been studied by several groups.[31,32,183–185]

3.1.2. Spin diffusion (SD)

This is a polarization transfer process among homonuclear spin systems in a laboratory frame mediated by motion or dipolar interactions. When the motion is the driving force, SD is also called spin exchange.[186] When SD is driven by dipolar coupling, SD has fundamentally the same mechanism as CP. This can be found from the calculation of the spin diffusion rate,[146,187,188] where a projection operator is used in the same way as in the calculation of the cross-relaxation rate. SD has customarily two types: spatial SD and spectral SD, the former occurs in unresolved spin systems while the latter in spectrally resolved spin systems. The spatial SD was studied largely before 1980 after SD was introduced by Bloembergen.[189] There are numerous publications on this topic, both theoretical treatments[81,189–192] and its applications.[193–198] Detailed discussion on spatial SD, based on coherence state theory, has been exploited by Sodickson and Waugh.[199] However, quantification of the information from SD is much better with the spectral SD. The emergence and prosperity of spectral SD depend on high-resolution solid-state NMR,[4–9] with the selection excitation[200–202] and exchange[203,204] spectroscopic techniques. The SD process

is energy-conserving which is easily met in spatial SD, but is the central problem in spectral SD where the diffusion partners have different resonance frequencies. In extreme cases, the diffusion partners exchange their spatial positions and the diffusion is automatically accomplished and no particular energy-compensating schemes are needed. When the diffusion partners are coupled with an abundant spin system (bath), e.g., protons, the energy difference can be borrowed from the bath. This depends on the sample spinning:[146,205] when the sample spins at low speed, the spin diffusion rate is not affected by the spinning; when the spinning speed is moderate, the spin diffusion can be enhanced by the spinning; when the spinning speed is so high that the proton dipolar interaction is significantly reduced, the spin diffusion is quenched by the spinning. When proton decoupling is needed, this method cannot be used. Several ways of compensating the energy difference have been proposed based on rotational resonance and multi-pulse selective excitation, and these have been excellently summarized elsewhere.[146] The former is straightforward and works the same way as in dipolar recoupling (Section 5.4). The latter involves the selection pulse sequences which should satisfy the following conditions: (1) highly selective; (2) the effective Hamiltonian depends less on the frequency difference between the selected nuclei; (3) the dipolar interaction is maximally reintroduced. Experimentally, SD can be studied with one- and two-dimensional (1D, 2D) spectroscopic methods. When the diffusion partners are large, a two-dimensional experiment is necessary.[33,206–209] During mixing, spin lattice relaxation also contributes to polarization transfer. The effect of spin relaxation can easily be removed by phase cycling[206] as shown in Fig. 6. This procedure is especially important for short T_1 systems such as quadrupole systems.[205] The most commonly investigated nucleus is ^{13}C.[146] Although other nuclei, including ^{19}F,[210] ^{15}N,[211–213] and ^{31}P,[214–219] have been studied, most reports focus on the proton-driven spectral SD. By means of multi-pulse decoupling during the evolution time, proton spectral SD has also been investigated.[220,221] There are a number of spectral SD studies involving quadrupolar nuclei on spin-1 systems, based mainly on the spin exchange of ^{2}H[222–234] systems, and two pieces of work on ^{14}N[187,188] with single crystal samples. The ^{2}H spectrum is broad and, under the MAS condition, special care should be exercised to avoid misleading effects caused by the spinning sidebands.[34,223] There appears to be only one publication dealing with the spectral SD of ^{23}Na[205] (spin-3/2) system. The main reasons for this are (1) the spectral overlapping or broadening, even for the central transition and (2) the short relaxation times in quadrupolar systems. The application of SD rests on the fact that the diffusion rate is related to the distance between the participating nuclei. Therefore, it can be used, for instance, to determine internuclear distances,[81,186,187,198,206,216–218,235] polymer structure,[186,198,207,235,236] heterogeneity[190,191,195–197,207] and phase transitions.[207] An example of spectral SD applied to the molecular sieve VPI-5

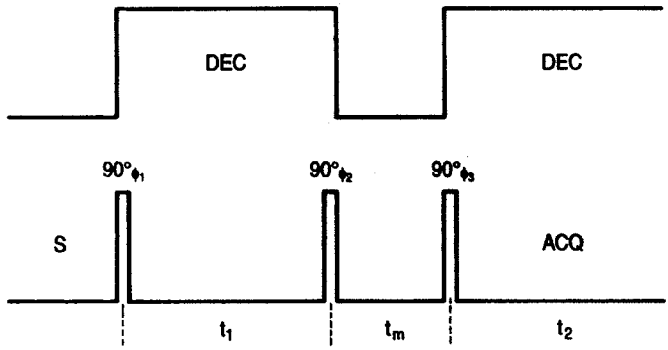

Fig. 6. The spin diffusion pulse sequence. The phase alterations are $\phi_1 = \phi_3 = X$, $\phi_2 = X, -X$ and $\phi_{REC} = -Y, Y$ in addition to the CYCLOPS. Phase cycling removes the instrumental errors and zero-frequency signals (e.g., owing to spin-lattice relaxation) in the first dimension.

is shown in Fig. 7 where the appearance of cross-peaks reflects the vicinity of the spin pairs. The effect of MAS on SD is also demonstrated, corresponding to the fast spinning case,[146,205] i.e., MAS reduces the diffusion rate.

The other important problem in polarization transfer in solid-state NMR is the determination of the equilibrium state. Because of the different magnitudes of various interactions, the system may reach a temporary equilibrium, or quasi-equilibrium, with a small environment whereas it finally reaches the equilibrium with the possible largest environment. For CP, a quasi-equilibrium is reached with both spin species having equal spin temperatures and then arrives at a final equilibrium with the lattice. The calculation of equilibrium needs no knowledge of the coupling between the system and the environment provided that the interaction is weak. The quasi-equilibrium state is determined by the conserved quantities defined by the system Hamiltonian. For example, relaxation in the laboratory frame can be regarded as the projection of an initial density operator onto the Zeeman Hamiltonian which defines the final equilibrium state. More demonstrations of this technique have been excellently shown by Ernst's group[136,138,188] and by Meier's review.[146] This technique can be generalized to more cases.

3.2. Irreversible processes

In the above subsection, and many parts of the following sections, a nuclear spin system is treated as a coherently evolving system where thermodynamically irreversible effects are neglected. In reality, the dynamical characteristics of a spin system are equally important to NMR spectroscopists. While the peak positions or lineshapes of an NMR spectrum reflect the geometric

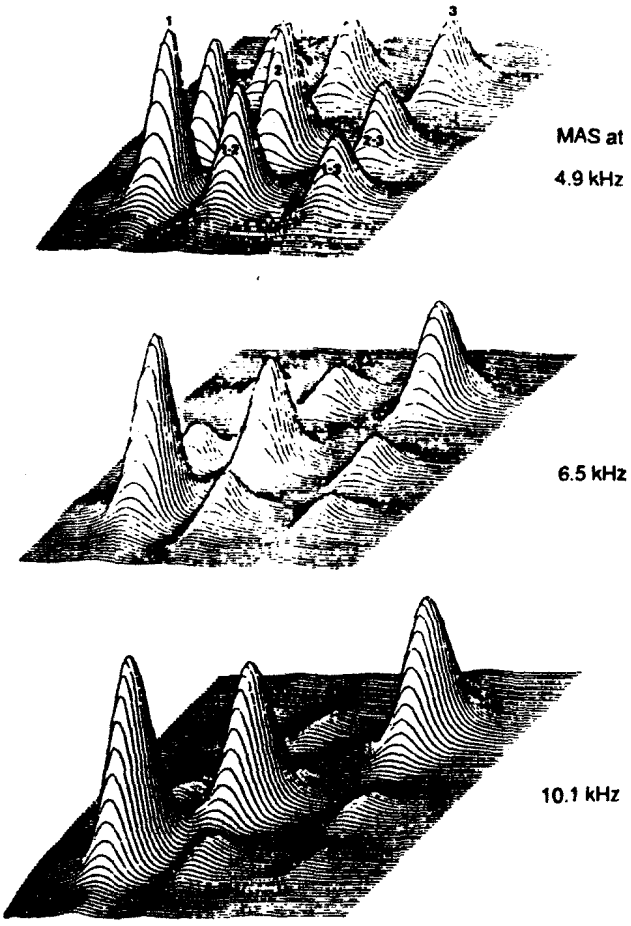

Fig. 7. Experimental 2D ^{31}P spin diffusion spectra of hydrated VPI-5 recorded with the mixing time of 3 s and MAS speeds of 4.9 kHz (top), 6.5 kHz (middle) and 10.1 kHz (bottom), respectively (used from Kolodziejski *et al.*[218] with permission).

and electronic structures of the system under investigation, the dynamical processes represent its internal motion. Generally speaking, a dynamic process corresponds to the problem of approaching equilibrium, including spin relaxation, spin diffusion, spin exchange, self-decoupling, etc. Microscopically, a nuclear spin system evolves according to the Liouville equation which is invariant under time reversal and describes the reversibility of the process. Conversely, the macroscopic relaxation, or diffusion, is described by irreversible equations that are variable under time reversal. The compromise between the microscopic and macroscopic descriptions of a nuclear spin system is intimately related to the general problem in nonequilibrium statistical mechanics, i.e., how to obtain, with certain reasonable

assumptions, an irreversible equation from the fundamentally reversible microscopic dynamical equation. Several formalisms have been proposed but all are based on the principle of the coarse graining technique. The projection operator formalism[40,69–73] is found to be the most successful formalism to translate coarse graining into a concise mathematical form. This formalism is especially suitable to NMR problems because a projection operator can be constructed usually by a small number of spin angular-momentum operators. It has another advantage that is very attractive to NMR spectroscopists, i.e., the calculation of lineshapes and dynamical processes is treated in a unified framework. In other words, the coherent and incoherent processes are treated in the same way but with different definitions of projection operators. For coherent situations, e.g., the lineshape calculation, the relevant Liouville space is the whole Liouville space defined by the coherent Hamiltonian. For incoherent processes, the irreversibility corresponds to a projection of the whole Liouville space (determined by the coherent and also the incoherent Hamiltonians) onto the relevant sub-Liouville space which, in many cases, is determined by the coherent part of the total Hamiltonian, or by the observables we are interested in. The projection is actually a procedure of coarse graining which brings about irreversibility, while the reduced density operator evolves into its equilibrium value. A universal differential–integral equation,[40,72] which can be used to explain lineshape and relaxation in a unified manner, can be derived provided that adequate approximations are taken based on physical considerations. This framework has an obvious strong advantage over Redfield's relaxation theory,[33,87,237] which is widely used in liquid-state NMR, in that the latter invokes second-order approximations and generally indicates an exponential process, while the projection operator formalism can cover more general situations, e.g., nonexponential relaxation. In practice, two extreme cases are distinguished depending upon the difference between the rates at which the spin system evolves and the environment "fluctuates": when the environment fluctuates much faster than the system decays, i.e., at the "weak collision limit", the environment and the system can be well separated. Conversely, if the environment fluctuates at a rate that is similar to the characteristic decay rate of the system, the environment should be included in the system.[238,239] It should be pointed out that weak collisions are more often encountered in dynamic processes in solids because of the weakness of the interactions involved.

The actual fluctuation spectrum in a solid sample is very complex with a broad distribution of correlation times. A number of widely used models for spectral density functions in solids[240–255] is summarized in Beckman's review paper,[256] where exponential correlation is assumed. However, it is possible that there is a nonexponential correlation case, as recently confirmed by Spiess' group with 3D and 4D methods.[257] The BPP model[240] which is the simplest, is mostly applied both in solid and solution NMR.

For a real spin system, the most important problem in the calculation and analysis of the relaxation is the mechanism of fluctuation. Generally, all interactions contribute to relaxation. For spin-1/2 systems, the chemical shift and dipolar interactions are comparable and both contribute to relaxation; the separation of the two contributions is generally difficult and therefore a more demanding problem is how to obtain the correct information of motion in a spin-1/2 system. Whereas for a quadrupolar system, the quadrupolar interaction is dominant and in most cases only this interaction should be considered in relaxation. The relaxation mechanism is relatively simple and so there have been more applications of quadrupole relaxation to the extraction of dynamical information in solids. ^{2}H is especially unique for this purpose because both dipolar and shielding interactions are weak. There are large quantities of work on this subject which have been reviewed in a recent paper by Hoatson and Vold.[258]

Other important examples of dynamic processes are polarization transfer rates such as cross-relaxation rate and spin diffusion rate which are discussed in the previous two subsections.

4. SUPPRESSION OF INTERACTIONS

Because the spin interactions in solids are generally anisotropic, the resulting spectra are broad and featureless for static solids. To obtain useful information, some interactions should be suppressed. Therefore, various types of techniques have been developed in solid-state NMR to average out internal interactions. As pointed out above, these methods fall into two categories: sample spinning and multi-pulse irradiation. The former manipulates the spatial part and involves rotation of the sample in real space, the latter acts in spin space. In principle, an $SO(3)$ rotation can average all orders of the internal interactions because irreducible tensors form a basis of the irreducible representations of the $SO(3)$ group. In liquids, an $SO(3)$ rotation may occur naturally. For solids, it is technically impossible to realize an $SO(3)$ rotation, but it is possible to implement a rotation corresponding to certain subgroup of $SO(3)$ and certain orders of interactions can be averaged out by the rotation. For example, sample spinning around a fixed axis at the magic angle can average the first-order terms of an internal interaction, proper combination of four $\pi/2$ pulses can average out the first-order terms of a homogeneous interaction. Detailed correspondence between the symmetry operation and the removal of an interaction is shown in Fig. 8.

4.1. Mechanical averaging in real space

When a sample rotates around an axis, the spatial part of the internal interactions becomes time-dependent. The time average of the interactions over a rotation period, associated with other techniques such as homo- and/or

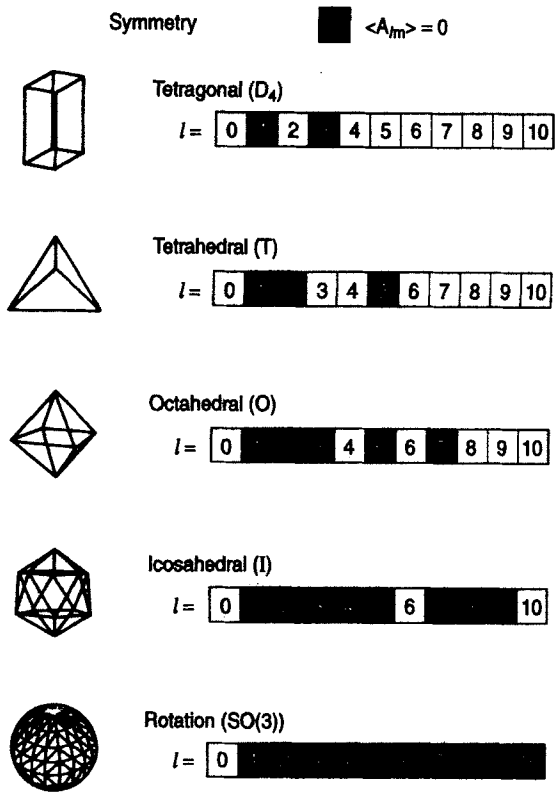

Fig. 8. Averaging of spherical harmonics under subgroups of $SO(3)$. The tinted numbers are the orders of harmonics which are averaged out by the corresponding manipulations (adapted, with permission, from Samoson *et al.*[259]).

hetero-nuclear decoupling if necessary, usually represents suppression of the interactions. Consequently, it can give the spectra of a specific spin species with higher resolution. To the accuracy of nth order, the anisotropic part of an internal interaction is expressed as the secular (except weight 0) components of tensors up to rank $2n$. When the sample undergoes a rotation in space, a factor $P_{2n}(\cos\theta)$ appears in that component, where θ is the angle between the rotation axis and the applied magnetic field. Consequently, there exist one or more special angles for each order of the internal interactions, which will be averaged out when the sample rotates at those angles. Therefore, if the higher orders of interactions, and also the first order need to be averaged out at the same time, a single-axis rotation is insufficient. Experimentally, it is now possible to obtain the sample rotation around two axes at the same time or at different periods of experimentation. However, it should be noted that rotation around a single axis at a time is still most commonly used.

4.1.1. Rotation around one axis (MAS, off-MAS)

First-order inhomogeneous interactions can be averaged out when the sample is spun at the magic angle. However, the complete removal of the anisotropy of the interactions can be realized only when the fast spinning condition is satisfied. When the spinning rate is slower than the anisotropy of the interaction, i.e., slow spinning condition,[3] each of the isotropic peaks is flanked by a series of sidebands. The fast spinning condition is readily met for dipolar interactions among most nuclei, which are in most cases less than 2 kHz (for heteronuclear) or 5 kHz (for homonuclear), but it is generally not met for dipolar interactions involving protons and fluorine nuclei whose gyromagnetic ratios are large. Therefore, when protons or fluorine nuclei are present, the MAS-only spectrum generally has insufficient resolution, as shown by Maciel and coworkers[260] who raised the spinning speed to as high as 23 kHz. For chemical shift interactions, the fast-spinning condition also generally cannot be met, especially in high magnetic fields. Considering that the effective quadrupolar interaction is typically tens or hundreds of kHz, the fast spinning condition is difficult to realize. Nonetheless, because the intensity of a broad spectrum of a static sample is centred on a series of central and sidebands, the spectrum has much better resolution and apparent sensitivity.

It is intriguing that all of sidebands and the central band have the same phase and the spectrum is absorptive. For a single crystal or a crystalline powder sample, the MAS spectrum is not absorptive.[261–262] After averaging over the spinning angle (γ), the spectrum becomes absorptive.[261] A pictorial interpretation of this phenomenon is given by Levitt.[263] When the sample is spun at off magic angle the central peaks become broadened. Under fast spinning conditions, the central peak is a static spectrum multiplied by a scaling factor.[3,264,265] However, the central and the sidebands may become distorted relative to the static spectrum under slow spinning conditions.[266,267] The relationship between the spinning rate and the distortion under various conditions has been discussed elsewhere.[267]

The situation is much more complicated for homogeneous interactions, and extensive studies are underway. However, to date, the studies have centred on spin pairs or systems with weak homogeneous interactions. The spin-pair systems are the most thoroughly studied[43–52,268] and several important phenomena have been discovered, such as rotational resonance[44–53,193,194] and the geometric phase,[49] which are further reviewed in the following sections.

Precisely setting the magic angle is an important problem in solid-state NMR. A number of methods have been proposed, including using the observation of the narrowest linewidth of a standard sample,[269] using laser reflection,[270] from the intensity ratio of the sidebands to the central band of a half-integer quadrupole spin system,[271] and from the observation of the

longest FID signal etc.[264,272,273] In practice, the method of observing the length of an FID signal of hexamethylbenzene or deuterated hexamethylbenzene is the most convenient and widely used. An accuracy of ±0.05 to ±0.1° is usually achieved, which is acceptable for most experiments. It is recommended that a standard sample is used for each nuclear species so that it is not necessary to retune the probe and preamplifier after setting the magic angle with the standard sample.[274]

4.1.2. Variable angle spinning (VAS)

Initially, this method was proposed for half-integer quadrupole spin systems.[275–277] The second-order interaction should be included in the total Hamiltonian of such a system. Therefore, the lineshape of the central transition, which is not affected by the first-order interaction, is dominated by the second-order terms. Information on the quadrupolar interaction parameters is contained in the lineshape. For a single-site system, the quadrupole interaction parameters can be obtained by means of a lineshape simulation. However, the simulation could bring about large errors when the system contains more than one magnetically nonequivalent site. For better accuracy, it is suggested that the simulation be undertaken at different angles, i.e., VAS method which has found considerable widespread applications.[278–282] However, it should be pointed out that VAS itself does not usually produce high-resolution NMR spectra for quadrupole systems.

In recent years, VAS has been generalized to two-dimensional correlation spectroscopy, mainly in two applications. One is the measurement of the chemical shift tensors of spin-1/2 systems. This method is termed VACSY (variable angle correlation spectroscopy),[283,284] the power of which is shown by Fig. 9,[283] where the chemical shift spectrum of an eight-site system is separated with satisfactory reliability. VACSY has also been used in dynamic study.[285] The drawback of a VACSY spectrum is that it is not purely absorptive. Using linear predictions, it has recently been shown that the phase artefacts in a VACSY spectrum can be removed.[286] The other two-dimensional version of VAS is correlated VAS proposed by Grandinetti *et al.*[287] by which the correlation between the evolution at different angles can be established. Correlated VAS is closely linked to dynamic angle spinning (DAS) which is discussed below. DAS can be regarded as a special case of correlated VAS. VACSY has been extended to three and four dimensions.[288–290]

4.1.3. Dynamic angle spinning (DAS)

To average out the higher-order terms in a Hamiltonian, the sample must undergo a rotation around more than one axis, either at the same time, or at different periods in an experiment. The latter is referred to as dynamic

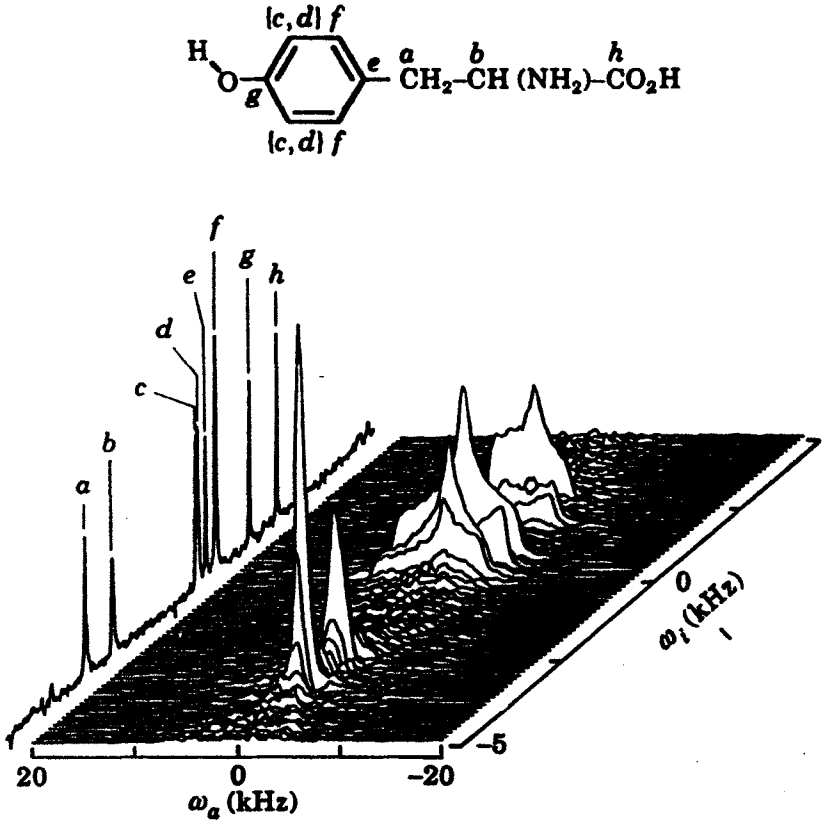

Fig. 9. Two-dimensional isotropic-anisotropic chemical shift correlation spectrum of L-tyrosine, showing the isotropic projection and the assignment of the peaks to each site in the molecule. A set of 65 signals were digitized at rates of 12 kHz over a range of angles. Experimental data were then interpolated over a regular grid composed of 128 × 256 points and Fourier transformed. (Adapted with permission from Frydman *et al.*[283])

angle spinning which is a two-dimensional technique. This technique is specifically designed to obtain high-resolution spectra of the central transition of half-integer quadrupolar spin systems because that transition is not subjected to first-order quadrupole interaction and the second-order terms are not negligible. In the first stage of development of this method, the spinning axis is along one direction in the first dimension and along the other in the second dimension[24,25,287,291–294] (Fig. 10a). In a DAS spectrum obtained in this way, the first dimension is free of first- and second-order interactions so it is high resolution, while the second dimension keeps the first-order interaction so it is broad. Moreover, a DAS spectrum is not purely absorptive. These problems were solved afterwards. By switching to a second

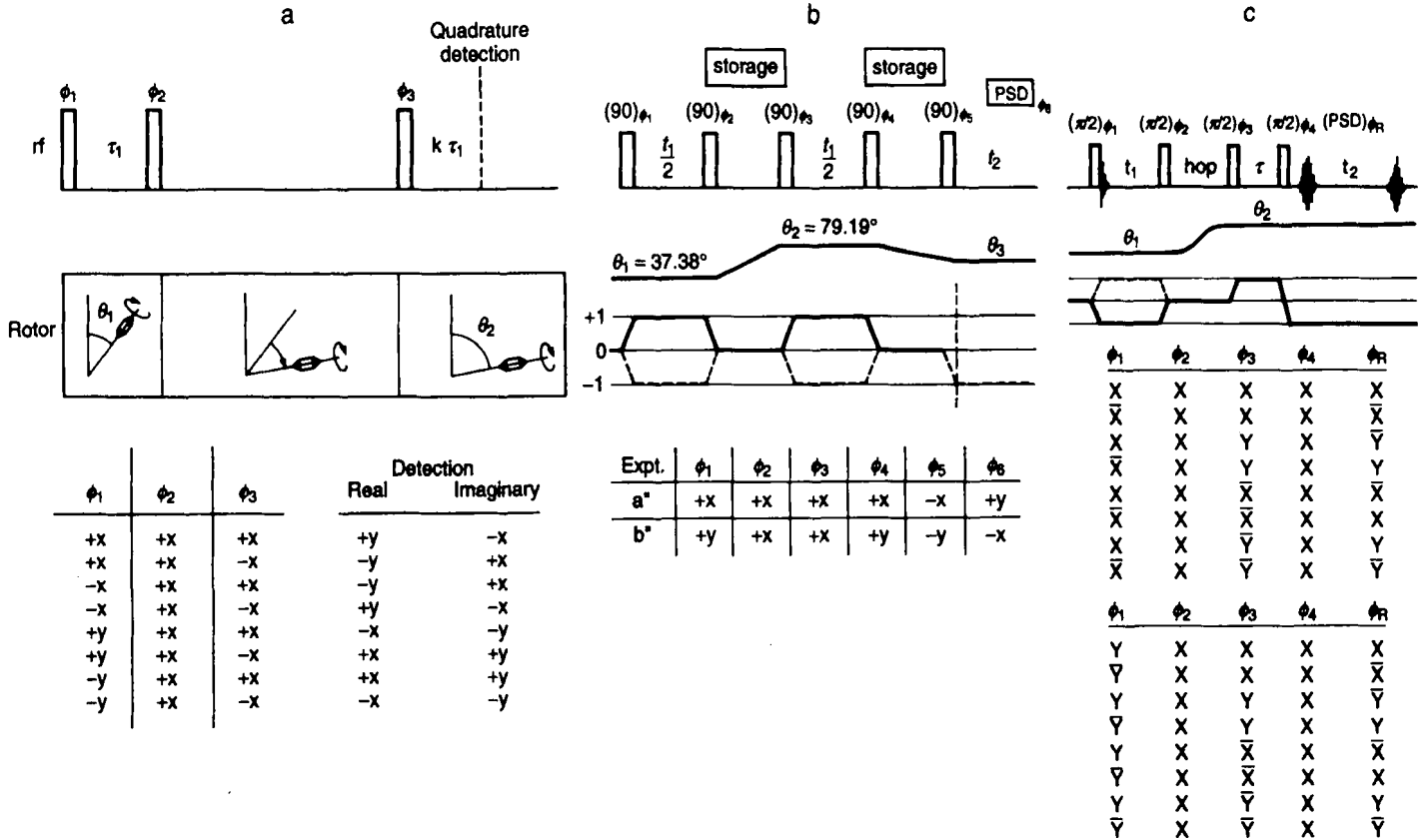

ϕ_1	ϕ_2	ϕ_3	Detection Real	Detection Imaginary
+x	+x	+x	+y	−x
+x	+x	−x	−y	+x
−x	+x	+x	−y	+x
−x	+x	−x	+y	−x
+y	+x	+x	−x	−y
+y	+x	−x	+x	+y
−y	+x	+x	+x	+y
−y	+x	−x	−x	−y

Expt.	ϕ_1	ϕ_2	ϕ_3	ϕ_4	ϕ_5	ϕ_6
a*	+x	+x	+x	+x	−x	+y
b*	+y	+x	+x	+y	−y	−x

ϕ_1	ϕ_2	ϕ_3	ϕ_4	ϕ_R
X	X	X	X	X
$\bar{X}$	X	X	X	$\bar{X}$
X	X	Y	X	$\bar{Y}$
$\bar{X}$	X	Y	X	Y
X	X	$\bar{X}$	X	$\bar{X}$
$\bar{X}$	X	$\bar{X}$	X	X
X	X	$\bar{Y}$	X	Y
$\bar{X}$	X	$\bar{Y}$	X	$\bar{Y}$

ϕ_1	ϕ_2	ϕ_3	ϕ_4	ϕ_R
Y	X	X	X	X
$\bar{Y}$	X	X	X	$\bar{X}$
Y	X	Y	X	$\bar{Y}$
$\bar{Y}$	X	Y	X	Y
Y	X	$\bar{X}$	X	$\bar{X}$
$\bar{Y}$	X	$\bar{X}$	X	X
Y	X	$\bar{Y}$	X	Y
$\bar{Y}$	X	$\bar{Y}$	X	$\bar{Y}$

Fig. 10. Three types of DAS pulse sequence, phase cycling and rotor axis orientations. (a) A basic DAS experiment where all pulses are selective 90° pulses calibrated for the particular axis orientations (used from Mueller *et al.*[291] with permission); (b) A more versatile pure-phase experiment, allowing axis flip to any angle θ_3 during acquisition. The Z filter mixes the two coherence orders during the flip. The time τ for the Z filter is set equal to the storage time needed for the axis flip (from Mueller *et al.*[295] with permission); (c) A combined shifted-echo and hypercomplex DAS experiment with two phase cycling schemes corresponding to the acquisition of real (upper) and imaginary (bottom) part of t_1 evolution, respectively (from Grandinetti *et al.*[296] with permission).

spinning axis[295] (Fig. 10b) so that the detection is at the magic angle, the second dimension of a DAS spectrum is free of first-order interaction. It can be proved that the spectrum recorded in this way is purely absorptive.[295] In addition, the correlation between chemical shift anisotropy and quadrupolar interactions can be obtained by appropriately setting the third angle. A disadvantage brought about is the loss of sensitivity because of an extra storage sequence. By carefully analysing the phase cycling characteristics, the initial pulse sequence has been modified[296] (Fig. 10c) so that the absorptivity of the spectrum is guaranteed with minimal loss of sensitivity. The applications of DAS have been increasing since it appeared in the determination of quadrupolar and chemical shift parameters.[294,297–302] The combination of CP with DAS was exploited by Baltisberger *et al.*[303] for ^{1}H–^{23}Na and by Gann *et al.*[304] for ^{1}H–^{17}O. DAS was also incorporated with reversed CP ^{31}P–^{27}Al by Fyfe *et al.*[305] A typical ^{17}O DAS spectrum of coesite is shown in Fig. 11, where five different oxygen sites are elegantly resolved. Finally, it should be noted that the DAS method is the same as SASS[306,307] in principle; however, the former is aimed at the removal of the second-order quadrupole interaction, particularly with special phase cycling, and SASS is mostly directed to spin-1/2 systems and the spinning axis usually switches in the way of the first version of DAS.

4.1.4. Double rotation (DOR)

Because DAS is a two-dimensional experiment it is time consuming, as are any two-dimensional experiments. But a more intrinsic limitation comes from the fact: for a spin system with a large quadrupolar interaction (such that its second-order interaction is sufficient to obscure a spectrum), both relaxation times are generally small and this may disqualify the use of DAS for certain systems. Another method has therefore been developed in which the sample is spun around two axes simultaneously.[26,308–311] Each rotor spins at the first- and second-order magic angles, respectively; therefore both the first- and second-order interactions can be averaged out. When both the inner and outer rotors are spinning at frequencies higher than the second-order spinning speed, a DOR spectrum is subject to neither the first-order nor the second-order interactions. To avoid the interference between the inner and outer rotors, the ratio of the spinning rate of the two rotors is preferably larger than 5.[312] A DOR spectrum is not purely absorptive in general but the absorptivity can be realized with acquisition asynchronically respect to the outer rotor. A typical DOR spectrum of sodium oxalate is shown in Fig. 12. Recently, DOR has also been incorporated with CP.[313] The applications of DOR have been demonstrated in a series of compounds which are summarized by Chmelka and Zwanziger.[294] DOR is also found to be useful for spin-1/2 systems.[314]

The DOR technique does not have the problem of sensitivity loss and,

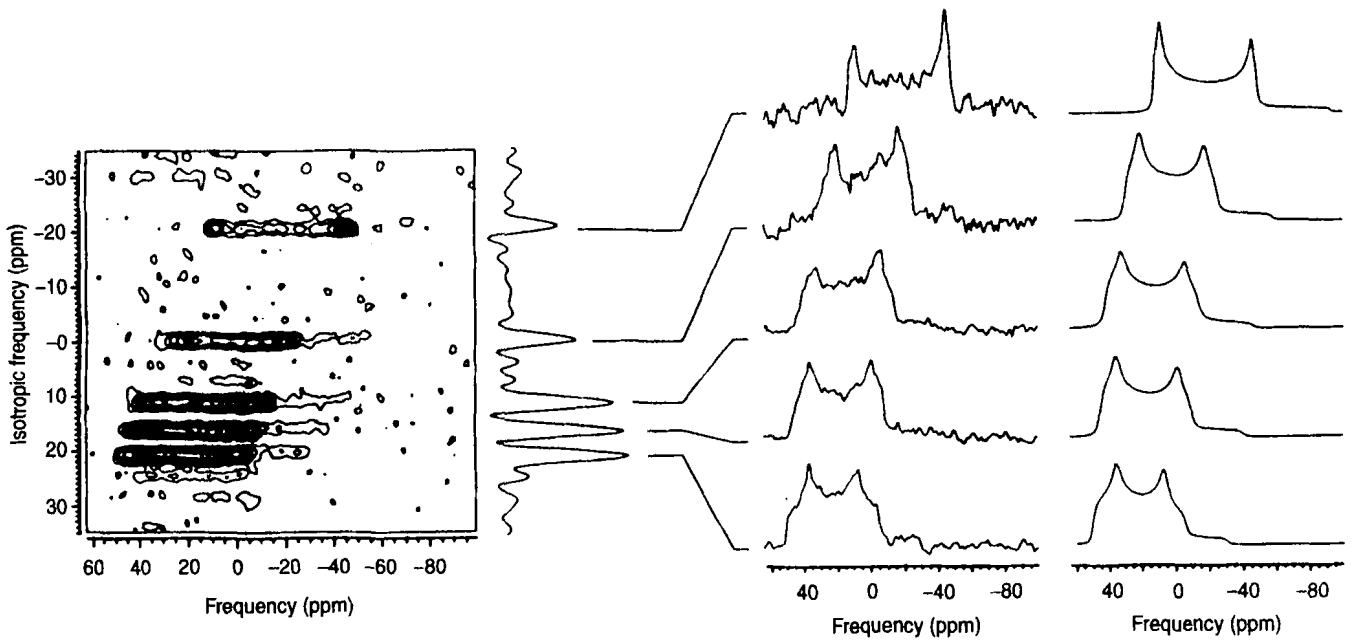

Fig. 11. Two-dimensional DAS spectrum of ^{17}O in coesite at 11.7 T. The projection of the isotropic shift dimension is shown at the top. The contour lines are drawn at levels of 7, 16, 25, 34, 43, 52, 61, 71, 79, 88, and 97% of the maximum point in the spectrum. The spectrum is referenced relative to ^{17}O-labelled H_2O. Also shown are cross-sections from the two-dimensional DAS spectrum taken parallel to the anisotropic (54.7°) dimension for the five sites in coesite. Best-fit simulations of the five sites are shown alongside each cross-section. (Reproduced from Grandinetti *et al.*[300] with permission.)

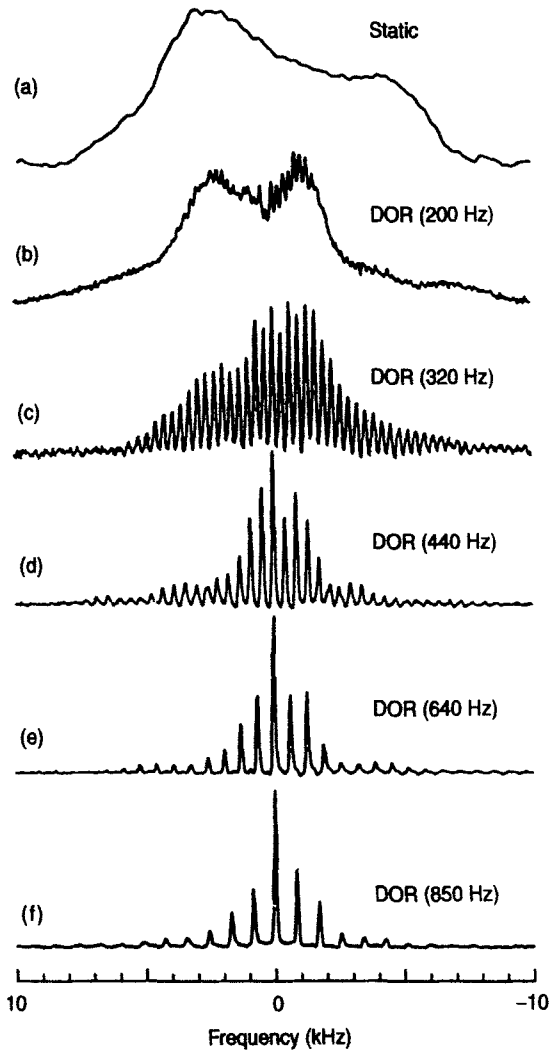

Fig. 12. DOR spectra of ^{23}Na of sodium oxalate, with different spinning speeds. The quadrupolar coupling constant is 405 kHz, the asymmetric parameter is 0.72, and the Larmor frequency is 105.8 MHz. (Reproduced from Sun *et al.*[312] with permission.)

in principle, it applies to any system. However, its popularity may be hampered because of dependence requirement on mechanical technology.

It is worth noting that there has been a promising method proposed recently by Frydman and Harwood[315] to overcome the difficulties with DAS and DOR. This method is simpler as only conventional MAS is employed.[315] Physically, this method is also interesting. The effective (first- and second-

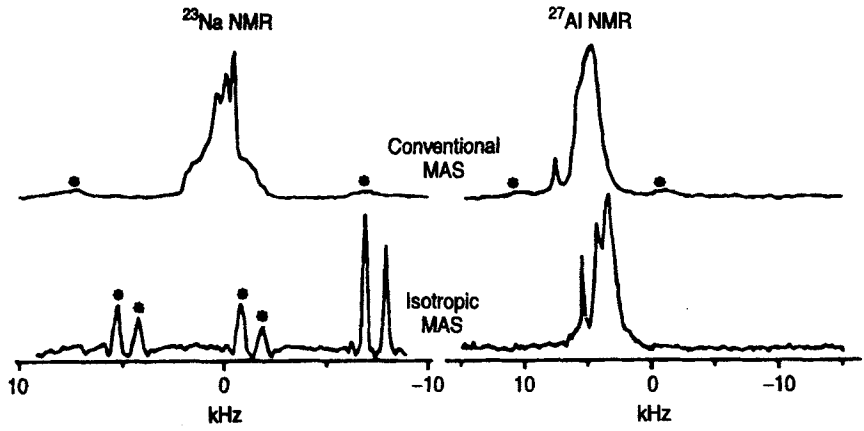

Fig. 13. Comparison between the conventional (top) and isotropic (bottom) MAS NMR spectra of multicomponent mixtures. Asterisks correspond to spinning sidebands. The sodium system contained approximately equimolar mixtures of Na_2SO_4 and $Na_2C_2O_4$; the aluminium system was a mixture of CaA zeolite and Linde-13X faujasite (from Frydman and Harwood[315] with permission).

order) quadrupolar coupling constants have two "external parameters" which are varied by the experimenter: the direction of the spin axis and the order of a transition. Both DAS and DOR average out second-order interactions by changing the spinning direction. As pointed out by Frydman and Harwood,[315] both external parameters can be changed so that the second-order interaction is averaged out without invoking DAS and DOR. With recourse to exciting different orders of multiquantum coherence in the first dimension by adequate phase cycling, a series of MAS spectra can be obtained and the DAS- or DOR-equivalent correlation spectrum (Fig. 13) can be reconstructed similarly to VACSY. In this method, the mechanical requirements and problems caused by short relaxation times disappear instead of an extensive computer reconstruction of a series of VAS or MAS spectra.

4.1.5. Sideband suppression

Whenever the spinning speed is smaller than the anisotropy of an internal interaction, there are sidebands flanking the central peaks. The presence of sidebands is unwelcome in most experiments because it complicates a spectrum and shares energy with the central peaks so that the overall sensitivity is reduced. Therefore, the removal or suppression of sidebands has been an interesting problem in the NMR of rotating solids. The simplest method for obtaining sideband-free spectra is by using synchronical acquisition,[3] i.e., the dwell time is equal to the spinning period. The

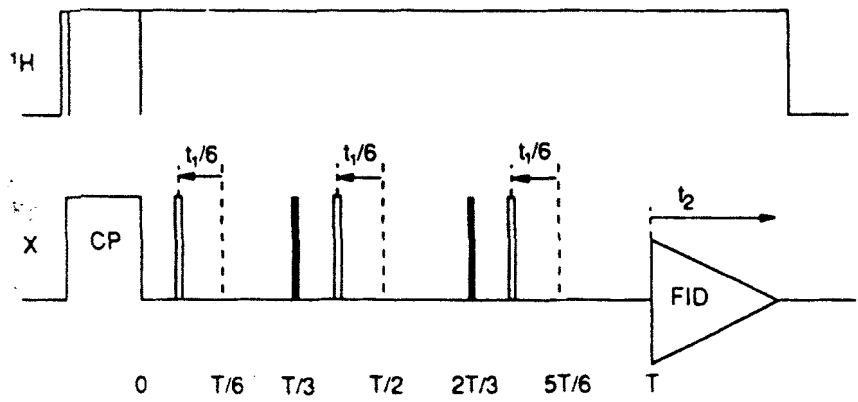

Fig. 14. Pulse sequence of the 5-π-pulse experiment used in the pseudo-two-dimensional spinning-sideband-suppression experiment. All pulses in the observe channel are π pulses. The constant delay T must be a multiple of the rotor period τ_r but not $3\tau_r$. (Reproduced from Gan[329] with permission.)

applicability of this method is severely limited because the spectral width is the spinning speed. Dixon *et al.*[316,317] invented the earliest four-pulse sequence (TOSS) which is easy to perform and is widely used in experiments. However, possible deviation in the TOSS experiments from the idealized conditions, e.g., accurate timing with infinite-narrow pulse width, might cause residual sidebands with significant intensities. Accordingly, several modifications have been made on TOSS to improve its function.[318–321] Thorough analyses of TOSS under various conditions can be found in the literature.[320–323] The analytical solutions of TOSS have been found.[321,324] Five-, six-, and nine-π pulse versions of TOSS have been proposed based on the symmetry consideration[321] which leads to a modification of the previous theory[322,323] on an understanding of the sidebands and thus might be important in ordered materials.[321] A method of suppressing sidebands that is totally different from TOSS has been proposed by Hong and Harbison[325] in which the evolution of the chemical shift interaction is suppressed by intense r.f. irradiation. The application of this method, however, is limited because the r.f. field should be kept on during the course of the time interval before acquisition. By means of TOSS or its variants, the sidebands are removed from a spectrum, but the overall sensitivity of the spectrum is determined by the intensity of the central peaks. Under slow spinning speeds, this loss of sensitivity may become intolerable. The intensity of the central peaks can be restored by a two-dimensional method in which a TOSS–reverse TOSS experiment is used.[326–328] The F1 projection gives an isotropic spectrum without loss of intensity.[327] A less time-consuming pseudo-two-dimensional method has been proposed by Gan[329] (Fig. 14) based on a magic-angle hopping (MAH) scheme.[330,331] More recently, it has been

generalized to quadrupolar spin systems by Nakai and Kuwakara,[332] this has a greater sensitivity than the eight-pulse sequence proposed by Dixon[333] for quadrupolar spins or the four-pulse sequence proposed by Carduner.[334]

The above description is directed to single-axis spinning, which is the method used most in practice. Naturally, there are sidebands in a DAS and in a DOR spectrum as well. The suppression of this type of sidebands is more difficult than chemical shift sidebands. The positions of the sidebands are not necessarily displaced from the central peaks by integer numbers of the sample spinning frequency.[287–312] The sideband properties in DAS and DOR spectra have been discussed by several authors. Gann *et al.*[335] proposed a method, similar to MAH, of suppressing DAS sidebands by using synchronized π pulses, i.e., dynamic angle hopping (DAH). Samoson and Tegenfeldt[336] suggested a DOR sidebands-suppressing method.

4.2. Pulse averaging in spin space

Sample spinning is an effective method of suppressing inhomogeneous interactions or homogeneous interactions of small magnitude, but it is not sufficient for homogeneous interactions such as the dipolar interaction in proton and fluorine systems because mechanical limitations make it difficult to achieve a stable spinning speed higher than about 20 kHz, which is still smaller than the homonuclear dipolar interactions in many proton and fluorine systems. In contrast, for the r.f. field, it is easy to obtain a strength greater than the strongest dipolar interactions. Therefore, the averaging of the interaction is undertaken in spin space, i.e., dipolar decoupling is applied.

Using CW decoupling, heteronuclear and also homonuclear dipolar interactions are averaged out.[39,40,337–339] Generally, to decouple effectively a dipolar interaction, the r.f. field should be on or near resonance and its strength should be larger than the square root of the second moment of the dipolar interaction.[338,339] If the r.f. field is weak, or irradiated far off-resonance, there will be evident residual broadening or alternatively the spectral peaks may be shifted and split into multiplets.[39,40,340,341] Because CW decoupling is windowless, it is mostly used for heteronuclear decoupling.

By means of multi-pulse sequence, spin decoupling can be more diverse and more flexible. For example, it is easy to realize a decoupling scheme where the homonuclear dipolar interactions are decoupled while the heteronuclear interactions are preserved, or vice versa. The basic idea of averaging interactions by a pulse sequence is the same as for fast-sample spinning, i.e., by manipulating the interactions so that they change rapidly and periodically. The early experiment of Lee and Goldburg[342,343] is the spin space version of MAS, where the magnetization is rotated in spin space at the magic angle; some improvements were later made by Haeberlen and

Waugh.[12,39] This technique has some difficulties in practice, for example, it is not easy to carry out phase cycling. Recently, Bielecki *et al.*[344] showed that this technique, when combined with frequency switching, is particularly useful in low-power heteronuclear experiments for decoupling homonuclear dipolar interactions while remaining heteronuclear dipolar interactions. They also noticed the following merits of this technique: large scaling factor, short cycling time, fewer adjustable parameters, and insensitiveness to pulse imperfections. On the whole, however, the decoupling method is based on a different principle which is more successful and more useful in practice — decoupling by means of echo sequences, which was initiated by Waugh, Mansfield and their coworkers[10,11,345–348] This was experimentally proved first by using a Carr–Purcell sequence.[40] A series of multi-pulse sequences was invented in the following decades.[349–360]

Because a multi-pulse sequence is periodic, the average Hamiltonian theory can be used.[12,33,39,40,361] However, care should be exercised with the convergence condition which may be unfulfilled in an improper representation. The selection of a proper representation is essential so that external interactions, such as the Zeeman interaction with the static magnetic field, and the r.f. interaction, should not appear explicitly in the total Hamiltonian. Because of this, the average Hamiltonian theory used in the multi-pulse description is referred to as coherent averaging Hamiltonian theory,[12] where the coherent evolution of the spin states instead of the spectral lineshape is emphasized. The frame where the representation is defined is actually toggling with respect to the rotating frame and therefore is termed toggling–rotating frame.[12,33,39,40] When the r.f. field is set well off-resonance, a representation transformation in addition to rotating and toggling may be needed and this extra transformation also provides further averaging of the interaction, called second averaging.[351,352] The extensive demonstrations of the application of coherent averaging Hamiltonian theory to analysing multi-pulse sequences have been summarized in several books.[39,40] A real pulse has finite width and always has imperfections in amplitude, phase, timing and offset, etc. The error estimation is an important part of work in designing new pulse sequences. This is undertaken by calculating the change of the average Hamiltonian caused by certain errors in pulse. This procedure is more complicated than calculating the averaging Hamiltonian of an ideal pulse sequence. Rhim *et al.*[355] completed detailed error analysis of several types of multi-pulse sequences. They concluded that, for example, WHH-4[347] (Fig. 15a) is less sensitive to phase error than to errors arising from pulse-width and r.f. homogeneity and both offset and phase transients have no first-order contributions to errors in the average Hamiltonian.

All multi-pulse sequences fulfil certain symmetry requirements and therefore a basic sequence can be used as a building-block to construct more complicated but more efficient sequences. HW-8[12,39] and MREV-8[349,353,354] (Fig. 15b), which are less sensitive to r.f. field inhomogeneity were proposed

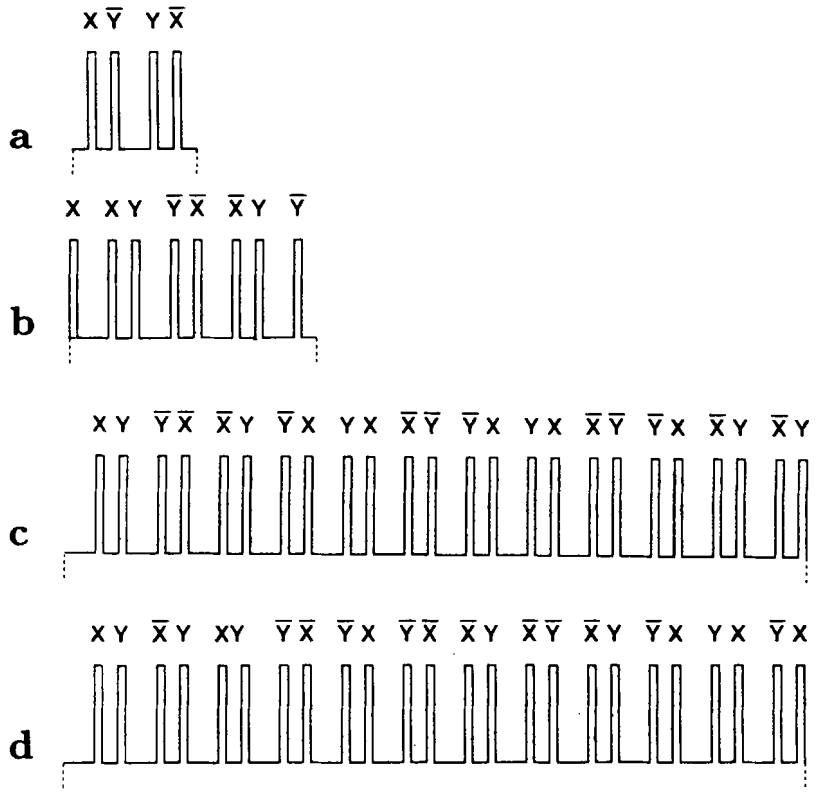

Fig. 15. Four multi-pulse sequences for suppressing homonuclear dipolar interaction: (a) WAHUHA, (b) MREV-8, (c) BR-24 and (d) CORY-24. One cycle is drawn for each sequence. The longer delays are double the length of the shorter ones.

in this way based on WHH-4. Only the 0th and first-order average Hamiltonians are removed in WHH-4, HW-8 and MREV-8. Higher-order terms can be removed by using BR-24[357–359] and BR-52[360] (Fig. 15c) designed by Burum and Rhim. BR-24 was recently modified by Cory,[361] and now it is called CORY-24 (Fig. 15d), which further improves resolution and tolerance to errors. Based on exact numerical computation, a new type of semi-windowless homonuclear dipolar decoupling sequence, which has better stability, has been reported by Liu *et al.*[362] All the aforementioned pulse sequences are windowed. As pointed out by Burum *et al.*,[363] homonuclear decoupling can be realized by totally windowless sequences such as BLEW-12 and BLEW-48, where a decoupling effect similar to BR-24 is achieved by the use of a lower r.f. field. Another windowless multipulse sequence, windowless isotropic mixing (WIM) proposed by Ernst and his coworkers [33,364,365] which can decouple homonuclear interactions while retaining the heteronuclear dipolar coupling, has been combined with the spin echo

sequence (WIMSE) and found to be useful in spectral editing[366] and heteronuclear correlation spectroscopy.[367]

In principle, these multi-pulse sequences can be used for homonuclear and for heteronuclear dipolar decouplings. However, the homonuclear decoupling is not usually required in heteronuclear decoupling. Moreover, the heteronuclear decoupling can be averaged out by lower r.f. field pulses because the heteronuclear couplings are weaker than the homonuclear ones. Therefore, heteronuclear decoupling is carried out by CW irradiation in many heteronuclear experiments. However, the bandwidth is often insufficient in CW decoupling. Therefore, in the last decade, theoretical and experimental efforts have focused on the use of multi-pulses in heteronuclear decoupling. A series of broad-band heteronuclear decoupling sequences has been invented including ALPHA, proposed by Fung *et al.*[369,370] which also performs well in liquid crystals, and COMARO by Pines and coworkers,[371–373] which works at low r.f. power, is insensitive to pulse errors, has especially good tolerance to r.f. field offset, and can also be applied to quadrupolar systems. However, COMARO may be ineffective under MAS because of interference between the pulse cycling and sample rotation. In addition, TREV[374] proposed by Takegoshi and McDowell can be used for heteronuclear decoupling. Pratum[375] has compared the performance of CW, ALPHA, COMARO and TREV and concluded that, for diamagnetic samples, they behave similarly to each other except that TREV requires greater r.f. power, but for paramagnetic materials like clay, CW is ineffective and ALPHA and COMARO are good. A very simple two-pulse sequence (TPPM) based on phase modulation, which effectively suppresses the residual line broadening left by CW decoupling, has been proposed by Bennett *et al.*[376] Further developments in heteronuclear decoupling are expected in systems with more than two spin species or where quadrupolar spins are involved.

In summary, the multi-pulse scheme is an effective method to average out the dipolar interactions, especially it is indispensable for homonuclear decoupling of abundant spins with high gyromagnetic ratios.

4.3. Combinated rotation and multi-pulse spectroscopy (CRAMPS)

For most nuclear spin species, sample rotation is sufficient to average out the internal interactions, either inhomogeneous or homogeneous. However, for solids that contain protons or fluorines, sample spinning alone, even at a spinning rate as high as 20 kHz, the spectrum is still unsatisfactorily resolved. This has been demonstrated by Maciel and coworkers;[377,378] in a heteronuclear experiment, CW or pulse decoupling, in addition to MAS, which averages chemical shift anisotropy, is necessary to suppress the dipolar interactions. This is actually the combination of sample rotation and multi-pulse (CRAMPS) technique used in heteronuclear experiments. How-

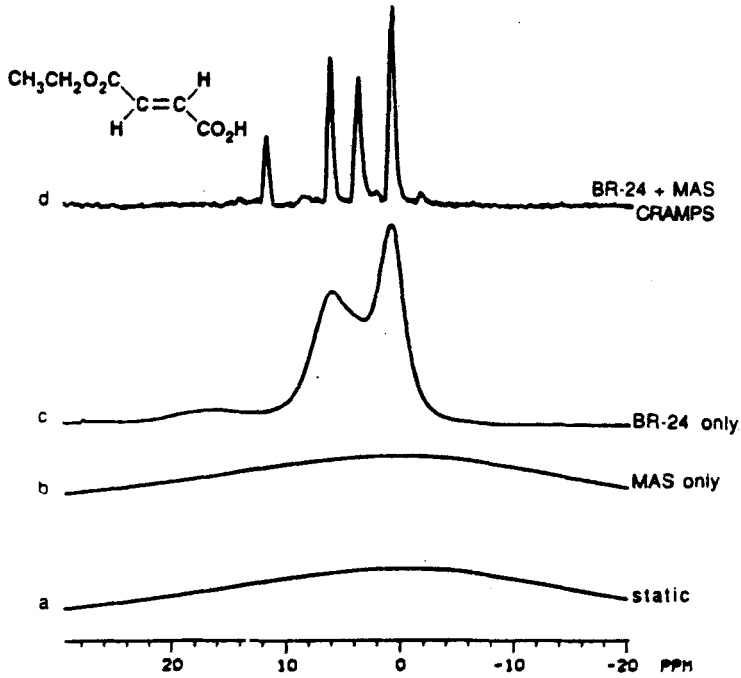

Fig. 16. 187 MHz ^{1}H NMR spectra of *trans*-ethylfumarate: (a) single pulse, no MAS; (b) single pulse with 2 kHz MAS; (c) multi-pulse with BR-24, no MAS; and (d) CRAMPS using BR-24 and 2 kHz MAS. (Reproduced from Maciel *et al.*[387] with permission.)

ever, historically, CRAMPS was specifically named to describe those homonuclear experiments involving protons[13,379–388] or fluorine,[13,385,389–391] although there were few reports on the use of CRAMPS in studying ^{31}P systems.[389] This is because these two spin species are abundant and have large gyromagnetic ratios and there are some unique and stringent requirements on the multi-pulse sequences used to suppress the dipolar interactions among these spins, which has been detailed in a monograph[383] and review papers.[387,391] The CRAMPS spectrum of fumaric acid monoethyl ester[387] is shown in Fig. 16 where protons of all groups are highly resolved. The most-used multi-pulse sequences in CRAMPS experiments are MREV-8 and BR-24, which average out the dipolar interactions up to the first- and second-order terms, respectively. The CRAMPS experiments based on TREV have been reported recently by Maciel and his coworkers[392–396] who have shown that TREV works for plastic as well as rigid solids and is insensitive to offsets. Besides, CRAMPS based on Cory[361] has been reported which shows a better tolerance to experimental imperfections than that based on BR-24 and MREV-8 but a slightly smaller scaling factor. A time-

suspension pulse-sequence, which suppresses both bilinear and linear terms of spin operators and thus is insensitive to r.f. field offset, was reportedly useful in imaging.[397]

Homonuclear high-power experiments require intensive pulsing, accurate timing, amplitude and phase stabilities, and good r.f. homogeneity; therefore, it is the most demanding technique in solid-state NMR experiments. The spectrometer generally should be carefully tuned up before the experiment[353,386,391,398,399] The transmitter, preamplifier and probe should be adjusted to their optimum performance. Coils may need to be rewound for better homogeneity. Through decades of efforts, with the development of electronics and computers, digital phase shifters are now installed on most newly produced commercial instruments and CRAMPS experiments have become less "painful" provided that certain procedures are followed.[386] For proton systems, the chemical shift range is usually less than 20 p.p.m.; the low spinning rate is sufficient to average out its anisotropy. The low spinning speed also ensures that there is no interplay between the multi-pulse and sample rotation.[13,383] For fluorine, the chemical shift is large, even larger than homonuclear dipolar interactions in high magnetic fields. The CRAMPS works less effectively compared with protons. Some efforts have been made to accommodate this difficulty, including rotor-pulse synchronization to obtain more reliable sidebands[390,400,401] and quadrature detection to cover wider spectral range.[400–402] The application of the CRAMPS technique to time–domain experiments has been explored by Caravatti *et al.*[403] and Bronniman *et al.*[404] to enable more detailed investigation of the dynamics in proton systems. Using dephasing prior to multipulse, these methods partly circumvent the problems brought about by insufficient resolution. Two-dimensional resolved spectra similar to NOESY are obtained[403] by the time–domain CRAMPS technique. The application of CRAMPS to imaging can be found in the review by Cory.[37]

Before concluding this section, it is noteworthy that an interesting and somewhat surprising observation of high-resolution proton spectra of solids has recently been reported by Ding and McDowell.[84–86] They found that a high-resolution proton spectrum can be obtained simply by single-pulse excitation with a long delay before acquisition.

4.4. Nutation

This method is used to suppress the chemical shift interaction by means of r.f. irradiation and single-point acquisition or indirectly, acquisition during the nutation pulse in a two-dimensional manner. The principle of nutation is based on two facts. One is that, similar to the r.f. interaction, the chemical shift Hamiltonian is linear to spin operators. The other is that, the r.f. field amplitude can be easily set to values that are much larger than the chemical

shift so that during the pulsing, the latter contributes negligibly to the evolution of a spin system. Dipolar and quadrupolar coupling information can be obtained by nutation spectroscopy. Over the last decade, it has been used in spin-1/2 systems, such as ^{13}C,[405–408] but more often in quadrupolar systems, such as ^{23}Na (spin-3/2),[409–416] ^{27}Al (spin-5/2),[411,412,417–421] ^{55}Mn,[422,425] ^{45}Sc (spin-7/2)[412] and ^{14}N (spin-1)[426–428] systems.

For spin-1/2 systems, the nutation provides dipolar coupling constants. One-dimensional spectroscopy with single-point acquisition is usually used because the dipolar coupling is not too large and the spectral dwell time (between pulses) is short enough to cover the spectral range. For quadrupolar systems, unless the quadrupolar coupling is weak, one-dimensional single acquisitions cannot provide a sufficiently wide spectral range. Therefore, two-dimensional spectroscopy is employed,[412–425] where the projection on the F1 axis corresponds to the nutation spectrum, which is independent of the chemical shift interaction. Two extreme cases[425] where the nutation spectrum is very simple and contains only one sharp peak, occur when the r.f. field amplitude is much larger and much smaller than the quadrupolar coupling constants, respectively. For the former case, the sharp peak is at the position with the frequency of the r.f. field amplitude; for the latter case, the peak appears at the frequency equal to the r.f. field amplitude times $I + 1/2$ where I is the spin quantum number. This fact is very useful in practice, especially in qualitative estimations of quadrupolar coupling constants of systems with highly inequivalent sites, e.g., molecular sieves. The resolution of a nutation spectrum thus can be adjusted by the selection of the r.f. field.[412] When a nutation spectrum is used to get the best resolution, the r.f. field should be set to the value where most peaks are sharp. However, to obtain accurate values of the quadrupole parameters, this highly resolved spectrum might not be suitable and intermediate cases are more useful because the intermediate case corresponds to a structural lineshape. The quadrupole parameters can then be obtained by means of the lineshape simulation.[412] Because the nutation time is usually tens of microseconds, which is much less than a period of a moderate sample rotation, nutation experiments are undertaken mainly on static samples. It is reported that the sample spinning employed in nutation spectroscopy can increase resolution and improve lineshape structure.[414] MAS helps to decrease broadening arising from chemical shift, dipolar and quadrupolar interactions so that the resolution of the second dimension is enhanced by sample spinning. However, this is not a generally correct conclusion for the first dimension (nutation dimension) and only holds when the (effective) quadrupolar coupling constant is small with respect to the r.f. field amplitude.[429] Theoretical investigations of the effect of the sample rotation on nutation spectra have been reported.[415,429] The nutation spectrum is usually broadened by MAS when the effective quadrupolar coupling constant is much larger than the r.f. field;[429] therefore, the spectral resolution worsens with the use of sample

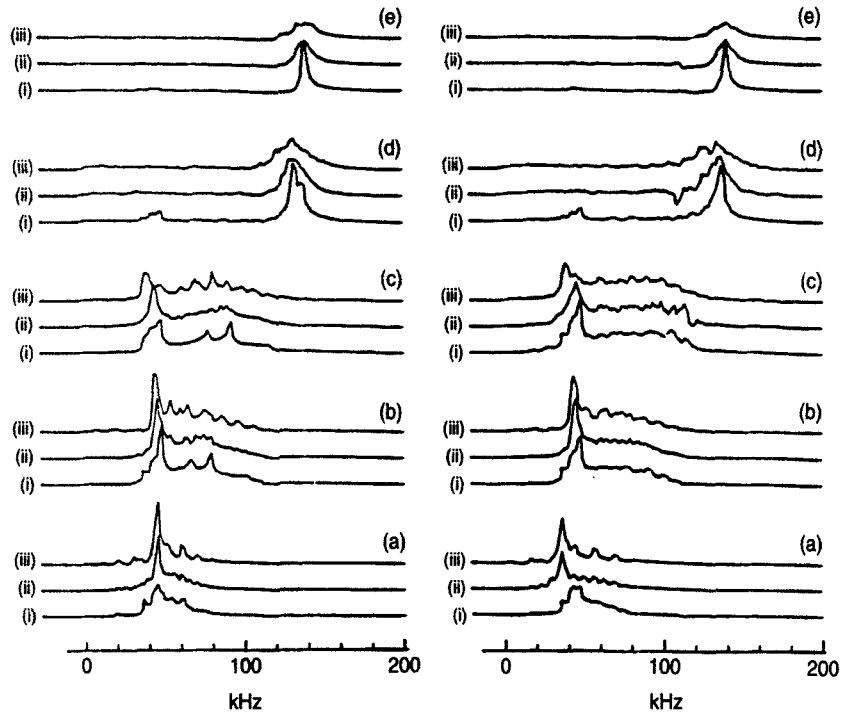

Fig. 17. The central transition nutation spectra of spin-5/2.

(a) $\frac{\omega_q}{\omega_1} = 0.3$, (b) $\frac{\omega_q}{\omega_1} = 1.0$, (c) $\frac{\omega_q}{\omega_1} = 2.5$, (d) $\frac{\omega_q}{\omega_1} = 5.0$,

The bottom (i) spectra are static ones, middle (ii), spinning speed $\omega_r = 5$ kHz and top (iii), $\omega_r = 10$ kHz. (Reproduced from Ding and McDowell[429] with permission.)

rotation. The effect of MAS on the nutation spectrum is shown in Fig. 17. Because central transition has the best sensitivity, nutation spectra are usually recorded using this. By introducing a conversion pulse before acquisition, Nielsen *et al.*[415] carried out a systematic survey of the multi-quantum nutation spectra, including the MAS effect, and concluded that the multi-quantum MAS nutation spectra are generally more time-consuming, more subject to experimental imperfections and more insensitive to asymmetric parameters, than their central transition counterparts. These properties may be advantageous for systems with very different quadrupolar coupling constants but with almost identical chemical shifts or for systems where both of these coupling constants are large. It is reported that if the nutation pulse is replaced by a rotary echo, the peaks belonging to sites with different relaxation times can be better resolved.[430] Conversely, Man[424] proved that

when the nutation pulse is replaced by two in-phase and slightly separated pulses, with the second one increasing its length, the nutation spectrum may provide a precise measurement of the quadrupole coupling constant of a powder sample whose central transition is featureless. To minimize the zero-frequency signal in a nutation spectrum, the r.f. field should be set exactly on resonance.[412,425] The off-resonance nutation method shown by Kentgens and coworkers[431,432] can extend the applicability of nutation spectroscopy, but a frequency-stepping device is needed in the experiment. Nutation spectroscopy, especially that of quadrupole systems, has been widely used in practical applications in zeolites[418] and superionic conductors.[433,434]

5. RECOVERY OF INTERACTIONS

Under MAS or multi-pulses, anisotropies and even isotropies are averaged out, so that spectral resolution and sensitivity are enhanced. In practice, however, the priority of a study is not only the resolution or sensitivity, it also includes the acquisition of accurate values of the anisotropies which are intimately related to the structure and dynamics of solids. Moreover, there are cases where interactions should be restored to ensure certain mechanisms, e.g., dephasing and relaxation effects. Therefore, there is an important problem in solid-state NMR: how to recover the internal interactions, especially when they are averaged out by MAS, r.f. irradiation, or both. Recovering an interaction would appear to be the reverse problem of removing it, i.e., by interrupting the manipulations that cause averaging. It is not quite as simple in reality because, by recovery of interactions, it is meant that only certain interactions of interest are, fully or partly, restored while all other interactions remain suppressed so that the resolution of the spectrum is retained. This can be seen when introducing a conflicting mechanism to cancel the averaging effect caused by MAS or r.f. irradiation. It should be noted that, however, in some cases, anisotropic information can be acquired simply by using multidimensional separation. There are a variety of ways of providing a conflicting mechanism: these fall into several categories elaborated below. This classification is, however, rather artificial. To obtain highly resolved spectra with anisotropies recovered experimentally frequently requires the use of two- or multi-dimensional techniques or more than one set of experiments. Moreover, different methods of recovering interactions may be used in the same experiment.

5.1. Static or slow spinning

By simply neither spinning nor irradiating a sample, all the anisotropies of the interactions are preserved. However, there are too few realistic systems

whose spectra can be unambiguously resolved. Ideally, this technique is suitable for single-crystal samples where both the resolution and sensitivity may be good enough. For powder samples, this may apply to systems where there are only few (one or a spin pair) magnetically inequivalent sites or only one type of interaction is involved. Pulse or CW decoupling is usually required to obtain a satisfactory spectrum. This technique can be performed in one- or two-dimensional spectroscopy (e.g., to obtain chemical shift and dipolar coupling parameters,[33,39,81,435–445] associated with numerical simulation. The ambiguity of interaction parameters extracted from these spectra has been analysed by Nakai and McDowell.[443–445] The early Carr–Purcell sequence can be used to produce Pake patterns of isolated spin pairs. Ishii and Terao[446] noted recently that improved experimental performance can be achieved if the π pulses are replaced by composite pulses. A good example of using a static sample to separate the dipolar interaction was shown by Oas and coworkers.[447–449] Their method is based on the work of Kaplan *et al.*[450] who pointed out that the chemical shift powder spectrum of a nucleus dipolar coupled to a neighbour can be used to extract the full set of values of the chemical shift tensor (principal values and directions in the molecular frame). By this method, Oas and coworkers[447–449] successfully measured the ^{13}C–^{15}N dipolar coupling tensor and also the chemical shift tensors of ^{13}C, and ^{15}N in several peptides. When considering the difficulty in preparing single crystals for biological samples, this method also provides a good demonstration of using powder samples to obtain the values of all elements of interaction tensors. Another excellent example of using static solids to obtain coupling information is the spin echo double-resonance (SEDOR) method invented by Wang and Slichter[14,15,451,452] for studying weak heteronuclear dipolar interactions in static solids. Using the imperfection of a spin echo under the influence of a dipolar interaction,[14,450] SEDOR can separate the information on dipolar interactions. This is a differential spectrum experiment. In the first step, a π pulse is applied only to the observing channel so the heteronuclear interaction is refocused. In the second experiment, both the observing and decoupling channels receive a π pulse and the acquired spectrum will include information on heteronuclear dipolar coupling. The differential spectrum of the two experiments then contains dipolar-only information. As a simple method of separating dipolar information, SEDOR has found a number of applications in surface adsorption,[15] catalysis,[451] and diffusion,[452] among others. Furthermore, SEDOR has been extended to three-channel experiments by Oas *et al.*[447–449,453] and Schneider *et al.*[454] The static samples associated with two-dimensional experiments which have been investigated generally have better separation, for example, in correlating chemical shift and dipolar coupling in heteronuclear[438,453–455] and homonuclear spin pair systems.[444,445] This method is generally classified as separation of local fields and a comprehensive summary can be found in the monograph by Ernst *et al.*[33] Two-dimensional spectroscopy can also be

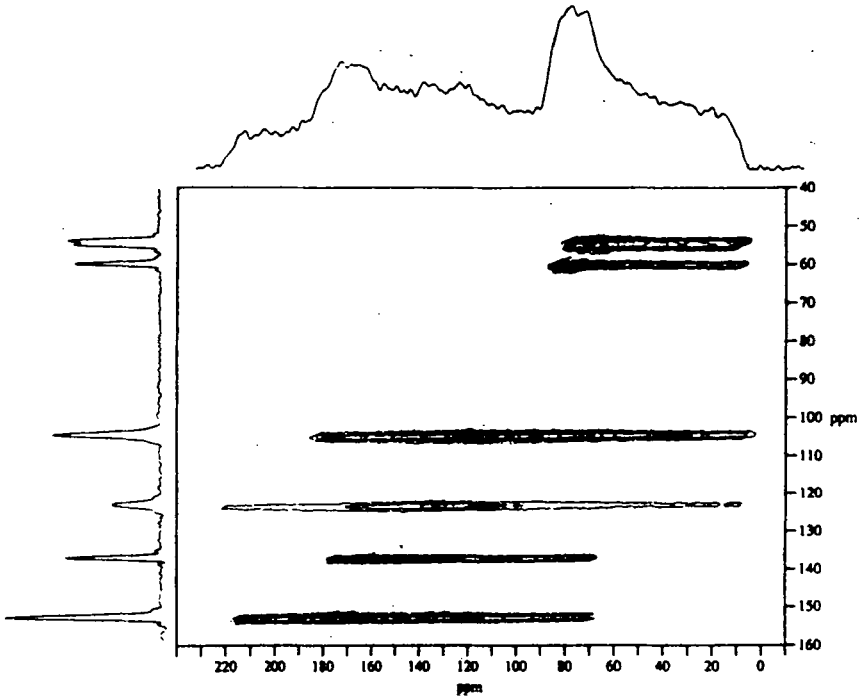

Fig. 18. Contour plot of the central portion of the 1,2,3-trimethoxybenzene 2D MAT spectrum obtained by shearing the experimentally acquired spectrum by 45°. The contour interval is 4% and the lowest contour plotted is 4% of the maximum peak height. The isotropic shifts of the carbons can be read from the vertical axis and the anisotropic shifts can be read from the corresponding horizontal slices. (Reproduced from Hu *et al.*[458] with permission.)

performed when the resolution is not important in one dimension, e.g., the stop-and-go cross-polarization method.[157]

In fact, when the spinning rate is much smaller than the anisotropy of the interaction, the sample can be safely considered to be static and the anisotropy is kept in the spectrum. Gan[456] and Hu *et al.*[457–459] recently proposed magic-angle turning where the sample rotates at hundreds and even tens of Hz so that the chemical shift anisotropies as well as isotropies can be read from a correlation spectrum (Fig. 18).

Even at moderate spinning rates, the anisotropies may be extracted when the slow spinning condition is satisfied. For example, the anisotropy of the interaction can be determined by the simulation of the intensities of the sidebands.[460–462] This method is simple in principle and in practice because it is a one-dimensional method; however, it works optimally only when the spinning speed is at least several times slower than the minimum anisotropy of

the system under study and when the isotropic positions are known beforehand. Therefore, this method is especially useful for quadrupolar spin systems wherever the first-order interaction is dominant because the typical effective quadrupole coupling constant is several tens to several hundreds of kHz and the slow spinning condition is always met. Indeed, this fact has been used in ^{2}H studies[463] and satellite transition spectroscopy (STRAS)[464–466] of half-integer quadrupolar systems. For systems with multi-magnetically inequivalent sites and for the central transition which is not subject to first-order interactions, this method might be useful if it is associated with the recently proposed simple method of obtaining a high-resolution spectrum of a half-integer quadrupole system where only MAS is used.[315] For heteronuclear dipolar interactions which are usually of the order of 2 kHz, the slow spinning condition is usually not satisfied, moreover, it is always entangled with homonuclear dipolar interactions; thus, this method generally cannot be used. For more general systems, however, two-dimensional separation methods should be used, in which both the isotropic and anisotropic chemical shifts are kept in the first dimension while only the isotropic shifts are kept in the second dimension by sideband suppression techniques. A comprehensive analysis and systematic comparison of these correlation methods can be found in a recent publication by Antzutkin *et al.*[467] They also propose a new separation method based on a five-pulse scheme by which the first dimension contains only the anisotropic information so that better sensitivity can be reached for sites with large shift anisotropies. An example of the use of their pulse sequence to separate sidebands is shown in Fig. 19.

5.2. Off magic-angle spinning

The MAS technique is effective because of the fact that the interaction Hamiltonian includes a static term proportional to the scale factor $P_2(\cos\theta)$. Consequently, the anisotropy can be partly restored when the samples rotate at an angle other than the magic angle. This method can be implemented in one-dimensional experiments, for example, in the measurement of chemical shift anisotropy,[323,468–473] working optimally when the fast spinning condition is fulfilled[266,267] and there are only a few magnetically inequivalent sites. Two- or multi-dimensional spectroscopy is more useful for better spectral assignments. Two types of experiments have been proposed. The first way is switching angle sample spinning (SASS)[474–477] where the sample rotates off the magic angle in the first dimension while it is switched to the magic angle during the detection. It is carried out in a similar way to a DAS experiment, but with different phase cycling and different ways of switching the spinning axis, as mentioned in Section 4.3.3. SASS has found important applications in the measurement of chemical shift tensors, and the chemical shift–dipolar correlation.[476–481] The second way is VACSY,[283,284] as introduced in Section

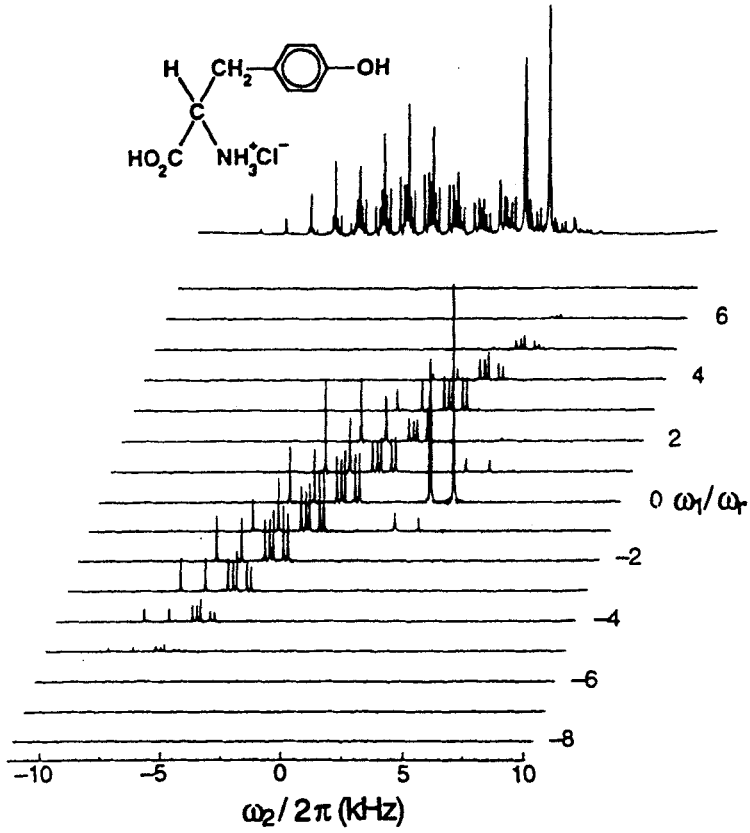

Fig. 19. ^{13}C spectra of L-tyrosine hydrochloride powder at a rotor frequency of 1.03 kHz. Top: 1D MAS spectrum (3888 transients). Bottom: 2D-PASS spectrum showing sidebands separated in the ω_1 dimension. The ω_1 slices are labelled with the order of the sidebands, k. Sixteen t_1 increments were taken, each the sum of 243 transients. (Reproduced from Antzutkin *et al.*[467] with permission.)

3.2, which does not require spinning axis switching, but needs a set of correlation spectra at different angles. It applies to chemical shift isotropy–anisotropy correlations and to chemical shift–quadrupolar coupling correlations.[315] Considering the limitations arising from mechanical restriction and relaxation times in SASS, VACSY appears more promising. It also represents a trend in NMR, where the hardware limitations are overcome by software.

5.3. Turning off or interrupting decoupling

Most solid-state NMR experiments on rare nuclei employ heteronuclear high-power decoupling for satisfactory resolution. Alla and Lippmaa[482]

pointed out that the carbons in different functional groups can be distinguished by the effective dipolar coupling constants if the decoupling is interrupted for tens of microseconds before acquisition. This method, now called dipolar dephasing, reintroduces the effect of the dipolar interactions on the lineshape so that the local structural information can be extracted from it.[483–488] Opella and Frey[489] found that dipolar dephasing can be used to suppress the signal of the carbons directly bonded to protons so that the spectrum can be simplified and then assigned. This method is useful when the heteronuclear dipolar interaction is strong. For weak dipolar interactions the dephasing time will be too long. Alemany *et al.*,[490] Munowitz *et al.*,[491] and Harbison *et al.*[492] have modified the dephasing sequence to overcome the effects of phase distortion and chemical shift anisotropy. By means of numerical computation, Newman[493] deduced how sample spinning and spin diffusion affect dephasing and pointed out that the signal of the nonprotonated nuclei in a dephasing spectrum is significantly changed if the chemical shift anisotropy is large. This simple procedure can also be used in homonuclear systems, as shown by Stoll,[488] or in cross-polarization-depolarization experiments.[494] It should be noted that this method is not used to obtain the values of the dipolar couplings in solids.

5.4. Rotational resonance and rotary resonance

As early as the 1960s, Andrew *et al.*[193,194] observed that when the spinning sidebands of two coupled nuclei overlap, the cross-relaxation between them is enhanced. This phenomenon was later found to have more significance and now is referred to as rotational resonance. As shown in Fig. 20, when the isotropic difference of the interaction between two spins is an integral number of times the spinning speed, the dipolar interaction between them, which is averaged out by MAS, is recovered. This can be well described by the use of average Hamiltonian theory.[48–53,216,268,495–497] Under the rotational resonance condition, the periodic terms in the total Hamiltonian which otherwise would be zero over a spinning period, become independent of time. Using the Floquet formalism, rotational resonance can be given in a more intuitive explanation,[63] i.e., the energy level anti-crossing of the relevant Floquet states. Rotational resonance is selective so it is especially useful in selection experiments. In a rotating frame, this condition can occur only in homonuclear systems because the resonance difference between different spin species is usually much larger than any spinning speed that is mechanically possible. However, heteronuclear rotational resonance can be realized in special frames. For example, in CP experiments at high spinning speed, the Hartmann–Hahn matching condition is split into a number of sideband matchings, as shown in Section 3.1. The sideband matching condition is actually the rotational resonance condition for heteronuclear systems in a tilted

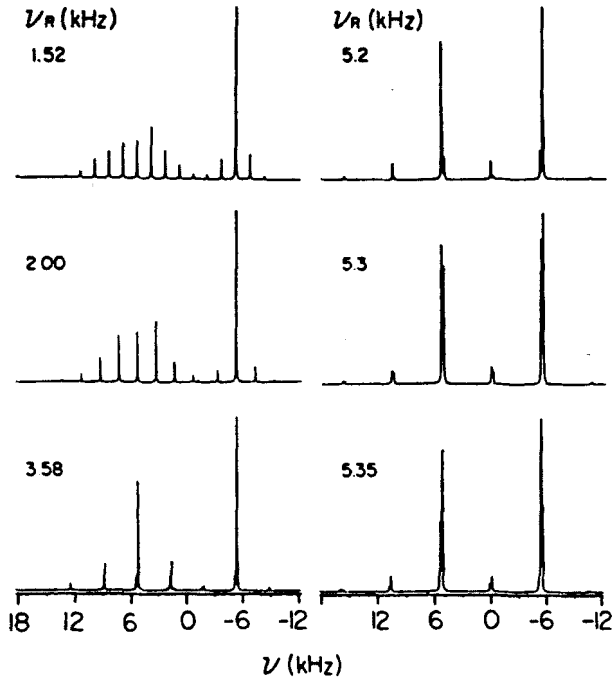

Fig. 20. Calculated MAS powder spectra of the glycine molecule at six different rotor frequencies, passing through the match conditions $N = 7, 3, 2$ are shown. From the spectra shown it is evident that the spectral lineshapes are most intensely affected when the match condition with $N = 2$ is met. The parameters of the glycine molecule, ignoring the J coupling, at magnetic field of 7.4 T were used. (Reproduced from Schmidt and Vega[61] with permission.)

rotating frame. Rotational resonance combined with a multi-pulse sequence which scales down isotropic interactions has been demonstrated by Spencer *et al.*,[496] where new rotational resonance conditions are shown. As a very simple mechanism of recovering dipolar interactions, rotational resonance has also been widely applied to many spin species in addition to ^{13}C,[146] such as ^{31}P,[50–53,60,193,194,217,219,268,497] and ^{15}N,[498] and found to have an enormous number of applications, such as in spectral lineshape analysis,[44–53,61–63,268,495–499] spin diffusion,[45,146,193,194,217,500,501] spin selection,[502] multi-quantum excitation[503] and structural determination.[504] The rotational resonance phenomenon has been found even in quadrupolar nuclei such as ^{23}Na and ^{27}Al,[505] where the recovered interaction is, of course, the quadrupolar interaction.

Another phenomenon similar to rotational resonance is rotary resonance where the modulation of interactions is introduced by the r.f. field in addition to sample spinning. When the r.f. field strength is an integral

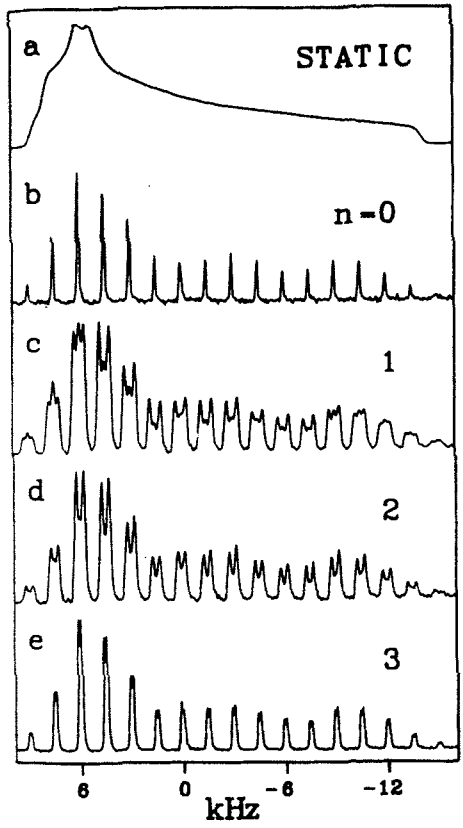

Fig. 21. (a) ^{1}H-decoupled ^{31}P NMR spectrum of polycrystalline ^{15}N-labelled *N*-methyldiphenylphosphoramidate, without sample rotation. The ^{31}P-shielding anisotropy and asymmetry parameters are −21.24 kHz and 0.19, respectively. (b) With magic-angle sample rotation at 1.5 kHz. (c)–(e) indicate when an r.f. irradiation is on at the N-15 isotropic shift frequency. The irradiation intensity fulfils the rotary resonance conditions $\omega_{11} = n\omega_r$, $n = 1$, 2, and 3. (Reproduced from Oas *et al.*[506] with permission.)

number of times the spinning rate, the MAS averaged dipolar interaction is restored, as shown in Fig. 21. This phenomenon can serve as a way of recovering the heteronuclear dipolar interactions in a rotating frame[47,506,507] and also homonuclear dipolar interactions in a tilted rotating frame.[508] The essence of this method is the cancellation of the mechanical averaging by a rotation in spin space. Its application includes the sideband enhancement,[509] the evaluation of heteronuclear coupling constants[47,507,508] and the analysis of sample spinning on spin diffusion[146,510] and on heteronuclear decoupling.[511]

5.5. Echo dephasing

The methods discussed in this section aim at the recovery of the interactions, especially dipolar interactions, which are averaged out or substantially reduced by MAS. Therefore, most of the methods are suitable for dipolar interactions between nuclei with low gyromagnetic ratios which are usually weak and can be averaged by moderate or even low spinning rates for MAS, or for strong interactions but under fast spinning conditions.

There is an increasing number of methods involving echo dephasing. The foundation of this type of method is that the MAS effect can be concealed by certain r.f. pulse sequences if the amplitude, spacing and phase of the pulses are set appropriately. More specifically, the purpose of these methods is to prevent a rotational echo from appearing (echo dephasing) because the presence of an echo means that the interactions are focused. The purposes of recovering an interaction are: (1) obtaining information on that interaction and (2) facilitating certain processes, e.g., coherence transfer, under MAS by the fast spinning condition. Generally, for the first purpose, differential spectrum experiments or two-dimensional experiments are carried out. It is convenient to classify these methods into two categories: heteronuclear and homonuclear experiments.

5.5.1. Heteronuclear echo dephasing

This method can be regarded as an extension of spin echo double-resonance (SEDOR) to rotating solids. When used on spinning samples, however, nontrivial modifications should be undertaken. The representative of this method is rotational echo double-resonance (REDOR) experiments proposed by Gullion and Schaefer[16] where one π pulse is applied to each channel per rotor cycle to dephase the rotational echo (Fig. 22). Like SEDOR, this is a differential experiment and two independent experiments are required. One spectrum contains no information on dipolar interactions while the other does. In this case the dipolar couplings can be found from the differential spectrum. For reliable values of dipolar constants, a series of REDOR spectra are needed and numerical simulation is necessary. The basic REDOR technique was extended, mainly by Gullion and Schaefer, in different directions,[512–525] including association with DANTE selected excitation,[512] spinning axis flipping,[513] sequences minimizing r.f. offset effects,[515,516] with quadrupolar nuclei as coupling partner,[517–521] two-dimensional spectroscopy[522,523] and transferred echo double resonance (TEDOR).[524,525] A comprehensive review on REDOR, among other topics, appeared recently.[526] The π pulse imperfections may have serious effects on the dephasing; it is suggested that the π pulses undergo phase cycling schemes such as MLEV and XY.[527–529] Gullion[528] showed that XY-8 is more advantageous than MLEV-8. Li and Evans[529–531] discussed the effects of large

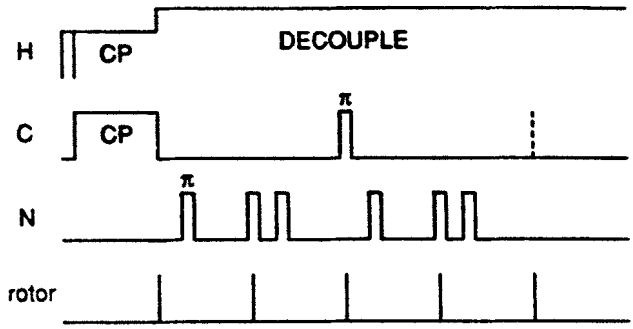

Fig. 22. Pulse sequence for ^{13}C–^{15}N REDOR NMR. Carbon magnetization is prepared CP from protons and then evolves under proton decoupling and the influence of two ^{15}N π pulses per rotor period. The first ^{15}N π pulse is placed at one-half the rotor period ($P = 2$), or one-third ($P = 3$), or one-fourth ($P = 4$), and so on, including delays as short as one-seventh ($P = 7$) of the period. The second pulse ^{15}N π pulse occurs at the completion of each rotor period. A single ^{13}C π pulse replaces the ^{15}N π pulse in the middle of the evolution period and refocuses isotropic chemical shifts. The illustration is for four rotor cycles with $P = 7$. (Reproduced from Gullion and Schaefer[16] with permission.)

chemical shift anisotropy on the REDOR experiment and proposed the use of TOSS; they also proposed a new REDOR pulse-timing scheme[531] to reduce the possible heating effects of intense pulsing. Because the REDOR Hamiltonian is independent of the chemical shift interaction, spin-pair systems are studied in most REDOR experiments, and even an ideal TOSS sequence can restore only the central band intensity, hence the requirement of TOSS in REDOR experiments is not imperative and its merits are not evident. Li and Evans proposed improvements in excitation pulse sequences[532,533] and showed that supercycled XY-8 phase cycling has a better pulse imperfection tolerance and produces greater sensitivity. Recently, Mueller *et al.*[534,535] obtained an analytical REDOR solution and proposed a promising scheme called REDOR transform in which the dipolar coupling constants are directly shown on the frequency axis. The application of the REDOR technique covers a wide range of systems, from simple compounds,[16,517–523] to zeolites,[536–539] peptides,[540] proteins,[541] bacteria[542] and even insects.[543] Another recoupling scheme, called TRAPDOR (transfer of population double resonance) which uses population transfer, instead of coherence transfer, as in REDOR, has been proposed; this is designed especially for the recoupling of spin-1/2 and quadrupolar spins.[544–546] In TRAPDOR, continuous irradiation is applied to the quadrupolar nuclei, π pulses are not used, so it has better tolerance to pulse imperfections. Studies on recovering heteronuclear dipolar interactions to facilitate certain processes at high-speed MAS have also been carried out by several authors (see high-speed CPMAS, reviewed in Section 3.1).

5.5.2. Homonuclear echo dephasing

There are many ways of recoupling homonuclear spins. Homonuclear experiments are different from their heteronuclear counterparts because of two facts: (1) unlike heteronuclear dipolar interactions, the homonuclear dipolar Hamiltonian contains flip-flop terms, and (2) experiments are undertaken in one channel. There are basic and improved DRAMA[547–551] (Fig. 23), SEDRA,[552–555] USEME,[556–558] CROWN[559] sequences. In basic DRAMA (dipolar recoupling at the magic angle),[526,547] two $\pi/2$ pulses are applied in each rotor cycle to produce a spin echo in the spin space to cancel the rotational echo. A π pulse is applied at an odd number of rotor cycles to reduce the effects of the chemical shift interaction. The basic length of a DRAMA cycle thus includes four rotor cycles with eight $\pi/2$ pulses and two π pulses. DRAMA performs best when the isotropic chemical shift difference between the two coupled spins is small. The basic DRAMA sequence is sensitive to chemical shift anisotropy but it can be improved by the application of π pulses. Further refinement of DRAMA pulse sequences has been proposed by Tycko and Smith[549] by consideration of symmetry. The use of the XY-8 phase cycling scheme has been investigated by Zhu *et al.*[550] who noted that this phase cycling can remove the offset effects more effectively than previous sequences. The shortcomings of basic DRAMA can also be removed by MELODRAMA, i.e., DRAMA incorporated with spin locking, proposed by Sun *et al.*,[551] which is insensitive to both isotropic chemical shift difference and anisotropic chemical shifts. SEDRA (simple excitation for dephasing of rotational-echo amplitude)[552] can be regarded as the homonuclear version of REDOR. Because the two coupled spins are the same, there is one π pulse applied per rotor cycle. The basic SEDRA cycle contains two rotor cycles to refocus both the isotropic and anisotropic chemical shifts. To minimize the effects of the pulse imperfections and offset effects, a single π pulse is suggested to phase cycle according to the XY-8 scheme.[552–554] A similar scheme is r.f. driven recoupling (RFDR).[560] It is the same as SEDRA, but recoupling is accomplished by longitudinal polarization transfer. Controlled SEDRA (CEDRA)[555] was proposed to improve SEDRA, which is easy to implement, not very sensitive to pulse imperfections, but difficult to calibrate. SEDRA can be incorporated with two-dimensional experiments, either in the transverse, such as in DICSY,[561] and *t*-SEDRA[553,554] (Fig. 24a), or in the longitudinal direction, such as in RFDR[560] (Fig. 24b) and BDR,[562] the first two establish spin correlation while the last two establish the spin exchange. Another type of recoupling mechanism is suggested by Fujiwara *et al.*,[556] which utilizes unified spin echo and magic echo (USEME); this recoupling method is based on the fact that MAS averages dipolar coupling in real space while magic echo does this in spin space. The authors showed that if magic echo pulse and MAS are applied simultaneously, the dipolar interaction can be restored.[556,557] This sequence

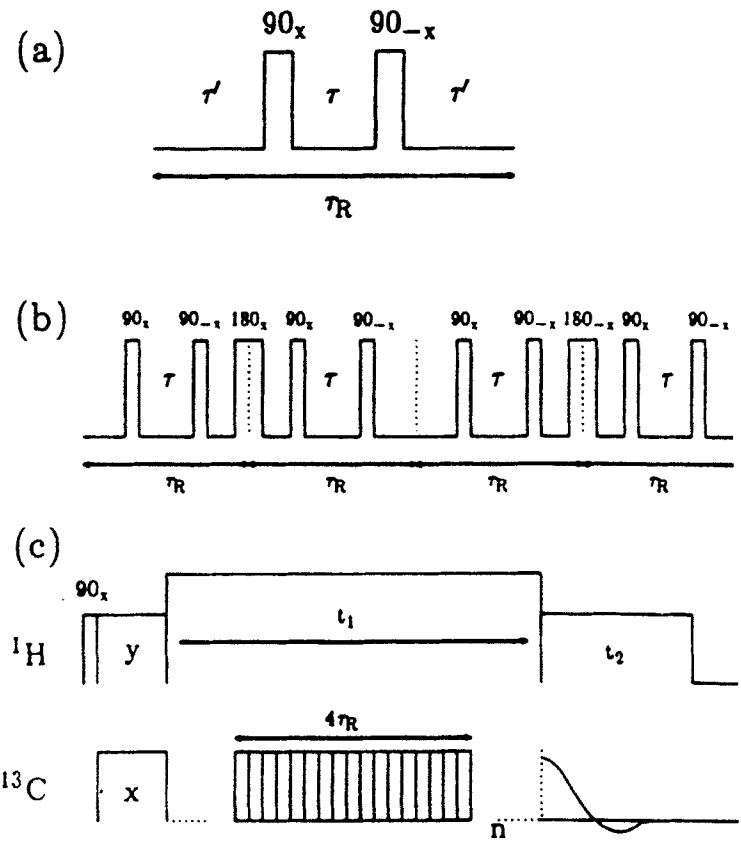

Fig. 23. Three versions of DRAMA pulse sequence. (a) Pulse sequence element that leads to non-zero average nuclear magnetic dipole–dipole couplings in a MAS NMR experiment. τ_R is the sample rotation period. As usual, θ_α denotes an r.f. pulse that rotates spin angular momenta by the angle θ about the axis α in the rotating frame. (b) Pulse sequence based on part (a) with the additional property that it averages out chemical shift anisotropy to 0th order and resonance offsets to 0th and first-order in coherent averaging theory. (c) Two-dimensional NMR experiment used to obtain experimental dipolar powder pattern spectra with MAS. Cross-polarization and proton decoupling are employed. The sequence in part (b) is applied in t_1, ^{13}C NMR signals are acquired in t_2. $T_1 = 4nt_R$, with n incremented from 0 to its maximum value. (Reproduced from Tycko and Dabbagh[547] with permission.)

is independent of isotropic and anisotropic chemical shift interactions. The method was subsequently modified by Baldus *et al.*[558] and applied to broad-band spin diffusion enhancement at high-speed MAS. USEME is a windowless sequence. Recently, another two windowless recoupling sequences were published,[563,564] which have characteristics similar to USEME. SEDRA (CEDRA), RFDR and DICSY depend on chemical shift differences

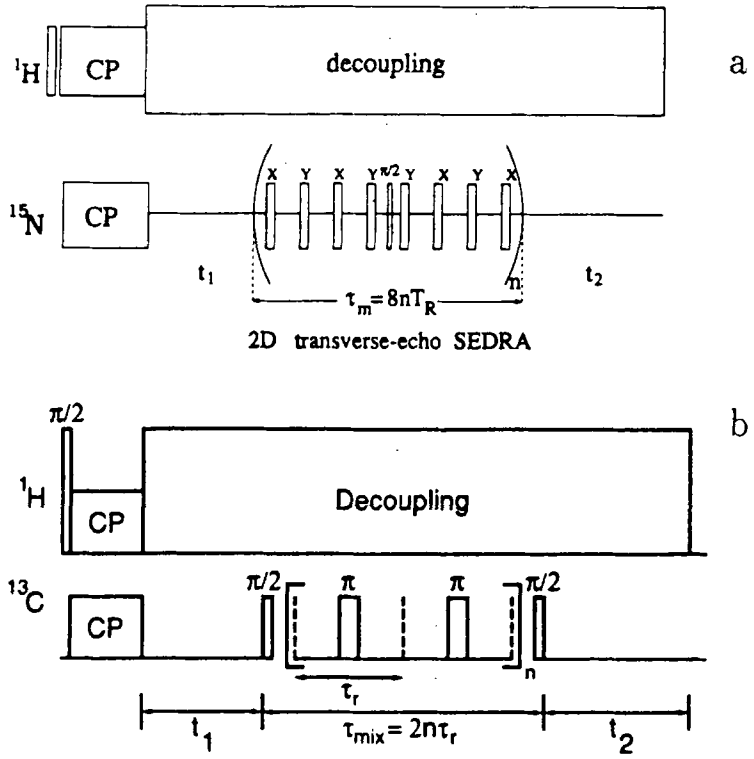

Fig. 24. (a) Two-dimensional transverse-echo SEDRA with t-SEDRA in the mixing time. The phase of the $\pi/2$ pulse is altered with x and y (reproduced from Weintraub *et al.*[554] with permission). (b) Two-dimensional homonuclear correlation (RFDR). The $\pi/2$ pulses set up longitudinal exchange. Mixing is accompanied by rotor-synchronized π pulses. (Reproduced from Benett *et al.*[560] with permission.)

and anisotropies, RFDR works best for spin pairs with large chemical shift differences, but is not very sensitive to the anisotropy. The dipolar nutation experiment[405–408] is extended to spinning solids and is called CROWN (combination of rotation with nutation).[559] It does not use δ-type pulses, but finite-width pulses. Demonstration of the recoupling function is given by Jores *et al.*[559] The effects of chemical shift interactions, and pulse imperfections, have not yet been studied.

To conclude this section, we state that interactions can be recovered simply from high-order effects because the MAS can average only out the first-order terms. When quadrupolar spins are involved, this is practically feasible because the second-order terms become evident. For example, the dipolar information can be extracted from the broadened CPMAS spectrum of a spin-1/2 nucleus bonded to a quadrupolar spin. This phenomenon can date

back to the observations of the dipolar splittings of single crystal spectra of the proton bonded to ^{55}Mn[565] and ^{13}C bonded to ^{14}N.[566,567] Later, a similar broadening was observed in the CPMAS spectra of ^{13}C bonded to ^{14}N.[568–570] This broadening is from the second-order quadrupole–dipole interference.[571–580] In addition to the C–N system, other systems such as P-Cu,[581] Sn-Cl,[582,583] C-As,[584] C-D[585,586] and C-H[84,86,382,388] have also been investigated. The effect of J coupling on lineshape has also been analysed.[579,587]

6. MULTI-QUANTUM COHERENCE

It is necessary first to clarify the definition of the multi-quantum transition in NMR. In NMR, especially in multi-quantum NMR spectroscopy, an n-quantum transition is defined as the process in which there are n quanta participating. As pointed out by Mehring,[40] this definition is different from that in general quantum mechanics but they are frequently confused in the literature. According to the latter, for a spin-1/2 system in high magnetic field, there is only a single quantum transition. The quantum mechanical definition is more in conformity with the (magnetic dipole forbidden) high-order transition induced by a strong CW r.f. field.[588–592] For multi-quantum transitions excited by coherent pulses, NMR definition is more convenient and is now adopted by most authors. Zero- and single-quantum transitions can be regarded as two special cases.

Multi-quantum spectroscopy is important in solid-state NMR because it has several valuable advantages:[33,40,593–597] (1) it can be used to simplify a crowded spectrum because the higher the order of the transitions, the fewer in number they are; (2) it can directly reflect structural and dynamic information because the creation of a high-order quantum transition requires many spins to evolve cooperatively; (3) in some cases, multi-quantum decoupling is less demanding; (4) the effect of a gradient field on an n-quantum transition (in spin-1/2 systems) is n times that of a single quantum transition.

Coherent pulsed multi-quantum spectroscopy in solids was initiated by Pines *et al.*[17] who successfully measured the chemical shift tensor of protons distributed in heavy ice, D_2O, by doublequantum decoupling. They also demonstrated that the double- quantum decoupling is more efficient. The Pines group,[17,598–600] Emid [601] and the Ernst group[602,603] have also studied double-quantum CP between spin-1/2 and deuterium, mediated by dipole order. Suter and Ernst[187,188] investigated the double-quantum spin diffusion in spin-1 systems including ^2H and ^{14}N. For quadrupolar spin systems, the magnetic dipole forbidden transitions can be excited by r.f. pulses because of the presence of the strong quadrupolar interactions. This fact has been used by Tycko and coworkers[604,605] who proposed the overtone NMR of ^{14}N;

it is actually the double quantum NMR of spin-1 systems with large electric field gradient tensors. The spectral width is dramatically reduced in the overtone spectroscopy. Considering the natural abundance of the ^{14}N nucleus in organic and biological materials, this method is useful for structural determination, as shown by Opella and other workers.[604–614] Combined with fundamental transition and the two-dimensional heteronuclear correlation method, overtone NMR is useful to determine the structure of compounds such as peptides. As shown in Fig. 25, the possibilities of the orientation of a peptide plane of single-crystal *N*-acetyl-D,L-valine (NAV) are reduced to two.[614] A simple and direct observation of a double-quantum transition of ^2H (with weak quadrupole coupling constants) by means of Raman magnetic resonance (RMR)[615] has been proposed by Yang and Ye.[616] The "Fictitious" operator formalism[33,617–619] and the multipole operator formalism[620–623] have been proposed to deal with the multi-quantum transition of quadrupolar systems. The latter is more general and concise and it is closer to the physical picture at zero or low field. Some of its applications have been shown.[620–623] In high fields, a direct relationship between them can easily be established by operator transformation. The operator set defined by the Fictitious operator formalism is overcomplete but it is more intuitive because in high-field NMR, one is interested in the magnetic quantum number. The multi-quantum solid-state NMR of spin-1/2 systems and that of quadrupolar systems differ in many aspects. Generally speaking, the excitation, manipulation and detection of the multi-quantum coherences (MQC) of quadrupolar systems are much more complicated than that of spin-1/2 systems. This is because of the presence of the strong quadrupolar interaction which renders a poorer magnetic quantum number, so the frequency of an MQC may not be a multiple of a single quantum coherence. Moreover, the strong quadrupolar interaction causes the excited MQCs to be highly anisotropic. Therefore, although the multi-quantum spectroscopy of solids began from the study of quadrupolar systems, more work has been accomplished for spin-1/2 systems where MQC is created by dipolar coupling.

The basic scheme of MQC spectroscopy in solids[17–20,33,40,593–597] is the same as that in liquids, i.e., MQC is prepared by a certain pulse sequence followed by an evolution under the internal Hamiltonian and then is converted by a mixing pulse into a magnetization that can be detected by a dipole coil (Fig. 26a). The simplest multi-quantum pulse sequence is shown in Fig. 26b. An essential difference between MQC in solids and in liquids is that MQC is, in most cases, created by dipolar interactions in solids while it is created by *J* coupling in liquids. The dipolar interaction is stronger and anisotropic and the excited MQCs are anisotropic and dephase easily, so the pulse sequence shown in Fig. 26b is used optimally in solids with weak dipolar interaction, such as pseudo-isolated molecules[18,19,593] and rare spin species in single crystals.[624] For general cases such as protons and ^{19}F, which are abundant and are strongly coupled in solids, Fig. 26b should be modified. Two major

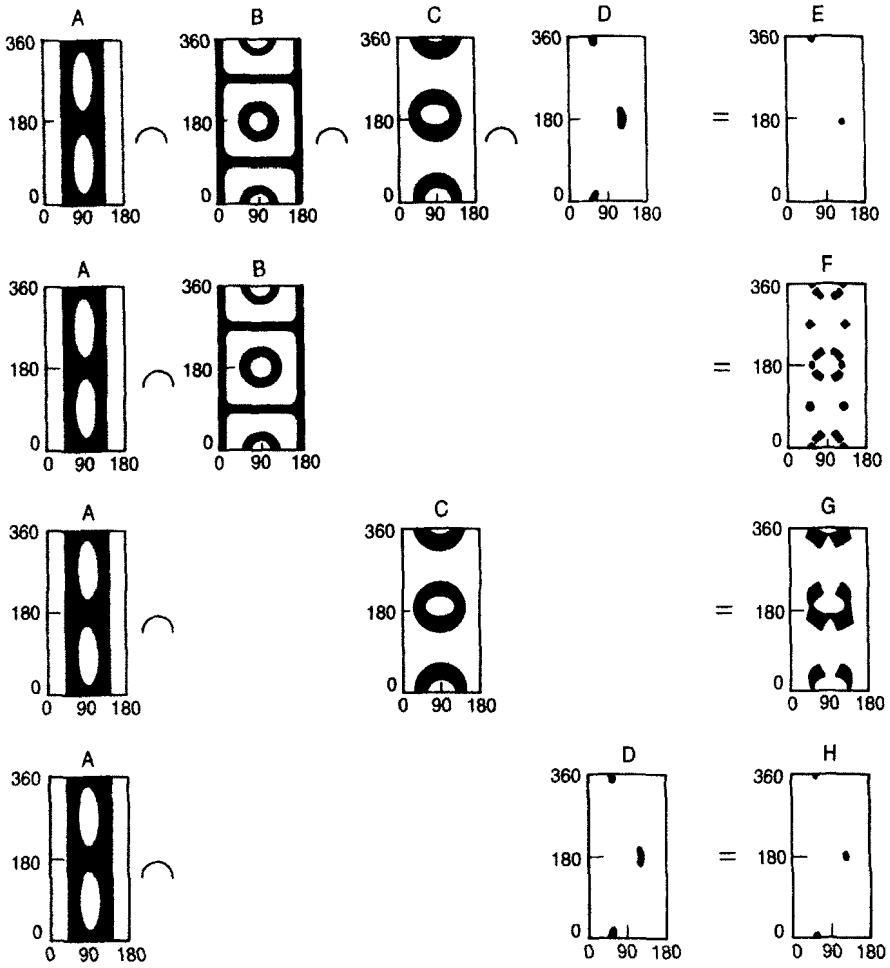

Fig. 25. Restriction plots calculated from the experimental spectral data associated with one molecule in the unit cell of NAV: (A) ^{14}N overtone shift, (B) $^{14}N/^{1}H$ dipolar splitting, (C) ^{1}H chemical shift, (D) $^{1}H/^{14}N$ dipolar splittings, (E) the intersection of all four types of experimental data, (F) the intersection of the data obtained with a ^{14}N separated local field experiment alone, (G) the intersection of the data with the ^{14}N overtone shift and ^{1}H chemical shift alone, and (H) the intersection of the data obtained with ^{14}N overtone shift and $^{1}H/^{14}N$ dipolar splitting alone. (Reproduced from McNamara *et al.*[614] with permission.)

improvements have been made. One is by selective excitation,[19,20] which can decrease the number of MQCs so that the MQC spectrum becomes simpler and the interference between different orders of MQC is reduced thus enhancing sensitivity. The other important improvement[20,21] is produced by using the time-reversal sequence[349] (see Fig. 26c) by which the propagator in the preparation period is the reciprocal of that in the mixing period. Using

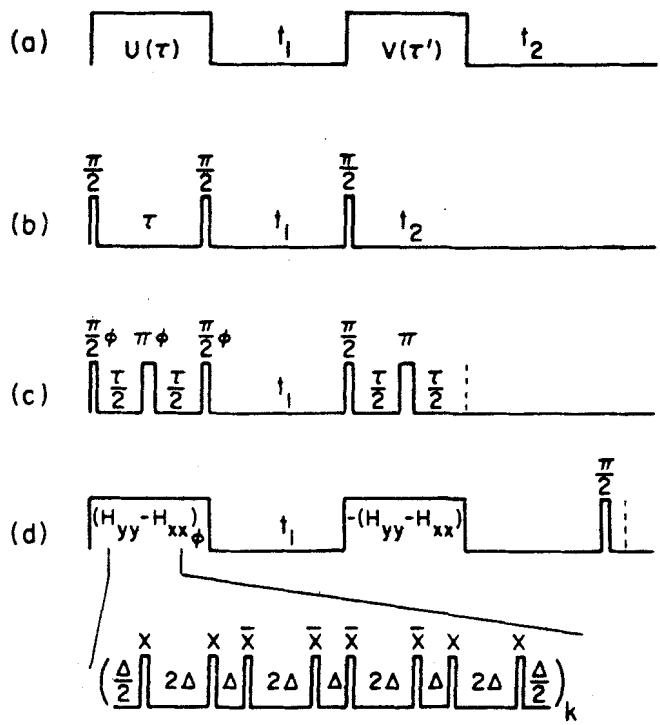

Fig. 26. Multi-pulse sequences: (a) schematic pulse sequence showing relevant periods; (b) nonselective three-pulse experiment; (c) even-selective sequence with preparation pulses phase shifted by an amount $\phi = \Delta\omega t_1$ (TPPI) to separate n-quantum orders; (d) time-reversed preparation and mixing periods with preparation $\pi/2$ pulses phase shifted by an amount ϕ (TPPI). The preparation and mixing periods are composed of cycles of eight-pulse sequences shown below. A delay of about 1.6 ms separates the mixing period from the final detecting pulse to allow transients to decay away. (Reproduced from Yen and Pines[21] with permission.)

this technique, the phase of all orders of MQC excited is the same so there is no cancellation arising from the interference among different orders of MQC. Consequently, the MQC spectrum is purely absorptive, while the sensitivity is increased. Yen and Pines[21] were the first to demonstrate the usefulness of this method in MQC in solids by observing the proton MQC up to order 22 in adamantane. This sequence was further perfected so that it works more efficiently and higher orders of MQC are observed. MQCs up to 100th order for protons in adamantane have been reported by Baum *et al.*[625] Scruggs and Gleason[626] applied this method to ^1H–^{19}F heteronuclear MQC and they observed a 22-quantum coherence with 180 spins correlated. Because of the relief brought about by the time-reversal sequence, all orders of MQC can be recorded in a spectrum, as shown by Suter *et al.*[627]

The time-reversal sequence is particularly useful for determining the size of spin clusters in solids because, on the one hand, MQC in a multi-spin system decays fast rapidly owing to strong dipolar couplings, while on the other, it takes longer to excite higher orders of MQC. Using this method, Pines' group[628,629] studied the relationship between the hydrogen concentration and bonding in hydrogenated noncrystalline silicon and showed that, at low hydrogen concentration, the bonding occurs in clusters with the size of about six to seven atoms while the cluster size increases with hydrogen concentration until an infinite network is formed. This method was also used by Gleason and coworkers[630,631] and Emid[632] to investigate the microstructures of hydrogenated noncrystalline silicons and hydrogenated noncrystalline silicon carbonates. When the clusters are relatively isolated from each other, the number of spins in a cluster can be conveniently counted by determining the highest order of MQC in the cluster. This spin-counting technique is especially useful for aphormous systems, as shown by Ryoo *et al.*[633] who have studied the distribution of the hexamethylbenzene molecules adsorbed in zeolites and concluded, from MQC spectra, that there are about 16 protons in each cluster; because there are 18 protons in each hexamethylbenzene molecule, this counting is reliable.

A unique MQC method has been proposed by Emid and Greyghton[634] and Shykind *et al.*[635] In their scheme, the evolution time is fixed and the phase of the preparation pulses is changed step by step. Therefore, the variable in the first dimension is the phase instead of time. The acquired signal is then Fourier transformed with respect to the phase variable. Because there is no broadening factor in the first dimension, the MQC spectrum along the first frequency axis is a spike spectrum with infinite resolution (Fig. 27). This technique performs well with a phase shifter installed in the spectrometer because phase increments as small as 0.1° may be required in some cases. This is no longer a limitation because phase shifters are available on most commercial machines. The demonstration of the advantages of this method were demonstrated by Shykind *et al.*[635]

The theoretical description of the evolution of MQC in a dipolar coupled multi-spin system was widely carried out by Munowitz and coworkers.[595,636–638] A "walk model" was proposed where the generation of MQC is regarded as a density operator walking in Liouville space according to certain rules. Under the second-order approximation, the excitation rates can be evaluated.[636] For special spin configurations, especially when the number of spins is not large, the evolution of MQC can be exactly calculated by numerical simulation.[638–641] When the configuration comprises a large number of spins and when the relaxation effect should be included, approximations should be used. A comprehensive discussion of the generation of MQC in dipolar coupled multi-spin systems can be found in Lacelle's review paper[642] where a series of models is elaborated and some elegant physical sights are shown.

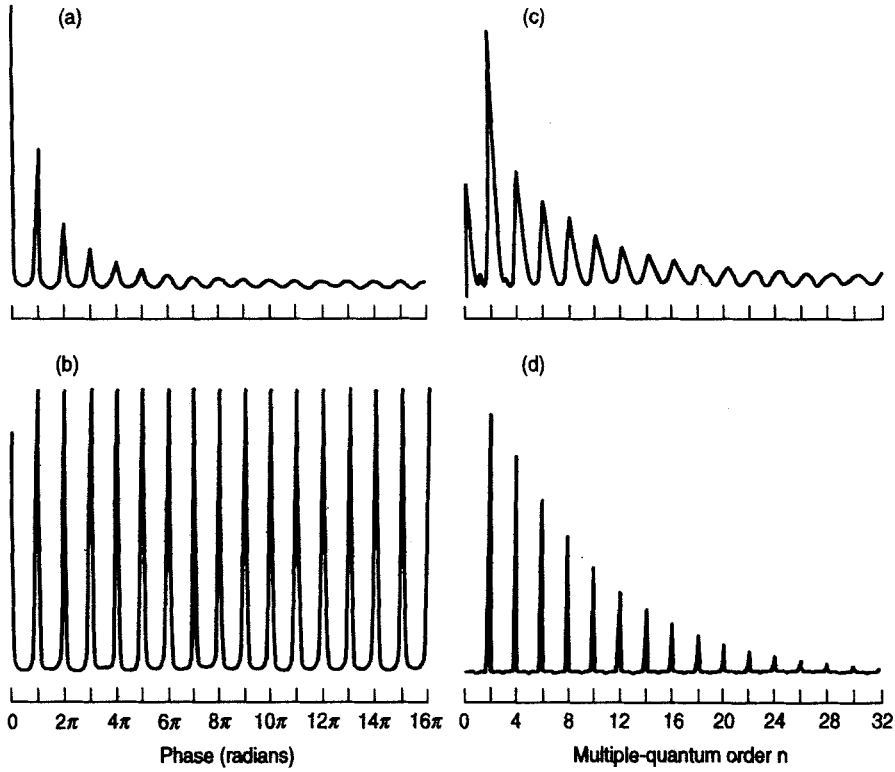

Fig. 27. Multi-quantum NMR signals of hexamethylbenzene. (a) Time-domain MQ interferogram using the TPPI method and the pulse sequence shown in Fig. 26d. The experimental parameters used are $\Delta = 2.5\,\mu s$, $t_p = 3\,\mu s$, $\Delta' = 8\,\mu s$, unit cycle time $\tau_c = 66\,\mu s$, number of cycles $m = \pi/\tau_c = 8$, $\Delta t_1 = 100\,\mu s$, and $\Delta\phi = \pi/32$. The spectrum was obtained on a 180 MHz spectrometer. (b) Similar to (a) but using phase-incremented method. Here, $\Delta = 2\,\mu s$, $t_p = 4\,\mu s$, $\Delta' = 8\,\mu s$, $\tau_c = 72\,\mu s$, $m = 8$, fixed $t_1 = 100\,\mu s$, $\Delta\phi = \pi/128$ radians. A 100 MHz spectrometer was used. Notice that, for this even-quantum excitation, the signal is periodic over π radians. The signal is strictly periodic over full 2π radians, and the data over the first 2π have been translated to fill 16π radians, to facilitate comparison with (a). (c) A Fourier transform of (a) with respect to t_1 yields a spectrum with broadlines, each appearing at even MQ orders. The intensity of the zero-quantum line is arbitrary. (d) Fourier transform of (b) with respect to ϕ in the phase-incremented MQ experiment. The MQ lines are now infinitely narrow, as expected; the apparent width arises from the plotter connecting the data points. (Reproduced from Shykind *et al.*[635] with permission.)

The pulse sequences shown in Fig. 26 may not be efficient for rotating samples when the rotation significantly affects the dipolar interactions that generate MQC. This situation occurs when the dipolar interaction is weak, either because of a large spin separation or a small gyromagnetic ratio. One remedy is to set the excitation time to much less than a spinning period so

that MQC is established before it is refocused by sample spinning.[643] Levitt *et al.*[46] and Meier and Earl[644] proposed to modulate the pulse phases in the sequence to cancel the effect of sample spinning. The resolution of MQC spectra can be enhanced because the detection is undertaken with MAS[46,644–647] This technique is useful for weakly coupled multi-spin systems. Ba and Veeman[645–647] have shown that similar results can be obtained with the modification of the pulses in preparation and mixing periods. Associated with the method proposed by Emid and Greyghton.[634] they demonstrated the applicability of MQC detection by CPMAS to obtain an MQC spectrum that was highly resolved in both dimensions. For spin systems with low gyromagnetic ratios, the effect of the chemical shift anisotropy emerges and the various methods of recovering dipolar interactions under MAS, introduced in Section 4, should be employed to obtain the corresponding MQC spectra. The methods most used are static or slow spinning samples[45,643] with off-magic-angle spinning,[648] rotational resonance or rotary resonance,[502,503] and DRAMA and its variants.[159,548,649–652] It is important to be familiar with the advantages and disadvantages of these methods because it is crucial in deciding which sequence should be utilized for a specific system.

7. ZERO FIELD

The presence of a strong applied magnetic field reduces the spatial symmetry from $SO(3)$ to $SO(2)$ and the internal Hamiltonian from a scalar to a tensor, which generally corresponds to a broad spectrum for a powder sample. The broad spectra can be narrowed by the various methods introduced in Section 3, but for some small interactions, such as J coupling or for systems with inequivalent sites with similar coupling constants, it is difficult to determine the coupling constants even by using narrowed spectra. For example, the dipolar coupling constants of ^2H systems, which have large quadrupolar coupling constants, cannot easily be evaluated from the highest resolved spectra. Therefore, the restoration of the $SO(3)$ symmetry, i.e., the removal of the static magnetic field, becomes necessary in these situations. Three different techniques have been proposed to date.

7.1. Pure zero-field method

This is the most straightforward method for recovering the $SO(3)$ symmetry of the systems. The spins are in zero field at all times, from excitation to evolution to detection. There are practical difficulties in the use of this method: first, the sensitivity is too low; second, the usual Faraday induction detector, whose induction voltage is proportional to the oscillating frequency, cannot be used. These difficulties can be overcome by the use of SQUID

technology and the pure zero-field spectra of a series of compounds have been obtained.[653,654]

7.2. Field cycling

To acquire sufficient sensitivity, the indirect method was proposed.[22,655–669] The spin systems are polarized and detected in high magnetic field to achieve high sensitivity but the excitation and evolution are carried out in zero field to record zero-field evolution information. This is a two-dimensional method, i.e., high-field–zero-field correlation spectroscopy. Because the evolution and detection are undertaken in different fields, experimentally, the sample needs to shuttle from zero field to high field. This technique is sensitive, especially for systems with a short T_2. A comprehensive introduction to this method is given by Zax *et al.*[22] One example of a zero-field–high-field correlation spectrum is shown in Fig. 28. The general procedure of calculating a zero-field lineshape was shown by Zax *et al.*[22] When a low-frequency pulse is applied[657,658] or when dynamics[659–664] are considered, the calculation should be changed accordingly. The Pines group[668,670–672] and the Ernst group[658] investigated the effects of direct currents or low-frequency pulses on zero-field evolution and their remedies. They also explored the possibility of the application of pulse sequences, and phase cycling to zero-field NMR. Various applications of field cycling zero-field NMR have been found, such as in liquid crystals[673–675] and spin diffusion.[676] Zero-field cycling has also been "transplanted" to NQR.[677,678] Because the phase shift cannot be utilized for direct current pulses, while low-frequency pulses bring about extra time-dependence of the Hamiltonian, there are still difficulties in this method.

7.3. Zero field in high magnetic field

The spin systems are always in a high magnetic field and the scalar part of the internal interactions is extracted by r.f. pulse sequences. This is actually a virtual zero-field method. The basic principle of this method is that although the secular part of the internal Hamiltonian is a rank-2 tensor, it can be expanded in terms of different ranks of tensors where the 0th-rank tensor is the scalar and the higher-rank tensors are averaged out by appropriate pulses and sample rotation. Tycko gave the detail theoretical analysis of this method and found numerically a series of r.f. pulse sequences and the requirements on sample spinning.[23,679–682] Sun and Pines[683] proposed numbers of exact solutions and found some new sequences. There are some direct advantages in this method in that there is no need to modify spectrometer hardware and the sensitivity and resolution are high. The disadvantages are that the scalar recovered by this method is scaled down

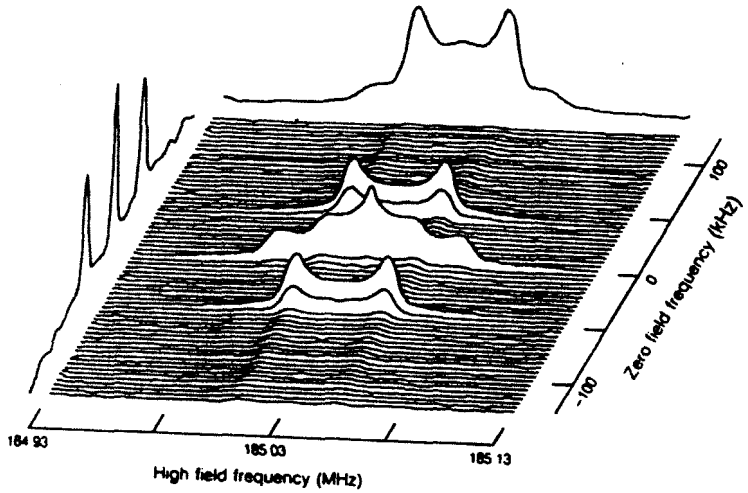

Fig. 28. Two-dimensional zero-field–high-field dipolar correlation spectrum of polycrystalline $Ba(ClO_3)_2.H_2O$. For each of 64 values of t_1, the zero-field interval, the high-field FID after a solid echo sequence is accumulated and stored. A double real Fourier transform in t_1 and t_2 is applied to the signal $S(t_1, t_2)$. At the left and top are projections of the zero-field and high-field spectra. In the centre, the correlations between the two frequency domains. Signals which appear at zero frequency in ω_1 correlate most strongly with signals from orientations of the two-spin system which are nearly at the edges of the high-field powder pattern. Zero-field signals which appear at ±42 kHz correlate to orientations which appear near the peaks (at ±21 kHz) of the high-field powder pattern. (Reproduced from Zax *et al.*[22] with permission.)

and the scaling factor is sensitive to pulse imperfections and the synchronization of the sample spinning and pulsing, which should become less and less as the development of modern spectrometer technology increases.

At this point, it is worth noting the difference between zero-field NMR and NQR. For quadrupolar spin systems, NQR is zero-field NMR. However, there are differences in practice. For instance, NQR is usually directed to systems with large quadrupolar coupling constants so that the sensitivity is good, while zero-field NMR deals mainly with those systems with smaller quadrupolar coupling constants and particularly, the dipolar, scalar couplings are emphasized. Moreover, the Hamiltonian in NQR is not a scalar but instead a tensor with privileged directions decided by the electric field gradient principal axes.

ACKNOWLEDGEMENTS

The authors are grateful to Dr G. A. Webb for his encouragement and helpful comments on this work. This work was financially supported by the National

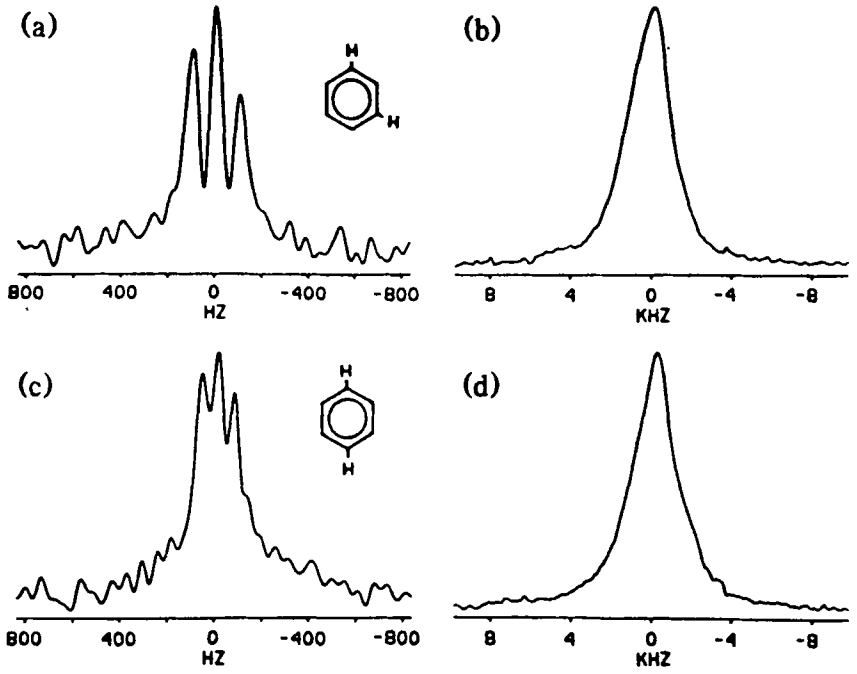

Fig. 29. (a) Untruncated high-field proton NMR spectrum of 4% meta-$C_6H_2D_4$ in 96% C_6D_6, in which the orientation dependence of the proton–proton dipolar couplings has been removed by spinning of the sample about an axis at 75° to the static magnetic field and application of the r.f. pulse sequence shown in Fig. 2 of Tycko.[679] The spectrum resembles the zero-field NMR spectrum of randomly oriented pairs of coupled nuclei. (b) Single-pulse spectrum of 4% meta-$C_6H_2D_4$ in 96% C_6D_6. Note the different frequency scale. (c) Untruncated spectrum of 4% *para*-$C_6H_2D_4$ in 96% C_6D_6, showing the dependence of the dipolar splittings on the internuclear distance. (d) Single-pulse spectrum of 4% *para*-$C_6H_2D_4$ in 96% C_6D_6. All spectra were obtained at approximately −35°C. (Reproduced from Tycko[679] with permission.)

Natural Science Foundation of China. S. D. gratefully acknowledges the support of K. C. Wong Education Foundation, Hong Kong.

REFERENCES

1. E. R. Andrew, A. Bradbury and R. G. Eades, *Nature*, 1958, **182**, 1659.
2. I. J. Lowe, *Phys. Rev. Lett.*, 1959, **2**, 285.
3. M. M. Maricq and J. S. Waugh, *J. Chem. Phys.*, 1979, **70**, 3300.
4. A. G. Anderson and S. R. Hartman, *Phys. Rev.*, 1960, **126**, 2033.
5. S. R. Hartman and E. L. Hahn, *Phys. Rev.*, 1962, **128**, 2042.
6. A. Pines, M. G. Gibby and J. S. Waugh, *J. Chem. Phys.*, 1972, **56**, 1776.

7. A. Pines, M. G. Gibby and J. S. Waugh, *J. Chem. Phys.*, 1973, **59**, 569.
8. J. Schaefer and E. O. Stejskal, *J. Am. Chem. Soc.*, 1976, **98**, 1031.
9. E. O. Stejskal, J. Schaefer and J. S. Waugh, *J. Magn. Reson.*, 1977, **28**, 105.
10. E. D. Ostraff and J. S. Waugh, *Phys. Rev. Lett.*, 1966, **16**, 1097.
11. P. Mansfield and D. Ware, *Phys. Lett.*, 1966, **22**, 133.
12. U. Haeberlen and J. S. Waugh, *Phys. Rev.*, 1968, **175**, 453.
13. B. C. Gerstein, R. G. Pembleton, R. C. Wilson and L. M. Ryan, *J. Chem. Phys.*, 1977, **66**, 362.
14. C. P. Slichter, *Principles of Magnetic Resonance*, 3rd edn. Springer-Verlag, Berlin, 1990.
15. P. K. Wang, C. P. Slichter and J. H. Sinfelt, *Phys. Rev. Lett.*, 1984, **53**, 82.
16. T. Gullion and J. Schaefer, *J. Magn. Reson.*, 1989, **81**, 196.
17. A. Pines, D. J. Ruben, S. Vega and M. Mehring, *Phys. Rev. Lett.*, 1976, **36**, 110.
18. S. Emid, A. Bax, J. Konijnendijk, J. Smidt and A. Pines, *Physica*, 1979, **B96**, 333.
19. S. Emid, J. S. Smidt and A. Pines, *Chem. Phys. Lett.*, 1980, **73**, 496.
20. W. S. Warren, D. P. Weitekamp and A. Pines, *J. Chem. Phys.*, 1980, **73**, 2084.
21. Y. S. Yen and A. Pines, *J. Chem. Phys.*, 1983, **78**, 3579.
22. D. B. Zax, A. Bielecki, K. T. Zilm, A. Pines and D. P. Weitekamp, *J. Chem. Phys.*, 1985, **83**, 4877.
23. R. Tycko, *J. Magn. Reson.*, 1987, **75**, 193.
24. A. Llor and J. Virlet, *Chem. Phys. Lett.*, 1988, **152**, 248.
25. B. F. Chmelka, K. T. Mueller, A. Pines, J. Stebbins, Y. Wu and J. W. Zwanziger, *Nature*, 1989, **42**, 339.
26. A. Samoson, E. Lippmaa and A. Pines, *Mol. Phys.*, 1988, **65**, 1013.
27. L. J. Friedman, P. Millet and R. C. Richardson, *Phys. Rev. Lett.*, 1981, **47**, 1078.
28. J. S. Waugh, O. Gonen and P. L. Kuhns, *J. Chem. Phys.*, 1987, **86**, 3816.
29. H. Wernan, M. Godlewski and B. Monemar, *Phys. Rev.*, 1988, **B38**, 12525.
30. C. von Borczyskowski, *Adv. Magn. Reson.*, 1988, **12**, 113.
31. R. A. Wind, M. J. Duijvestijn, C. VanderLugt, A. Manenschijn and J. Vreind, *Progr. NMR Spectrosc.*, 1985, **17**, 33.
32. M. J. Duijvestijn, A. Manenschijn, J. Schmidt and R. A. Wind, *J. Magn. Reson.*, 1985, **64**, 461.
33. R. R. Ernst, G. Bodenhausen and A. Wokaun, *Principles of Nuclear Magnetic Resonance in One and Two Dimensions*, Clarendon Press, Oxford, 1987.
34. K. Schmidt-Rohr and H. W. Spiess, *Multidimensional Solid State NMR and Polymers*, Academic Press, London, 1994.
35. P. T. Callaghan, *Principles of NMR Microscopy*. Clarendon Press, Oxford, 1991.
36. P. Jezzard, J. J. Attard, T. A. Carpenter and L. D. Hall, *Progr. NMR Spectrosc.*, 1991, **23**, 1.
37. D. G. Cory, *Annu. Rep. NMR Spectrosc.*, 1992, **24**, 87.
38. P. Blümer and B. Blümich, *NMR: Basic Principles Prog.*, 1994, **30**, 209.
39. U. Haeberlen, *High Resolution NMR in Solids: Selective Averaging*. Academic Press, New York, 1976.
40. M. Mehring, *Principles of High Resolution NMR in Solids*. Springer-Verlag, Berlin, 1983.
41. M. M. Maricq, *Phys. Rev.*, 1982, **B25**, 6622.
42. M. M. Maricq, *Adv. Magn. Reson.*, 1990, **14**, 151.
43. D. P. Raleigh, G. S. Harbison, T. G. Neiss, J. E. Roberts and R. G. Griffin, *Chem. Phys. Lett.*, 1987, **138**, 285.
44. D. P. Raleigh, M. H. Levitt and R. G. Griffin, *Chem. Phys. Lett.*, 1988, **146**, 71.
45. B. H. Meier, *J. Am. Chem. Soc.*, 1987, **109**, 7937.
46. M. H. Levitt, T. G. Oas and R. G. Griffin, *Isr. J. Chem.*, 1988, **28**, 271.

47. Z. Gan and D. M. Grant, *Mol. Phys.*, 1989, **67**, 1419.
48. M. H. Levitt, D. P. Raleigh, F. Greuzet and R. G. Griffin, *J. Chem. Phys.*, 1990, **92**, 6347.
49. T. Nakai, R. Challoner and C. A. McDowell, *Chem. Phys. Lett.*, 1991, **180**, 13.
50. R. Challoner, T. Nakai and C. A. McDowell, *J. Chem. Phys.*, 1991, **94**, 7038.
51. R. Challoner, T. Nakai and C. A. McDowell, *J. Magn. Reson.*, 1991, **94**, 433.
52. K. Eichele, G. Wu and R. E. Wasylishen, *J. Magn. Reson.*, 1993, **A101**, 157.
53. M. Goldman, R. J. Grandinetti, A. Llor, Z. Olejniczak, J. R. Sachleben and J. W. Zwanziger, *J. Chem. Phys.*, 1992, **97**, 8947.
54. J. H. Shirley, *Phys. Rev.*, 1965, **138**, 979.
55. Y. Zur, M. H. Levitt and S. Vega, *J. Chem. Phys.*, 1983, **78**, 5293.
56. Y. Zur and S. Vega, *J. Chem. Phys.*, 1983, **79**, 548.
57. A. Schmidt and S. Vega, *J. Chem. Phys.*, 1987, **87**, 6895.
58. S. Vega, E. T. Olejniczak and R. G. Griffin, *J. Chem. Phys.*, 1984, **80**, 4832.
59. D. B. Zax, G. Goleman, D. Abramovich and S. Vega, *Adv. Magn. Reson.*, 1990, **14**, 214.
60. A. Kubo and C. A. McDowell, *J. Chem. Phys.*, 1990, **92**, 7156.
61. A. Schmidt and S. Vega, *J. Chem. Phys.*, 1992, **32**, 215.
62. T. Nakai and C. A. McDowell, *J. Chem. Phys.*, 1992, **96**, 3452.
63. A. Schmidt and S. Vega, *J. Chem. Phys.*, 1992, **96**, 2655.
64. T. Nakai and C. A. McDowell, *Mol. Phys.*, 1992, **77**, 569.
65. O. Weintraub and S. Vega, *J. Magn. Reson.*, 1993, **A105**, 245.
66. D. Abramovich and S. Vega, *J. Magn. Reson.*, 1994, **A105**, 30.
67. D. Abramovich, S. Vega, J. Quant and S. J. Glaser, *J. Magn. Reson.*, 1995, **A115**, 222.
68. M. P. Augustine, K. W. Zilm and D. B. Zax, *J. Chem. Phys.*, 1993, **98**, 9432.
69. H. Mori, *Prog. Theor. Phys. Jpn.*, 1965, **33**, 423.
70. H. Mori, *Prog. Theor. Phys. Jpn.*, 1965, **34**, 399.
71. T. Shimizu, *J. Phys. Soc. Jpn.*, 1970, **28**, 811.
72. F. Lado, J. D. Memory and G. W. Parker, *Phys. Rev.*, 1971, **B4**, 1406.
73. D. Kivelson and K. Ogan, *Adv. Magn. Reson.*, 1974, **7**, 71.
74. G. W. Parker and F. Lado, *Phys. Rev.*, 1973, **B8**, 3081.
75. D. E. Demco, J. Tegenfeldt and J. S. Waugh, *Phys. Rev.*, 1975, **B11**, 4133.
76. J. Jeener, *Adv. Magn. Reson.*, 1982, **10**, 2.
77. P. Borckmans and D. Walgraef, *Phys. Rev.*, 1968, **167**, 282.
78. P. Borckmans and D. Walgraef, *Phys. Rev. Lett.*, 1968, **21**, 1516.
79. P. Resibois and M. De Leener, *Phys. Rev.*, 1966, **152**, 305.
80. J. H. van Vleck, *Phys. Rev.*, 1948, **74**, 1148.
81. A. Abraham, *Principles of Nuclear Magnetism*. Clarendon Press, Oxford, 1961.
82. S. J. K. Jensen and E. K. Hansen, *Phys. Rev.*, 1973, **B7**, 2910.
83. M. Engelberg and I. J. Lowe, *Phys. Rev.*, 1974, **B10**, 822.
84. S. Ding and C. A. McDowell, *J. Magn. Reson.*, 1994, **A111**, 212.
85. S. Ding and C. A. McDowell, *J. Magn. Reson.*, 1995, **A115**, 141.
86. S. Ding and C. A. McDowell, *J. Magn. Reson.*, 1995, **A117**, 171.
87. M. Goldman, in *Nuclear Magnetic Double Resonance* (ed. B. Maraviglia). North-Holland, Amsterdam, 1993.
88. J. Wei and E. Norman, *J. Math. Phys.*, 1963, **4**, 575.
89. J. Wei and E. Norman, *Proc. Am. Math. Soc.*, 1964, **15**, 327.
90. G. Campolieti and B. C. Sanctuary, *J. Chem. Phys.*, 1989, **91**, 2108.
91. G. Theimer and G. Bodenhausen, *Appl. Magn. Reson.*, 1992, **3**, 981.
92. G. Theimer and G. Bodenhausen, *Appl. Magn. Reson.*, 1992, **3**, 1071.
93. C. J. Lee, N. Murali and W. S. Warren, *Adv. Magn. Reson.*, 1990, **14**, 241.

94. H. Kessler, M. Gehrke and C. Griesnger, *Angew. Chem.*, 1988, **100**, 507.
95. C. A. Fyfe, H. Gies and Y. Feng, *J. Am. Chem. Soc.*, 1989, **111**, 7702.
96. W. Kolodziejski, P. J. Barrie, H. He and J. Klinowski, *J. Chem. Soc. Chem. Commun.*, 1991, 961.
97. W. Kolodziejski and J. Klinowski, *Solid State NMR*, 1992, **1**, 41.
98. A. J. Vega, *J. Am. Chem. Soc.*, 1988, **110**, 1049.
99. C. A. Fyfe, H. Gies, Y. Feng and G. T. Kokotailo, *Nature*, 1989, **341**, 223.
100. C. A. Fyfe, H. Gies, H. Grondey and G. T. Kokotailo, *J. Am. Chem. Soc.*, 1990, **112**, 3264.
101. R. E. Walstedt, D. C. McArthur and E. L. Hahn, *Phys. Lett.*, 1965, **15**, 7.
102. R. E. Slusher and E. L. Hahn, *Phys. Rev.*, 1968, **166**, 332.
103. D. A. McArthur, E. L. Hahn and R. E. Waldstedt, *Phys. Rev.*, 1969, **188**, 609.
104. D. V. Lang and P. R. Moran, *Phys. Rev.*, 1970, **B1**, 53.
105. H. Stokes and D. C. Allion, *Phys. Rev.*, 1977, **B15**, 1271.
106. T. T. P. Chueng and R. Yaris, *J. Chem. Phys.*, 1979, **72**, 3604.
107. S. Ding and C. Ye, *Solid State NMR*, 1992, **1**, 321.
108. D. L. Vander Hart, *J. Magn. Reson.*, 1982, **72**, 13.
109. X. Wu, S. Zhang and X. Wu, *J. Magn. Reson.*, 1988, **77**, 343.
110. X. Wu, S. Zhang and X. Wu, *Phys. Rev.*, 1988, **B37**, 9827.
111. S. Zhang and X. Wu, *Chem. Phys. Lett.*, 1989, **156**, 82.
112. S. Zhang and X. Wu, *Chem. Phys. Lett.*, 1989, **150**, 333.
113. S. Zhang and X. Wu, *Chem. Phys. Lett.*, 1989, **166**, 92.
114. S. Zhang and X. Wu, *Chem. Phys. Lett.*, 1989, **156**, 79.
115. S. Zhang, X. Wu, H. Zhang and X. Wu, *Chem. Phys. Lett.*, 1990, **165**, 465.
116. X. Wu and K. T. Zilm, *J. Magn. Reson.*, 1991, **93**, 265.
117. D. G. Gory, *Chem. Phys. Lett.*, 1988, **152**, 431.
118. X. Wu, X. Xie and X. Wu, *Chem. Phys. Lett.*, 1989, **162**, 325.
119. L. Jelinski and M. Melchoir, in *NMR Spectroscopic Techniques* (eds C. R. Dybowsk and R. Lichter), Dekker, New York, 1987.
120. N. Zumbulyadis and J. M. O'Reilley, *J. Magn. Reson.*, 1989, **82**, 613.
121. X. Wu and K. T. Zilm, *J. Magn. Reson.*, 1993, **A102**, 205.
122. X. Wu and K. T. Zilm, *J. Magn. Reson.*, 1993, **A104**, 119.
123. X. Wu and K. T. Zilm, *J. Magn. Reson.*, 1993, **A104**, 154.
124. X. Wu, S. T. Burns and K. T. Zilm, *J. Magn. Reson.*, 1994, **A111**, 29.
125. R. Sangill, N. Rastrup-Anderson, H. Bildsøe, H. J. Jakobsen and N. C. Nielsen, *J. Magn. Reson.*, 1994, **A107**, 67.
126. O. W. Sørensen, *Progr. NMR Spectrosc.*, 1989, **21**, 503.
127. A. G. Redfield, *J. Magn. Reson.*, 1991, **92**, 642.
128. O. W. Sørensen, *J. Magn. Reson.*, 1991, **93**, 648.
129. M. H. Levitt, *J. Magn. Reson.*, 1992, **99**, 1.
130. L. Emsley and A. Pines, in *Nuclear Magnetic Double Resonance* (ed. B. Maraviglia), North-Holland, Amsterdam, 1993.
131. N. C. Nielsen and O. W. Sørensen, *J. Magn. Reson.*, 1992, **99**, 214.
132. N. C. Nielsen and O. W. Sørensen, *J. Magn. Reson.*, 1992, **99**, 494.
133. J. Stoustrap, O. Shedletzky, S. J. Glaser, C. Griesinger, N. C. Nielsen and O. W. Sørensen, *Phys. Rev. Lett.*, 1995, **74**, 2921.
134. N. C. Nielsen and O. W. Sørensen, *J. Magn. Reson.*, 1995, **A114**, 24.
135. N. C. Nielsen, T. Shulte-Herbrüggen and O. W. Sørensen, *Mol. Phys.*, 1995, **85**, 1205.
136. M. H. Levitt, D. Suter and R. Ernst, *J. Chem. Phys.*, 1986, **84**, 4243.
137. S. Zhang, B. H. Meier, S. Appelt, M. Mehring and R. R. Ernst, *J. Magn. Reson.*, 1993, **A101**, 60.
138. S. Zhang, B. H. Meier and R. R. Ernst, *J. Magn. Reson.*, 1994, **A108**, 30.

139. E. O. Stejskal, J. S. Waugh and J. S. Waugh, *J. Magn. Reson.*, 1977, **28**, 105.
140. R. C. Ziegler, R. A. Wind and G. E. Maciel, *J. Magn. Reson.*, 1988, **79**, 299.
141. M. Sardashthi and G. E. Maciel, *J. Magn. Reson.*, 1987, **72**, 467.
142. R. A. Wind, S. F. Dec, H. Lock and G. E. Maciel, *J. Magn. Reson.*, 1986, **79**, 186.
143. S. Ding, C. A. McDowell and C. Ye, *J. Magn. Reson.*, 1994, **A109**, 1.
144. S. Ding, C. A. McDowell and C. Ye, *J. Magn. Reson.*, 1994, **A109**, 6.
145. B. H. Meier, *Chem. Phys. Lett.*, 1992, **188**, 201.
146. B. H. Meier, *Adv. Magn. Reson. Opt. Reson.*, 1994, **18**, 1.
147. T. M. Barbara and E. H. Williams, *J. Magn. Reson.*, 1992, **99**, 439.
148. O. B. Persen, X. Wu, I. Kustanovich and S. O. Smith, *J. Magn. Reson.*, 1993, **A104**, 334.
149. O. B. Persen, X. Wu and S. O. Smith, *J. Magn. Reson.*, 1994, **A106**, 127.
150. G. Metz, X. Wu and S. O. Smith, *J. Magn. Reson.*, 1994, **A110**, 219.
151. S. Hediger, B. H. Meier and R. R. Ernst, *Chem. Phys. Lett.*, 1993, **213**, 627.
152. S. Hediger, B. H. Meier, N. D. Kuru, G. Bodenhausen and R. R. Ernst, *Chem. Phys. Lett.*, 1994, **223**, 283.
153. A. C. Kolbert and S. L. Gann, *Chem. Phys. Lett.*, 1994, **224**, 86.
154. S. Hediger, B. H. Meier and R. R. Ernst, *Chem. Phys. Lett.*, 1995, **240**, 449.
155. S. Zhang, C. L. Czekaj and W. T. Ford, *J. Magn. Reson.*, 1994, **A111**, 87.
156. B. Q. Sun, P. R. Costa and R. G. Griffin, *J. Magn. Reson.*, 1995, **A112**, 191.
157. S. Hediger, B. H. Meier and R. R. Ernst, *J. Chem. Phys.*, 1995, **102**, 4000.
158. A. C. Kolbert and A. Bielecki, *J. Magn. Reson.*, 1995, **A116**, 29.
159. H. Geen, J. J. Titman and H. W. Spiess, *Chem. Phys. Lett.*, 1993, **213**, 145.
160. A. C. Kolbert, H. J. de Groot and R. G. Griffin, *J. Magn. Reson.*, 1989, **85**, 60.
161. C. S. Blackwell and R. L. Pattn, *J. Phys. Chem.*, 1984, **88**, 6135.
162. H. D. Morris and P. D. Ellis, *J. Am. Chem. Soc.*, 1989, **111**, 6045.
163. H. D. Morris, S. Bank and P. D. Ellis, *J. Phys. Chem.*, 1990, **94**, 3121.
164. J. Rocha and J. Klinowski, *J. Chem. Soc. Chem. Commum.*, 1991, 1121.
165. L. Kellberg, M. Linsten and J. Klinowski, *Chem. Phys. Lett.*, 1991, **182**, 120.
166. J. Rocha, S.W. Carr and J. Klinowski, *Chem. Phys. Lett.*, 1991, **187**, 401.
167. C. A. Fyfe, H. Grondey, K. T. Mueller, K. C. Wong-Moon and T. Markus, *J. Am. Chem. Soc.*, 1992, **114**, 5876.
168. P. J. Barrie, *Chem. Phys. Lett.*, 1993, **208**, 48.
169. S. Ding and C. A. McDowell, *J. Magn. Reson.*, 1995, **A114**, 80.
170. D. E. Wassner, *Z. Phys. Chem.*, 1987, **152**, 51.
171. R. G. Bryant, S. Ganapathy and S. D. Kennedy, *J. Magn. Reson.*, 1987, **72**, 376.
172. T. H. Walter, G. L. Turner and E. Oldfield, *J. Magn. Reson.*, 1988, **76**, 106.
173. S. L. Gann, J. H. Baltisberger, E. W. Wooten, H. Zimmermann and A. Pines, *Bull. Magn. Reson.*, 1993, **16**, 68.
174. R. K. Harris and G. J. Nosbitt, *J. Magn. Reson.*, 1988, **78**, 245.
175. A. J. Vega, *J. Magn. Reson.*, 1992, **96**, 50.
176. A. J. Vega, *Solid State NMR*, 1992, **1**, 17.
177. S. Hayashi and K. Hayamizu, *Chem. Phys. Lett.*, 1993, **203**, 319.
178. F. Deng, Y. Du, C. Ye, K. Wang, T. Chen, D. Ding, J. Wang and H. Li, *Appl. Magn. Reson.*, 1994, **6**, 537.
179. J. C. Edwards and P. D. Ellis, *Magn. Reson. Chem.*, 1990, **28**, S59.
180. R. Tycko, P. L. Stewart and S. J. Opella, *J. Am. Chem. Soc.*, 1986, **108**, 5419.
181. N. Zumbulyadis and J. M. O'Reilly, *J. Am. Chem. Soc.*, 1993, **115**, 4408.
182. J. Schaefer, E. O. Stejskal, J. R. Garbow and R. A. McKay, *J. Magn. Reson.*, 1984, **59**, 150.
183. M. Goldman, *Spin Temperature and NMR in Solids*. Clarendon Press, Oxford, 1970.
184. R. A. Wind, L. Li, H. Lock and G. E. Maciel, *J. Magn. Reson.*, 1988, **79**, 577.

185. R. A. Wind and H. Lock, *Adv. Magn. Reson.*, 1990, **15**, 51.
186. D. L. Vander Hart, *J. Magn. Reson.*, 1987, **72**, 13.
187. D. Suter and R. R. Ernst, *Phys. Rev.*, 1982, **B25**, 6038.
188. D. Suter and R. R. Ernst, *Phys. Rev.*, 1985, **B32**, 5608.
189. N. Bloembergen, *Physica*, 1949, **15**, 386.
190. D. C. Douglass and G. P. Jones, *J. Chem. Phys.*, 1966, **45**, 956.
191. V. J. McBrierty and D. C. Douglass, *Phys. Rep.*, 1980, **63**, 63.
192. T. T. P. Cheung, *Phys. Rev.*, 1981, **B23**, 1404.
193. E. R. Andrew, A. Bradbury, R. G. Eads and V. T. Wynn, *Phys. Lett.*, 1963, **4**, 99.
194. E. R. Andrew, S. Clough, L. F. Farnell, T. D. Gledhill and I. Roberts, *Phys. Lett.*, 1966, **21**, 505.
195. D. C. Douglass and V. J. McBrierty, *J. Chem. Phys.*, 1971, **54**, 4085.
196. V. J. McBrierty, D. C. Douglass and T. K. Kwei, *Macromolecules*, 1978, **11**, 1265.
197. A. C. Lind, *J. Chem. Phys.*, 1977, **66**, 3482.
198. D. L. VanderHart and A. N. Garroway, *J. Chem. Phys.*, 1979, **71**, 2773.
199. D. K. Sodickson and J. S. Waugh, *Phys. Rev.*, 1995, **B52**, 6467.
200. G. Bodenhausen, R. Freeman and G. A. Morris, *J. Magn. Reson.*, 1976, **23**, 171.
201. G. A. Morris and R. Freeman, *J. Magn. Reson.*, 1976, **29**, 433.
202. P. Caravatti, G. Bodenhausen and R. R. Ernst, *J. Magn. Reson.*, 1983, **55**, 88.
203. J. Jeneer, B. H. Meier, P. Bachmann and R. R. Ernst, *J. Chem. Phys.*, 1979, **71**, 4546.
204. S. Macura and R. R. Ernst, *Mol. Phys.*, 1980, **41**, 95.
205. S. Ding and C. A. McDowell, *Mol. Phys.*, 1995, **85**, 283.
206. N. M. Szeverenyi, M. J. Sullivan and G. E. Maciel, *J. Magn. Reson.*, 1982, **47**, 462.
207. P. Caravatti, J. A. Deli, G. Bodenhausen and R. R. Ernst, *J. Am. Chem. Soc.*, 1982, **104**, 5506.
208. C. E. Bronniman, N. M. Szeverenyi and G. E. Maciel, *J. Chem. Phys.*, 1983, **79**, 3964.
209. N. M. Szeverenyi, A. Bax and G. E. Maciel, *J. Am. Chem. Soc.*, 1983, **105**, 2579.
210. N. Zumblyadis, P. M. Roberts and W. T. Ferrar, *J. Magn. Reson.*, 1987, **72**, 388.
211. T. A. Cross, M. H. Frey and S. J. Opella, *J. Am. Chem. Soc.*, 1983, **105**, 7471.
212. M. H. Frey and S. J. Opella, *J. Am. Chem. Soc.*, 1984, **106**, 1515.
213. K. M. Morden and S. J. Opella, *J. Magn. Reson.*, 1986, **70**, 476.
214. C. Connor, A. Naito and C. A. McDowell, *Chem. Phys. Lett.*, 1985, **113**, 123.
215. N. J. Clayden, *J. Magn. Reson.*, 1986, **68**, 360.
216. A. Kubo and C. A. McDowell, *J. Chem. Phys.*, 1988, **89**, 63.
217. A. Kubo and C. A. McDowell, *J. Chem. Soc., Faraday Trans.*, 1988, **184**, 3713.
218. W. Kolodziejski, H. He and J. Klinowski, *Chem. Phys. Lett.*, 1992, **191**, 117.
219. R. Challoner, J. Kümmerlen and C. A. McDowell, *Mol. Phys.*, 1994, **83**, 687.
220. G. C. Campbell and D. L. VanderHart, *J. Magn. Reson.*, 1992, **96**, 69.
221. J. Hu and C. Ye, *J. Magn. Reson.*, 1992, **99**, 576.
222. M. Alla, R. Eckman and A. Pines, *Chem. Phys. Lett.*, 1980, **71**, 148.
223. W. Schajor, N. Pilsewski, H. Zimmermann and U. Haeberlen, *Chem. Phys. Lett.*, 1980, **76**, 409.
224. C. Ye, R. Eckman and A. Pines, *J. Magn. Reson.*, 1983, **55**, 334.
225. H. W. Spiess, *Chem. Rev.*, 1991, **91**, 1321.
226. C. Schmidt, S. Wefing, B. Blümich and H. W. Spiess, *Chem. Phys. Lett.*, 1986, **130**, 84.
227. S. Wefing and H. W. Spiess, *J. Chem. Phys.*, 1988, **89**, 1219.
228. S. Wefing, S. Kaufmann and H. W. Spiess, *J. Chem. Phys.*, 1988, **89**, 1234.
229. C. Schmidt, B. Blümich and H. W. Spiess, *J. Magn. Reson.*, 1988, **79**, 269.
230. S. Kaufmann, S. Wefing, D. Schafer and H. W. Spiess, *J. Chem. Phys.*, 1990, **95**, 197.

231. C. Boeffel, Z. Luz, R. Poupko and Z. Zimmermann, *J. Magn. Reson.*, 1989, **85**, 329.
232. T. H. Lin, R. R. Vold and R. L. Vold, *J. Magn. Reson.*, 1991, **95**, 71.
233. K. Müller, Z. Luz, R. Poupko and H. Zimmermann, *Liq. Cryst.*, 1992, **11**, 547.
234. D. Reichert, Z. Olender, R. Roupko, H. Zimmermann and Z. Luz, *J. Chem. Phys.*, 1993, **98**, 7699.
235. P. M. Herich, M. Linder and J. M. Hewitt, *J. Chem. Phys.*, 1987, **85**, 7077.
236. M. Linder, P. M. Henrichs, J. M. Hewitt and D. J. Massa, *J. Chem. Phys.*, 1985, **82**, 1585.
237. A. G. Redfield, *Adv. Magn. Reson.*, 1965, **1**, 1.
238. C. P. Slichter and D. G. Allion, *Phys. Rev.*, 1964, **A135**, 1099.
239. D. Wolf, *Spin Temperature and Nuclear Spin Relaxation in Matter.* Clarendon Press, Oxford, 1979.
240. N. Bloembergen, E. M. Purcell and R. V. Pound, *Phys. Rev.*, 1948, **73**, 679.
241. R. Kubo and K. Tomita, *Proc. Phys. Soc. Jpn.*, 1954, **9**, 888.
242. D. W. Davison and R. H. Cole, *J. Chem. Phys.*, 1951, **19**, 1484.
243. K. G. Conn, P. A. Beckman, C. W. Mallory and F. B. Mallory, *J. Chem. Phys.*, 1987, **77**, 20.
244. P. Fang, *Physica*, 1961, **27**, 68.
245. K. S. Cole and R. H. Cole, *J. Chem. Phys.*, 1941, **9**, 341.
246. J.-M. Chezeau, J. H. Strange and C. Brot, *J. Chem. Phys.*, 1972, **56**, 1380.
247. L. A. Dissado and R. M. Hill, *Phil. Magz.*, 1980, **B41**, 625.
248. R. M. Fuoss and J. G. Kirkwood, *J. Am. Chem. Soc.*, 1941, **63**, 385.
249. P. W. Drake, R. Pridham and R. Meister, *J. Chem. Phys.*, 1968, **48**, 2272.
250. H. W. Spiess, *NMR: Basic Principles Progr.*, 1978, **15**, 59.
251. E. R. Andrew, D. J. Bryant, E. M. Cashell and Q. A. Meng, *Phys. Lett.*, 1980, **A88**, 487.
252. E. R. Andrew, D. J. Bryant and E. M. Cashell, *Chem. Phys. Lett.*, 1980, **69**, 551.
253. H. Frolich, *Theory of Dielectrics.* 1958, Oxford.
254. A. M. Albano, P. A. Beckman, M. E. Carrington, E. E. Fisch, F. A. Fusco, A. E. O'Neill and M. E. Scott, *Phys. Rev.*, 1984, **B30**, 2334.
255. D. W. McCall, D. C. Douglass and E. W. Anderson, *J. Chem. Phys.*, 1959, **30**, 1272.
256. P. A. Beckman, *Phys. Reps.*, 1988, **171**, 85.
257. K. Schmidt and H. W. Spiess, *Phys. Rev. Lett.*, 1991, **66**, 3020.
258. G. L. Hoatson and R. L. Vold, *NMR: Basic Principles Progr.*, 1994, **32**, 1.
259. A. Samoson, B. Q. Sun and A. Pines, in *Pulsed Magnetic Resonance: NMR, ESR and Optics, in Recognition of E. L. Hahn* (ed.) D. M. S. Bagguley. Oxford, 1992, p. 80.
260. S. F. Dec, C. E. Bronnimann, R. A. Wind and G. E. Maciel, *J. Magn. Reson.*, 1989, **82**, 454.
261. D. P. Raleigh, E. T. Olejniczak and R. G. Griffin, *J. Chem. Phys.*, 1988, **89**, 1333.
262. M. Munowitz, *J. Magn. Reson.*, 1987, **73**, 338.
263. M. H. Levitt, *J. Magn. Reson.*, 1989, **82**, 427.
264. C. Ye, B. Q. Sun and G. E. Maciel, *J. Magn. Reson.*, 1986, **70**, 241.
265. E. M. Menger, D. P. Raleigh and R. G. Griffin, *J. Magn. Reson.*, 1985, **63**, 579.
266. N. K. Sethi, D. W. Alderman and D. M. Grant, *Mol. Phys.*, 1990, **71**, 271.
267. S. Ding, J. Hu and C. Ye, *Solid State NMR*, 1992, **1**, 103.
268. W. P. Power and G. Wasylishen, *Ann. Rep. NMR Spectr.*, 1991, **23**, 1.
269. E. R. Andrew, *Phil. Trans. R. Soc. Lond.*, 1981, **A299**, 560.
270. G. Bodenhausen, P. Caravatti, J. Deli and R. R. Ernst, *J. Magn. Reson.*, 1982, **48**, 143.
271. J. S. Frye and G. E. Maciel, *J. Magn. Reson.*, 1982, **48**, 125.
272. C. L. Khetrapal, B. S. A. Kumar, V. Ramanathan and N. Suryaparakash, *J. Magn. Reson.*, 1987, **73**, 516.

273. R. C. Crossby and J. F. Haw, *J. Magn. Reson.*, 1989, **82**, 367.
274. A. Kubo and C. A. McDowell, *J. Magn. Reson.*, 1991, **92**, 409.
275. A. Samoson, E. Kundla and E. Lippmaa, *J. Magn. Reson.*, 1982, **49**, 350.
276. S. Ganapathy, S. Schraman and E. Oldfield, *J. Chem. Phys.*, 1987, **77**, 4360.
277. S. Ganapathy, J. Shore and E. Oldfield, *Chem. Phys. Lett.*, 1990, **169**, 301.
278. F. Lefebvre, J.-P. Amoureux, C. Fernandez and E. G. Derouane, *J. Chem. Phys.*, 1988, **86**, 6070.
279. J.-P. Amoureux, C. Fernandez and F. Lefebvre, *Magn. Reson. Chem.*, 1990, **28**, 5.
280. S. F. Dec and G. E. Maciel, *J. Magn. Reson.*, 1990, **87**, 153.
281. J. Skibsted, H. Bildøe and H. J. Jakobsen, *J. Magn. Reson.*, 1991, **92**, 669.
282. Z. Zheng, Z. Gan, N. K. Sethi, D. W. Alderman and D. M. Grant, *J. Magn. Reson.*, 1991, **95**, 509.
283. L. Frydman, G. C. Chingas, Y. K. Lee, P. J. Grandinetti, M. A. Eastman, G. A. Barral and A. Pines, *Isr. J. Chem.*, 1992, **32**, 161.
284. L. Frydman, G. C. Chingas, Y. K. Lee, P. J. Grandinetti, M. A. Eastman, G. A. Barral and A. Pines, *J. Chem. Phys.*, 1992, **97**, 4800.
285. L. Frydman, S. Vallabaneni, Y. K. Lee and L. Emsley, *J. Chem. Phys.*, 1994, **101**, 111.
286. Y. K. Lee, R. L. Vold, G. L. Hoatson, Y.-Y. Lin and A. Pines, *J. Magn. Reson.*, 1995, **A112**, 112.
287. P. J. Grandinetti, Y. K. Lee, J. H. Baltisberger, B. Q. Sun and A. Pines, *J. Magn. Reson.*, 1993, **A102**, 195.
288. L. Frydman, Y. K. Lee, L. Emsley, G. C. Chingas and A. Pines, *J. Am. Chem. Soc.*, 1993, **115**, 4825.
289. Y. K. Lee, L. Emsley, R. G. Larsen, K. Schmidt-Rohr, M. Hong, L. Frydman, G. C. Chingas and A. Pines, *J. Chem. Phys.*, 1994, **101**, 1852.
290. R. G. Larsen, Y. K. Lee, B. He, J. O. Yang, Z. Luz, H. Zimmermann and A. Pines, *J. Chem. Phys.*, 1995, **103**, 9844.
291. K. T. Mueller, B. Q. Sun, G. C. Chingas, J. W. Zwanziger, T. Tarao and A. Pines, *J. Magn. Reson.*, 1990, **86**, 470.
292. K. T. Mueller, G. C. Chingas and A. Pines, *Rev. Sci. Instr.*, 1991, **62**, 1445.
293. K. T. Mueller, Y. Wu, B. F. Chmelka, J. Stebbins and A. Pines, *J. Am. Chem. Soc.*, 1991, **113**, 32.
294. B. F. Chmelka and J. W. Zwanziger, *NMR: Basic Principles Progr.*, 1994, **33**, 79.
295. K. T. Mueller, E. W. Wooten and A. Pines, *J. Magn. Reson.*, 1991, **92**, 620.
296. P. J. Grandinetti, J. H. Baltisberger, A. Llor, Y. K. Lee, U. Werner, M. A. Eastman and A. Pines, *J. Magn. Reson.*, 1993, **A103**, 72.
297. J. H. Baltisberger, S. L. Gann, E. W. Wooten, T. H. Chang, K. T. Mueller and A. Pines, *J. Am. Chem. Soc.*, 1992, **114**, 7489.
298. K. T. Mueller, J. H. Baltisberger, E. W. Wooten and A. Pines, *J. Phys. Chem.*, 1992, **96**, 7001.
299. I. Farnan, P. J. Grandinetti, J. H. Baltisberger, J. F. Stebbins, U. Werner, M. A. Eastman and A. Pines, *Nature*, 1992, **358**, 31.
300. P. J. Grandinetti, J. H. Baltisberger, I. Farnan, J. F. Stebbins, U. Werner and A. Pines, *J. Phys. Chem.*, 1995, **99**, 12341.
301. E. W. Wooten, K. T. Mueller and A. Pines, *Accts Chem. Res.*, 1992, **25**, 209.
302. D. Freude and J. Hasse, *NMR: Basic Principles Progr.*, 1993, **29**, 1.
303. J. H. Baltisberger, S. L. Gann, P. J. Grandinetti and A. Pines, *Mol. Phys.*, 1994, **81**, 1109.
304. S. L. Gann, J. H. Baltisberger, E. W. Wooten, H. Zimmermann and A. Pines, *Bull. Magn. Reson.*, 1994, **16**, 68.
305. C. A. Fyfe, K. C. Wong-Moon, H. Grondey and K. T. Mueller, *J. Phys. Chem.*, 1994, **98**, 2139.

306. A. Bax, N. M. Szeverenyi and G. E. Maciel, *J. Magn. Reson.*, 1983, **55**, 494.
307. T. Terao, T. Fujii, T. Onodera and A. Saika, *Chem. Phys. Lett.*, 1984, **107**, 145.
308. A. Samoson and A. Pines, *Rev. Sci. Instr.*, 1989, **60**, 3239.
309. Y. Wu, B. F. Chmelka, A. Pines, M. E. Davis, P. J. Grobet and P. A. Jacobs, *Nature*, 1990, **346**, 550.
310. A. Samoson and E. Lippmaa, *J. Magn. Reson.*, 1989, **84**, 410.
311. Y. Wu, B. Q. Sun, A. Pines, A. Samoson and E. Lippmaa, *J. Magn. Reson.*, 1990, **89**, 297.
312. B. Q. Sun, J. H. Baltisberger, Y. Wu, A. Samoson and A. Pines, *Solid State NMR*, 1992, **1**, 267.
313. Y. Wu, D. Lewis, J. S. Frye, A. R. Palmer and R. A. Wind, *J. Magn. Reson.*, 1992, **100**, 425.
314. Y. Wu, Z. Y. Peng, Z. Olejniczak, B. Q. Sun and A. Pines, *J. Magn. Reson.*, 1993, **A102**, 29.
315. L. Frydman and J. S. Harwood, *J. Am. Chem. Soc.*, 1995, **117**, 5367.
316. W. T. Dixon, *J. Chem. Phys.*, 1982, **77**, 1800.
317. W. T. Dixon, J. Schaefer, M. D. Seficik, E. O. Stejskal and R. A. McKay, *J. Magn. Reson.*, 1982, **49**, 341.
318. M. A. Hemminga and P. A. de Jäager, *J. Magn. Reson.*, 1983, **51**, 339.
319. N. C. Nielsen, H. Bildsøe and H. J. Jakobsen, *J. Magn. Reson.*, 1988, **80**, 149.
320. Z. Song, O. N. Antzutkin, X. Feng and M. H. Levitt, *Solid State NMR*, 1993, **2**, 143.
321. O. N. Antzukin, Z. Song, X. Feng and M. H. Levitt, *J. Chem. Phys.*, 1994, **100**, 130.
322. D. P. Raleigh, E. T. Olejniczak, S. Vega and R. G. Griffin, *J. Magn. Reson.*, 1987, **72**, 238.
323. D. P. Raleigh, E. T. Olejniczak and R. G. Griffin, *J. Chem. Phys.*, 1988, **89**, 1333.
324. S. J. Long, *J. Magn. Reson.*, 1993, **A104**, 345.
325. J. Hong and G. S. Harbison, *J. Magn. Reson.*, 1993, **A105**, 128.
326. A. C. Kolbert and R. G. Griffin, *Chem. Phys. Lett.*, 1990, **166**, 87.
327. H. Geen and G. Bodenhausen, *J. Chem. Phys.*, 1992, **97**, 2928.
328. H. Geen and G. Bodenhausen, *J. Am. Chem. Soc.*, 1993, **115**, 1579.
329. Z. Gan, *J. Magn. Reson.*, 1994, **A109**, 253.
330. A. Bax, N. M. Szeverenyi and G. E. Maciel, *J. Magn. Reson.*, 1983, **52**, 147.
331. N. M. Szeverenyi, A. Bax and G. E. Maciel, *J. Magn. Reson.*, 1985, **61**, 440.
332. T. Nakai and D. Kuwakara, *Chem. Phys. Lett.*, 1996, **249**, 205.
333. W. T. Dixon, *J. Magn. Reson.*, 1985, **64**, 332.
334. K. R. Carduner, *J. Magn. Reson.*, 1989, **81**, 312.
335. S. L. Gann, J. H. Baltisberger and A. Pines, *Chem. Phys. Lett.*, 1993, **210**, 405.
336. A. Samoson and J. Tegenfeldt, *J. Magn. Reson.*, 1994, **A110**, 238.
337. L. R. Sales and R. M. Cotts, *Phys. Rev.*, 1958, **111**, 853.
338. A. N. Garroway, W. B. Moniz and H. A. Resing, *ACS Symp. Ser.*, 1979, **103**, 67.
339. A. N. Garroway, D. L. VanderHart and W. L. Earl, *Phil. Trans. Roy. Soc. London*, 1981, **A299**, 609.
340. A. Bax, T. E. Early and G. E. Maciel, *J. Magn. Reson.*, 1982, **52**, 35.
341. K. Takagoshi and C. A. McDowell, *J. Magn. Reson.*, 1986, **66**, 14.
342. M. Lee and W. I. Goldburg, *Phys. Rev. Lett.*, 1963, **11**, 255.
343. M. Lee and W. I. Goldburg, *Phys. Rev.*, 1965, **A140**, 1261.
344. A. Bielecki, A. C. Kolbert and M. H. Levitt, *Chem. Phys. Lett.*, 1989, **155**, 341.
345. P. Mansfield and D. Ware, *Phys. Rev.*, 1968, **168**, 318.
346. J. S. Waugh and C. H. Wang, *Phys. Rev.*, 1967, **162**, 209.
347. J. S. Waugh, L. M. Huber and U. Haeberlen, *Phys. Rev. Lett.*, 1968, **20**, 180.
348. P. Mansfield, K. H. B. Richards and D. Ware, *Phys. Rev.*, 1970, **B1**, 2048.
349. W. K. Rhim, A. Pines and J. S. Waugh, *Phys. Rev.*, 1971, **B3**, 684.

350. P. Mansfield, M. Orchard, D. C. Stalker and K. H. B. Richards, *Phys. Rev.*, 1973, **B7**, 90.
351. U. Haeberlen, J. D. Ellett Jr and J. S. Waugh, *J. Chem. Phys.*, 1973, **55**, 53.
352. A. Pines and J. S. Waugh, *J. Magn. Reson.*, 1972, **8**, 354.
353. W. K. Rhim, D. D. Elleman and R. W. Vaughan, *J. Chem. Phys.*, 1973, **58**, 1772.
354. W. K. Rhim, D. D. Elleman and R. W. Vaughan, *J. Chem. Phys.*, 1973, **59**, 3740.
355. W. K. Rhim, D. D. Elleman, L. B. Schreiber and R. W. Vaughan, *J. Chem. Phys.*, 1974, **60**, 4595.
356. A. N. Garroway, P. Mansfield and D. C. Stalker, *Phys. Rev.*, 1975, **B11**, 121.
357. D. P. Burum and W. K. Rhim, *J. Chem. Phys.*, 1979, **70**, 3553.
358. D. P. Burum and W. K. Rhim, *J. Chem. Phys.*, 1979, **71**, 944.
359. D. P. Burum and W. K. Rhim, *J. Magn. Reson.*, 1979, **34**, 241.
360. W. K. Rhim, D. P. Burum and D. D. Elleman, *J. Chem. Phys.*, 1979, **71**, 3139.
361. D. G. Cory, *J. Magn. Reson.*, 1991, **94**, 526.
362. H. Liu, S. J. Glasser and G. P. Drobny, *J. Chem. Phys.*, 1990, **93**, 7543.
363. D. P. Burum, M. Linder and R. R. Ernst, *J. Magn. Reson.*, 1981, **44**, 173.
364. P. Caravatti, G. Bodenhausen and R. R. Ernst, *Chem. Phys. Lett.*, 1982, **89**, 363.
365. P. Caravatti, L. Braunchweiler and R. R. Ernst, *Chem. Phys. Lett.*, 1983, **100**, 305.
366. D. P. Burum and A. Bielecki, *J. Magn. Reson.*, 1991, **95**, 184.
367. D. P. Burum and A. Bielecki, *J. Magn. Reson.*, 1991, **94**, 645.
368. J. S. Waugh, *J. Magn. Reson.*, 1982, **50**, 30.
369. B. M. Fung, D. S. L. Mui, I. R. Bonnell and E. L. Enwall, *J. Magn. Reson.*, 1984, **58**, 254.
370. D. S. L. Mui, B. M. Fung, I. R. Bonnell and E. L. Enwall, *J. Magn. Reson.*, 1985, **64**, 124.
371. K. V. Schenker, D. Suter and A. Pines, *J. Magn. Reson.*, 1983, **73**, 90.
372. D. Suter, K. V. Schenker and A. Pines, *J. Magn. Reson.*, 1987, **73**, 99.
373. D. Suter, A. Pines, J. H. Lee and G. Drobny, *Chem. Phys. Lett.*, 1988, **144**, 324.
374. K. Takegishi and C. A. McDowell, *Chem. Phys. Lett.*, 1985, **100**, 116.
375. T. K. Pratum, *J. Magn. Reson.*, 1990, **88**, 384.
376. A. E. Bennett, C. M. Rienstra, M. Auger, K. V. Lakshmi and R. G. Griffin, *J. Chem. Phys.*, 1995, **103**, 6951.
377. S. F. Dec, R. A. Wind, G. E. Maciel and F. E. Anthonio, *J. Magn. Reson.*, 1986, **70**, 355.
378. S. F. Dec, C. E. Bronnimann, R. A. Wind and G. E. Maciel, *J. Magn. Reson.*, 1989, **82**, 454.
379. R. G. Pembleton, L. M. Ryan and B. C. Gerstein, *Rev. Sci. Instr.*, 1977, **48**, 1286.
380. L. M. Ryan, R. E. Taylor, A. J. Paff and B. C. Gerstein, *J. Chem. Phys.*, 1980, **72**, 508.
381. B. C. Gerstein, *Phil. Trans. R. Soc. London*, 1981, **A299**, 521.
382. C. G. Scheler, U. Haubenreisser and H. Rosenberger, *J. Magn. Reson.*, 1981, **44**, 134.
383. B. C. Gerstein and C. R. Dybowski, *Transient Techniques in NMR of Solids*. Academic Press. Orlando, 1985.
384. C. E. Bronniman, B. L. Kawkins, M. Zhang and G. E. Maciel, *Anal. Chem.*, 1988, **60**, 1743.
385. R. K. Harris, P. Jakkson and G. J. Nesbitt, *J. Magn. Reson.*, 1989, **85**, 294.
386. D. P. Burum, *Concepts Magn. Reson.*, 1990, **2**, 213.
387. G. E. Maciel, C. E. Bronnimann and B. L. Hawkins, *Adv. Magn. Reson.*, 1990, **14**, 125.
388. A. Naito, A. Root and C. A. McDowell, *J. Phys. Chem.*, 1991, **95**, 3578.
389. R. K. Harris, P. Jackson, P. J. Wilkes and P. S. Belton, *J. Magn. Reson.*, 1987, **73**, 178.

390. K. A. Smith and D. P. Burum, *J. Magn. Reson.*, 1989, **84**, 85.
391. R. K. Harris and P. Jackson, *Chem. Rev.*, 1991, **91**, 1427.
392. M. L. Buszko, C. E. Bronnimann and G. E. Maciel, *J. Magn. Reson.*, 1993, **A103**, 183.
393. M. L. Buszko and G. E. Maciel, *J. Magn. Reson.*, 1993, **A104**, 172.
394. M. L. Buszko and G. E. Maciel, *J. Magn. Reson.*, 1994, **A107**, 151.
395. Y. Sun, J. Xiong, H. Lock, M. L. Buszko, J. A. Hasse and G. E. Maciel, *J. Magn. Reson.*, 1994, **A110**, 1.
396. M. L. Buszko and G. E. Maciel, *J. Magn. Reson.*, 1994, **A110**, 7.
397. D. G. Cory, J. B. Miller and A. N. Garroway, *J. Magn. Reson.*, 1990, **90**, 205.
398. U. Haubenreisser and B. Schnabel, *J. Magn. Reson.*, 1979, **35**, 175.
399. D. P. Burum, M. Linder and R. R. Ernst, *J. Magn. Reson.*, 1981, **43**, 463.
400. D. G. Cory, J. B. Miller and A. N. Garroway, *J. Magn. Reson.*, 1990, **87**, 202.
401. L. G. Butler, D. G. Cory, K. M. Dooley, J. B. Miller and A. N. Garroway, *J. Am. Chem. Soc.*, 1992, **114**, 125.
402. D. P. Burum, D. G. Cory, K. K. Gleason, D. Levy and A. Bielecki, *J. Magn. Reson.*, 1993, **A104**, 347.
403. P. Caravatti, P. Neuenschwander and R. R. Ernst, *Macromolecules*, 1985, **18**, 119.
404. C. E. Bronniman, R. C. Ziegler and G. E. Maciel, *J. Am. Chem. Soc.*, 1988, **110**, 2023.
405. C. S. Yannoni and R. D. Kendrick, *J. Chem. Phys.*, 1981, **74**, 747.
406. D. Horne, R. D. Kendrick and C. S. Yannoni, *J. Magn. Reson.*, 1983, **52**, 191.
407. C. S. Yannoni and T. C. Clarke, *Phy. Rev. Lett.*, 1983, **51**, 1191.
408. M. Engelsbery and C. S. Yannoni, *J. Magn. Reson.*, 1990, **88**, 393.
409. A. Samoson and E. Lippmaa, *Phys. Rev.*, 1983, **B28**, 6567.
410. G. A. Tijink, R. Janssen and W. S. Veeman, *J. Am. Chem. Soc.*, 1987, **109**, 7301.
411. A. Samoson, E. Lippmaa, G. Engelhardt, U. Lohse and H. G. Jerchkewitz, *Chem. Phys. Lett.*, 1987, **134**, 589.
412. A. P. M. Kentgens, *Two Dimensional Solid State NMR*. Nijmegen, 1987.
413. A. P. M. Kentgens, J. J. M. Lemmens, F. M. M. Geurts and W. S. Veeman, *J. Magn. Reson.*, 1987, **71**, 62.
414. G. Engelhandt, J. Ch. Buhl and J. Felsche, *Chem. Phys. Lett.*, 1988, **153**, 332.
415. N. C. Nielsen, H. Bildse and H. J. Jakobsen, *J. Magn. Reson.*, 1992, **97**, 149.
416. N. C. Nielsen, H. Bildse and H. J. Jakobsen, *J. Magn. Reson.*, 1992, **98**, 665.
417. A. P. M. Kentgens, K. F. M. Scholle and W. S. Veeman, *J. Chem. Phys.*, 1983, **87**, 4357.
418. F. M. M. Geurts, A. P. M. Kentagens and W. S. Veeman, *Chem. Phys. Lett.*, 1985, **120**, 206.
419. P. P. Man and J. Klinowski, *Chem. Phys. Lett.*, 1988, **147**, 581.
420. H. Hamdan and J. Klinowski, *J. Chem. Soc. Chem. Commun.*, 1989, 240.
421. J. A. M. Vander Mijden, R. Janssen and W. S. Veeman, *Mol. Phys.*, 1990, **69**, 53.
422. P. P. Man, *J. Magn. Reson.*, 1987, **67**, 78.
423. P. P. Man, *Mol. Phys.*, 1990, **69**, 337.
424. P. P. Man, *Chem. Phys. Lett.*, 1990, **168**, 227.
425. A. Samoson and E. Lippmaa, *J. Magn. Reson.*, 1988, **79**, 255.
426. G. Y. Li and X. Wu, *Chem. Phys. Lett.*, 1990, **168**, 518.
427. D. Wang, G. Y. Li and X. Wu, *J. Magn. Reson.*, 1987, **74**, 464.
428. G. Y. Li and X. Wu, *Rev. Sci. Instr.*, 1988, **59**, 569.
429. S. Ding and C. A. McDowell, *J. Magn. Reson.*, 1995, **A112**, 36.
430. R. Janssen, G. A. H. Tijink and W. S. Veeman, *J. Chem. Phys.*, 1988, **88**, 518.
431. A. P. M. Kentgens, *J. Magn. Reson.*, 1993, **A104**, 302.
432. P. J. Dirken, G. H. Nachtegal and A. P. M. Kentgens, *Solid State NMR*, 1995, **5**, 189.

433. H. Ohki and N. Nakamura, *Z. Naturforsch.*, 1992, **47a**, 319.
434. N. Nakamura, *Z. Naturforsch.*, 1994, **49a**, 337.
435. D. L. VanderHart and H. S. Gutowsky, *J. Chem. Phys.*, 1968, **49**, 261.
436. K. W. Zilm and D. M. Grant, *J. Am. Chem. Soc.*, 1981, **103**, 2913.
437. K. W. Zilm, G. G. Webb, A. H. Cowley, M. Pakulski and A. Orendt, *J. Am. Chem. Soc.*, 1988, **110**, 2032.
438. M. Linder, A. Hohener and R. R. Ernst, *J. Chem. Phys.*, 1980, **73**, 4959.
439. M. J. Duijvestjn, A. Manenschijn, J. Smidt and R. A. Wind, *J. Magn. Reson.*, 1985, **64**, 461.
440. W. E. Maas, A. P. M. Kentgens and W. S. Veeman, *J. Chem. Phys.*, 1987, **87**, 6854.
441. T. Nakai, J. Ashida and T. Terao, *J. Chem. Phys.*, 1988, **88**, 4069.
442. D. P. Weleky, G. Dabbagh and R. Tycko, *J. Magn. Reson.*, 1993, **A104**, 10.
443. T. Nakai and C. A. McDowell, *Chem. Phys. Lett.*, 1994, **217**, 234.
444. T. Nakai and C. A. McDowell, *J. Am. Chem. Soc.*, 1994, **116**, 6373.
445. T. Nakai and C. A. McDowell, *Solid State NMR*, 1995, **4**, 163.
446. Y. Ishii and T. Terao, *J. Magn. Reson.*, 1995, **A115**, 116.
447. T. G. Oas, C. J. Hartzell, T. J. McMahon, G. P. Drobny and F. W. Dahlquist, *J. Am. Chem. Soc.*, 1987, **109**, 5956.
448. T. G. Oas, C. J. Hartzell, F. W. Dahlquist and G. P. Drobny, *J. Am. Chem. Soc.*, 1987, **109**, 5962.
449. C. J. Hartzell, M. Whitefield, T. G. Oas and G. P. Drobny, *J. Am. Chem. Soc.*, 1987, **109**, 5967.
450. S. Kaplan, A. Pines, R. G. Griffin and J. S. Waugh, *Chem. Phys. Lett.*, 1974, **25**, 78.
451. P. K. Wang, J. P. Ansermet and C. P. Slichter, *Phys. Rev. Lett.*, 1985, **55**, 2731.
452. S. E. Shore, J. P. Ansermet, C. P. Slichter and J. H. Sinfelt, *Phys. Rev. Lett.*, 1987, **58**, 953.
453. T. G. Oas, C. J. Hartzell, G. P. Drobny and F. W. Dahlquist, *J. Magn. Reson.*, 1989, **81**, 395.
454. D. M. Schneider, R. Tycko and S. J. Opella, *J. Magn. Reson.*, 1987, **73**, 568.
455. R. Hester, J. L. Ackerman, B. L. Neff and J. S. Waugh, *Phys. Rev.*, 1976, **A36**, 1081.
456. Z. Gan, *J. Am. Chem. Soc.*, 1992, **114**, 8307.
457. J. Hu, D. W. Alderman, C. Ye, R. J. Pugmire and D. M. Grant, *J. Magn. Reson.*, 1993, **A103**, 82.
458. J. Hu, A. M. Orendt, D. W. Alderman, R. J. Pugmire, C. Ye and D. M. Grant, *Solid State NMR*, 1994, **3**, 181.
459. J. Hu, W. Wang, F. Liu, M. S. Solum, D. W. Alderman, R. J. Pugmire and D. M. Grant, *J. Magn. Reson.*, 1995, **A113**, 210.
460. J. Herzfeld and A. E. Berger, *J. Chem. Phys.*, 1982, **73**, 6021.
461. D. W. Alderman, M. S. Solum and D. M. Grant, *J. Chem. Phys.*, 1986, **84**, 3717.
462. D. Freude, D. Maas and H. Pfeiffer, *J. Magn. Reson.*, 1990, **88**, 172.
463. J. H. Kristensen, H. Bildsøe and N. C. Nielsen, *J. Magn. Reson.*, 1991, **95**, 443.
464. A. Samoson, *Chem. Phys. Lett.*, 1985, **119**, 29.
465. J. Skibstedt, N. C. Nielsen, H. Bildsøe and H. J. Jakobsen, *J. Magn. Reson.*, 1991, **95**, 88.
466. C. Jäger, J. Rocha and J. Klinowski, *Chem. Phys. Lett.*, 1992, **188**, 208.
467. O. N. Antzutkin, S. C. Sheker and M. H. Levitt, *J. Magn. Reson.*, 1995, **A115**, 7.
468. E. O. Stejskal, J. Schaefer and R. A. McKay, *J. Magn. Reson.*, 1977, **25**, 569.
469. N. J. Clayden, *Chem. Phys. Lett.*, 1986, **131**, 517.
470. H. Muira, T. Terao and A. Saika, *J. Chem. Phys.*, 1986, **84**, 3717; **85**, 2458.
471. Z. Gan and D. M. Grant, *J. Magn. Reson.*, 1990, **90**, 522.
472. N. Sethi, D. M. Grant and R. J. Pugmire, *J. Magn. Reson.*, 1987, **71**, 476.

473. C. Ye, R. Fu, J. Hu, L. Hou and S. Ding, *Magn. Reson. Chem.*, 1993, **31**, 699.
474. A. Bax, N. M. Szeverenyi and G. E. Maciel, *J. Magn. Reson.*, 1983, **55**, 494.
475. G. E. Maciel, N. M. Szeverenyi and M. Sadashti, *J. Magn. Reson.*, 1984, **64**, 365.
476. J. H. Iwamiya, M. F. Davis and G. E. Maciel, *J. Magn. Reson.*, 1990, **88**, 199.
477. T. Terao, T. Fujii, T. Onedera and A. Saika, *Chem. Phys. Lett.*, 1984, **107**, 145.
478. J. Ashida, T. Nakai and T. Terao, *Chem. Phys. Lett.*, 1990, **168**, 523.
479. T. Terao, H. Miura and A. Saika, *J. Chem. Phys.*, 1986, **85**, 3816.
480. T. Nakai, J. Ashida and T. Terao, *J. Chem. Phys.*, 1988, **88**, 6049.
481. T. Nakai, T. Terao and H. Shirakawa, *Chem. Phys. Lett.*, 1988, **145**, 90.
482. M. Alla and E. Lippmaa, *Chem. Phys. Lett.*, 1976, **37**, 260.
483. M. E. Stoll, A. J. Vega and R. W. Vaughan, *J. Chem. Phys.*, 1976, **65**, 4093.
484. M. E. Stoll, A. J. Vega and R. W. Vaughan, *Phys. Rev.*, 1977, **A16**, 1521.
485. M. E. Stoll, A. J. Vega and R. W. Vaughan, *J. Chem. Phys.*, 1977, **67**, 2029.
486. M. E. Stoll, A. J. Vega and R. W. Vaughan, *J. Chem. Phys.*, 1978, **69**, 5458.
487. M. E. Stoll, E. K. Wolff and M. Mehring, *Phys. Rev.*, 1978, **A17**, 1561.
488. M. E. Stoll, *Phil. Trans. R. Soc. London*, 1981, **A299**, 565.
489. S. J. Opella and M. H. Frey, *J. Am. Chem. Soc.*, 1979, **101**, 5854.
490. L. B. Alemany, D. M. Grant, T. D. Alger and R. J. Pugmire, *J. Am. Chem. Soc.*, 1983, **105**, 6697.
491. M. G. Munowitz, R. G. Griffin, G. Bodenhausen and T. H. Huang, *J. Am. Chem. Soc.*, 1981, **103**, 2529.
492. G. S. Harbison, P. P. J. Mulder, H. Pardoen, J. Lugtenburg, J. Herzfeld and R. G. Griffin, *J. Am. Chem. Soc.*, 1985, **107**, 4809.
493. R. H. Newman, *J. Magn. Reson.*, 1990, **86**, 176; 1992, **96**, 370.
494. X. Wu, S. Zhang and X. Wu, *Chem. Phys. Lett.*, 1989, **162**, 321.
495. D. P. Raleigh, G. S. Harbison, T. G. Neiss, J. E. Roberts and R. G. Griffin, *Chem. Phys. Lett.*, 1987, **138**, 285.
496. R. G. Spencer, K. W. Fishbein, M. H. Levitt and R. G. Griffin, *J. Chem. Phys.*, 1994, **100**, 5533.
497. D. P. Raleigh, F. Greuzet, S. K. Das Gupta and M. H. Levitt, *J. Am. Chem. Soc.*, 1989, **111**, 4502.
498. R. Challoner and R. K. Harris, *Chem. Phys. Lett.*, 1994, **228**, 589.
499. N. C. Nielsen, F. Greuzet and R. G. Griffin, *J. Magn. Reson.*, 1993, **A103**, 245.
500. M. G. Colomb, B. H. Meier and R. R. Ernst, *Chem. Phys. Lett.*, 1988, **146**, 189.
501. W. Maas and W. S. Veeman, *Chem. Phys. Lett.*, 1988, **149**, 170.
502. T. Nakai and C. A. McDowell, *J. Magn. Reson.*, 1995, **A112**, 199.
503. N. C. Nielsen, F. Greuzet, R. G. Griffin and M. H. Levitt, *J. Chem. Phys.*, 1992, **96**, 5668.
504. J. M. Griffiths, T. A. Ashburn, M. Auger, P. R. Costa, R. G. Griffin and P. T. Lansbury Jr, *J. Am. Chem. Soc.*, 1995, **117**, 3539.
505. W. Sun, J. T. Stephen, L. D. Potter and Y. Wu, *J. Magn. Reson.*, 1995, **A116**, 181.
506. T. G. Oas, R. G. Griffin and M. H. Levitt, *J. Chem. Phys.*, 1988, **89**, 692.
507. D. P. Raleigh, A. C. Kolbert, T. G. Oas, M. H. Levitt and R. G. Griffin, *J. Chem. Soc. Faraday Trans.*, 1988, **184**, 3691.
508. K. Takegoshi, K. Nomura and T. Terao, *Chem. Phys. Lett.*, 1995, **232**, 424.
509. A. C. Kolbert, D. P. Raleigh, R. G. Griffin and M. H. Levitt, *J. Magn. Reson.*, 1989, **89**, 133.
510. P. Robyr, B. H. Meier and R. R. Ernst, *Chem. Phys. Lett.*, 1989, **162**, 417.
511. T. Nakai and C. A. McDowell, *Chem. Phys. Lett.*, 1994, **227**, 639.
512. Y. Pan and J. Schaefer, *J. Magn. Reson.*, 1990, **90**, 341.
513. Y. Pan, T. Gullion and J. Schaefer, *J. Magn. Reson.*, 1990, **90**, 330.
514. T. Gullion and J. Schaefer, *Adv. Magn. Reson.*, 1989, **13**, 57.

515. T. Gullion, R. A. McKay and A. Schmidt, *J. Magn. Reson.*, 1991, **94**, 362.
516. T. Gullion and J. Schaefer, *J. Magn. Reson.*, 1991, **92**, 439.
517. J. R. Garbow and T. Gullion, *J. Magn. Reson.*, 1991, **95**, 442.
518. A. Schmidt, R. A. McKay and J. Schaefer, *J. Magn. Reson.*, 1992, **96**, 644.
519. A. L. Blumerdeldt, D. J. Coster and J. J. Fripiat, *Chem. Phys. Lett.*, 1994, **231**, 491.
520. T. Gullion, *Chem. Phys. Lett.*, 1995, **246**, 325.
521. S. M. Holl, R. A. McKay, T. Gullion and J. Schaefer, *J. Magn. Reson.*, 1990, **89**, 620.
522. T. Gullion, M. D. Poliks and J. Schaefer, *J. Magn. Reson.*, 1988, **80**, 553.
523. U. Bork, T. Gullion, A. W. Hing and J. Schaefer, *J. Magn. Reson.*, 1990, **88**, 523.
524. A. W. Hing, S. Vega and J. Schaefer, *J. Magn. Reson.*, 1992, **96**, 205.
525. A. W. Hing, S. Vega and J. Schaefer, *J. Magn. Reson.*, 1993, **A103**, 151.
526. A. E. Bennet, R. G. Griffin and S. Vega, *NMR: Basic Principles Progr.*, 1994, **33**, 1.
527. T. Gullion, D. B. Baker and M. S. Conradi, *J. Magn. Reson.*, 1990, **89**, 479.
528. T. Gullion, *J. Magn. Reson.*, 1993, **A101**, 320.
529. Y. Li and J. N. S. Evans, *J. Magn. Reson.*, 1995, **A116**, 150.
530. Y. Li and J. N. S. Evans, *J. Magn. Reson.*, 1994, **A109**, 256.
531. Y. Li and J. N. S. Evans, *J. Chem. Phys.*, 1994, **101**, 10211.
532. Y. Li and J. N. S. Evans, *Chem. Phys. Lett.*, 1995, **241**, 79.
533. Y. Li and J. N. S. Evans, *Chem. Phys. Lett.*, 1995, **246**, 527.
534. K. T. Mueller, *J. Magn. Reson.*, 1995, **A113**, 81.
535. K. T. Mueller, T. P. Jarvie, D. J. Aurentz and B. W. Roberts, *Chem. Phys. Lett.*, 1995, **242**, 535.
536. A. L. Blumerdeldt, D. J. Coster and J. J. Fripiat, *J. Phys. Chem.*, 1994, **99**, 15181.
537. C. A. Fyfe, K. T. Mueller, H. G. Grandey and K. C. Wong-Moon, *J. Phys. Chem.*, 1993, **97**, 13484.
538. C. A. Fyfe, K. T. Mueller, H. G. Grandey and K. C. Wong-Moon, *Chem. Phys. Lett.*, 1992, **199**, 198.
539. R. C. Anderson, T. Gullion, J. M. Joers, M. Shapiro, E. B. Villhauer and H. P. Weber, *J. Am. Chem. Soc.*, 1995, **117**, 10546.
540. A. M. Christensen and J. Schaefer, *Biochem.*, 1993, **32**, 2868.
541. S. M. Holl, G. R. Marshall, D. D. Beusen, K. Kociolek, A. S. Redlinski, M. T. Leplawy, R. A. McKay, S. Vega and J. Schaefer, *J. Am. Chem. Soc.*, 1992, **114**, 4830.
542. T. M. Forrest, G. E. Wilson, Y. Pan and J. Schaefer, *J. Bio. Chem.*, 1991, **266**, 24485.
543. A. M. Christensen, J. Schaefer, K. J. Kramer, T. D. Morgan and T. L. Hopkins, *J. Am. Chem. Soc.*, 1991, **113**, 6799.
544. E. R. H. van Eck, R. J. Jannsen, W. E. J. R. Maas and W. S. Veeman, *Chem. Phys. Lett.*, 1990, **174**, 428.
545. C. P. Grey and W. S. Veeman, *Chem. Phys. Lett.*, 1992, **192**, 379.
546. C. P. Grey, W. S. Veeman and A. J. Vega, *J. Chem. Phys.*, 1993, **98**, 7711.
547. R. Tycko and G. Dabbagh, *Chem. Phys. Lett.*, 1990, **173**, 461.
548. R. Tycko and G. Dabbagh, *J. Am. Chem. Soc.*, 1991, **113**, 9444.
549. R. Tycko and S. O. Smith, *J. Chem. Phys.*, 1993, **98**, 932.
550. W. Zhu, C. A. Klug, M. E. Merritt and J. Schaefer, *J. Magn. Reson.*, 1994, **A109**, 134.
551. B. Q. Sun, P. R. Costa, D. Kocisko, P. T. Lamsbury and R. G. Griffin, *J. Chem. Phys.*, 1995, **102**, 702.
552. T. Gullion and S. Vega, *Chem. Phys. Lett.*, 1992, **194**, 423.
553. O. Weintraub, S. Vega, C. Hoegler and H. H. Limbach, *J. Magn. Reson.*, 1994, **A109**, 14.
554. O. Weintraub, S. Vega, C. Hoegler and H. H. Limbach, *J. Magn. Reson.*, 1994, **A110**, 12.

555. W. Zhu, C. A. Klung and J. Schaefer, *J. Magn. Reson.*, 1994, **A108**, 121.
556. T. Fujiwara, A. Ramamoorthy, K. Nagayama, K. Hioka and T. Fujito, *Chem. Phys. Lett.*, 1993, **212**, 81.
557. A. Ramamoorthy, T. Fujiwara and K. Nagayama, *J. Magn. Reson.*, 1993, **A104**, 366.
558. M. Baldus, M. Tomaselli, B. H. Meier and R. R. Ernst, *Chem. Phys. Lett.*, 1994, **230**, 329.
559. R. M. Jores, R. Rosanske, T. Gullion and J. R. Garbow, *J. Magn. Reson.*, 1994, **A106**, 123.
560. A. E. Benett, J. H. Ok, R. G. Griffin and S. Vega, *J. Chem. Phys.*, 1992, **96**, 8624.
561. J. H. Ok, R. G. S. Spencer, A. E. Benett and R. G. Griffin, *Chem. Phys. Lett.*, 1992, **197**, 389.
562. D. K. Sodickson, M. H. Levitt, S. Vega and R. G. Griffin, *J. Chem. Phys.*, 1993, **98**, 6742.
563. Y. K. Lee, N. D. Kurur, M. Helmle, O. G. Johannessen, N. C. Nielsen and M. H. Levitt, *Chem. Phys. Lett.*, 1995, **242**, 304.
564. D. M. Gregory, D. J. Mitchell, J. A. Stringer, S. Kiihne, J. C. Shiels, J. Callahan, M. A. Mehta and G. P. Drobny, *Chem. Phys. Lett.*, 1995, **246**, 654.
565. D. L. VanderHart, H. S. Gutowsky and R. C. Farrar, *J. Am. Chem. Soc.*, 1967, **89**, 5056.
566. R. G. Griffin, A. Pines and J. S. Waugh, *J. Chem. Phys.*, 1975, **63**, 3976.
567. M. E. Stoll, R. W. Vaughan, R. B. Saillant and T. Cole, *J. Chem. Phys.*, 1974, **61**, 2896.
568. S. J. Opella, M. H. Frey and T. A. Cross, *J. Am. Chem. Soc.*, 1979, **101**, 5856.
569. M. H. Frey and S. J. Opella, *J. Chem. Soc. Chem. Commun.*, 1980, **11**, 474.
570. C. J. Groombridge, R. K. Harris, K. J. Packer, B. J. Say and S. F. Tanner, *J. Chem. Soc. Chem. Commun.*, 1980, **4**, 174.
571. J. G. Hexem, M. H. Frey and S. J. Opella, *J. Am. Chem. Soc.*, 1981, **103**, 224.
572. J. G. Hexem, M. H. Frey and S. J. Opella, *J. Chem. Phys.*, 1982, **77**, 3847.
573. S. J. Opella, J. G. Hexem, M. H. Frey and T. A. Cross, *Phil. Trans. R. Soc. London*, 1981, **A299**, 665.
574. G. E. Baliman, C. J. Groombridge, R. K. Harris, K. J. Packer, B. J. Say and S. F. Tanner, *Phil. Trans. R. Soc. London*, 1981, **A299**, 643.
575. A. Naito, S. Ganapathy and C. A. McDowell, *J. Chem. Phys.*, 1981, **74**, 5393.
576. A. Naito, S. Ganapathy and C. A. McDowell, *J. Magn. Reson.*, 1982, **48**, 367.
577. N. Zumbulyadis, D. M. Hendricks and R. L. Young, *J. Chem. Phys.*, 1982, **75**, 1603.
578. A. C. Olivieri, L. Frydman and L. E. Diaz, *J. Magn. Reson.*, 1987, **75**, 50.
579. R. K. Harris and A. C. Olivieri, *Progr. NMR Spectrosc.*, 1992, **24**, 435.
580. Z. Gan and D. M. Grant, *J. Magn. Reson.*, 1990, **90**, 522.
581. E. M. Menger, W. S. Veeman, *J. Magn. Reson.*, 1982, **46**, 251.
582. R. K. Harris, *J. Magn. Reson.*, 1988, **78**, 389.
583. D. C. Apperley, B. Haiping and R. K. Harris, *Mol. Phys.*, 1989, **68**, 1277.
584. D. L. Sastry, A. Naito and C. A. McDowell, *Chem. Phys. Lett.*, 1988, **146**, 422.
585. A. C. Olivieri, L. Frydman, M. Grasselli and L. E. Diaz, *Magn. Reson. Chem.*, 1988, **26**, 281; 615.
586. A. C. Olivieri, *Solid State NMR*, 1992, **1**, 201.
587. K. Eichele and R. E. Wasylishen, *Solid State NMR*, 1992, **1**, 159.
588. W. A. Anderson, *Phys. Rev.*, 1956, **104**, 850.
589. J. I. Kaplan and S. Meiboom, *Phys. Rev.*, 1957, **106**, 4991.
590. S. Yatsiv, *Phys. Rev.*, 1952, **103**, 1522.
591. P. Bucci, M. Martinell and S. Santucci, *J. Chem. Phys.*, 1970, **52**, 4041.
592. P. Bucci, M. Martinell and S. Santucci, *J. Chem. Phys.*, 1970, **53**, 4524.
593. G. Bodenhausen, *Progr. NMR Spectrosc.*, 1981, **14**, 137.

594. D. P. Weitekamp, *Adv. Magn. Reson.*, 1983, **11**, 111.
595. M. Munowitz and A. Pines, *Adv. Chem. Phys.*, 1987, **66**, 1.
596. T. J. Norwood, *Progr. NMR Spectrosc.*, 1992, **24**, 295.
597. G. P. Drobny, *Ann. Rev. Chem. Phys.*, 1985, **36**, 451.
598. A. Pines, S. Vega and M. Mehring, *Phys. Rev.*, 1978, **B18**, 112.
599. D. Suwelack, M. Mehring and A. Pines, *Phys. Rev.*, 1979, **B19**, 238.
600. S. Vega, T. W. Shattuck and A. Pines, *Phys. Rev.*, 1980, **A22**, 638.
601. S. Emid, *J. Magn. Reson.*, 1981, **42**, 147.
602. P. Brunner, M. Reinhold and R. R. Ernst, *J. Chem. Phys.*, 1980, **73**, 1086.
603. M. Reinhold, P. Brunner and R. R. Ernst, *J. Chem. Phys.*, 1980, **74**, 184.
604. R. Tycko, *J. Am. Chem. Soc.*, 1986, **108**, 3531.
605. R. Tycko, P. L. Stewart and S. J. Opella, *J. Am. Chem. Soc.*, 1986, **108**, 5419.
606. M. Bloom and M. A. Legros, *Can. J. Chem.*, 1986, **64**, 1522.
607. P. L. Stewart, K. G. Valentine and S. J. Opella, *J. Magn. Reson.*, 1987, **71**, 45.
608. R. Tycko and S. J. Opella, *J. Chem. Phys.*, 1987, **86**, 1761.
609. K. V. Ramanthan and S. J. Opella, *J. Magn. Reson.*, 1988, **78**, 367.
610. A. N. Garroway and J. B. Miller, *J. Magn. Reson.*, 1989, **82**, 591.
611. L. E. Chirlian and S. J. Opella, *Adv. Magn. Reson.*, 1990, **14**, 183.
612. K. Takegoshi and K. Hikichi, *Chem. Phys. Lett.*, 1993, **206**, 450.
613. S. J. Opella, *Ann. Rev. Chem. Phys.*, 1994, **45**, 659.
614. R. McNamara, C. H. Wu, L. E. Chirlian and S. J. Opella, *J. Am. Chem. Soc.*, 1995, **117**, 7805.
615. C. S. Yannoni, R. D. Kendrick and P. K. Wang, *Phys. Rev. Lett.*, 1987, **58**, 345.
616. D. Yang and C. Ye, *Solid State NMR*, 1993, **2**, 147.
617. S. Vega and A. Pines, *J. Chem. Phys.*, 1977, **66**, 5624.
618. S. Vega, *J. Chem. Phys.*, 1978, **68**, 5518.
619. A Wokaun and R. R. Ernst, *J. Chem. Phys.*, 1977, **67**, 1752.
620. T. K. Malstead, P. A. Osment, B. C. Sanctuary, T. Takegoshi and I. Lowe, *J. Magn. Reson.*, 1986, **67**, 267.
621. M. S. Krishan, N. Lee, B. C. Sanctuary and T. G. Halstead, *J. Magn. Reson.*, 1988, **80**, 214.
622. G. Camplieti, B. C. Sanctuary and B. R. Cole, *J. Magn. Reson.*, 1990, **88**, 457.
623. N. Lee, M. E. Lam, B. C. Sanctuary and M. A. Keniry, *J. Magn. Reson.*, 1991, **92**, 455.
624. E. M. Menger, S. Vega and R. G. Griffin, *J. Magn. Reson.*, 1984, **56**, 338.
625. J. Baum, M. Munowitz, A. N. Garroway and A. Pines, *J. Chem. Phys.*, 1985, **83**, 2015.
626. B. E. Scruggs and K. K. Gleason, *J. Magn. Reson.*, 1992, **99**, 149.
627. D. Suter, S. B. Liu, J. Baum and A. Pines, *Chem. Phys.*, 1987, **114**, 103.
628. J. Baum, K. K. Gleason, A. Pines, A. N. Garroway and J. A. Reimer, *Phys. Rev. Lett.*, 1986, **56**, 1377.
629. J. Baum and A. Pines, *J. Am. Chem. Soc.*, 1986, **108**, 1447.
630. K. K. Gleason, M. A. Petrich and J. A. Reimer, *Phys. Rev.*, 1987, **B36**, 3259.
631. M. A. Petrich, K. K. Gleason and J. A. Reimer, *Phys. Rev.*, 1987, **B36**, 9722.
632. S. Emid, *Physica*, 1985, **B128**, 79.
633. R. Ryoo, S. B. Liu, L. C. de Menorval, K. Takegoshi, B. Chmelka, M. Treooke and A. Pines, *J. Chem. Phys.*, 1987, **91**, 6575.
634. S. Emid and J. H. N. Greyghton, *Physica*, 1985, **B128**, 81.
635. D. N. Shykind, J. Baum, S. B. Liu, A. Pines and A. N. Garroway, *J. Magn. Reson.*, 1988, **76**, 149.
636. M. Munowitz, A. Pines and M. Mehring, *J. Chem. Phys.*, 1987, **86**, 3172.
637. M. Munowitz and M. Mehring, *Chem. Phys.*, 1987, **116**, 79.

638. M. Munowitz, *Mol. Phys.*, 1990, **71**, 959.
639. J. B. Murdoch, W. S. Warren, D. P. Weitekamp and A. Pines, *J. Magn. Reson.*, 1984, **60**, 205.
640. T. M. Barkara, R. Tycko and D. P. Weitekamp, *J. Magn. Reson.*, 1985, **62**, 54.
641. B. E. Scruggs and K. K. Gleason, *Chem. Phys.*, 1992, **166**, 367.
642. S. Lacelle, *Adv. Magn Reson. and Opt. Reson.*, 1991, **16**, 173.
643. E. M. Menger, S. Vega and R. G. Griffin, *J. Am. Chem. Soc.*, 1986, **108**, 2215.
644. B. H. Meier and W. L. Earl, *J. Chem. Phys.*, 1986, **85**, 4905.
645. Y. Ba and W. S. Veeman, *Isr. J. Chem.*, 1992, **32**, 173.
646. Y. Ba and W. S. Veeman, *Solid State NMR*, 1993, **2**, 131.
647. Y. Ba and W. S. Veeman, *Solid State NMR*, 1994, **3**, 249.
648. R. Tycko, *J. Am. Chem. Soc.*, 1994, **116**, 2217.
649. H. Geen, J. J. Titman, J. Gottwald and H. W. Spiess, *Chem. Phys. Lett.*, 1994, **227**, 79.
650. W. Sommer, J. Gottwald and H. W. Spiess, *J. Magn. Reson.*, 1995, **A113**, 131.
651. H. Geen, J. J. Titman, J. Gottwald and H. W. Spiess, *J. Magn. Reson.*, 1995, **A114**, 264.
652. J. Gottwald, D. E. Demco, R. Graf and H. W. Spiess, *Chem. Phys. Lett.*, 1995, **243**, 314.
653. J. Chang, C. Connor, E. L. Hahn, H. Huber and A. Pines, *J. Magn. Reson.*, 1989, **82**, 387.
654. C. Connor, *Adv. Magn. Reson.*, 1990, **15**, 201.
655. N. F. Ramsey and R. V. Pound, *Phys. Rev.*, 1951, **81**, 278.
656. D. T. Edmonds, *Phys. Rep.*, 1977, **29**, 233.
657. J. M. Millar, A. M. Thayer, A. Bielecki, D. B. Zax and A. Pines, *J. Chem. Phys.*, 1985, **83**, 934.
658. R. Kreis, A. Thomas, W. Studer and R. Ernst, *J. Chem. Phys.*, 1988, **89**, 6623.
659. J. W. Hennel, A. Birczynski, S. F. Sagnowski and M. Stachurowa, *Z. Phys.*, 1985, **B60**, 49.
660. J. M. Millar, A. M. Thayer, D. B. Zax and A. Pines, *J. Am. Chem. Soc.*, 1986, **108**, 5113.
661. P. Jones, M. Luzar and A. Pines, *J. Chem. Phys.*, 1986, **85**, 4873.
662. P. Meier, G. Kothe, P. Jones, M. Trecoske and A. Pines, *J. Chem. Phys.*, 1987, **87**, 6867.
663. Yu. A. Serebrennikov, *Chem. Phys.*, 1987, **112**, 253.
664. Yu. A. Serebrennikov, *Adv. Magn. Reson.*, 1990, **17**, 47.
665. D. P. Weitekamp, A. Bielecki, D. B. Zax, K. W. Zilm and A. Pines, *Phys. Rev. Lett.*, 1983, **50**, 1807.
666. R. Kreis, D. Suter and R. Ernst, *Chem. Phys. Lett.*, 1985, **118**, 120.
667. D. B. Zax, A. Bielecki, K. W. Zilm and A. Pines, *Chem. Phys. Lett.*, 1984, **105**, 550.
668. A. M. Thayer and A. Pines, *J. Magn. Reson.*, 1986, **70**, 518.
669. T. P. Javrie, K. Takagoshi, D. Suter and A. Pines, *Chem. Phys. Lett.*, 1989, **158**, 325.
670. C. J. Lee, D. Suter and A. Pines, *J. Magn. Reson.*, 1987, **75**, 110.
671. A. Llor, Z. Olejiniczak and A. Pines, *J. Chem. Phys.*, 1995, **103**, 3966.
672. A. Llor, Z. Olejiniczak and A. Pines, *J. Chem. Phys.*, 1995, **103**, 3982.
673. A. M. Thayer, M. Luzar and A. Pines, *J. Magn. Reson.*, 1987, **72**, 567.
674. A. M. Thayer, J. M. Millar, M. Luzar, T. P. Jarvie and A. Pines, *J. Chem. Phys.*, 1986, **90**, 1577.
675. A. M. Thayer and M. Luzar, *Mol. Phys.*, 1987, **62**, 573.
676. D. Suter, T. P. Jarvie, B. Sun and A. Pines, *Phys. Rev. Lett.*, 1987, **59**, 106.
677. A. Bielecki, J. B. Murdoch, D. P. Weitekamp, D. B. Zax, K. W. Zilm, H. Zimmermann and A. Pines, *J. Chem. Phys.*, 1984, **80**, 2232.

678. A. Bielecki, D. B. Zax, K. W. Zilm and A. Pines, *Rev. Sci. Inst.*, 1986, **57**, 393.
679. R. Tycko, *Phys. Rev. Lett.*, 1988, **60**, 2734.
680. R. Tycko, *J. Chem. Phys.*, 1990, **92**, 5776.
681. R. Tycko, *Adv. Magn. Reson.*, 1990, **14**, 203.
682. R. Tycko, G. Dabbagh, J. C. Duchamp and K. T. Zilm, *J. Magn. Reson.*, 1990, **89**, 205.
683. B. Q. Sun and A. Pines, *J. Magn. Reson.*, 1995, **A109**, 157.

High-pressure NMR

LANCE BALLARD AND JIRI JONAS

Department of Chemistry, School of Chemical Sciences and Beckman Institute for Advanced Science and Technology, University of Illinois, Urbana, Illinois 61801, USA

1. INTRODUCTION

It is not surprising that we experience a major expansion in applications of high-pressure NMR spectroscopy to problems in chemistry, biochemistry and physics.[1,2] Advances in superconductivity magnet technology have resulted in the development of superconducting magnets capable of attaining a high homogeneity of the magnetic field over the sample volume, so that even without sample spinning, high resolution can still be achieved. The ability to record high-resolution NMR spectra on dilute spin systems opened a new field of high-pressure NMR spectroscopy, which deals with pressure effects on biochemical systems.[3]

In this chapter we review the literature in the period from 1993 to the present; several detailed review articles dealing with high-pressure NMR appeared in 1992 and 1993.[4–6] In view of our own interest, the main emphasis of this report is on high-resolution, high-pressure NMR instrumentation and applications to studies of biochemical systems.

It is appropriate to summarize briefly the fundamental reasons why it is important to carry out high-pressure experiments on chemical or biochemical

ANNUAL REPORTS ON NMR SPECTROSCOPY
VOLUME 33 ISBN 0-12-505333-9

systems. During experiments at constant pressure, a change in temperature produces both a change in density and a change in kinetic energy of the molecules. Therefore, in order to separate the effects of density (volume) and temperature on a dynamic process one has to use both pressure and temperature as experimental variables. The use of pressure allows one to extend the range of measurements above the boiling point of a liquid, and also permits the study of supercritical dense fluids. Studies of simple liquids indicated that volume effects often determine the mechanism of a specific dynamic process, whereas temperature only changes the frequency of the motions without actually affecting the mechanism.

For studies of biochemical systems, one should point out several additional reasons for high-pressure experiments. Because noncovalent interactions play a primary role in the stabilization of biochemical systems, the use of pressure allows one to change, in a controlled way, the intermolecular interactions without the major perturbations produced by changes in temperature and/or chemical composition. Pressure affects chemical equilibria and reaction rates. The following standard equations define the reaction volume ΔV, and the activation volume, $\Delta V\ddagger$:

$$\Delta V = -\left[\frac{RT\,\partial \ln K}{\partial P}\right]_T, \quad \Delta V\ddagger = -\left[\frac{RT\,\partial \ln k}{\partial P}\right]_T \tag{1}$$

where K is the equilibrium constant, and k is the reaction rate.
Although proteins are known to undergo pressure denaturation, few details are known about this important process or how it is related to thermal- or solvent-induced denaturation. According to the high-pressure phase diagram of water, even at -15°C water is still a liquid. Therefore, protein solutions can be measured at subzero temperatures to investigate their cold-denaturation behaviour. Finally, the phase behaviour and dynamics of phospholipid membranes can be explored more completely by carrying out experiments at high pressure. The lipid-phase transitions are influenced by pressure, and unique high-pressure gel phases are produced.

Pressures used to investigate biochemical systems range from 0.1 MPa to 1 GPa (0.1 MPa = 1 bar; 1 GPa = 10 kbar); such pressures only change intermolecular distances and affect conformations but do not change covalent bond distances or bond angles. Pressures in excess of 30 GPa are required to change the electronic structure of a molecule.[7]

This report is organized as follows. The next section (Section 2) deals with high-pressure NMR instrumentation and covers the main design features of high-pressure, high-resolution NMR. In Section 3, we include a discussion of two specific applications of high-pressure NMR for the study of model membranes. Section 4 includes several examples of high-resolution two-dimensional (2D) NMR experiments on chemical and biochemical systems performed recently in our laboratory. In order to inform the reader about

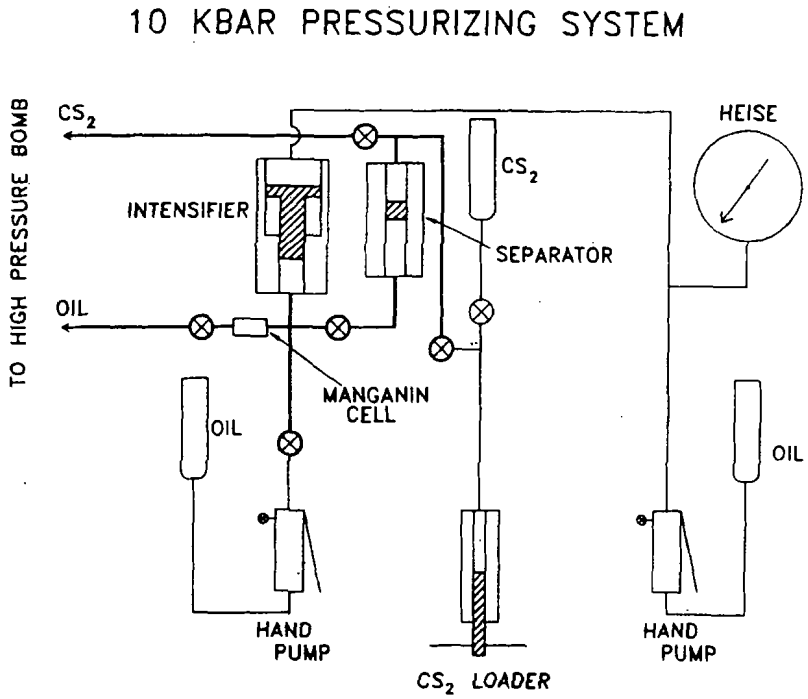

Fig. 1. Schematic diagram of the high-pressure generating equipment.

the wide spectrum of applications of high-pressure NMR spectroscopy, an overview of recent high-pressure NMR studies is provided in tabular form in Section 5.

2. NMR INSTRUMENTATION FOR HIGH-PRESSURE WORK

Nearly all the components necessary for building a high-pressure setup, such as piston hand pumps, high-pressure tubing and valves, intensifiers, and high-pressure separators, are currently available from commercial sources. The high-pressure setup consists of three main parts: (1) the pressure-generating system, (2) the pressure-measuring system, and (3) the NMR probe, which is located in a high-pressure vessel.

Figure 1 shows a schematic drawing of the high-pressure generating system used in our laboratory, illustrating the relative simplicity of the standard equipment used to generate high hydrostatic pressure.[8] This system can produce hydrostatic pressure up to 1 GPa.

In our laboratory, we have used high-resolution, high-pressure NMR spectroscopy to investigate simple molecular liquids for over two decades. Early on, we predicted that this high-pressure technique would be applied

Table 1. Performance characteristics of some selected high-pressure, high-resolution NMR probes.

Probe Type[a]	Pressure[b] (bars)	Temperature (K)	Sample Ø[c] (mm)	Resolution[d] ($\times 10^{-9}$)	^{1}H frequency (MHz)	Ref.
C-P-N	*c.* 2500	–[e]	1	8.0	100	10
C-P-R	*c.* 2500	–[e]	1.5	3.0	100	10
C-S-R	*c.* 140	–[e]	3.4	1.4	360	11
C-FS-R	*c.* 1000	–[e]	[f]	1.1	300	12
HPV	3700	263–353	1.5	10	60	13
HPV	5000	203–473	6	5.0	180	14
HPV	2500	213–423	5	5.0	200	15
HPV	300	n.a	[g]	2.3	300	16
HPV	6000	150–450	3	6.7	300	17
HPV	6000	263–353	10	3.0	300	18
HPV	9000	263–353	8	3.0	300	19
HPV	2500	233–423	5	1.0	400	20
HPV	2200	n.a.	5	10	400	21

[a]C = capillary; P = pyrex; S = sapphire; FS = fused silica; N = nonrotating; R = rotating; HPV = high-pressure vessel, nonrotating.
[b]Pressure represents typical reported working pressure for capillary (c) probes and the highest test pressure reported for high-pressure vessel (HPV) probes.
[c]Sample Ø represents the tube inner diameter for the thick-walled tubes of capillary-style systems, and the tube outer diameter for the thin-walled tubes of high-pressure vessel-style systems.
[d]Resolution represents the best reported resolution values, not necessarily the "typical" resolution.
[e]Temperature range depends on the temperature range of the commercial probe being used.
[f]Tube consists of fused silica capillary (360 μm outside diameter, 100 μm internal diameter) looped several times to fit inside a 5-mm NMR tube.
[g]Torroid cavity-style coil.
n.a. – data not available.

to studies of biological systems.[9] However, initial progress in this area has been slow because of technical difficulties and the need for specialized equipment.

A survey of performance features of high-resolution, high-pressure NMR probes is given in Table 1. Several features of NMR probe design[18] are essential for biochemical applications of the high-pressure NMR technique: high resolution, high sensitivity, wide pressure and temperature ranges, large sample volume, reliable r.f. feedthroughs, contamination-free sample cells, ease of assembly and use, and suitability for superconducting magnets.

For clarity, Fig. 2 is a schematic diagram of a high-resolution NMR probe

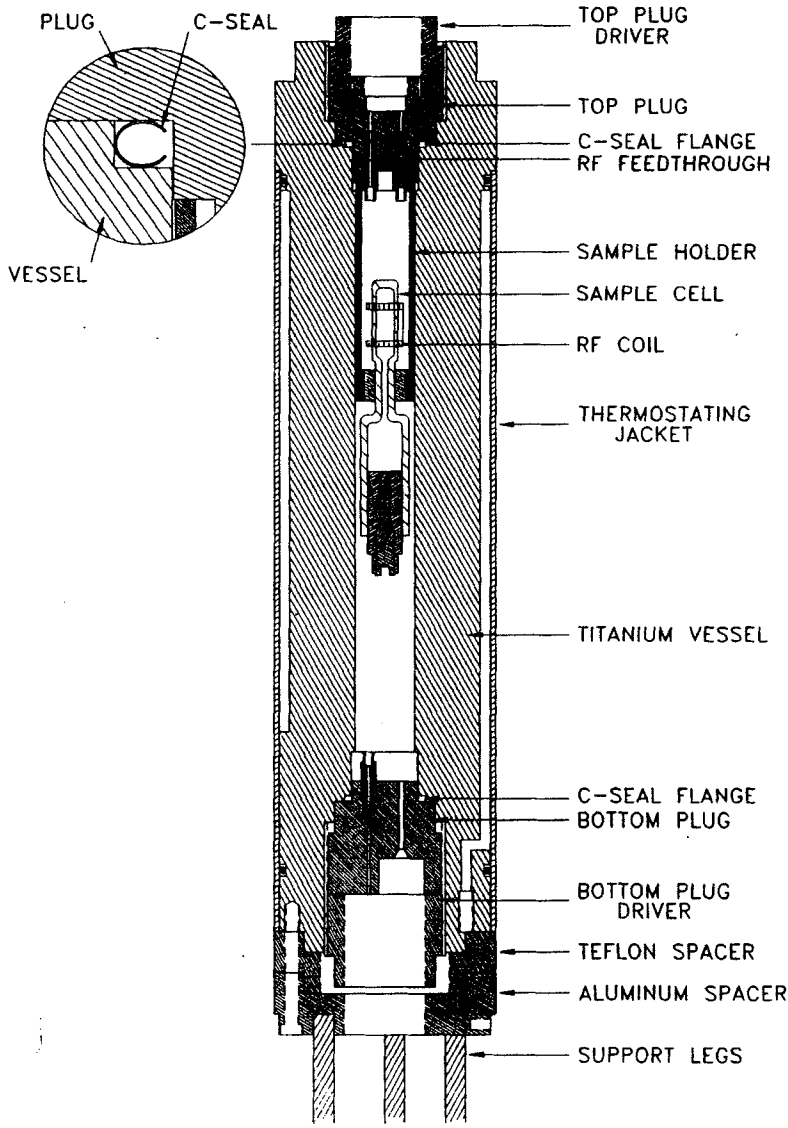

Fig. 2. Schematic drawing of the high-pressure, high-resolution NMR probe. The C-seal is shown in inset.

used in our laboratory. Details of the construction are given in the original references.[18] To make the reader aware of specialized high-pressure NMR probes, Table 2 lists the main performance features of high-temperature, low-temperature, and special-application NMR probes.

Table 2. Selected high-pressure NMR probes for special applications.

Feature	Pressure (bar)	Temperature (K)	^{1}H NMR[a] frequency (MHz)	Ref.
High temperature	2000	298–973	60	22
	10 000	298–600	180	23
Low temperature	7000	77–300		24
	10 000	100–300		25
	15 000	2–100		26
	3000	80–380		27
Stopped flow	2000	243–353	270	28
Homogenous catalysis with stirring	2000	223–423	180	29

[a]Proton Larmor frequency is listed only for those probes where proton tuning is specified.

3. HIGH-PRESSURE NMR STUDIES OF MODEL MEMBRANES

Interest in pressure as an experimental variable has been growing in studies of membranes by a variety of experimental techniques, including IR and Raman spectroscopy, light transmission, fluorescence spectroscopy, X-ray diffraction, neutron scattering, and NMR. By applying high pressure to membrane systems, one can observe changes in the dynamics of the component lipids and new pressure-induced phases. Temperature–pressure phase diagrams have been generated for several phospholipid systems. In our laboratory, we have initiated systematic high-pressure NMR studies on model phospholipid membranes. Table 3 summarizes these studies, two of which are discussed in the next section. First, the effects of pressure on the lateral diffusion of phospholipid molecules in sonicated pure DPPC and 1-palmitoyl-2-oleoylphosphotidylcholine (POPC) vesicles in D_2O were examined using the high-pressure proton NMR rotating frame spin-lattice relaxation method. Second, selected results of our high-pressure ^{2}H NMR study of the effects of pressure on the structure and dynamics of selectively denaturated 1,2-dipalmitoyl-*sn*-glycero-3-phosphatidylcholine (DPPC) multilamellar aqueous dispersion are discussed.

3.1. Pressure effects on lateral self-diffusion of phosphatidylcholines in sonicated unilamellar vesicles[38]

Lateral diffusion of phospholipids in model membranes at ambient pressure has been studied using a variety of techniques including fluorescence recovery

Table 3. NMR studies of the pressure effects on model membranes.[a]

System	Experiment	Result	Ref.
DPPC[b]	Natural abundance ^{13}C, T_1, T_2	Phase transitions	30
DMPC[c] POPC[d]	^1H 2D-NOESY	NOE build-up curves	31
DPPC-d_{62}	^2H lineshapes	Phase diagram; Order parameter; Pressure reversal of the anesthetic effect of tetracaine	32, 33
DPPC(TTC)[e]	^{31}P lineshapes, T_1	Structure and dynamics of the head group; Phase diagram	34
DPPC-d_2 (2,2); (9,9); (13,13)	^2H lineshapes, T_1, T_2	Order parameters; Chain motions	35
DPPC(TTC)	^1H T_1, 2D NOESY	Dynamics; Location of TTC; Spin-diffusion	36
DPPC-d_{62}-cholesterol	^2H lineshapes	Phase diagram	37
DPPC POPC	^1H T_1 and Tiρ	Lateral diffusion	38

[a]Pressure range from 0.1 MPa to 500 MPa.
[b]DPPC, dipalmitoylphosphatidylcholine.
[c]DMPC, dimyristoylphosphatidylcholine.
[d]POPC, palmitoyloleylphosphatidylcholine.
[e]TTC, tetracaine.

after photobleaching (FRAP),[39] spin-labelled ESR,[40] pulsed field gradient NMR (PFG-NMR),[41,42] quasielastic neutron scattering (QENS),[43,44] excimer fluorescence[45] and others.[46–48] In general the values previously reported for the lateral diffusion coefficient (D) range from 10^{-9} to $10^{-6}\,cm^2\,s^{-1}$ in the liquid crystalline phase and from 10^{-10} to $10^{-7}\,cm^2\,s^{-1}$ in the gel phase at ambient pressure.

The NMR rotating frame spin-lattice relaxation time ($T_{1\rho}$) method,[47,49] which has been used successfully in our laboratory in studies of pressure effects on diffusion in highly viscous liquids,[50,51] was used in this study to measure lateral diffusion of the phospholipid molecules in DPPC and POPC vesicles. An advantage of this method is that the diffusion coefficient is found directly from measured quantities without estimations of molecular parameters or the effects of the addition of spin or fluorescence probes to

the bilayers. If intermolecular dipolar interactions modulated by translational motion contribute significantly to the proton relaxation, the rotating frame spin-lattice relaxation rate ($1/T_{1\rho}$) is a function of the square root of the spin-locking field angular frequency ($\omega_1^{1/2}$) according to the following equation:[47,49]

$$\frac{1}{T_{1\rho}} = C\omega_1^{1/2} + \frac{1}{T_2} \tag{2}$$

where C is a constant that contains the lateral diffusion coefficient and $1/T_2$ is the spin–spin relaxation rate. By taking the derivative of equation 1 with respect to $\omega_1^{1/2}$ and applying the resulting equation to motion in only two dimensions, an equation is obtained by which the lateral diffusion coefficient can be determined directly:[47]

$$\frac{d(1/T_{1\rho})}{d(\omega_1^{1/2})} = -3\sqrt{3}\gamma^4\hbar^2 n/40D^{3/2} \tag{3}$$

where γ is the gyromagnetic ratio, $\hbar$ is Planck's constant divided by 2π, n is the spin density (spins ml^{-1}) and D is the lateral diffusion coefficient. However, there are two experimental requirements that must be met for this equation to be valid.[49] The first is that the angular frequency of the spin-locking field (ω_1) must be greater than the strength of the local dipolar field (H_{loc}) or $\omega_1 = \gamma H_1 > \gamma H_{loc}$, where H_1 is the strength of the applied spin-locking r.f. field. The second requirement on the use of equation (2) in determining the lateral diffusion coefficient is that $(\omega_1\sigma^2/D)^{1/2} \leq 2$, where σ is the molecular diameter.

In this study, we measured the lateral diffusion coefficients of the phospholipid molecules in sonicated pure DPPC and pure POPC vesicles at pressures ranging from 1 bar to 5 kbar by using the proton $T_{1\rho}$ method. We used sonicated vesicles (unilamellar vesicles) to achieve better resolution, and the choline methyl (NMe_3) proton resonance is well resolved from the palmitoyl methylene $(CH_2)_n$ proton resonance. Also the NMe_3 proton resonance of the sonicated vesicles is still sharp even at the pressure of 5 kbar. For the pressure effects on the lateral diffusion coefficient, each of the two phosphatidylcholine systems was measured at temperatures above its main chain-melting transition temperature (T_m).[52] The DPPC vesicles ($T_m = 41°C$) were studied at temperatures ranging from 50°C to 70°C. The POPC vesicles ($T_m = -5°C$) were measured at temperatures from 5°C to 35°C. Three distinct ranges of the values of the lateral diffusion coefficients of DPPC under increasing pressure have been attributed to different phases: the liquid-crystalline (LC) phase, the pressure-induced gel I (GI) phase, and the pressure-induced interdigitated gel (Gi) phase.[53–57] Two distinct ranges of the values of the lateral diffusion coefficients of POPC have been attributed

to the LC phase and the GI.[55,56] It is noteworthy that the LC and GI phases exist in both multilamellar and sonicated vesicles of DPPC and POPC[58] and the interdigitated gel phase exists in both multilamellar and sonicated DPPC vesicles.[59] The activation volume for diffusion of DPPC and POPC vesicles in the LC phase and the activation energy for diffusion of DPPC and POPC vesicles in the LC and GI phases were also determined. Lateral diffusion coefficients and line width data at various pressures and temperatures were used to construct pressure–temperature phase diagrams of sonicated pure DPPC and POPC vesicles.

3.2. High-pressure ^{2}H NMR study of the dynamics of selectively deuterated DPPC in multilamellar aqueous dispersions[35]

The ^{2}H NMR lineshapes and relaxation times T_1 and T_2, of 1,2-dipalmitoyl-*sn*-glycero-3-phosphocholine selectively deuterated at (2′,2′-^{2}H),(9′,9′-^{2}H), and (13′,13′-^{2}H) on both chains were measured as a function of pressure from 1 bar to 5 kbar at 50°C. As shown in our previous study,[60] this pressure range permits us to explore the phase behaviour of DPPC from the LC phase through various gel phases such as the Gel I ($P_{\beta'}$), Gel II ($L_{\beta'}$), Gel III, Gel X, and the interdigitated gel phase, Gel i. The main goals of this study were as follows: (1) to determine the effects of pressure on deuterium lineshapes and relaxation times T_1 and T_2 of the different segments of DPPC; (2) to obtain order parameters as a function of pressure in the LC phase; (3) to determine pressure effects on the first moment $M1$, for the various high-pressure gel phases; (4) to compare the motional behaviour of the different chain segments and their response to pressure in the different phases; (5) to determine whether changing S_{CD} by increasing pressure in the LC phase yields linear T_1^{-1} versus S_{CD}^2 and T_2^{-1} versus S_{CD}^2 relationships for the different deuterated segments studied in multilamellar DPPC dispersions.

Because a number of high-pressure NMR studies of the effects of pressure on the lineshapes have been recently reported, the following illustrative example focuses on T_1 and T_2 relaxation experiments.[35] In this study, T_1 and T_2 relaxation times were measured employing multi-pulse sequences in order to detect motions with different frequencies. Because many types of motions are involved in this system, it is not surprising to find a complicated relaxation behaviour as shown in Figs 3 and 4. A quantitative evaluation of these motional rates requires comprehensive computer simulation and appropriate molecular modelling[61] which are beyond the scope of this study. In the following paragraphs, we discuss the main features of the relaxation results in a qualitative way.

The spin lattice relaxation time, T_1, is sensitive to motions with a correlation time τ_c near ω_0^{-1}; therefore, motions with correlation times in the

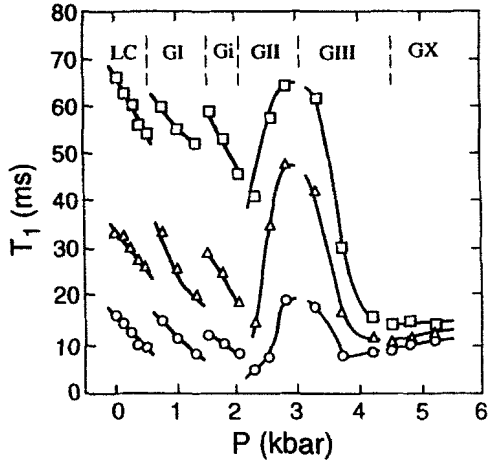

Fig. 3. The spin-lattice relaxation time, T_1, as a function of pressure for 1,2(2′,2′-^{2}H) DPPC(O), 1,2,(9′,9′-^{2}H)DPPC(Δ); and 1,2(13′, 13′-^{2}H)DPPC(□) samples at 50°C. The pressure range of this study allowed observation of the liquid-crystalline (LC), Gel I (GI), inter-digitated gel (Gi), Gel II (GII), Gel III (GIII), and Gel X (GX) phase regimes.

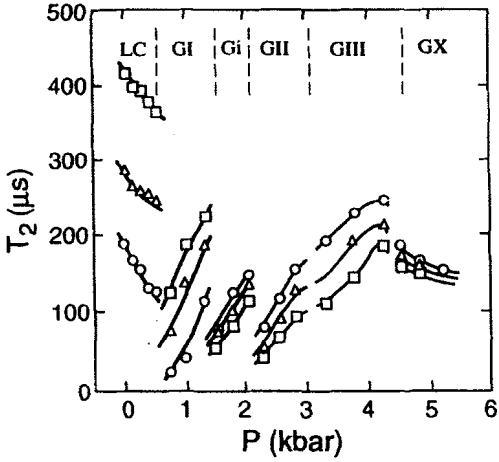

Fig. 4. The spin-spin relaxation time, T_2, as a function of pressure for 1,2(2′,2′-^{2}H)DPPC(O), 1,2(9′,9′-^{2}H)DPPC(Δ), and 1,2(13′, 13′-^{2}H)DPPC(□) samples at 50°C.

range from 10^{-8} to 10^{-11} s are accessible from spin-lattice relaxation measurements. In the LC phase, the different T_1 values observed for deuterons on the *sn*-1 and *sn*-2 chains indicate clearly that the motional states of the C-2 segment of the *sn*-1 chain are different from those of the *sn*-2 chain. The order of T_1 values in the LC phase is C-13 > C-9 > C-2, indicating a

greater motional freedom towards the end of the acyl chain. The three discontinuities at phase transitions LC/Gel I, Gel I/Gel i, and Gel i/Gel II indicate abrupt changes in rates for different modes of motion among these phases. In the Gel I and Gel i phases, the largest T_1 for the C-13 segment shows that the C-13 segment is the most mobile in the fast correlation time region (10^{-8}–10^{-11} s). As illustrated in Fig. 3, the T_1 values increase with pressure in the Gel II phase, reach a maximum at the phase transition between Gel II/Gel III, and then decreases in the Gel III phase. A further increase in pressure results in a local minimum near the phase transition between Gel III/Gel X and a slight increase in the Gel X phase. All three segments approach a common T_1 value in the Gel X phase, suggesting a common motional mode in the Gel X phase which is, most likely, the *trans*-gauche isomerization. Inspection of Fig. 3 shows that the order of magnitude of T_1 is C-13 > C-9 > C-2 in all the phases maintaining the same order of motional rates for the three segments.

In comparison with T_1, the spin–spin relaxation time T_2 is more sensitive to motions with correlation times near $(e^2qQ/h)^{-1}$. Therefore, T_2 measurements provide information on motions with correlation times in the intermediate to slow range (10^{-4}–10^{-8} s). In the LC phase, the same T_2 values are obtained for the C-2 segment of the two chains, indicating the same segmental motional rate in the intermediate correlation time region. The variation of T_2 with chain position represents different motional rates for different segments in the LC phase. The order of magnitude of T_2 is C-13 > C-9 > C-2, indicating the greatest mobility for the C-13 segment in agreement with the T_1 results; the T_2 values also decrease with increasing pressure in the LC phase, indicating a motionally narrowed regime. Much reduced T_2 values are observed just below the main phase transition, resulting in a significant echo intensity loss in the spectra. In the Gel I phase, the T_2 values increase with increasing pressure, indicating a slow correlation time regime. The same trend was also observed in DMPC bilayers[62] at the transition between the LC and the gel phases. Figure 4 shows three discontinuities in T_2 values at the phase transitions for LC/Gel I, Gel I/Gel i, and Gel i/Gel II, indicating different dynamic properties for the system in the different gel phases. The T_2 values increase with pressure in the Gel I, Gel i, Gel II, and Gel III phases; there is also a local maximum near the phase transition between Gel III and Gel X. A further increase in pressure causes a decrease in T_2 values in the Gel X phase where all segments approach the same T_2 value, indicating a common motional mode in the Gel X phase.

Figure 4 also shows a variation of T_2 values with the chain position in all of the phases. Our results are different from those for DMPC bilayers obtained by Mayer *et al.*,[62] where the same T_2 value was observed in the gel phases for all chain positions except for the terminal methyl group. The differences reflect the different dynamic properties of these two phospholipids and also the differences in the dynamics of the thermotropic and barotropic gel phases. In contrast to the LC and Gel I phases, the order of T_2 values becomes

C-2 > C-9 > C-13 for Gel i through Gel X phase, possibly reflecting slow axial motions, and the greater range of motions of the C-2.

The availability of experimental pressure dependencies for T_1, T_2, and S_{CD} as determined for the selectively deuterated DPPC molecules in the LC phase, allowed us to test whether linear T_1^{-1} versus S_{CD}^2 and T_2^{-1} versus S_{CD}^2 relationships;[63,64] also hold for changing pressures. One should point out that there is still a difference of opinion whether this linear relationship signifies collective motions for various chains.[63–66] In our experiments a linear relationship between T_1^{-1} and S_{CD}^2 is indeed observed. We find that all data points fall on the same straight line for 1,2(9′,9′-^{2}H)DPPC and 1,2(13′,13′-^{2}H)DPPC, at all pressures in the LC phase at 50°C ($T_1^{-1} = 738.8\,s^{-1}\,S_{CD}^2 + 1.59\,s^{-1}$). In contrast, the T_1^{-1} versus S_{CD}^2 for C-2 *sn*-2 deuterons and *sn*-1 deuterons does not fall on the same straight line and have an intercept value which is nonphysical (<0). As with T_1 data, there is a linear relationship between T_2^{-1} and S_{CD}^2. The data for the C-9 and C-13 segments falls on the same straight line with the following equation: $T_2^{-1} = 5.329 \times 10^4\,s^{-1}\,S_{CD}^2 + 1480\,s^{-1}$. Once again, there are two lines with different slopes and intercepts for the C-2 segments of the two chains, suggesting that the motions for the C-2 segments are not correlated with the other two segments. In contrast to the DMPC bilayers the cooperative chain motions apparently do not extend to the C-2 segment.[63] However, our results are in agreement with the conclusions of Brown[63] and Watnick *et al.*[64] that the cooperative motions extend from at least C-9 toward the end of the acyl chains. The chain carbons near the glycerol backbone may act as anchor groups in DPPC bilayers and do not obey the common linear relationship observed for positions 9 and 13.

4. APPLICATIONS OF TWO-DIMENSIONAL NMR TECHNIQUES AT HIGH PRESSURE

4.1. High-pressure two-dimensional NOESY study of complex liquid of 2-ethylhexyl benzoate[67]

Two-dimensional nuclear Overhauser effect spectroscopy (NOESY) has proven to be a valuable technique in determining the conformations of large polypeptides[68–71] and oligonucleotides.[72] The slow motional regime in which such molecules lie (where $\omega\tau > 1$) causes the zero quantum transition to be extremely important in determining the rate of cross-relaxation. Cross-relaxation in the homonuclear case is described by the expression[70,72]

$$R_{ij}^C = \frac{\gamma^4 \hbar^2}{10 r_{ij}^6} [6J_2(2\omega) - J_0(0)] \tag{4}$$

where γ is the gyromagnetic ratio, r_{ij} is the internuclear distance, $J_2(2\omega)$ is

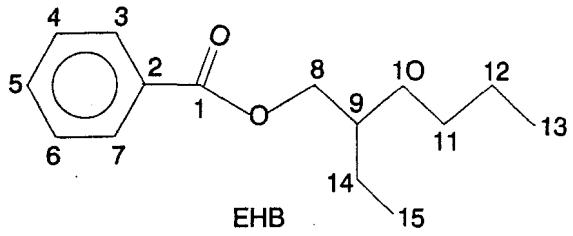

Fig. 5. Structural formula of 2-ethylhexylbenzoate (EHB). Carbons are numbered according to international rules.

the double-quantum spectral density, and $J_0(0)$ is the zero-quantum spectral density. Because cross-relaxation rates are large in magnitude in the slow motional regime, the NOESY experiment is especially suited to studying the conformations of large, slow-moving molecules in solution. The technique has rarely been employed in the study of smaller molecules.[73] The motional regime in which such smaller molecules fall is often such that the cross-relaxation rates are near zero, resulting in small cross-peaks in the 2D spectrum and long evolution times. Lengthy T_1s can also make NOESY experiments extremely long if three to five times the maximum T_1 is used as a preparation period. It would therefore be advantageous to decrease the rotational rates of small molecules in order to bring the molecular motion into the slow motional regime. In one-dimensional NOE studies of the antibiotic echinomycin, slow molecular motion was achieved by use of a highly viscous solvent.[74] In this study, the application of high pressure at low temperatures was used to slow down molecular motion in the complex fluid 2-ethylhexyl benzoate (EHB), shown in Fig. 5. This fluid has been the subject of previous transport and relaxation studies carried out in our laboratory.[51,75,76] The high-pressure/low-temperature NMR capability allowed the 2D NOESY experiment to be performed in the slow motional regime, as indicated by the presence of positive cross-peaks in a phase-sensitive NOESY spectrum. In order to separate intramolecular and intermolecular cross-relaxation interactions, NOESY cross-peak evolution rates were measured as a function of the mole fraction of EHB in perdeuterated EHB-d_{22}. Cross-relaxation rates at infinite dilution were assumed to occur only from intramolecular interactions. We have therefore assumed that cross-relaxation between two protons occurs at a significantly greater rate than in a multi-step spin diffusion process. Spin diffusion is expressed in the quadratic and higher-order terms in the Taylor expansion describing the mixing coefficient a_{kl} (which governs the intensity of the peaks in a NOESY spectrum):[70,77]

$$a_{kl}(\tau_m) = \left(\delta_{kl} - R_{kl}\tau_m + \frac{1}{2}\sum_j R_{kj}R_{jl}\tau_m^2 + \ldots \right) M_Z \qquad (5)$$

where $\delta = 1$ when $k = 1$ and $\delta = 0$ when $k \neq 1$, and τ_m is the mixing time. In this study, the NOESY cross-peaks occurring between protons k and I arise due to magnetization transfer from proton k to deuterium j to proton I. Our analysis considered the quadratic and higher-order terms to be negligible because R_{kj} (and R_{jk}) should be less than R_{kl} and peak intensities were analysed at small values of τ_m.

The primary objective of this study was to determine whether pressure could be used to slow down the rotational motion of a small molecule so that its conformation could be studied in the negative cross-relaxation rate regime. To our knowledge, EHB is the smallest molecule ever studied by NOESY. The second objective was to investigate the effect of pressure on cross-relaxation in EHB. It was also hoped that some insight could be gained into the preferential conformation of EHB under such conditions of high density. Finally, we sought further dynamical information about EHB because the cross-relaxation rate is dependent on the rate of molecular motion.

Figure 6 shows a 1D ^{1}H spectrum of 10% EHB in EHB-d_{22} at −20°C and 1000 bar along with a 2D NOESY spectrum taken under the same conditions with a mixing time of 200 ms. Of particular interest are the cross-peaks occurring between aromatic and methyl protons. We believe the cross-peaks to be the result of through-space dipolar coupling and not the result of spin diffusion propagating through the molecule. The reader is directed to the original reference[67] for a quantitative explanation. Figure 6 also shows cross peaks between protons connected to carbon 8 and the methyl protons. Additional cross-peaks exist between chain methylene protons and aromatic protons. The experimental NOESY spectra showed a drastic effect of pressure on the cross-peak evolution rate (equal to the cross-relaxation rate).

In order to separate the intermolecular and intramolecular contributions to cross-relaxation, values of the cross-relaxation rate R_{ij}^C were plotted as a function of mole fraction of EHB in EHB-d_{22}. The experimental points were least-squares fit to a straight line and the y-intercept was taken to be the intramolecular contribution to the total cross-relaxation rate. This analysis neglects any cross-relaxation due to deuterium.

From the experimental data we were able to determine both the intramolecular and intermolecular relaxation rates as a function of pressure and temperature. The availability of shear viscosities and self-diffusion coefficients of EHB, which were measured earlier in our laboratory, provided the opportunity to test the dependence of the experimental cross-relaxation rates on viscosity and/or diffusion of EHB. The reorientational correlation time τ_c describing overall molecular motion is coupled to the η/T term through the Debye equation, which in a modified form is[78]

$$\tau_c = KV_H \frac{\eta}{kT} + \tau_H \tag{6}$$

where K is a parameter indicative of the ratio of the mean square

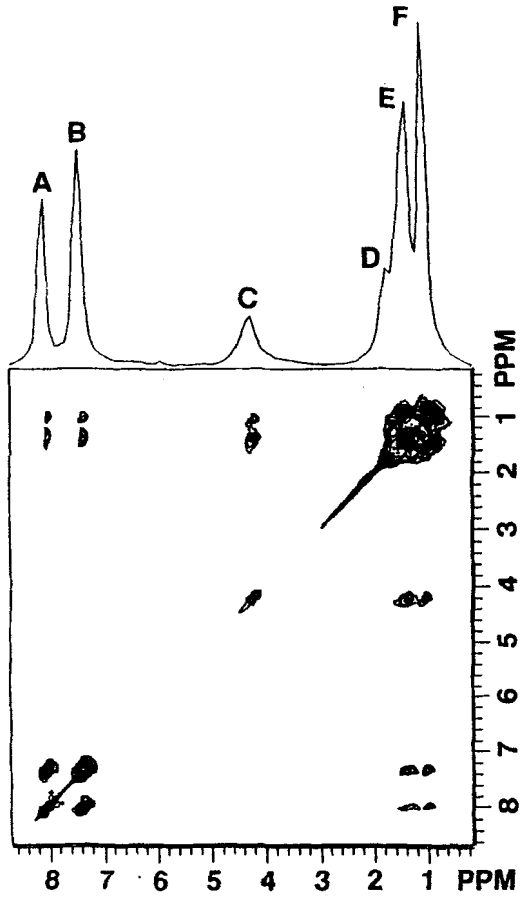

Fig. 6. One- and two-dimensional NOESY spectra of 10% EHB in EHB-d_{22} at −20°C a 1 kbar. Proton assignments for the carbon atoms (C#) in the numbered EHB structure (Fig. 5) are as follows: A-C3, C7; B-C4, C5, C6; C-C8; D-C9; E-C10, C11, C12, C14; F-C13, C15.

intermolecular torques on the solute molecules to the intermolecular forces on the solvent molecules, V_H is the hydrodynamic volume swept out by the reorienting vector, and τ_H is a zero viscosity intercept.[78] The relationship between cross-relaxation rate and viscosity can be further explored by considering that EHB molecular motion definitely lies in the $\omega\tau_c > 1$ regime. Using the analysis given in detail in the original study[67] one can show that in the slow motional regime a proportionality between the magnitude of the cross-relaxation rate and the shear viscosity is expected:

$$|R_{ij}^{C}|\,\alpha\tau_c = KV_H\frac{\eta}{kT} + \tau_H \tag{7}$$

where $\omega\tau_c > 1$.

In order to test the validity of equation (7) for the EHB system, we plotted $|R_{ij}^C|$ as a function of η/T, an example of which is shown in Fig. 7. The linear behaviour of the plot indicates good agreement with equation (7). Analogous plots for A–F, B–E and B–F relaxation rates as a function of η/T also showed good linearity. The linearity of the $|R_{ij}^C|$ versus η/T plots implies that overall rotation is extremely important in determining intramolecular cross-relaxation rates and that reorientation of each of the relaxation vectors is adequately described by one correlation time.

An investigation of intermolecular cross-relaxation can also be made. Intermolecular cross-relaxation rates equal to the differences between rates in the neat EHB liquid and corresponding intramolecular rates were calculated. It is expected that the rate of intermolecular relaxation should be related to the rate of diffusion. In the pressure and temperature range covered in the study, the EHB density changes by about 7% and the translational diffusion coefficient changes by about an order of magnitude,[75] so that R_{inter}^C should be more heavily dependent on D.

The limited resolution available under high-pressure/low-temperature conditions did not permit differentiation between the methyl group on the hexyl chain and the methyl group on the ethyl chain. It can therefore not be determined whether the aromatic-methyl crosspeaks are due to the hexyl chain or the ethyl chain or both of the chains being close enough to the ring in order to have cross-relaxation. In order to gain some qualitative insight into the conformational possibility of one or both of the chains folding back to be close to the ring, possible minimum conformational energy structures

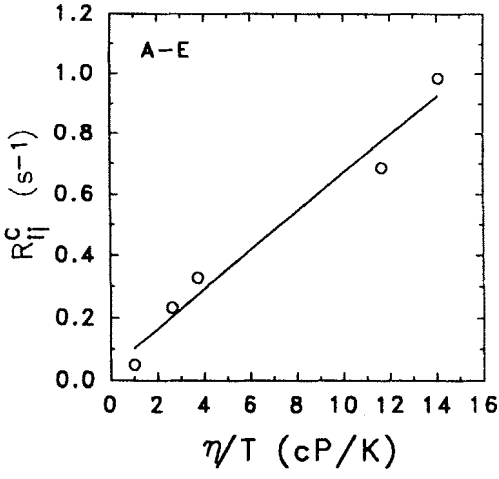

Fig. 7. The linear dependence of the intramolecular cross-relaxation rate on η/T for the cross-peaks between hydrogens on ring carbons 3, 7 and hydrogens on side-chain carbons 10, 11, 12, 14 (see Fig. 5).

of EHB were analysed using Allinger's MM2 force field parameters.[79] The calculations give qualitative information only because no intermolecular interactions are assumed and although distances between atoms can be constricted, the total volume cannot.

In view of the approximate nature of the discussion above one can only conclude that at high-pressure and low-temperature conditions, EHB exists in conformations where one or both of the chains are bent over toward the ring to allow a significant amount of cross-relaxation to occur between methyl and aromatic protons.

4.2. Pressure-induced dissociation of Arc repressor[80]

The results of our recent study of the pressure dissociation of Arc repressor are a good illustration of the unique information provided by advanced 2D NMR techniques at high pressures. To approach the question of how a protein acquires its biological three-dimensional structure or conformation, a perturbation is typically applied to the system. This perturbation can be chemical, such as pH extremes, urea or guanidine hydrochloride, or physical, such as temperature or pressure. However, the equilibrium between the "native state" (N) and the denatured state (D) might be affected in a different manner, depending on the nature of the perturbation. The subset of denatured states relevant to the equilibrium with the native state has been only transiently obtained, for example, by dilution of a denaturing agent. Therefore, to determine how a protein correctly folds from a random coil state into a native three-dimensional structure, one has to find a way to stabilize and characterize the folding intermediates. Several studies indicate that the folding intermediates have a compact structure, termed molten globule, with a secondary structure similar to the native state but with a disordered tertiary structure.

Arc repressor is a small, DNA-binding dimeric protein, consisting of 53 amino acid residues (M_r 13 000). It represses transcription from the P_{ant} promoter of *Salmonella* bacteriophage P22.[81–83] Arc repressor belongs to a family of proteins that have an antiparallel β-sheet as the interfacial DNA-binding motif.[84–86] A tertiary structure model for Arc repressor has been proposed[85] based upon homology between Arc repressor and the *Escherichia coli* Met repressor and on 2D NMR data.[87,88] This model consists of an intertwined dimer in which residues 8–14 of each monomer participate in the formation of an antiparallel β-sheet. Arc repressor dimer dissociates reversibly into subunits with increasing pressure, at fixed protein concentration, or with dilution, at constant pressure.[89] The Arc repressor monomer obtained by compression is compact, and, as measured by its rotational diffusion, has a much smaller molecular volume than that of Arc repressor denatured by urea. The dissociated Arc repressor exposes a nonpolar

core and binds bis(8-anilinonaphthalene-1-sulfonate) strongly.[89] Thus, the properties of the Arc repressor dissociated by pressure agree with the characteristic properties of a molten globule.[90–92] Previous fluorescence studies clearly showed that the pressure-dissociated form of the Arc repressor retains significant three-dimensional structure in contrast to the urea-denatured or temperature-denatured forms of the protein. A preliminary high-pressure NMR study from our laboratory suggested that the pressure-induced molten globule state of Arc repressor monomer adopts a β-strand, γ-turn, β-strand structure in the residue 8–14 region.[93]

Our study using high-pressure, high-resolution NMR techniques including 2D techniques had several goals. First, we wanted to use 1D and 2D NMR techniques to determine how different the pressure-dissociated Arc repressor monomer was from the monomer forms obtained by thermal or urea denaturation. Second, we wanted to provide experimental evidence for the existence of a pressure-induced predissociated state of Arc repressor which was suggested by our preliminary NMR experiments. Third, we wanted to partially characterize the structure of the predissociated state and the molten globule monomer state of Arc repressor. Finally, we also wanted to show that pressure is a more easily controlled and less drastic perturbation of protein structure than thermal or chemical denaturation.

The 2D NOESY spectra in the αH–αH region, where the NOE cross-peaks in the β-sheet region (residues 8–14) can be observed, show that the pressure-dissociated monomer is different from the thermal or urea denatured states. Figure 8 compares the NOESY spectra in the αH–αH region for the native state, the pressure-induced monomer state, the thermally denatured state, and the urea-denatured state. The most important finding is that NOE cross-peaks between α-H of Gln-9 and Arg-13 occur even in the pressure-denatured form, indicating the proximity of these two residues.[93] In contrast, no NOEs were observed between α-Hs of Gln-9 and Arg-13 in the NOESY spectra of Arc repressor at 70°C, nor in the presence of 7 M urea. This observation directly proves that Gln-9 and Arg-13 were no longer close to each other in the thermally or chemically denatured states.

The relative changes in 1D spectra of both aromatic and aliphatic regions at 1 kbar with respect to 1 bar indicated that there must be some changes in structure of Arc repressor prior to its dissociation. In this pressure range, there is no dissociation of 1 mM Arc repressor dimer according to the fluorescence emission and polarization experiments.[89]

Conclusive experimental evidence for the existence of a pressure-induced predissociated state of Arc repressor comes from the 2D NOESY experiments in the αH–αH region of the β-sheet residues (residues 8–14) performed at high pressure. Figure 9 shows the NOESY spectra in the αH–αH region in the pressure range from 1 bar to 5 kbar at 20°C. As expected, at 1 bar we observe a strong cross-peak between Gln-9 and Arg-13 (see Fig. 11) which indicates the presence of the intermonomer β-sheet in the Arc repressor

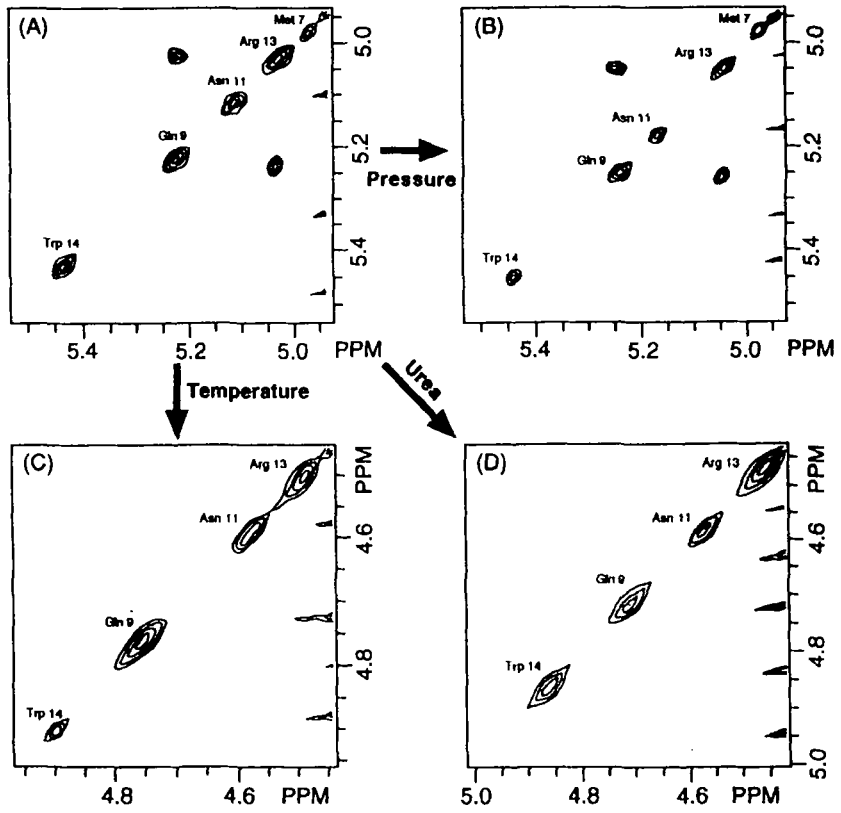

Fig. 8. Comparison of an expanded region of NOESY spectra showing the αH–αH correction in the β-sheet region of Arc repressor among the native state (A), pressure-induced molten globule state (B), thermally denatured state (C), and urea-denatured state (D).

dimer as proposed by Breg *et al.*[85,87] The increase in pressure to 500 bar does not produce significant changes in the NOESY spectra, but they change drastically at 1 kbar. At 1 kbar there appears an additional cross-peak between Gln-9 and Trp-14 and a cross-peak between Met-7 and Gln-9. Essentially the same NOESY spectrum persists at 1.5 kbar, but at 2 kbar only the cross-peak Gln-9 and Arg-13 persists. This cross-peak remains unchanged at pressures up to 5 kbar, i.e., in the pressure regime where Arc repressor dissociates into its molten globule monomers. This experimental evidence suggests that the conformation of the predissociated state could be intermediate between the antiparallel intermonomer β-sheet of native dimer[85] and the intramolecular β-sheet of the molten globule monomer.[93] The structures of the predissociated state and the molten globule monomer were obtained from molecular dynamics calculations and energy minimizations. The

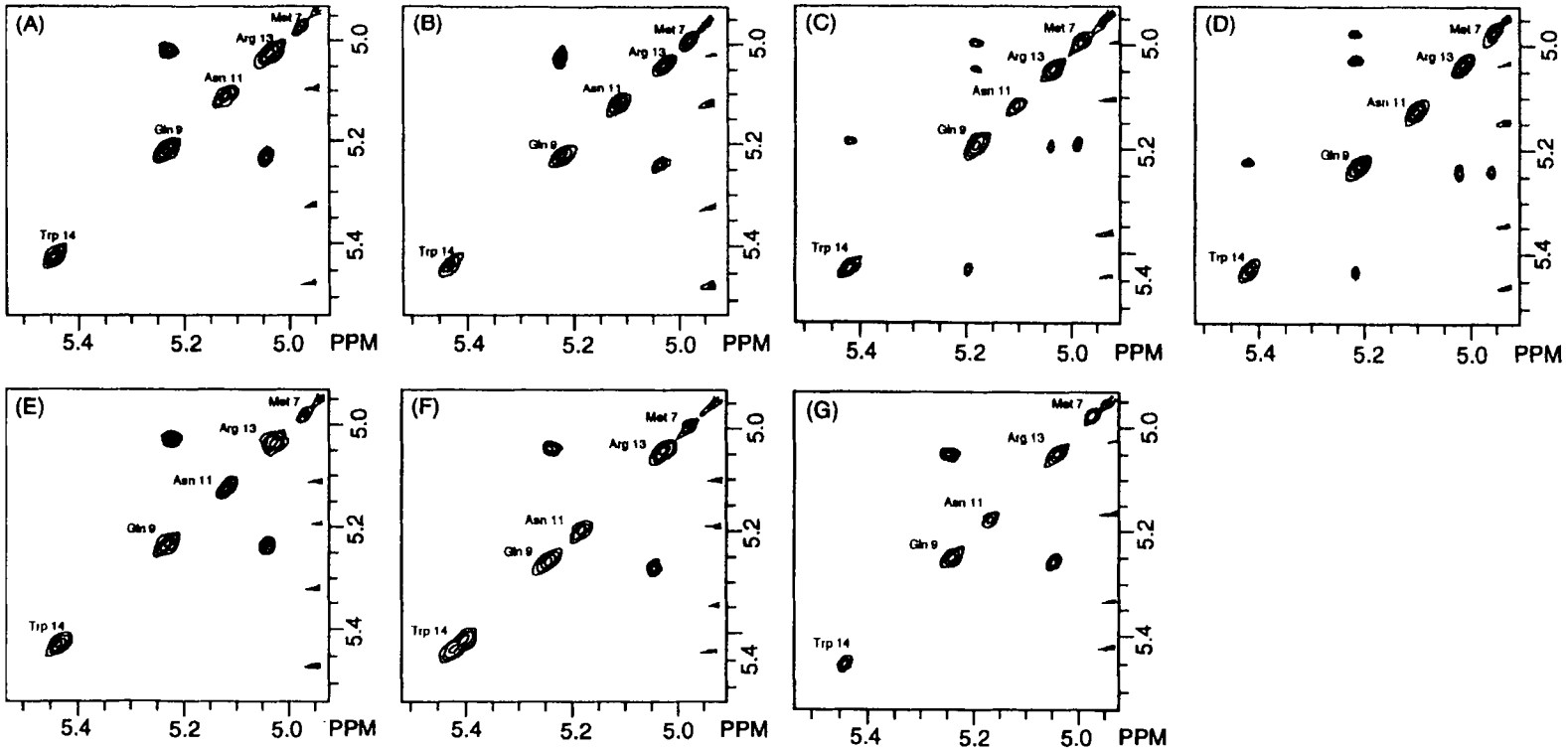

Fig. 9. Expanded region of NOESY spectra of Arc repressor at various pressures at 20°C: 1 bar (A), 500 bar (B), 1 kbar (C), 1.5 kbar (D), 2.5 kbar (E), 3.5 kbar (F), 5.0 kbar (G).

predissociated dimer may be related to the transition state in the protein folding theory described by Creighton,[94] corresponding to a high-energy distorted form of the native conformation. Further increases in pressure cause the dissociation of the predissociated state into molten globule monomers.

4.3. Pressure- and cold-denaturation of proteins[95]

Most studies dealing with protein denaturation have been carried out at atmospheric pressure using various physicochemical perturbations, such as temperature, pH, or denaturants as experimental variables. Compared with varying temperature, which produces simultaneous changes in both volume and thermal energy, the use of pressure to study protein solutions perturbs the environment of the protein in a continuous, controlled way by changing only intermolecular distances.[96] In addition, by taking advantage of the phase behaviour of water, high pressure can substantially lower the freezing point of an aqueous protein solution. Therefore, by applying high pressure one can investigate in detail not only pressure-denatured proteins, but also cold-denatured proteins in aqueous solution.

All globular proteins appear to be subject to denaturation by low temperatures, referred to as cold denaturation. Because this type of protein denaturation should occur at subzero temperatures in aqueous solutions at neutral pH, investigators have prevented freezing of water by different means, including protein solutions emulsified in oil,[97] supercooled aqueous solutions[98,99] and cryosolvents such as methanol.[98] Another way to depress the freezing point of aqueous protein solutions is to use high pressure, taking advantage of the high-pressure phase behaviour of water.[100]

In recent studies, we carried out cold denaturation experiments on Ribonuclease A and specifically used 2D NMR spectroscopy to determine the hydrogen exchange rates of individual backbone amide protons of this protein to confirm the presence of partially folded structures in the pressure-denatured and cold-denatured states. Our experiments had the following specific objectives: (1) to investigate the pressure unfolding of Ribonuclease A; (2) to study pressure-assisted cold unfolding; (3) to use hydrogen exchange experiments to compare the unfolded structures of Ribonuclease A produced by cold, heat, and pressure denaturation.

RNase A is a single-domain protein, a pancreatic enzyme which catalyses the cleavage of single-stranded RNA. This protein consists of 124 amino acid residues with a molecular mass of 13.7 kDa. It has traditionally served as a model for protein folding because it is small, stable and has a well-known native structure. The $\varepsilon 1$ protons of the four RNase A histidine residues are well-resolved from other protons in the ^1H NMR spectrum of the native protein in D_2O; they have been used in this work to monitor the structural changes of four distinct segments in the molecule during cold, heat and pressure denaturation processes. His-12 and His-119 are part of the catalytic

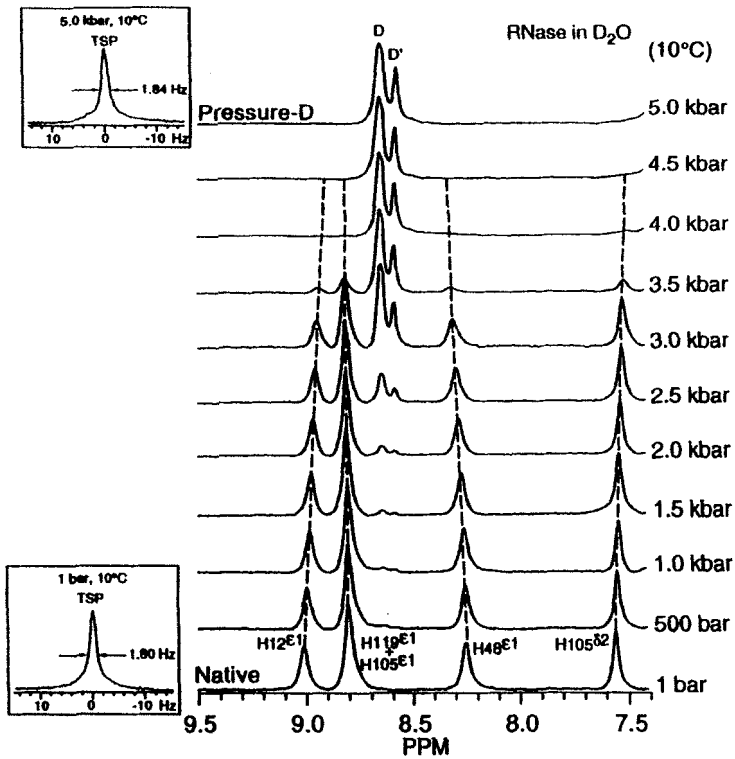

Fig. 10. The histidine region of the ^{1}H NMR spectrum of RNase A in D_2O at various pressures (10°C; pH*2.0). The standard in the insets is sodium 3-(trimethylsilyl)tetradeuteriopropionate.

site of native RNase A, and His-48 is at the hinge of the active site crevice. His-48, His-105, and His-119 are in the β-sheet fold, which forms the backbone of the molecule. His-12 is in an α-helix near the *N*-terminus. The folding pathway of the protein has been extensively studied. Several studies on RNase A strongly suggest that its folding proceeds through intermediates, including an early hydrogen-bonded intermediate and a late native-like intermediate.[101–106] Theoretical and experimental evidence suggests that nonrandom structures exist in the denatured protein. Circular dichroism (CD) and Fourier transform-infrared (FTIR) data indicate that there is a significant amount of structure in thermally denatured RNase A,[107,108] although a stable hydrogen-bonded structure could not be detected by amide proton protection experiments.[109]

The ε1 proton peaks of the four histidine residues are well resolved from other proton peaks in the 1D ^{1}H spectrum of the native RNase A in D_2O. They have been assigned and used to probe the folding and unfolding processes of the protein. Figure 10 shows the behaviour of the histidine region

proton spectrum during pressure unfolding at pH* 2.0, 10°C. With increasing pressure, the intensity of the native histidine peaks decreases. At about 4 kbar, all native histidine resonances disappear, indicating that the protein is pressure denatured. As pressure increases, two denatured resonances of the histidine residues, D and D', are observed. The chemical shift of resonance D is very similar to the composite resonance observed in the thermally denatured state and in the urea or guanidine hydrochloride denatured states of the protein.[110–112] The interesting feature in the pressure unfolding process is that in addition to the composite denatured histidine resonance D, another denatured histidine resonance, D', appears as the pressure increases. This resonance was not observed in either the thermal-denatured state or in the urea or guanidine hydrochloride-denatured states. In the completely pressure-denatured state, the intensity ratio of D to D' is 3:1, suggesting that D' comes from one of the four histidine residues. In order to assign the D' resonance, a magnetization transfer NMR experiment[113,114] was performed. It was found that the intensity of resonance D' decreased when the native His-12 peak was selectively irradiated. The result of the magnetization transfer test indicates that resonance D' comes from the His-12, and that resonance D comes from histidines 48, 105 and 119.

Because the simple appearance of resonance D' does not allow one to arrive at unambiguous conclusions about the presence or absence of secondary structure in the pressure and/or cold denaturated states, we decided to carry out a hydrogen-exchange experiment to test for the presence of partially folded structures in the pressure-denatured state. The hydrogen exchange behaviour contains information about the structure and conformational dynamics of proteins, resolved to the level of individual amino acid residues. The protection against exchange of the amide proton of each amino acid residue imposed by the protein structure is expressed by the protection factor, $P = k_{rc}/k_{obs}$, where k_{rc} is the hydrogen exchange rate calculated using a random coil model, and k_{obs} is the hydrogen exchange rate measured experimentally.

The experimental hydrogen exchange rate k_{obs} was obtained by fitting the measured cross-peak intensifies in 2D COSY NMR spectra to the exponential function, $I = I_0 \exp(-kt)$ The data measured at eight experimental times was used to obtain the experimental hydrogen exchange rates at high pressure. The cross-peaks between the NH and CαH hydrogens of residues of RNase A in 2D COSY NMR spectra were assigned according to the literature.[115,116] Of 119 backbone NHs in RNase A, approximately 40 amide protons are stable to exchange with D_2O in the native state, and they can be recorded by a COSY NMR spectrum. Only 33 of the 40 amide protons show cross-peaks of sufficient intensity to allow determination of the exchange rate in the pressure described in detail in the original reference; these were used to probe the stable hydrogen-bonded structure in the pressure-denatured protein.

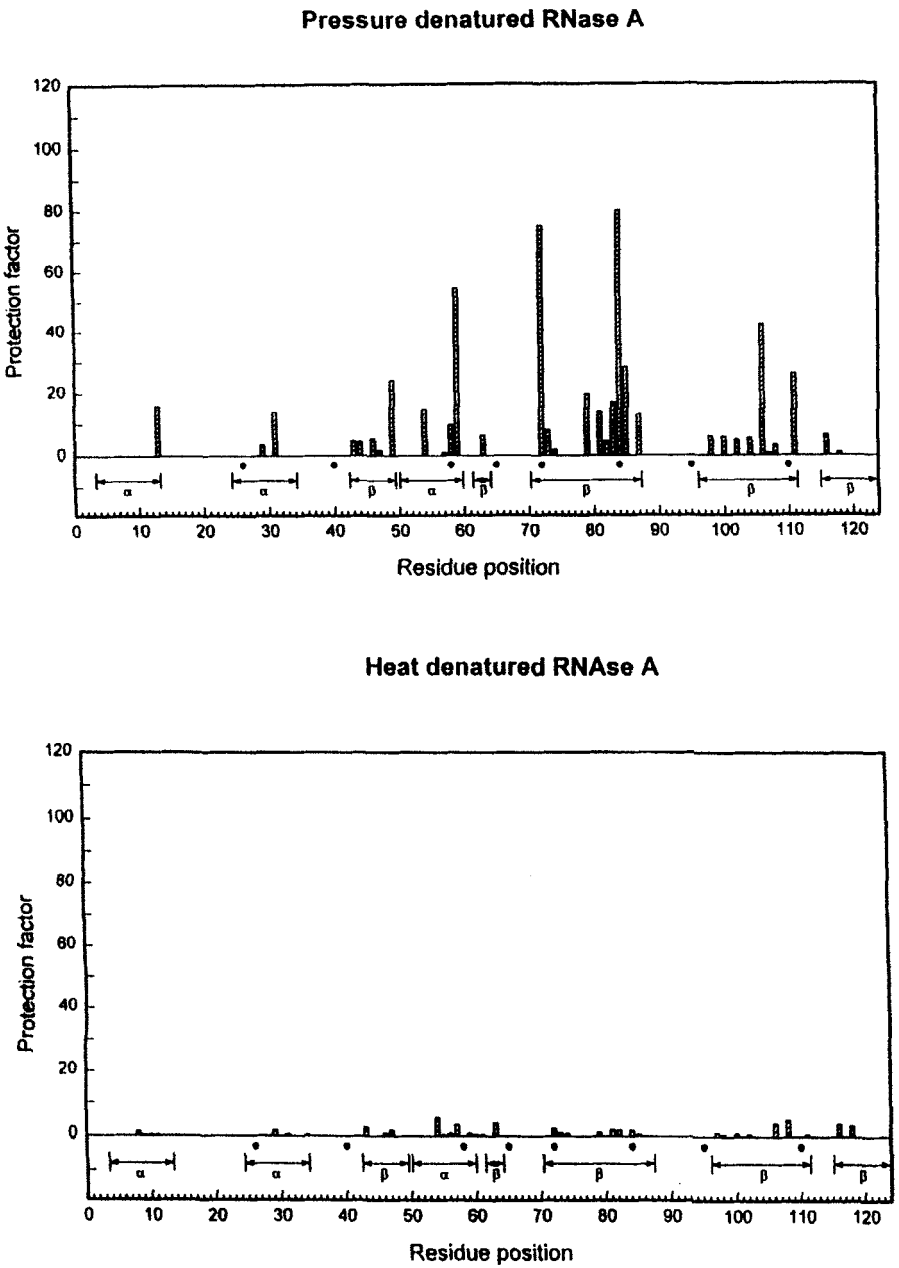

Fig. 11. Comparison of the protection factors for the amide exchange in the pressure-denatured (upper) and the heat-denatured (lower) RNase.

Table 4. High-pressure kinetic studies of solvent exchange in inorganic systems

System	Solvent	Pressure (bar)	Temperature (K)	Nuclei	Ref.
$[Cu(DMF)_6]^{2+}$, $[Cu(H_2O)_6]^{2+}$	DMF, H_2O	2000	217–300	^{17}O	118
$[Ln(PDTA)(H_2O)_2]^-$ (Ln = Tb, Dy, Er, Tm, Yb) $[Er(EDTA)(H_2O)_2]^-$	H_2O	2000	272–292	^{17}O	119
$[Ln(DTPA\text{-}BMA)(H_2O)]$ (Ln = Nd, Eu, Tb, Dy, Ho)	H_2O	2000	n.a.	^{17}O	120
$[M(en)_3](CF_3SO_3)_2$ (M = Co, Fe, Mn)	en	2000	278–332	^{14}N	121
$[Cp^*M(H_2O)_3]^{2+}$ (M = Rh, Ir)	H_2O	2000	288–333	^{17}O	122
Review of Lanthanide Systems		–	–	^{17}O	123
$Cu(tren)H_2O^{2+}$	H_2O	2000	321	^{17}O	124
$[M(CH_3NH_2)_5H_2O]^{3+}$ (M = Cr(III), Co(III), Rh(III))	H_2O	2000	264–281	^{17}O	125
$[Gd(DTPA\text{-}BMA)(H_2O)]$	H_2O	2000	291	^{17}O	126
$[Gd(H_2O)_8]^{3+}$, $[Gd(PDTA)(H_2O)_2]^-$	H_2O	2000	n.a.	^{17}O	127
$[Gd(H_2O)_8]^{3+}$, $[Gd(PDTA)(H_2O)_2]^-$	H_2O	2000	298–300	^{17}O	128
$[Rh_2(CH_3CN)_{10}]^{4+}$	CH_3CN	2000	314	^1H	129
$[UO_2(HMPA)_4]^{2+}$, $[UO_2(TMPA)_5]^{2+}$	HMPA or TMPA in CD_2Cl_2	2000	304	^1H	130
$[Ti(DMF)_6]^{3+}$	DMF	2000	242–270	^1H,^{17}O	131
$[TiO(DMSO)_5]^{2+}$	DMSO	2000	257–295	^1H	132
$[V(DMSO)_6]^{3+}$	DMSO	2000	311–349	^1H	133
$[Ni(en)_3]^{2+}$	en	2700	383	^1H	134
$[Al(DMF)_6]^{3+}$	DMF-d_7	2000	243–353	^1H	28
Review	–	–	–	–	5

DMF = dimethylformamide; PDTA = 1,3-propylenediamine-*N*,*N*,*N*′,*N*′-tetraacetate; EDTA = ethylenediaminetetraacetate; DTPA-BMA = diethylenetriaminepentaacetate-bis(methylamide); en = ethylenediamine; tren = 2,2′,2″-triaminotriethylamine; HMPA = hexamethylphosphoramide; TMPA = trimethyl phosphate; DMSO = dimethylsulfoxide; n.a. – data not available.

Table 5. Miscellaneous high-pressure NMR studies of inorganic systems.

System	Study	Pressure (bar)	Temperature (K)	Nuclei	Ref.
Et_4NBr (aqueous)	T_1	2250	190–350	^1H, ^2H	135
$NbH_3(C_5H_3(Si(CH_3)_3)_2)$	Hydrogen pair tunnelling frequency	5000	250–370	^1H	136
Me_4NBr (aqueous)	T_1, D	2250	230–360	^2H	137
$[Ir_2Rh_2(CO)_{11}PPh_3]$	PPh_3 migration	1840	324	^{31}P	138
$HCo(CO)_4$, $HMn(CO)_5$, etc.	H-atom transfer, ligand transfer rctn. kinetics	370	350–473	^{59}Co, ^{55}Mn, ^1H, ^{13}C	139
Sodium (I) cryptates of C221 and C222	Dissociation in en	2000	304	^{23}Na	140
$Cr(acac)_3$ in various perdeuterated solvents, $Ni[en]_3^{2+}$ in en	Paramagnetic relaxation effects on non-exchanging systems	2000	298	^1H, ^{14}N	141
Discussion of H_2O pressure properties, and properties of aqueous alkali solutions	–	n.a.	n.a.		142
$[Ru_3(CO)_9\{\mu_3\text{-}(\eta^3\text{-}1,3,5\text{-trithiane})\}]$ and $[Ru_3(t\text{-BuNC})(CO)_8\{\mu_3\text{-}(\eta^3\text{-}1,3,5\text{-trithiane})\}]$	CO site exchange	2000	253–280	^{13}C	143
Me_4NBr, Pr_4NBr, Bu_4NBr	T_1	2250	180–300	^2H	144
$[Ir_4(CO)_9(SCH_2)_3]$	CO site exchange	2000	274	^{13}C	145

Et = Ethyl; Ph = Phenyl; en = ethylenediamine; C221 = 4,7,13,16,21-pentaoxa-1,10-diazabicyclo[8.8.5]tricosane; C222 = 4,7,13,16,21,24-hexaoxa-1,10-diazabicyclo[8.8.8]hexacosane; acac = acetylacetone; Pr = Propyl; Bu = Butyl.

We found that in pressure-denatured and cold-denatured RNase A most of the interior amide groups exchange hydrogen atoms with the solvent more rapidly than in the folded state, but more slowly than in the fully unfolded state. Clearly, at least some secondary structure, which is more or less native, appears to persist in the pressure-denatured state to protect the NH

Table 6. High-pressure NMR studies using sapphire tubes.

System	Type of study	Pressure (bar)	Temperature (K)	Nuclei	Ref.
Monoorganopalladium (II) complexes with tridentate nitrogen donor ligands	CO insertion (catalysis)	10	295	^{1}H	146
$[MeC(CH_2PPh_2)_3]IrH(\eta^2(C,S)\text{-}C_{12}H_8S)$	CS insertion (catalysis)	5	323	$^{31}P\{^{1}H\}$	147
1-octene/Rhodium	Hydroformylation (catalysis)	20	296–333	$^{31}P\{^{1}H\}$	148
2-Ethylthiophenol	C-S scission (catalysis)	30	433		149
Benzyl-butyl-phthalate	SFC-NMR	250	321	^{1}H	150
cis-Methyl(carbonyl)platinum–diphosphine compounds	CO insertion (catalysis)	50	194–room	^{13}C, ^{31}P	151
Imine hydrogenation by rhodium(I)/phosphine complexes	Hydrogenation (catalysis)	138	183–room	^{1}H, ^{31}P	152
$[Pd(CH_3)CO)\{(S,S)BDPP\}]BF_4$	CO insertion (catalysis)	3	183	^{13}C, ^{31}P	153
Xe in liquid CO_2, N_2O, C_2H_6 or C_3H_8	Xe chemical shifts	*c.* 70	193–room	^{129}Xe	154
Supercritical CO_2/*n*-hexadecane mixtures	Self-diffusion	>200	308–333	^{1}H, ^{13}C	155
Supercritical CO_2	Self-diffusion	*c.* 74	304	^{13}C	156
Sapphire tube design/description	Tube design	–	–	–	157

hydrogens from exchange with solvent molecules, as illustrated in Fig. 11. The pressure-denatured state appears to display some characteristics of a molten globule or compact intermediate, which is a collapsed molecule with native-like secondary structure and a liquid-like interior.[91,117]

5. SURVEY OF RECENT HIGH-PRESSURE NMR STUDIES

As indicated in the introduction, this section presents recent high-pressure NMR studies in a tabular form. In Tables 4 to 11 we grouped together studies with the following common themes:

- High-pressure kinetic studies of solvent exchange in inorganic systems

Table 7. Various high-pressure studies of polymers and complex liquids.

System	Type of study	Pressure (bar)	Temperature (K)	Nuclei	Ref.
Bis(2-ethylhexyl) Phthalate	T_1 relaxation, NOE	3000	293	$^{13}C\{^1H\}$	158
2-Ethylhexylbenzoate	2D NOESY	3000	253–273	^1H	159
Vinylidene fluoride/trifluoroethylene copolymer (70/30)	T_1, $T_{1\rho}$	2000	370–410	^{19}F	160
Polyethylene	Quadrupole echo spectroscopy	2500	203–393	^2H	161
Polystyrene	T_1 relaxation	2250	293–403	^2H	162
Polystyrene	Quadrupole echo spectroscopy	1250	353–383	^2H	163
Polystyrene	Spin alignment echo	2250	373–388	^2H	163
Polycarbonate	T_1 relaxation	2500	233–298	^2H	164
Dicyclohexyl compounds	T_1 relaxation	2000	280–329	$^{13}C\{^1H\}$	165
2-Ethylhexylbenzoate, 2-Ethylhexyl-cyclohexanecarboxylate	T_1, T_2 relaxation	5000	253–353	$^{13}C\{^1H\}$	76
2-Ethylhexylbenzoate, 2-Ethylhexyl-cyclohexanecarboxylate	Self-diffusion coefficients, T_1 relaxation	4500	253–353	^1H, ^{13}C	51

Table 8. High-pressure studies of liquids confined to porous media.

Liquid	Porous media	Pressure (bar)	Temperature (K)	Nuclei	Ref.
Acetonitrile-d_3	Silica sol gel glass	5000	300	^2H, ^{14}N	166, 167
H_2O, D_2O	Rocks (sandstone, limestone)	2500	297	^1H, ^2H	168
Acetonitrile-d_3, pyridine-d_5, nitrobenzene-d_5, methylcyclohexane-d_{14}, and 2-ethylhexylbenzoate	Silica sol gel glass	5000	300	^2H, ^{13}C, ^{14}N	169
Pyridine-d_5, nitrobenzene-d_5	Silica sol gel glass	5000	300	^2H	170
Water	Natrolite (natural zeolite)	15 000	n.a.	^1H	171

n.a. – data not available.

Table 9. High-pressure NMR studies of solids.

System	Type of study	Pressure (bar)	Temperature (K)	Nuclei	Ref.
$Al_{65}Cu_{20}Ru_{15}$	T_1, isotropic Knight shift	1900	77	^{27}Al, ^{65}Cu	172
$La_{1.85}Sr_{0.15}CuO_4$, $YBa_2Cu_4O_8$	T_1, Knight shift (NQR)	15 000	4.2	^{63}Cu	173
Dimethyl sulphide		4500	60–200	^{1}H	174
C_{60}		n.a.	n.a.	^{13}C	175
C_{60}		3800	295	^{13}C	176
Rb_3C_{60}	T_1	6100	295	^{13}C	177
C_{60} and K_3C_{60}	Knight shift	12 000	200–343	^{13}C	178
C_{60}	T_1	5000	200–343	^{13}C	179
K_3C_{60}	Knight shift	8000	Room	^{13}C	180
As_2O_3, $LiIO_3$	(NQR stress/ pressure imaging)	140		^{127}I, ^{75}As	181
Methyl ethyl ketone	Field cycling	3300	4.2		182
Benzoic acid	T_1	4000	16–200	^{1}H	183
K_3C_{60}		n.a.	n.a.	^{13}C	184
Diacetyl	Field cycling	6250	80–200	^{1}H	185
K_3C_{60}		n.a.	n.a.	^{13}C	186
2,3-Butanedione	T_1	6250	4.2	^{1}H	187
He		20	0.9	^{3}He	188
Li, Na		80 000	250–300	^{7}Li,^{23}Na	189
H_2		n.a.	1.85–100	^{1}H	190

n.a. – data not available.

- Miscellaneous high-pressure NMR studies of inorganic systems
- High-pressure NMR studies using sapphire tubes
- Various high-pressure studies of polymers and complex liquids
- High-pressure studies of liquids confined to porous media
- High-pressure NMR studies of solids
- High-pressure NMR diffusion-related studies of simple molecules
- High-pressure NMR studies using diamond anvil cells

ACKNOWLEDGEMENTS

This work was supported in part by the Air Force Office of Scientific Research (AFOSR) under Grant F49620-93-1-0241, by the Augmentation

Table 10. High-pressure NMR diffusion-related studies of simple molecules.

System	Property measured	Pressure (bar)	Temperature (K)	Nuclei	Ref.
D_2O in organic solvents. Benzene, chloroform, acetonitrile	T_1	3000	303	^2H	191
Dimethyl ether	D	2000	185–458	^1H	192
D_2O, acetonitrile-d_3, chloroform-d_1, benzene-d_6	T_1	3000	279–328	^2H, ^{14}N	193
HF (liquid)	D	6000	195–419	^{19}F	194, 195
H_2O properties	T_1, D	n.a.	n.a.		142
superionic conductors		n.a.	n.a.		196
Sucrose/D_2O	T_1	2500	n.a.	^2H	197
Ethanol-d_1, 1-propanol-d_1, 2-propanol-d_1	D	2000 (gc)	158–478		198
Propane and tetradecane in binary mixtures	D	2000	n.a.		199
supercritical CO_2/*n*-hexadecane mixtures	T_1, D	>200 (st)	308–333	^1H, ^{13}C	155
n-Octane, toluene	D	3690	223–348		200
supercritical CO_2	T_1, D	~74 (st)	304	^{13}C	156
Review	–	–	–	–	4

gc = glass capillary; st = sapphire tube.

Table 11. High-pressure NMR studies by diamond anvil cells.

System	Type of study	Pressure (bar)	Temperature (K)	Nuclei	Ref.
Toluene, glycerol	T_1, T_2	16 000	room	^1H, ^{13}C	201
Glycerol	T_1, T_2 Chemical shifts	10 000	room	^1H	202
Li, Na	D, ΔV	80 000	250–300	^7Li, ^{23}Na	189
Solid H_2	(Probe design)	16 000	2–400	^1H	203
Na	(Probe design)	83 000		^2Na	204
Glycerol; methanol; benzyl alcohol; 1,2-propanediol	Chemical shifts	>10 000	n.a.	^1H	205
Solid H_2		n.a.	1.85–100	^1H	190

Awards for Science and Engineering Research Training (AASERT) under Grant F49620-93-1-0555, by the National Science Foundation under Grant NSF CHE 95-26237, and by the National Institutes of Health under Grant PHS 5 RO1 GM42452-05.

REFERENCES

1. J. Jonas, in *NMR Basic Principles and Progress*, Vol. **24** (ed. J. Jonas), p. 85. Springer-Verlag: Heidelberg, 1990.
2. J. Jonas and Y. T. Lee, *J. Phys. Condens. Matter*, 1991, **3**, 305.
3. J. Jonas and A. Jonas, *Annu. Rev. Biophys. Biomol. Struct.*, 1994, **23**, 287.
4. E. W. Lang and H.-D. Lüdemann, *Prog. NMR Spectrosc.*, 1993, **25**, 507.
5. R. van Eldik and A. E. Merbach, *Comments Inorg. Chem.*, 1992, **12**, 341.
6. J. Jonas, in *NATO ASI, Series C* (eds R. Winter and J. Jonas), Kluwer Academic Publishing: Dordrecht, 1993, **401**, 393.
7. H. G. Drickamer and C. W. Frank, *Electronic Transitions and the High Pressure Chemistry and Physics of Solids*. Chapman and Hall, New York, 1973.
8. J. Jonas, *Rev. Sci. Instrum.*, 1972, **43**, 643.
9. J. Jonas, *Science*, 1982, **216**, 1179.
10. H. Yamada, K. Kubo, I. Kakihara and A. Sera, in *High Pressure Liquids and Solutions*, (eds Y. Taniguchi, M. Senoo and K. Hara), p. 49. Elsevier Science, Amsterdam, 1994.
11. D. C. Roe, *J. Magn. Reson.*, 1985, **63**, 388.
12. C. R. Yonker, T. S. Zemanian, S. L. Wallen, J. C. Linehan and J. A. Franz, *J. Magn. Reson.*, 1995, **113A**, 102.
13. W. L. Earl, H. Vanni and A. E. Merbach, *J. Magn. Reson.*, 1978, **30**, 571.
14. J. Jonas, D. L. Hasha, W. J. Lamb, G. A. Hoffman and T. Eguchi, *J. Magn. Reson.*, 1981, **42**, 169.
15. D. L. Pisaniello, L. Helm, P. Meier and A. E. Merbach, *J. Am. Chem. Soc.*, 1983, **105**, 4528.
16. K. Woelk, J. W. Rathke and R. J. Klingler, *J. Magn. Reson.*, 1994, **109A**, 137.
17. F. Bachl and H.-D. Lüdemann, *High Press. Res.*, 1990, **6**, 91.
18. J. Jonas, P. Koziol, X. Peng, C. Reiner and D. M. Campbell, *J. Magn. Reson.*, 1993, **102B**, 299.
19. L. Ballard, C. Reiner and J. Jonas, *J. Mag. Res., Series A* (in press).
20. U. Frey, L. Helm and A. E. Merbach, *High Press. Res.*, 1990, **2**, 237.
21. A. Zahl, A. Neubrand, S. Aygen and R. van Eldik, *Rev. Sci. Instrum.*, 1994, **65**, 882.
22. T. H. DeFries and J. Jonas, *J. Magn. Reson.*, 1979, **35**, 111.
23. M. de Langen and K. O. Prins, *Rev. Sci. Instrum.*, 1995, **66**, 5218.
24. H. Huber, M. Mali, J. Roos and D. Brinkmann, *Rev. Sci. Instrum.*, 1984, **55**, 1325.
25. A. Trokiner, N. Dahan, H. Theveneau and P. Papon, *Rev. Sci. Instrum.*, 1984, **55**, 1616.
26. D. van der Putten, K. O. Prins and N. J. Trappeniers, *Rev. Sci. Instrum.*, 1985, **56**, 603.
27. P. W. E. Peereboom, K. O. Prins and N. J. Trappeniers, *Rev. Sci. Instrum.*, 1988, **59**, 1182.
28. S. Funahashi, K. Ishihara, S. Aizawa, T. Sugata, M. Ishii, Y. Inada and M. Tanaka, *Rev. Sci. Instrum.*, 1993, **64**, 130.
29. D. G. Vander Velde and J. Jonas, *J. Magn. Reson.*, 1987, **71**, 480.
30. J. Jonas, C. L. Xie, A. Jonas, P. J. Grandinetti, D. Campbell and D. Driscoll, *Proc. Natl Acad. Sci. USA*, 1988, **85**, 4115.

31. J. Jonas, R. Winter, P. J. Grandinetti and D. Driscoll, *J. Magn. Reson.* 1990, **87**, 536.
32. D. A. Driscoll, J. Jonas and A. Jonas, *Chem. Phys. Lipids*, 1991, **58**, 97.
33. D. A. Driscoll, S. Samarasinghe, S. Adamy, J. Jonas and A. Jonas, *Biochemistry*, 1991, **30**, 3322.
34. X. Peng and J. Jonas, *Biochemistry*, 1992, **31**, 6383.
35. X. Peng, A. Jonas and J. Jonas, *Biophys. J.*, 1995, **68**, 1137.
36. X. Peng, A. Jonas and J. Jonas, *Chem. Phys. Lipids*, 1995, **75**, 59.
37. S. Samarasinghe, Ph.D. Thesis, Univ. of Illinois, 1993.
38. B.-S. Lee, S. A. Mabry, A. Jonas and J. Jonas, *Chem. Phys. Lipids*, 1995, **78**, 103.
39. W. L. C. Vaz, R. M. Clegg and D. Hallmann, *Biochemistry*, 1985, **24**, 781.
40. P. F. Devaux and H. M. McConnell, *J. Am. Chem. Soc.*, 1972, **94**, 4475.
41. D. P. Hinton and C. S. Johnson, Jr, *J. Phys. Chem.*, 1993, **97**, 9064.
42. A.-L. Kuo and C. G. Wade, *Biochemistry*, 1979, **18**, 2300.
43. S. König, W. Pfeiffer, T. Bayerl, D. Richter and E. Sackmann, *J. Phys. II France*, 1992, **2**, 1589.
44. J. Tabony and B. Perly, *Biochim. Biophys. Acta*, 1990, **1063**, 67.
45. H.-J. Galla, W. Hartmann, U. Theilen and E. Sackmann, *J. Membrane Biol.*, 1979, **48**, 215.
46. D. B. Fenske, *Chem. Phys. Lipids*, 1993, **64**, 143.
47. R. W. Fisher and T. L. James, *Biochemistry*, 1978, **17**, 1177.
48. P. R. Cullis, *FEBS Lett.*, 1976, **70**, 223.
49. L. J. Burnett and J. F. Harmon, *J. Chem. Phys.*, 1972, **57**, 1293.
50. N. A. Walker, D. M. Lamb, J. Jonas and M. P. Dare-Edwards, *J. Magn. Reson.*, 1987, **74**, 580.
51. J. Jonas, S. T. Adamy, P. J. Grandinetti, Y. Masuda, S. J. Morris, D. M. Campbell and Y. Li, *J. Phys. Chem.*, 1990, **94**, 1157.
52. G. Cevc (ed.), *Phospholipids Handbook*, Marcel Dekker, New York, 1993.
53. L. F. Braganza and D. L. Worcester, *Biochemistry*, 1986, **25**, 7484.
54. L. F. Braganza and D. L. Worcester, *Biochemistry*, 1986, **25**, 2591.
55. R. Winter and P. Thiyagarajan, *Progr. Colloid Polym. Sci.*, 1990, **81**, 216.
56. R. Winter and W.-C. Pilgrim, *Ber. Bunsenges. Phys. Chem.*, 1989, **93**, 708.
57. S. K. Prasad, R. Shashidhar, B. P. Gaber and S. C. Chandrasehkar, *Chem. Phys. Lipids*, 1987, **43**, 227.
58. P. L.-G. Chong and G. Weber, *Biochemistry*, 1983, **22**, 5544.
59. H. Komatsu, P. T. Guy and E. S. Rowe, *Chem. Phys. Lipids*, 1993, **65**, 11.
60. X. Peng and J. Jonas, *Biochemistry*, 1992, **31**, 6383.
61. P. Meier, E. Ohmes and G. Kothe, *J. Chem. Phys.*, 1986, **85**, 3598.
62. C. Mayer, K. Muller, K. Weisz and G. Kothe, *Liq. Cryst.*, 1988, **3**, 797.
63. M. F. Brown, *J. Chem. Phys.*, 1984, **80**, 2832.
64. P. I. Watnick, P. Dea and S. I. Chan, *Proc. Natl Acad. Sci. USA*, 1990, **87**, 2082.
65. E. Rommel, F. Noack, P. Meier and G. Kothe, *J. Phys. Chem.*, 1988, **92**, 2981.
66. M. Bloom, E. Evans and O. G. Mouritsen, *Q. Rev. Biophys.*, 1991, **24**, 293.
67. S. T. Adamy, S. T. Kerrick and J. Jonas, *Z. Phys. Chem.*, 1994, **184**, 185.
68. A. Kumar, G. Wagner, R. R. Ernst and K. Wüthrich, *J. Am. Chem. Soc.*, 1981, **103**, 3654.
69. K. Wüthrich, M. Billeter and W. Braun, *J. Mol. Biol.*, 1984, **180**, 715.
70. P. A. Mirau and F. A. Bovey, *J. Am. Chem. Soc.*, 1986, **108**, 5130.
71. P. E. Wright, H. J. Dyson and R. A. Lerner, *Biochemistry*, 1988, **27**, 7167.
72. J. D. Baleja, J. Moult and B. D. Sykes, *J. Magn. Reson.*, 1990, **87**, 375.
73. N. H. Anderson, H. L. Eaton and X. Lai, *Magn. Reson. Chem.*, 1989, **27**, 515.
74. M. P. Williamson and D. H. Williams, *J. Chem. Soc. Chem. Commun.*, 1981, 165.
75. N. A. Walker, D. M. Lamb, S. T. Adamy, J. Jonas and M. P. Dare-Edwards, *J. Phys. Chem.*, 1988, **92**, 3675.

76. S. T. Adamy, P. J. Grandinetti, Y. Masuda, D. Campbell and J. Jonas, *J. Chem. Phys.*, 1991, **94**, 3568.
77. S. Macura and R. R. Ernst, *Molec. Phys.*, 1980, **41**, 95.
78. R. E. McClung and D. Kivelson, *J. Chem. Phys.*, 1968, **49**, 3380.
79. N. L. Allinger, *J. Am. Chem. Soc.*, 1977, **99**, 8127.
80. X. Peng, J. Jonas and J. L. Silva, *Biochemistry*, 1994, **33**, 8323.
81. M. M. Susskind, *J. Mol. Biol.*, 1980, **138**, 685.
82. R. T. Sauer, W. Krovatin, J. DeAnda, P. Youderian and M. M. Susskind, *J. Mol. Biol.*, 1983, **168**, 699.
83. A. K. Vershon, P. Youderian, M. M. Susskind and R. T. Sauer, *J. Mol. Biol.*, 1985, **260**, 12124.
84. K. L. Knight and R. T. Sauer, *Proc. Natl Acad. Sci. USA*, 1989, **86**, 797.
85. J. N. Breg, J. H. J. van Opheusden, M. J. M. Burgering, R. Boelens and R. Kaptein, *Nature*, 1990, **346**, 586.
86. S. E. V. Phillips, *Curr. Opin. Struct. Biol.*, 1991, **1**, 89.
87. J. N. Breg, R. Boelens, A. V. E. George and R. Kaptein, *Biochemistry*, 1989, **28**, 9826.
88. M. G. Zagorski, J. U. Bowie, A. K. Vershon, R. T. Sauer and D. J. Patel, *Biochemistry*, 1989, **28**, 9813.
89. J. L. Silva, C. F. Silveira, A. Correia, Jr and L. Pontes, *J. Mol. Biol.*, 1992, **223**, 545.
90. Y. Goto and A. L. Kink, *Biochemistry*, 1989, **28**, 945.
91. O. B. Ptitsyn, *J. Protein Chem.*, 1987, **6**, 273.
92. O. B. Ptitsyn, R. H. Pain, G. V. Semisotnov, E. Zerovnik and O. I. Razgulyaev, *FEBS Lett.*, 1990, **262**, 20.
93. X. Peng, J. Jonas and J. L. Silva, *Proc. Natl Acad. Sci. USA*, 1993, **90**, 1776.
94. T. E. Creighton, *Proc. Natl Acad. Sci. USA*, 1988, **85**, 5082.
95. J. Zhang, X. Peng, A. Jonas and J. Jonas, *Biochemistry*, 1995, **34**, 8631.
96. G. Weber and H. G. Drickamer, *Q. Rev. Biophys.*, 1983, **16**, 89.
97. F. Franks and R. H. M. Hatley, *Cryo-Lett.*, 1985, **6**, 171.
98. R. H. M. Hatley and F. Franks, *Cryo-Lett.*, 1986, **7**, 226.
99. A. Tamura, K. Kimura and K. Akasaka, *Biochemistry*, 1991, **30**, 11313.
100. T. DeFries and J. Jonas, *J. Chem. Phys.*, 1977, **66**, 5393.
101. K. H. Cook, F. X. Schmid and R. L. Baldwin, *Proc. Natl Acad. Sci. USA*, 1979, **76**, 6157.
102. F. X. Schmid and R. L. Baldwin, *J. Mol. Biol.*, 1979, **135**, 199.
103. P. S. Kim and R. L. Baldwin, *Biochemistry*, 1980, **19**, 6124.
104. F. X. Schmid, *Biochemistry*, 1983, **22**, 4690.
105. J. B. Udgaonkar and R. L. Baldwin, *Nature*, 1988, **335**, 694.
106. J. B. Udgaonkar and R. L. Baldwin, *Proc. Natl Acad. Sci. USA*, 1990, **87**, 8197.
107. A. M. Labhardt, *J. Mol. Biol.*, 1982, **114**, 181.
108. S. Seshadri, K. A. Oberg and A. L. Fink, *Biochemistry*, 1994, **33**, 1351.
109. A. D. Robertson and R. L. Baldwin, *Biochemistry*, 1991, **30**, 9907.
110. D. G. Westmoreland and C. R. Matthews, *Proc. Natl Acad Sci. USA*, 1973, **70**, 914.
111. F. W. Benz and G. C. K. Roberts, *J. Mol. Biol.* 1975, **91**, 345.
112. F. W. Benz and G. C. K. Roberts, *J. Mol. Biol.* 1975, **91**, 367.
113. C. M. Dobson and P. A. Evans, *Biochemistry*, 1984, **23**, 4267.
114. P. A. Evans, R. A. Kautz, R. O. Fox and C. M. Dobson, *Biochemistry*, 1989, **28**, 362.
115. M. Rico, M. Bruix, J. Santorio, C. Gonzalez, J. L. Neira, J. L. Nieto and J. Herranz, *Eur. J. Biochem.*, 1989, **183**, 623.
116. A. D. Robertson, E. O. Purisma, M. A. Eastman and H. A. Scheraga, *Biochemistry*, 1989, **28**, 5930.

117. P. S. Kim and R. L. Baldwin, *Annu. Rev. Biochem.*, 1990, **59**, 631.
118. D. H. Powell, P. Furrer, P.-A. Pittet and A. E. Merbach, *J. Phys. Chem.*, 1995, **99**, 16622.
119. N. Graeppi, D. H. Powell, G. Laurenczy, L. Zékány and A. E. Merbach, *Inorg. Chim. Acta*, 1995, **235**, 311.
120. D. Pubanz, G. González, D. H. Powell and A. E. Merbach, *Inorg. Chem.*, 1995, **34**, 4447.
121. S. Aizawa, K. Matsuda, T. Tajima, M. Maeda, T. Sugata and S. Funahashi, *Inorg. Chem.*, 1995, **34**, 2042.
122. L. Dadci, H. Elias, U. Frey, A. Hörnig, U. Koelle, A. Merbach, H. Paulus and J. S. Schneider, *Inorg. Chem.*, 1995, **34**, 306.
123. D. H. Powell, M. Favre, N. Graeppi, Ni Dhubhghaill, M. Orla, D. Pubanz and A. E. Merbach, *J. Alloys Compd.*, 1995, **225**, 246.
124. D. H. Powell, A. E. Merbach, I. Fábián, S. Schindler and R. van Eldik, *Inorg. Chem.*, 1994, **33**, 4468.
125. G. González, B. Moullet, M. Martinez and A. E. Merbach, *Inorg. Chem.*, 1994, **33**, 2330.
126. G. González, D. H. Powell, V. Tissières and A. E. Merbach, *J. Phys. Chem.*, 1994, **98**, 53.
127. D. H. Powell, G. González, V. Tissières, K. Micskei, E. Brücher, L. Helm and A. E. Merbach, *J. Alloys Compd.*, 1994, **207–208**, 20.
128. K. Micskei, D. H. Powell, L. Helm, E. Brücher and A. E. Merbach, *Magn. Reson. Chem.*, 1993, **31**, 1011.
129. P.-A. Pittet, L. Dadci, P. Zbinden, A. Abou-Hamdan and A. E. Merbach, *Inorg. Chim. Acta*, 1993, **206**, 135.
130. A. Abou-Hamdan, N. Burki, S. F. Lincoln, A. E. Merbach and S. J. F. Vincent, *Inorg. Chim. Acta*, 1993, **207**, 27.
131. I. Dellavia, L. Helm and A. E. Merbach, *Inorg. Chem.*, 1992, **31**, 2230.
132. I. Dellavia, L. Helm and A. E. Merbach, *Inorg. Chem.*, 1992, **31**, 4151.
133. I. Dellavia, P.-Y. Sauvageat, L. Helm, Y. Ducommun and A. E. Merbach, *Inorg. Chem.*, 1992, **31**, 792.
134. S. Soyama, M. Ishii, S. Funahashi and M. Tanaka, *Inorg. Chem.*, 1992, **31**, 536.
135. B. Liegl, S. Bradl, T. Schätz and E. W. Lang, *J. Phys. Chem.*, 1996, **100**, 897.
136. R. Wiedenbruch, M. Schick, A. Pampel, B. H. Meier, R. Meyer, R. R. Ernst, S. Chaloupka and L. M. Venanzi, *J. Phys. Chem.*, 1995, **99**, 13088.
137. S. Bradl, E. W. Lang, J. Z. Turner and A. K. Soper, *J. Phys. Chem.*, 1994, **98**, 8161.
138. G. Laurenczy, G. Bondietti, A. E. Merbach, B. Moullet and R. Roulet, *Helvetica Chim. Acta*, 1994, **77**, 547.
139. R. J. Klingler and J. W. Rathke, *J. Am. Chem. Soc.*, 1994, **116**, 4772.
140. S. Aizawa and S. Funahashi, *Bull. Chem. Soc. Jpn*, 1994, **67**, 1048.
141. H. D. Takagi, K. Matsuda, S. Aizawa, S. Funahashi, S. D. Kinrade and T. W. Swaddle, *Can. J. Chem.*, 1994, **72**, 2188.
142. H.-D. Lüdemann, *Pol. J. Chem.*, 1994, **68**, 1.
143. G. Laurenczy, A. E. Merbach, B. Moullet, R. Roulet, L. Hoferkamp and G. Süss-Fink, *Helvetica Chim. Acta*, 1993, **76**, 2936.
144. S. Bradl and E. W. Lang, *J. Phys. Chem.*, 1993, **97**, 10463.
145. A. Orlandi, U. Frey, G. Suardi, A. E. Merbach and R. Roulet, *Inorg. Chem.* 1992, **31**, 1304.
146. B. A. Markies, P. Wijkens, A. Dedieu, J. Boersma, A. L. Spek and G. van Koten, *Organometallics*, 1995, **14**, 5628.
147. C. Bianchini, J. A. Casares, M. V. Jiménez, A. Meli, S. Moneti, F. Vizza, V. Herrera and R. Sánchez-Delgado, *Organometallics*, 1995, **14**, 4850.

148. B. Moasser, W. L. Gladfelter and D. C. Roe, *Organometallics*, 1995, **14**, 3832.
149. C. Bianchini, V. Herrera, M. V. Jiménez, A. Meli, R. Sánchez-Delgado and F. Vizza, *J. Am. Chem. Soc.*, 1995, **117**, 8567.
150. K. Albert and U. Braumann, *Spec. Publ. Roy. Soc. Chem.*, 1995, **163**, 86.
151. I. Tóth, T. Kégl, C. J. Elsevier and L. Kollár, *Inorg. Chem.*, 1994, **33**, 5708.
152. G. E. Ball, W. R. Cullen, M. D. Fryzuk, W. J. Henderson, B. R. James and K. S. MacFarlane, *Inorg. Chem.*, 1994, **33**, 1464.
153. I. Tóth and C. J. Elsevier, *J. Am. Chem. Soc.*, 1993, **115**, 10388.
154. Y.-H. Lim, N. E. Nugara and A. D. King, Jr, *J. Phys. Chem.*, 1993, **97**, 8816.
155. P. Etesse, W. G. Chapman and R. Kobayashi, *Mol. Phys.*, 1993, **80**, 1145.
156. P. Etesse, A. M. Ward, W. V. House and R. Kobayashi, *Physica B*, 1993, **183**, 45.
157. D. C. Roe, *Adv. Chem. Ser.*, 1992, **230**, 33.
158. Y. J. Kim and J. Jonas, *J. Phys. Chem.*, 1995, **99**, 6777.
159. M. Stock-Schweyer, B. Meurer and G. Weill, *Polymer*, 1994, **35**, 2072.
160. A. S. Kulik and K. O. Prins, *Polymer*, 1993, **35**, 2307.
161. A. S. Kulik and K. O. Prins, *Polymer*, 1993, **34**, 4642.
162. A. S. Kulik and K. O. Prins, *Polymer*, 1993, **34**, 4635.
163. A. S. Kulik and K. O. Prins, *Polymer*, 1993, **34**, 4629.
164. M. T. Hansen, A. S. Kulik, K. O. Prins and H. W. Spiess, *Polymer*, 1992, **33**, 2231.
165. D. G. Gillies, S. J. Matthews and L. H. Sutcliffe, *Magn. Reson. Chem.*, 1991, **29**, 823.
166. S. Xu, Y. J. Kim and J. Jonas, *Chem. Phys. Lett.*, 1994, **218**, 329.
167. S. Xu, J.-P. Korb and J. Jonas, *Mater. Res. Soc. Symp. Proc.*, 1994, **346**, 925.
168. R. Chen, P. E. Stallworth, S. G. Greenbaum and R. L. Kleinberg, *J. Magn. Reson.*, 1994, **110A**, 77.
169. J. Jonas, J. Zhang and S. Xu, *Mater. Res. Soc. Symp. Proc.*, 1993, **290**, 95.
170. S. Xu, J. Zhang and J. Jonas, *J. Chem. Phys.*, 1992, **97**, 4564.
171. I. A. Belitskii, B. A. Fursenko, S. P. Gabuda, O. V. Kholdeev and Yu. V. Seretkin, *Phys. Chem. Miner.*, 1992, **18**, 497.
172. A. Shastri, D. B. Baker, M. S. Conradi, F. Borsa and D. R. Torgeson, *Phys. Rev. B: Condens. Matter*, 1995, **52**, 12681.
173. G.-Q. Zheng, T. Mito, Y. Kitaoka, K. Asayama and Y. Kodama, *Physica C*, 1995, **243**, 337.
174. P. J. McDonald and M. Pinter-Krainer, *Mol. Phys.*, 1995, **84**, 1021.
175. P. Auban-Senzier, R. Kerkoud, D. Jerome, F. Rachdi and P. Bernier, *Mater. Res. Soc. Symp. Proc.*, 1995, **359**, 261.
176. J. H. Walton and T. Gullion, *J. Phys. Chem.*, 1994, **98**, 13064.
177. St. Kluthe, J. Roos, M. Mali, D. Brinkmann, H. P. Lang, V. Thommen-Geiser and H.-J. Güntherodt, in *Prog. Fullerene Res., Int. Winter Sch. Electron. Prop. Novel Mater., 2nd* (ed. H. Kuzmany), p. 466. World Science, Singapore, 1994.
178. P. Auban-Senzier, R. Kerkoud, J. Godard, D. Jerome, J. Lambert, A. Zahab, F. Rachdi and P. Bernier, in *Prog. Fullerene Res., Int. Winter Sch. Electron. Prop. Novel Mater., 2nd* (ed. H. Kuzmany), p. 451. World Science, Singapore, 1994.
179. R. Kerkoud, P. Auban-Senzier, J. Godard, D. Jérome, J.-M. Lambert and P. Bernier, *Adv. Mat.*, 1994, **6**, 782.
180. R. Kerkoud, P. Auban-Senzier, D. Jerome, J.-M. Lambert, A. Zahab and P. Bernier, *Europhys. Lett.*, 1994, **25**, 379.
181. P. Nickel, H. Robert, R. Kimmich and D. Pusiol, *J. Magn. Reson.*, 1994, **111A**, 191.
182. P. J. McDonald, D. Vijayaraghavan, P. M. Debenham and A. J. Horsewill, *Physica B*, 1994, **202**, 346.
183. A. J. Horsewill, P. J. McDonald and D. Vijayaraghavan, *J. Chem. Phys.*, 1994, **100**, 1889.

184. G. Quirion, C. Bourbonnais, R. Kerkoud, E. Barthel, P. Auban, D. Jerome, J. M. Lambert, A. Zahab, P. Bernier and C. Fabre, *Springer Ser. Solid-State Sci.*, 1993, **117**, 334.
185. P. J. McDonald, D. Vijayaraghavan, P. M. Debenham and A. J. Horsewill, *Mol. Phys.*, 1993, **78**, 219.
186. G. Quirion, C. Bourbonnais, E. Barthel, P. Auban, P. Wzietek, D. Jerome, J. M. Lambert, A. Zahab and P. Bernier, *Synth. Met.*, 1993, **56**, 3154.
187. P. M. Debenham, P. J. McDonald, A. J. Horsewill and D. Vijayaraghavan, *Bull. Magn. Reson.*, 1993, **15**, 172.
188. V. A. Hopkins, Jr, M. J. McKenna and J. D. Maynard, *Physica B*, 1994, **194–196**, 1137.
189. D. Brinkman, in *Recent Trends High Pressure Res., Proc. AIRAPT Int. Conf. High Pressure Sci. Technol., 13th* (ed. A. K. Singh), p. 857. Oxford and IBH, New Delhi, 1992.
190. A. M. Ulug, M. S. Conradi and R. E. Norberg, *NATO ASI Ser., Ser. B*, 1991, **286**, 131.
191. C. Wakai and M. Nakahara, *J. Chem. Phys.*, 1995, **103**, 2025.
192. A. Heinrich-Schramm, W. E. Price and H.-D. Lüdemann, *Z. Naturforsch., A. Phys. Sci.*, 1995, **50**, 145.
193. C. Wakai and M. Nakahara, *J. Chem. Phys.*, 1994, **100**, 8347.
194. N. Karger, T. Vardag and H.-D. Lüdemann, *J. Chem. Phys.*, 1994, **100**, 8271.
195. N. Karger and H.-D. Lüdemann, *AIP Conf. Proc.*, 1994, **309**, 1321.
196. D. Brinkmann, in *Solid State Ionic Mater., Proc. Asian Conf. Solid State Ionics, 4th* (ed. B. V. R. Chowdari), p. 27. World Science, Singapore, 1994.
197. D. Girlich and H.-D. Lüdemann, *Z. Naturforsch., C: Biosci.*, 1994, **49**, 250.
198. N. Shaker-Gaafar, N. Karger, S. Wappmann and H.-D. Lüdemann, *Ber. Bunsenges. Phys. Chem.*, 1993, **97**, 805.
199. S. Wappmann, I. Tarassov and H.-D. Lüdemann, *Z. Naturforsch., A. Phys. Sci.*, 1993, **48**, 613.
200. K. R. Harris, J. J. Alexander, T. Goscinska, R. Malhotra, L. A. Woolf and J. H. Dymond, *Mol. Phys.*, 1993, **78**, 235.
201. J. L. Yarger, R. A. Nieman, G. H. Wolf and R. F. Marzke, *J. Magn. Reson.*, 1995, **114A**, 255.
202. R. F. Marzke, D. P. Raffaelle, K. E. Halvorson and G. H. Wolf, *J. Non-Cryst. Solids*, 1994, **172–174**, 401.
203. S.-H. Lee, M. S. Conradi and R. E. Norberg, *Rev. Sci. Instrum.*, 1992, **63**, 3674.
204. R. Bertani, M. Mali, J. Roos and D. Brinkmann, *Rev. Sci. Instrum.*, 1992, **63**, 3303.
205. K. E. Halvorson, D. P. Raffaelle, G. H. Wolf and R. F. Marzke, *NATO ASI Ser., Ser B*, 1991, **286**, 217.

Molybdenum-95 NMR Spectroscopy

JOHN MALITO

Department of Chemistry, Cork Regional Technical College, Rossa Avenue, Bishopstown, Cork, Ireland

1. MOLYBDENUM-95 NMR

1.1. Introductory remarks

Nuclear Magnetic Resonance of transition metal nuclei can provide direct information about the metal centre in different physical and chemical environments in three key manners. The chemical shift (δ, p.p.m.) can give some indication of the electronic environment about the metal nucleus; the

ANNUAL REPORTS ON NMR SPECTROSCOPY
VOLUME 33 ISBN 0-12-505333-9

line width (or width at half height, $\Delta\nu_{1/2}$, Hz) can inform about the degree of symmetry of the electric field at the nucleus; and the coupling constant (^nJ, Hz) can help to delineate molecular structure and possibly, intramolecular bonding. ^{95}Mo NMR has become an increasingly useful probe for the characterization of a wide variety of molybdenum complexes in different situations.

The ^{95}Mo nucleus is preferred to the ^{97}Mo nucleus even though they are of similar spin ($I = 5/2$) and resonate at very similar frequencies (6.51 versus 6.65 MHz)[1] because the former has a significantly higher natural abundance (15.72% *vs* 9.46%),[1,2] smaller quadrupole moment (0.12×10^{-28} m^2 *vs* 1.1×10^{-28} m^2)[3,4] and a greater sensitivity (relative to ^{13}C, 2.92 *vs* 1.87).[1,2] Consequently, much has been published in the area of ^{95}Mo NMR in the last 10 years since the last comprehensive review, by Minelli *et al.*[5] Other general reviews for Group 6 metal NMR in particular[6–8] and transition metal NMR in general have also been published.[9–13] This review is primarily concerned with ^{95}Mo NMR data from the 10-year period, 1985–1995, for all seven common oxidation states of molybdenum, Mo(0)–Mo(VI). Some notes on the developments in the areas of ^{53}Cr, ^{183}W and solid-state NMR over the same time period are included.

For a large and representative data base, one would expect that empirical methods could be used to relate chemical shift, line width and coupling constant data to several aspects of molecular structure.[5,14] In addition to differentiation of metal oxidation states, generalizations should also be possible for ligand properties and/or ligand effects, ring effects, and reaction conditions.[5,14] Discussion, with the latter possibilities in mind, follows the order of oxidation states, from Mo(0) to Mo(VI). Thus, chemical shifts are grouped in Tables based on ligand types for compounds with similar structures for the same Mo oxidation state. Wherever possible line width and coupling constant data are included as are the solvents used. The chemical shift data are treated in terms of shielding (upfield or low-frequency tendency) and deshielding (downfield or high-frequency tendency) terminologies. All data in the tables are for measurements made at ambient temperatures unless otherwise specified. Abbreviations used in the text are included in an appendix at the end of this chapter.

1.2. Background and parameters

There are several books to which one can refer for more detailed technical information[1,2] but, in general, chemical shifts for heavy and/or quadrupolar nuclei are rationalized on the basis of the Ramsey expression, equation (1)[15–18] for overall shielding (σ), made up of diamagnetic (σ_d) and paramagnetic (σ_p) contributions. The diamagnetic parameter, opposite in sign to the paramagnetic parameter, reflects the electron density in the immediate

vicinity of the nucleus and it is dominated by the core electrons. Thus, σ_d is unaffected by changes in the chemical environment and remains virtually constant for a given nucleus. It follows that σ_p should be the dominant parameter[5,19] and it is attributed, almost exclusively, to the relatively low energy metal d–d electronic transitions. Because σ_p is fairly localized, ligand field theory has been applied for overall shielding approximations.[20,21] A much simplified expression (equation 2) can be used to account for σ_p for the ^{95}Mo nucleus.[5,9,20]

$$\sigma = \sigma_d + \sigma_p \tag{1}$$

$$\sigma_p = -K.\Delta E^{-1}\{r^{-3}\}_{4d}\, k^2 \tag{2}$$

In equation (2), K is a collection of constants, ΔE is the mean effective excitation energy approximated by the HOMO-LUMO energy gap for the Mo 4d orbitals, $\{r^{-3}\}_{4d}$ and k^2 are terms associated with the nephelauxetic effect and the metal-ligand band covalency respectively.[22] A similar term for the imbalance of charge with respect to p electrons around the nucleus has been omitted because the p contributions to shielding are negligible in the case of molybdenum.[9] The negative sign for σ_p means that any increase in its absolute magnitude will correspond to deshielding of the molybdenum nucleus. Hence, deshielding is promoted by small magnitudes for both ΔE and r_d. Conversely, shielding should be enhanced for strong field ligands which tend to increase ΔE but reduce the radial term. For very high symmetry species, the chemical shift should be directly proportional to the ratio $\{r^{-3}\}_{4d}/\Delta E$.[23]

Clearly, the properties of the ligand (L) are important. This has been borne out by at least two independent MO studies on the Mo(VI) species, $[MoO_{4-n}X_n]^{2-}$ (X = S[24–27] or Se[24,25]), which suggest that changes in chemical shift reflect changes in the valence 4d orbitals caused by ligand substitution. These changes may be related to stabilization of the unoccupied 4d* and 4dπ* orbitals on Mo through participation with ligand orbitals. In comparing theoretical and experimental chemical shift values for $[MoO_{4-n}S_n]^{2-}$ ($n = 0-4$), Sun *et al.* found that shielding increases as n increases.[28]

The nature of the resulting Mo-L bond is also very important in determining the ^{95}Mo NMR chemical shift. An efficient σ-donor ligand will tend to raise the LUMO while an efficient π-acceptor ligand will tend to lower the HOMO. Either of these effects will lead to increased shielding but when comparing the overall effects caused by different ligands, the relative importance of both ligand donor and acceptor properties must be considered. For example, a build-up of negative charge at the molybdenum nucleus will tend to raise the HOMO and thereby lower ΔE (deshielding) while concomitantly decreasing the radial term as a consequence of the nephelauxetic effect (shielding). It has also been suggested that the chemical

shift should increase with ligand softness and that it is inversely proportional to the magnetically allowed d–d transitions.[24,25]

From the above it becomes apparent that there are three main factors to be considered in the interpretation of ^{95}Mo NMR chemical shifts with reference to equation (2): (1) the position of L in the spectrochemical series; (2) the nephelauxetic ratio or position of L in the nephelauxetic series; and (3) the nature of the Mo-L bond in terms of σ- and π- characteristics.

Juranic[20,29] considered these factors in some detail for d^6 systems, particularly Co(III), and discussed the differing effects of ligands in the more general terms of a magnetochemical series. That is, ligands can be ordered according to increased shielding of the metal nucleus. A ligand which is to precede another in the magnetochemical series must occupy a higher position in the spectrochemical series but a lower position in the nephelauxetic series.

For nuclei with $I > 1/2$ (e.g., ^{53}Cr, ^{95,97}Mo), the nuclei couple with an electric field gradient (q). This coupling, of magnitude proportional to the nuclear quadrupole moment (Q), provides a process for nuclear relaxation. For a given nucleus, I and Q are constant so the line widths observed will depend on the correlation time (τ_c) for molecular tumbling and the square of the electric field gradient (q^2). Increases in the electric field gradient and correlation time lead to quadrupolar and correlation time line-broadening, respectively. However, the line widths are also sensitive to temperature and generally increase as temperature decreases. This is also related to solvent viscosity which also shows an indirectly proportional dependence on temperature. Finally, q^2 is related to the degree of symmetry of the electronic distribution about the nucleus and the sharpest spectral lines are observed for the most uniformly spherical electronic environment, or as close as possible to a zero electric field gradient.

2. SOLUTION STATE NMR

2.1. Molybdenum (0) compounds

The major portion of transition metal NMR data available is for complexes of the d^6 electronic configuration.[20,30] This is very true for ^{95}Mo NMR because Mo(0) has a very rich and widespread chemistry relative to the other common oxidation states of molybdenum.[5,30,31–33]

A large accumulation of ^{95}Mo NMR data for Molybdenum (0) compounds is now presented. Some of these data have been previously reviewed[5,9,29,30] but are included here to ensure a more complete data set. The chemical shift data are discussed in terms of ligand types, based initially on the donor atom

(e.g., P versus N) but then further subcategorized on the basis of more specific ligand classes (e.g., phosphine versus phosphite). Some general conclusions, including nonligand effects (e.g., variations in temperature), are summarized at the end of this section for Mo(0) compounds.

^{95}Mo NMR chemical shifts are invariably measured relative to an external reference of aqueous alkaline (pH 11) 2M $[MoO_4]^{2-}$. Nevertheless, it is very convenient in discussion of Mo(0) compounds to refer to the hexacarbonyl species, $Mo(CO)_6$.[34] This compound was the first reported to be investigated by ^{95}Mo NMR spectroscopy[35] and is often a synthetic starting point for Mo(0) chemistry. Some ^{95}Mo NMR data for $Mo(CO)_6$ are presented in Table 1. There is very little solvent effect on the chemical shift although the most shielded values occur for solutions in hydrocarbon solvents wherein direct solvent interaction is least likely. In some cases (e.g., CH_3CN or THF), the solvent can coordinate and this will be discussed later.[41] Chemical shifts for $Mo(CO)_6$ also appear to be virtually unaffected by changes in some experimental conditions (e.g., sample concentration) which do affect chemical shifts observed for other less symmetrical Mo(0) compounds. Merlic and Adams,[37] however, reported a chemical shift dependence on temperature of 0.3 p.p.m. per degree Celsius. The high symmetry of $Mo(CO)_6$ leads to a negligible effective electric field gradient at the Mo nucleus and hence, relatively narrow line widths (i.e., <10 Hz). The small variations that are observed have been attributed to varying solvent viscosities.[5] The spin lattice relaxation time for $Mo(CO)_6$ has been measured as *c.* 7 s at ambient temperatures.[42] This T_1 value is deemed to be rather long for a quadrupolar nucleus but it is fully consistent with the lack of an effective relaxation mechanism.[37,42] The greater than 1 Hz line widths observed are therefore ascribed to temperature effects.[37]

2.1.1. Molybdenum carbonylate anions

^{95}Mo NMR data for several carbonylate species, $[Mo(CO)_5X]^-$ and $[Mo_2(CO)_{10}X]^-$ (X = halide, pseudohalide), are given in Table 2, arranged in order of increased deshielding of the Mo nucleus. Clearly, the chemical shifts observed are independent of the counter-ion present and show minimal susceptibility to solvent effects. The broader line widths, relative to those observed for $Mo(CO)_6$ (see Table 1), are most likely due to reduced symmetry at the Mo nucleus upon substitution of the CO ligands.[5] Brownlee *et al.*[43] have found that for $Mo(CO)_5L$ (L = Cl^-, py, PPh_3, $AsPh_3$ and $SbPh_3$) the spin lattice relaxation times (T_1) are due entirely to a quadrupolar mechanism with no scalar contribution to the line width where the Mo is bonded to another quadrupolar nucleus. Some related higher substitution anionic species are discussed later in this review (see Sections 2.1.4 and 2.1.5).

Table 1. ^{95}Mo NMR data for $Mo(CO)_6$ in different solvents.

Solvent	δ^{95}Mo (p.p.m.)	$\Delta\nu_{1/2}$(Hz)	Ref.
DMF	−1850	3	36
CH_3CN	−1855	10	36
CD_3CN	−1855	≤0.1	37
THF	−1855	3	38
$(CH_3)_2CO$	−1856	1	36
CH_2Cl_2	−1856	1	35, 39
	−1857	9	36
	−1858	0.14	37
$CDCl_3$	−1857	3	40
C_6H_6	−1858	4	40
$CHCl_3$	−1860	3	36
Toluene	−1861	4	36
iso-Octane	−1867	5	36

The magnetochemical series for X^-:

$$H^- > CN^- > I^- > NCO^- > NCS^- > NCSe^- > Br^- > N_3^- > NO_2^- > Cl^- > O_2CH^- > SeCN^- > ON_2^- \geq OCH_3^-$$

shows the normal halogen dependence[44] although the opposite trend has been observed in other situations (e.g., d^0 Mo(VI)).[45] The overall shift range of 545 p.p.m., observed for the monomeric pentacarbonyl species, reflects the importance of the ligand field strengths, polarizabilities, and electronegativities in determining the chemical shifts. Nevertheless, greatest shielding is observed for the more polarizable anions (H^-, Cl^- and I^-) while the more electronegative harder anions (e.g., O-donors) lead to deshielding. These trends indicate that the nephelauxetic term in equation (2) (i.e., $\{r^{-3}\}_{4d}$) is the dominant term for determining the chemical shifts in this situation but the relative π-acceptor abilities of some of the anions (e.g., NCO^-, NCS^- and $NCSe^-$) should not be ignored.

The data in Table 2 also show that ^{95}Mo NMR can be a useful probe for the qualitative investigation of product mixtures. Linkage isomers (e.g., NCSe versus SeCN),[46] bonding modes for potential ambidentate ligands (e.g., NO_2^- and $NCSe^-$)[46] and relatively unstable reactive species formed *in situ*[48] can all be identified and/or differentiated. Several of the species generated *in situ* by reaction of $Mo(CO)_6$ with OH^- and subsequent chemistry[48] have been implicated as intermediates for the water–gas-shift reaction.[50–53]

Table 2. ^{95}Mo NMR data for some monomeric and dimeric carbonylate anion species.

Compound	Solvent	δ^{95}Mo (p.p.m.)	$\Delta\nu_{1/2}$(Hz)	Ref.
$Na[Mo(CO)_5H]$	DMSO	−1980	50	46
$Na[Mo(CO)_5CN]$	DMSO	−1887	[a]	46
$[Bu_4N][Mo(CO)_5I]$	DMSO	−1660	[a]	46
$[Et_4N][Mo(CO)_5I]$	CD_2Cl_2	−1660	190	47
$K[Mo(CO)_5(NCO)]$	DMSO	−1604	[a]	46
$K[Mo(CO)_5(NCS)]$	DMSO	−1596	[a]	46
$K[Mo(CO)_5(NCSe)]$	DMSO	−1590	[a]	46
$[Et_4N][Mo(CO)_5Br]$	CD_2Cl_2	−1540	130	47, 48
	DMSO	−1540	[a]	46
$Na[Mo(CO)_5N_3]$	DMSO	−1523	[a]	46
$Na[Mo(CO)_5NO_2]$	DMSO	−1514	[a]	46
$[Et_4N][Mo(CO)_5Cl]$	CD_2Cl_2	−1513	110	47
	DMSO	−1513	[a]	46
$Na[Mo(CO)_5(O_2CH)]$	DMSO	−1495	[a]	46
	THF	−1494	[a]	48
	CH_3CN	−1491	[a]	48
$K[Mo(CO)_5(SeCN)]$	DMSO	−1438	[a]	46
$Na[Mo(CO)_5(OCH_3)]$	THF	−1435	[a]	46
$Na[Mo(CO)_5(O_2N)]$	DMSO	−1435	[a]	46
$Na[Mo_2(CO)_{10}H]$	CH_3CN	−1940	[a]	46
	DMSO	−1941	50	46
$[Et_4N][Mo_2(CO)_{10}H]$[b]	THF	−1937	30	49
$Na[MoW(CO)_{10}H]$	THF	−1916	[a]	48
$Na[MoCr(CO)_{10}H]$	THF	−1872	[a]	48
$K[Mo_2(CO)_{10}(NCS)]$	DMSO	−1370	[a]	48
$K[Mo_2(CO)_{10}(NCSe)]$	DMSO	−1360	[a]	48

[a]Not reported;
[b]$^1J(^{95}Mo–^1H) = 15$ Hz.

2.1.2. Phosphorus donor ligands

Mo(0) compounds containing phosphorus ligands form one of the largest classes of compounds for which ^{95}Mo NMR data are available. These data are arranged according to ligand type in Tables 3–6 for penta-, tetra-, tri- and higher substitution carbonyl compounds respectively. Data for related compounds containing arsine and stibine ligands are also included whereas data available for mixed phosphorus ligand-other donor atom ligand compounds appear in later sections (see 2.1.3 and 2.1.5).

Mono-phosphorus ligands are typically monodentate but the

Table 3. ^{95}Mo NMR data for $Mo(CO)_5P$ and related species.

P-donor ligand	Solvent	δ^{95}Mo (p.p.m.)	$\Delta\nu_{1/2}$ (Hz)	$^1J(^{95}Mo-^{31}P)$ (Hz)	Ref.
$P(Et)_3$	CH_2Cl_2	−1854 to −1856	6–10	131–133	36, 49
$P(CH_2CH_2CN)_3$	CH_2Cl_2	−1829	50	140	36
$P(^nBu)_3$	CH_2Cl_2	−1843	16–20	129	34, 36, 54
	Ligand	−1842	40	129	49
$P(^tBu)_3$	CH_2Cl_2	−1711	67	127	36, 54
$P(Cy)_3$	CH_2Cl_2	−1825	46	129	36, 54
$P(Me_2Ph)$	CH_2Cl_2	−1788	8	131	49
$P(Et_2Ph)$	CH_2Cl_2	−1815	11	132	49
$P(^nBu_2Ph)$	CH_2Cl_2	−1808	19	133	49
$P(MePh_2)$	CH_2Cl_2	−1772	30	135	36
$P(EtPh_2)$	CH_2Cl_2	−1789	30	137	36
$P(Ph)_3$	CH_2Cl_2	−1743	35–54	139–144	36, 47, 49
$As(Ph)_3$	CH_2Cl_2	−1757	112	–	36, 49, 54
$Sb(Ph)_3$	CH_2Cl_2	−1864	117	–	36, 47 49, 54
$P(C_6H_4$-p-$Cl)_3$	THF	−1741	90	140	36
$P(C_6H_4$-p-$F)_3$	THF	−1730	50	142	36
$P(m$-tolyl$)_3$	CH_2Cl_2	−1743	70	139	36
$P(p$-tolyl$)_3$	CH_2Cl_2	−1750	50	133	36
$P(C_6H_4$-pMeO$)_3$	CH_2Cl_2	−1744	60–70	138	36, 47, 54
$P(Ph_2Cl)$	$CDCl_3$	−1702	9	165	55
$P(Ph_2OC_6H_4$-p-H$)$	$CDCl_3$	−1775	34	161	55, 56
$P(Ph_2OC_6H_4$-p-Cl$)$	$CDCl_3$	−1774	40	161	56
$P(Ph_2OC_6H_4$-p-Me$)$	$CDCl_3$	−1776	39	162	55, 56
$P(Ph_2OC_6H_4$-p-^{t}Bu$)$	$CDCl_3$	−1775	40	164	56
$P(Ph_2OC_6H_4$-p-Ph$)$	$CDCl_3$	−1774	47	164	56
$P(Ph_2OC_6H_4$-p-OMe$)$	$CDCl_3$	−1778	40	162	56
$P(Ph_2OC_6H_4$-p-OPh$)$	$CDCl_3$	−1774	49	162	56
$P(Ph_2OC_6H_4$-p-SMe$)$	$CDCl_3$	−1775	43	161	56
$P(Ph_2OC_6H_4$-p-COPh$)$	$CDCl_3$	−1772	52	164	56
$P(Ph_2OC_6H_4$-p-CO_2Me$)$	$CDCl_3$	−1772	48	164	56
$P(Ph_2OC_6H_4$-p-COMe$)$	$CDCl_3$	−1772	50	164	56
$P(Ph_2OC_6H_4$-p-CHO$)$	$CDCl_3$	−1770	48	164	56
$P(Ph_2OC_6H_4$-p-CN$)$	$CDCl_3$	−1771	46	165	56
$P(Ph_2OC_6H_4$-p-$NO_2)$	$CDCl_3$	−1770	48	165	56
$P(Ph_2OMe)$	$CDCl_3$	−1791	[a]	156	57
$P(Ph_2OEt)$	$CDCl_3$	−1788	[a]	159	57
$P(Ph_2O^nPr)$	$CDCl_3$	−1788	[a]	159	57
$P(Ph_2S^nPr)$	$CDCl_3$	−1726	[a]	142	55
$P(Ph_2O^iPr)$	$CDCl_3$	−1783	[a]	156	57
$P(Ph_2S^iPr)$	$CDCl_3$	−1723	[a]	145	55
$P(Ph_2O^nBu)$	$CDCl_3$	−1788	[a]	159	57
$P(Ph_2O^sBu)$	$CDCl_3$	−1782	[a]	159	57
$P(Ph_2O^tBu)$	$CDCl_3$	−1788	[a]	159	57
$P(Ph_2OSiMe_3)$	$CDCl_3$	−1765	[a]	161	55
$P(Ph(OMe)_2)$	CH_2Cl_2	−1816	[a]	183	34
$P(Ph_2NH_2)$	$CDCl_3$	−1767	[a]	148	55
$P(Ph_2NHMe)$	$CDCl_3$	−1765	[a]	146	57

Table 3.– *cont.*

P-donor ligand	Solvent	δ^{95}Mo (p.p.m.)	$\Delta\nu_{1/2}$ (Hz)	$^1J(^{95}Mo–^{31}P)$ (Hz)	Ref.
$P(Ph_2NHEt)$	$CDCl_3$	−1763	[a]	146	57
$P(Ph_2NH^nPr)$	$CDCl_3$	−1763	[a]	146	55, 57
$P(Ph_2NH^iPr)$	$CDCl_3$	−1760	[a]	146	55, 57
$P(Ph_2NH^nBu)$	$CDCl_3$	−1764	[a]	149	57
$P(Ph_2NH^sBu)$	$CDCl_3$	−1760	[a]	151	57
$P(Ph_2NH^iBu)$	$CDCl_3$	−1763	[a]	146	57
$P(Ph_2NHSiMe_3)$	$CDCl_3$	−1725	[a]	149	55
$P(Ph_2NHPh)$	$CDCL_3$	−1736	[a]	150	55
$P(Ph_2NHC_6H_4$-*p*-Me)	$CDCL_3$	−1737	[a]	153	55
$\{PPh(NEt_2)\}_2$[b]	CH_2Cl_2	−1801	[a]	159	34
$P(NMe_2)_3$[b]	CH_2Cl_2	−1803	[a]	173	34
$P(Ph_2(SC_6H_4$-*p*-Me))[b]	$CDCl_3$	−1728	[a]	150	55, 56
$P(OMe)_3$	Ligand	−1864	5	218	34, 40, 49
	CH_2Cl_2	−1859	10	216	34, 40, 49
$P(OEt)_3$	Ligand	−1854	8	214	34, 40, 49
$P(O^nPr)_3$	CH_2Cl_2	−1851	20	215	36
$P(O^iPr)_3$	Ligand	−1835	15	215	34, 49
$P(O^nBu)_3$	Ligand	−1854	29	216	49
$P(OPh)_3$	CH_2Cl_2	−1819	36	234–237	34, 36, 49
$P((OCH_2)_3CEt)$[b]	CH_2Cl_2	−1858	20	227	34
$P(OCH_2C(Me)_2CH_2O)Cl$	$CDCl_3$	−1757	16	242	58
$P(OCH_2C(Me)_2CH_2O)Br$	$CDCl_3$	−1777	22	244	58
$P(OCh_2C(Me)_2CH_2O)O^nPr$	$CDCl_3$	−1857	7	221	58
$P(OCH_2C(Me)_2CH_2O)O^iPr$	$CDCl_3$	−1849	7	219	58
$P(OCH_2C(Me)_2CH_2O)S^nPr$	$CDCl_3$	−1772	23	213	58
$P(OCH_2C(Me)_2CH_2O)S^iPr$	$CDCl_3$	−1770	20	213	58
$P(OCH_2C(Me)_2CH_2O)NH^nPr$	$CDCl_3$	−1845	6	200	58
$P(OCH_2C(Me)_2CH_2O)NH^iPr$	$CDCl_3$	−1842	6	200	58
$P(OCH_2C(Me)_2CH_2O)O$-*p*-tolyl	$CDCl_3$	−1839	13	229	58
$P(OCH_2C(Me)_2CH_2O)S$-*p*-tolyl	$CDCl_3$	−1767	30	218	58
$P(OCH_2C(Me)_2CH_2O)NH$-*p*-tolyl	$CDCl_3$	−1828	11	215	58
$P(OCH_2C(Me)_2CH_2O)O^-Et_3NH^+$	$CDCl_3$	−1829	4	199	58
$P(OCH_2C(Me)_2CH_2O)OSiMe_3$	$CDCl_3$	−1831	6	226	58
$P(O(CH_2)_2CH(Me)O)Cl$	$CDCl_3$	−1750	[c]	244	59
$P(O(CH_2)_2CH(Me)O)O^nPr$	$CDCl_3$	−1845	[c]	198	59
$P(O(CH_2)_2CH(Me)O)S^nPr$	$CDCl_3$	−1767	[c]	205	59
$P(O(CH_2)_2CH(Me)O)NH^nPr$	$CDCl_3$	−1845	[c]	194	59
$P(O(CH_2)_2CH(Me)O)O$-*p*-tolyl	$CDCl_3$	−1829	[c]	278	59
$P(O(CH_2)_2CH(Me)O)S$-*p*-tolyl	$CDCl_3$	−1754	[c]	213	59
$P(O(CH_2)_2CH(Me)O)O^-Et_3NH^+$	$CDCl_3$	−1849	[c]	195	59
PTA	CH_3CN	−1877	[a]	126	60
PTAMeI	CH_3CN	−1860	[a]	127	60
PCl_3	MeC_6H_{11}	−1523	5–50	250	61
PCl_2Ph	$Cl(CH_2)_2Cl$	−1615	5–50	197	61
$PClPh_2$	$CDCl_3$	−1702	5–50	165	61
PBr_3	MeC_6H_{11}	−1396	5–50	242	61
PF_3	Ligand	−1860	[a]	284	62
DBP[d]	CH_2Cl_2	−1795	38	132	63, 64

Table 3.– *cont.*

P-donor ligand	Solvent	δ^{95}Mo (p.p.m.)	$\Delta\nu_{1/2}$ (Hz)	$^1J(^{95}Mo-^{31}P)$ (Hz)	Ref.
dppm	CH_2Cl_2	−1764	65	140	65
1/2 dppe[c]	CH_2Cl_2	−1778	70	123	65
	CH_3CN	−1780	52	133	65
1/2 dppp[c]	CH_2Cl_2	−1785	70	137	65
	CH_3CN	−1785	53	131	65
1/2 dppb[c]	CH_2Cl_2	−1789	65	133	65
	CH_3CN	−1788	64	132	65
1/2 dpppent[c]	CH_3CN	−1785	52	122	65
1/2 dpphex[c]	CH_3CN	−1784	70	140	65
tppe	CH_2Cl_2	−1707	[a]	127	66

[a]Not reported.
[b]Spectra measured at 40°C.
[c]$5 < \Delta\nu_{1/2} < 21$ Hz.
[d]See also references 63, 64 for data for Lithium dibenzophospholides.
[e]$[Mo_2(CO)_{10}(\mu\text{-}Ph_2P(CH_2)_nPPh_2)]$ ($n = 2$–6).

arylphosphines[60] can also coordinate through the aryl moiety in a π-bonding fashion (see Table 6). The diphosphorus ligands are typically chelating ligands[67] but can also coordinate in a monodentate manner at a single metal centre or in a bidentate manner by bridging two different metal centres.[68] Nevertheless, in all instances, relative to $Mo(CO)_6$, substitution of a CO ligand leads to deshielding of the Mo and further substitution leads to further deshielding in a relatively predictable way. Good correlations with various ligand parameters have been observed for ^{95}Mo NMR data for penta- and tetracarbonyl species of tertiary phosphines and/or tertiary phosphites.[49,55]

The data in Table 3 suggest the following shielding orders:

$$Sb > As > P;$$

$$PTA > PF_3 > P(OR)_3 > P(OCH_2C(Me)_2CH_2O)OR \geq P(Alk)_3 > P(OCH_2)_2CH(Me)O)OR \geq P(OCH_2C(Me)_2CH_2O)NHR > P(O(CH_2)_2CH(Me)O)NHR > P(OPh)_3 > PPh(OR)_2 > P(PH_2OR) \gg DBP > Ph_2P(CH_2)_nPPh_2 > P(Ph_2OC_6H_4\text{-}p\text{-}R) > P(OCH_2C(Me)_2CH_2O)X > P(OCH_2C(Me)_2CH_2)SR > P(Ph_2NHR) > P(O(CH_2)_2CH(Me)SR > P(O(CH_2)_2CH(Me)O)Cl > P(AR)_3 > P(Ph_2SR) \geq P(Ph_2SC_6H_4\text{-}p\text{-}R) > P(Ph_2Cl) > P(PhCl_2) > PCl_3 \gg PBr_3$$

There are several factors operative in determining the above shielding orders but the balance of steric and electronic effects is of prime importance. Steric congestion will introduce interbond angle distortions which should both alter the overall electronic symmetry and lengthen the Mo–P bond, increasing the net positive charge at molybdenum.[57,78–80] Thus, greater net

Table 4. ^{95}Mo NMR data for $Mo(CO)_4P_2$ and related species.

P-donor ligand	Geometry	Solvent	δ^{95}Mo (p.p.m.)	$\Delta\nu_{1/2}$ (Hz)	$^1J(^{95}Mo-^{31}P)$ (Hz)	Ref.
$P(Et)_3$	*cis*	CH_2Cl_2	−1764	20	125–129	49, 69 70
	trans	CH_2Cl_2	−1810	110	151	70
$P(CH_2CH_2CN)_3$	*cis*	DMF	−1737	210	128	70
$P(^nBu)_3$	*cis*	CH_2Cl_2	−1742	34	123–124	49, 54, 70
	trans	CH_2Cl_2	−1741	70	159	54, 70
$P(Cy)_3$	*trans*	CH_2Cl_2	−1765	90	134	70
$P(Me_2Ph)^a$	*cis*	CH_2Cl_2	−1670	20	130	34
$P(^nBu_2Ph)$	*cis*	CH_2Cl_2	−1688	76	140	49
$P(MePh_2)$	*cis*	CH_2Cl_2	−1637	57	133	54, 70
	trans	CH_2Cl_2	−1655	170	125	70
$As(MePh_2)$	*cis*	CH_2Cl_2	−1617	170	–	69
$P(EtPh_2)$	*cis*	CH_2Cl_2	−1657	80	130	54, 70
	trans	CH_2Cl_2	−1720	50	128	70
$P(Ph)_3$	*cis*	CH_2Cl_2	−1556	46	140	54, 70
$As(Ph)_3$	*cis*	CH_2Cl_2	−1577	190	–	54, 70
$Sb(Ph)_3$	*cis*	CH_2Cl_2	−1807	247	–	54, 70
	trans	Toluene	−1867	150	–	54, 70
$P(C_6H_4$-*p*-$MeO)_3$	*cis*	CH_2Cl_2	−1552	90	127	70
	trans	CH_2Cl_2	−1739	60	139	54, 70
$P(C_6H_4$-*p*-$F)_3$	*cis*	CH_2Cl_2	−1551	*b*	*b*	71
$P(Ph_2Cl)$	*cis*	CH_2Cl_2	−1522	70	166	72
$P(Ph_2OC_6H_4$-*p*-Me)	*cis*	CH_2Cl_2	−1654	90	157	72
$P(Ph_2OMe)$	*cis*	CH_2Cl_2	−1707	40	153	72
a	*cis*	CH_2Cl_2	−1677	30	161	34
$P(Ph_2OSiMe_3)$	*cis*	CH_2Cl_2	−1623	60	162	72
$P(Ph_2SC_6H_4$-*p*-Me)	*cis*	CH_2Cl_2	−1537	100	133	72
$P(Ph_2SEt)$	*cis*	CH_2Cl_2	−1540	150	140	72
$P(Ph_2NHC_6H_4$-*p*-Me)	*cis*	CH_2Cl_2	−1571	80	140	72
$P(Ph_2NH_2)$	*cis*	CH_2Cl_2	−1652	50	144	72
$P(Ph_2NHMe)$	*cis*	CH_2Cl_2	−1622	100	138	72
$P(Ph_2NHSiMe_3)$	*cis*	CH_2Cl_2	−1563	80	139	72
PTA	*cis*	CH_3CN	−1837	*b*	126	60
PTAMeI	*cis*	CH_3CN	−1819	*b*	127	60
$P(OMe)_3$	*cis*	CH_2Cl_2/C_6D_6	−1827	20	215	34, 49, 73
	trans	CH_2Cl_2/C_6D_6	−1844	60	235	34, 73
$P(OEt)_3$	*cis*	CH_2Cl_2	−1807	20	213	49, 54, 73
$P(O^nBu)_3$	*cis*	CH_2Cl_2	−1808	30	212	49
$P(O^iPr)_3$	*cis*	CH_2Cl_2	−1762	20	209	49
	trans	CH_2Cl_2	−1811	110	203	70
$P(OPh)_3$	*cis*	CH_2Cl_2	−1754	36	226–250	34, 49 49, 70
	trans	CH_2Cl_2	−1792	30	225–231	49, 70
$P(OCH_2CMe_2CH_2O)Cl$	*cis*	$CDCl_3$	−1640	45	246	74
$P(OCH_2CMe_2CH_2O)Br$	*cis*	$CDCl_3$	−1567	49	247	74
$P(OCH_2CMe_2CH_2O)O^nPr$	*cis*	$CDCl_3$	−1824	24	223	74
$P(OCH_2CMe_2CH_2O)O^iPr$	*cis*	$CDCl_3$	−1810	28	222	74

Table 4.– *cont.*

P-donor ligand	Geometry	Solvent	δ^{95}Mo (p.p.m.)	$\Delta\nu_{1/2}$ (Hz)	$^1J(^{95}Mo–^{31}P)$ (Hz)	Ref.
$P(OCH_2CMe_2CH_2O)S^nPr$	*cis*	$CDCl_3$	−1652	73	220	74
$P(OCH_2CMe_2CH_2O)$-NH^nPr	*cis*	$CDCl_3$	−1815	28	195	74
$P(OCH_2CMe_2CH_2O)$-NH^iPr	*cis*	$CDCl_3$	−1812	24	195	74
$P(OCH_2CMe_2CH_2O)$-OC_6H_4-*p*-Me	*cis*	$CDCl_3$	−1805	21	234	74
$P(OCH_2CMe_2CH_2O)$-SC_6H_4-*p*-Me	*cis*	$CDCl_3$	−1640	99	229	74
$P(OCH_2CMe_2CH_2O)$-$O_2H^-Et_3NH^+$	*cis*	$CDCl_3$	−1840	21	201	74
$P(OCH_2CMe_2CH_2O)$-$OSiMe_3$	*cis*	$CDCl_3$	−1774	30	227	74
	cis	CH_3CN	−1837	[b]	126	74
	cis	CH_3CN	−1819	[b]	127	75
DBP	*cis*	CH_2Cl_2	−1714	58	134	63, 64
PCl_3	*cis*	MeC_6H_{11}	−1206	5–50	250	61
PCl_2Ph	*cis*	$Cl(CH_2)_2Cl$	−1369	5–50	194	61
PBr_3	*cis*	CH_2Cl_2	−977	5–50	235	61
$P(OMe_2Ph)$	*cis*	CH_2Cl_2	−1740	5–50	184	61
dppm	*cis*	CH_2Cl_2	−1552	100	119–122	34, 49, 69
dppe	*cis*	CH_2Cl_2	−1775 to −1782	50	128–145	34,[a] 49, 69
dppp	*cis*	CH_2Cl_2	−1693	42	133–142	34, 49 69
dppb	*cis*	CH_2Cl_2	−1667	73	133	69
diars	*cis*	CH_2Cl_2	−1807	43	–	54
dpfe	*cis*	CH_2Cl_2	−1752	80	127	36
depe	*cis*	CH_2Cl_2	−1881	20	129	69
vpp	*cis*	CH_2Cl_2	−1805	73	135	69
dae	*cis*	CH_2Cl_2	−1779	70	–	69
$Ph_2PNHSiMe_2NHPPh_2$	*cis*	CH_2Cl_2	−1610	40	145	72
$Ph_2POSiMe_2OPPh_2$	*cis*	CH_2Cl_2	−1700	90	154	72
$Ph_2PNHSiMe(Ph)NHPPh_2$	*cis*	CH_2Cl_2	−1676	60	144	72
$Ph_2POSiMe(Ph)OPPh_2$	*cis*	CH_2Cl_2	−1685	50	155	72
$Ph_2P(1/2O_4Si)PPh_2$[c]	*cis*	CH_2Cl_2	−1710	50	153	72
$Ph_2P(NMe(CH_2)_2NMe)PPh_2$	*cis*	CH_2Cl_2	−1670	60	153	72
$Ph_2PCH_2P^tPr_2$[a]	*cis*	CH_2Cl_2	−1612	150	117	34
$Ph_2PCH_2P^tBu_2$[a]	*cis*	CH_2Cl_2	−1552	50	117	34
$Ph_2PCH_2PPh^iPr$[a]	*cis*	CH_2Cl_2	−1588	50	124	34
$(CH_2(PPh_2))_2$[a]	*cis*	CH_2Cl_2	−1578	140	125	34
$Ph_2PCH{=}CHPPh_2$[a]	*cis*	CH_2Cl_2	−1801	30	134	34
$(CH(PPh_2)_3$[a]	*cis*	CH_2Cl_2	−1538	100	127	34
$Ph_2P(S)CH_2PPh_2$[a]	*cis*	CH_2Cl_2	−1468	400	[b]	34
$Ph_2P(S)CH_2P^iPr_2$[a]	*cis*	CH_2Cl_2	−1545	400	[b]	34
tppe[d]	*cis*	CH_2Cl_2	−1555	[b]	105	66
tppe[e]	*cis*	CH_2Cl_2	−1712	[b]	132	66

[a]Spectra measured at 313 K.
[b]Not reported.
[c]$[Mo(CO)_4]_2\{(Ph_2P)O_2SiO_2(PPh_2)\}_2$.
[d]Four-membered chelate ring.
[e]Five-membered chelate ring.

Table 5. ^{95}Mo NMR data for $Mo(CO)_3P_3$ and related species.

P-donor ligand	Geometry	Solvent	δ^{95}Mo (p.p.m.)	$\Delta\nu_{1/2}$ (Hz)	$^1J(^{95}Mo–^{31}P)$ (Hz)	Ref.
$P(^nBu)_3$	fac	CH_2Cl_2	−1521	10	124	49
$P(MePh_2)$	fac	CH_2Cl_2	−1427	7	126	54
$P(EtPh_2)$	fac	CH_2Cl_2	−1414	20	124	69
$As(Ph)_3$	fac	$CDCl_3$	−1549	350	–	47
$Sb(Ph)_3$	fac	$CDCl_3$	−1669	50	–	47
$P(OMe)_3$	fac	CH_2Cl_2	−1756	10	214	34, 49
	mer	CH_2Cl_2/C_6D_6	−1780	200	210	34
$P(OMe_2Ph)$	fac	CH_2Cl_2	−1611	5–50	184	61
$P(OEt)_3$	fac	CH_2Cl_2	−1721	4	210	36, 40, 49
$P(OPh)_3$	fac	CH_2Cl_2	−1673	[a]	[a]	76
PTA	fac	CH_3CN	−1759	[a]	126	60
DBP	fac	CH_2Cl_2	−1494	15	126	63
PCl_3	fac	$CDCl_3$	−1885	3	251	47
	fac	CH_2Cl_2	−910	5–50	251	61
PCl_2Ph	fac	$Cl(CH_2)_2Cl$	−1124	5–50	198	61
$PClPh_2$	fac	CH_2Cl_2	−1320	5–50	154	61
PPh_3	fac	CH_2Cl_2	−1265	5–50	120	61
tppe	fac	CH_2Cl_2	−1504	[a]	120	66
triphos	fac	CH_2Cl_2	−1760	43	129	54

[a]Not reported.

Table 6. ^{95}Mo NMR data for $Mo(CO)_{6-n}P_n$ $(n>3)$ species.

Compound	Solvent	δ^{95}Mo (p.p.m.)	$\Delta\nu_{1/2}$ (Hz)	$^1J(^{95}Mo–^{31}P)$ (Hz)	Ref.
cis-$[Mo(CO)_2(P(OMe)_3)_4]$	CH_2Cl_2/C_6D_6	−1660	100	220	34
trans-$[Mo(CO)_2(P(OMe)_3)_4]$	CH_2Cl_2/C_6D_6	−1679	1600	[a]	34
$Mo(CO)(P(OMe)_3)_5$	CH_2Cl_2/C_6D_6	−1518	100	240	34
$Mo(P(OMe)_3)_6$	CH_2Cl_2/C_6D_6	−1358	15	256	34
cis-$[Mo(CO)_2(dppe)_2]$	THF	−1486	[a]	[a]	38
trans-$[Mo(CO)_2(dppe)_2]$	THF	−1451	[a]	[a]	38
cis-$[Mo(CO)_2(dptpe)_2]$[b,c]	THF	−1475	207	[a]	49
trans-$[Mo(CO)_2(dptpe)_2]$[b,c]	THF	−1802	121	[a]	49
$Mo(\eta^6\text{-}PhPMePh)(PMePh_2)_3$	THF	−1033	87	203	77
$Mo(\eta^6\text{-}PhPPh_2)(dppe)(PMe_3)$	THF	−1479	85	218	77

[a]Not reported.
[b]Assignments are tentative, see reference 49.
[c]Spectra measured at 330 K.

ligand steric bulk should promote deshielding and this appears to be the case (compare chemical shift data for $P(^nBu)_3$ and $P(^tBu)_3$ or for $P(OMe)_3$ and $P(OEt)_3$). Unfortunately, steric and electronic effects tend to be very closely and subtly inter-related.

It is tempting to conclude that the more basic trialkylphosphines, $P(Alk)_3$, provide greater shielding than the less basic triarylphosphines, $P(Ar)_3$, owing to a greater nephelauxetic effect and/or greater ligand field strength for the former. Clearly, it is the phenyl substituent which promotes deshielding, as can be seen from the observed shielding order, $P(Alk)_3 > P(Alk_2Ph) > P(AlkPh_2) > P(Ph)_3$. Introduction of the electron-withdrawing phenyl substituent will decrease the σ-donicity of the phosphorus atom but, at the same time, the phenyl substituent should increase the π-acidity of the molybdenum by affecting all the terms in the Ramsey expression. These two effects do not cancel each other, however, as there is a third, concomitant, effect. That is, introduction of a phenyl substituent will also tend to increase the net steric bulk of $P(Alk_{3-n}Ph_n)$ which will promote deshielding (see above).

Gray and coworkers[56,58,59,72,74] reported good correlations for ^{95}Mo chemical shift data with other experimental data, including multinuclear NMR data (^{13}C, ^{17}O, ^{31}P) for other NMR active nuclei present in the same compound once the steric parameter is more or less held constant and the electronic parameter left as a variable. For example, for the series of compounds, $[Mo(CO)_5(P(Ph_2OC_6H_4\text{-}p\text{-}R)]$,[56] it was found that the ^{95}Mo chemical shifts correlate fairly well with Taft parameters representative of the relative donor/acceptor properties of the *R* groups. Ultimately, there is a tendency toward deshielding as *R* becomes more electron-withdrawing and this can also be observed when comparing the ^{95}Mo chemical shifts for tertiary phosphines of similar steric bulk but differing basicities (compare $P(Et)_3$ and $P(CH_2CH_2CN)_3$ or $P(Ph)_3$ and $P(C_6H_4\text{-}p\text{-}F)_3$).

Thus, it becomes clear that in rationalizing chemical shifts observed, generalizations can only be made for series of closely related compounds. For example, Gray and Kraihanzel[72] have found that for *cis*-$[Mo(CO)_4(P(Ph_2XR))_2]$ and $[Mo(CO)_4(Ph_2PYPPh_2)]$, the ^{95}Mo chemical shift data correlate well with the longest wavelength visible absorption band. This suggests that the radial and Mo–P bond covalency terms as in equation (2) are more or less constant and that ΔE is the dominating parameter. Nevertheless, there are further complications. For the above compounds, and for the pentacarbonyls species, $[Mo(CO)_5(P(OCH_2C(Me)_2CH_2O)ER)]$,[58] $[Mo(CO)_5(P(O(CH_2)_2CH(Me)O)ER)]$,[59] and $[Mo(CO)_5(P(Ph_2ER))]$[55] (R = H, alkyl, aryl), the Mo is shielded as $E = O > N \gg S > Br > Cl$, which is not entirely consistent with the changes in the ER (or XR) electronegativities.[72] It is suggested[72] that the shielding order observed may be a function of ER donation from filled p-orbitals into unfilled phosphorus d-orbitals, thereby reducing the overall π-acidity of the phosphorus ligand.

Furthermore, it was found[58,59] that the effects of the three substituents at phosphorus upon the chemical shifts are not additive.

Steric and various bonding effects are also important in determining compound geometry. Mo–P dπ–dπ back bonding will stabilize the more thermodynamically favoured *cis*- and/or mer-isomers via a synergistic mechanism[81,82] whereas the avoidance of steric congestion should favour the *trans*- and/or fac-isomers.[81,82] For the last two cases, ΔE is expected to be larger so that the *trans*- and fac-isomers should be more shielded than their *cis*- and mer-counterparts; this is what is generally, but not always, observed.

Replacement of two *cis* monophosphines by a comparable chelating diphosphine ligand normally leads to increased shielding. This is attributed to a chelate ring effect[83] most likely due to angular distortions introduced within the coordination sphere. The shielding order observed for $Mo(CO)_4(Ph_2P(CH_2)_nPPh_2)$, $n = 2 > 1 > 3 > 4$,[34,38,69] is opposite to that observed for the ^{31}P chemical shifts of the phosphorus nuclei.[83,84] The dppe and depe compounds show similar chelate ring effects with respect to their monophosphine analogues but, as expected, the more basic depe ligand is 100 p.p.m. more shielding than the less basic dppe ligand. The ethylene backbone in vpp promotes greater shielding than the ethane backbone in dppe. These observations are in accordance with a π-delocalization onto the ring system.[85] Conversely, the ^{95}Mo chemical shifts for $[Mo_2(CO)_{10}(\mu\text{-}Ph_2P(CH_2)_nPPh_2)]$ are virtually independent of the value of n and are very similar to chemical shifts for their monophosphine analogues. Some interesting work has been reported[66] for the complexes, $[Mo(CO)_n(tppe)]$ (n = 3–5), wherein the tppe ligand can coordinate in five different modes. The data clearly demonstrate the effects of chelation, chelate ring size and double versus single chelation on the ^{95}Mo chemical shifts.

Unlike for δ^{95}Mo, $^1J(^{95}Mo\text{-}^{31}P)$ values appear to be insensitive to subtle changes in the substituents at phosphorus although one would expect that their magnitudes would be sensitive to substituent electronegativities. The major contributor to spin–spin coupling, the Fermi contact term, is increased by increased p-character in bonds leaving greater s-character at the nuclei.[84] For the overall shielding order (*vide supra*) there is no clear correlation between chemical shift and ^1J data. Nevertheless, the coupling constant magnitudes are expected to increase with increased phosphorus substituent electronegativities[86] and this does appear to be the case for $Mo(CO)_5(P(Ph_2ER))$ where ^1J values increase as E = S (142–145 Hz) < NH (146–151 Hz) < O (156–159 Hz) and for the series, $P(Alk)_3$ (127–140 Hz) < $P(Ph)_3$ (139–144 Hz) < $P(Ph_2OR)$ (156–159 Hz) < $P(Ph(OR)_2)$ (183 Hz) < $P(OR)_3$ (214–218 Hz). This, in turn, implies that increased Mo–P dπ-dπ back-bonding is a factor in increasing the magnitude of the coupling constant. The highest ^1J values thus far reported have been measured for ^{31}P NMR spectra for compounds of the

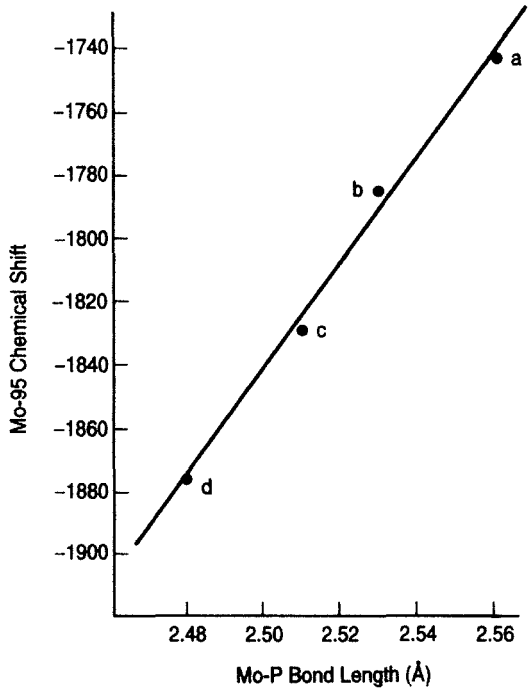

Fig. 1. Correlation between ^{95}Mo NMR chemical shifts and Mo–P bond lengths for: (a) $Mo(CO)_5(P(Ph)_3)$; (b) $[Mo_2(CO)_{10}(\mu\text{-dppp})]$; (c) $Mo(CO)_5(P(CH_2CH_2CN)_3$; (d) $Mo(CO)_5(PTA)$.

very effective π-acid, PF_3, in $Mo(CO)_{6-n}(PF_3)_n$ (n = 1, 2, 3, 6) with ^1J in the range, 279–290 Hz.[62]

Unfortunately, unlike the situation for ^{195}Pt NMR,[14] *cis/trans* and/or mer/fac isomers cannot readily be distinguished on the basis of coupling constant data. Thus, it is questionable whether higher coupling constants correspond to shorter Mo–P bonds, as has been suggested for comparable W(0) species.[84] There are only limited X-ray crystallography data available for molybdenum compounds containing phosphorus ligands but it is already clear that the Mo–P bond lengths measured for representative compounds such as, $Mo(CO)_5(PTA)$ (2.48 Å),[87] $Mo(CO)_5(P(CH_2CH_2CN)_3)$ (2.51 Å),[88] $Mo(CO)_5(P(Ph)_3)$ (2.56 Å),[88] and $[Mo_2(CO)_{10}(\mu\text{-dppp})]$ (2.532 Å),[65] do not correlate with the coupling constants measured for these compounds. However, for the same compounds, there appears to be a good correlation between the bond length data and corresponding δ^{95}Mo values (see Fig. 1) implying that shielding of the Mo nucleus corresponds with shorter, and presumably stronger, Mo–P bonds.

Finally, the line widths observed for the majority of compounds in Tables 3–6 are relatively narrow (i.e., < 100 Hz). Broader lines observed for certain compounds might be attributed to the presence of unresolved scalar coupling to other quadrupolar nuclei (e.g., ^{75}As, ^{121}Sb, ^{123}Sb) and/or to reduced symmetry at the molybdenum nucleus with a consequent enhancement of the quadrupolar contribution to the line width.[5,89] Line widths should be narrower for *cis*- and fac-isomers relative to their *trans*- and mer-counterparts[22,29] but often are not owing to steric congestion. Andrews *et al.*[34] have documented the expected changes in $\Delta\nu_{1/2}$ for $Mo(CO)_{6-n}(P(OMe)_3)$ (n = 0–6).

2.1.3. Nitrogen donor ligands

^{95}Mo NMR data for compounds containing nitrogen ligands are presented in Tables 7–10 for penta-, tetra-, tri- and higher substitution carbonyl species respectively. Both the line widths and chemical shifts observed show significant solvent dependencies. Chemical shifts for $[Mo(CO)_{6-n}(N)_n]$ (N = pip, py) are increasingly shielded as the solvent becomes more polar and the chemical shift sensitivity to solvent polarity increases as $n = 0 \ll 1 < 2$, the order also expected for increasing net molecular dipole moments for these compounds. Unlike its pentacarbonyl analogue, *cis*-$[Mo(CO)_4(pip)_2]$ is insoluble in the relatively non-polar solvents, C_6H_6 and $CHCl_3$.[90]

In all cases, substitution of a mono-ligating nitrogen ligand for CO leads to deshielding but the relative amount of deshielding becomes progressively smaller for each successive substitution, opposite to what is seen for the isocyanide compounds (see Section 2.1.5). The overall shielding orders observed for the penta- and tetracarbonyl species are quin > pyr > NCR ≥ pip > py and quin > pn > NCR > Et_3N > pyr > pip > py respectively. It is not clear why pyr appears at very different positions in these two series. For coordinating solvents, shielding increases according to increasing solvent polarity as py < Et_3N < $NCCH_2CH_3$ < $NCCH_3$. Solvent polarity is related to solvent acceptor number (AN)[99] which is a measure of solvent electrophilicity[100] and there is a qualitative correlation of the chemical shifts with AN. There is no apparent correlation, however, with the corresponding solvent donor number (DN)[99] which is directly related to solvent nucleophilicity.[100] For the cyclic ligands deshielding is observed upon ring saturation from pip to py while shielding occurs with ring contraction from py to pyr and with expansion to a double-ring system, py to quin. The addition of substituents to the ring system (saturated or unsaturated) leads to either shielding or deshielding, depending on both the electronic nature[90,92] and the position[90] of the ring substituent.

For compounds with substituted pyridine ligands, increased shielding correlates well with increasingly negative values for the ring-substituent

Table 7. ^{95}Mo NMR data for pentacarbonyl compounds containing nitrogen donor ligands.

N-donor ligand	Solvent	δ^{95}Mo (p.p.m.)	$\Delta\nu_{1/2}$ (Hz)	Ref.
$NCCH_3$	CH_3CN	−1440	39	36, 54
pip	C_6H_6	−1420	[a]	90
	$CHCl_3$	−1420	[a]	90
	CH_2Cl_2	−1433	80	36, 90
	THF	−1441	[a]	90
	$(CH_3)_2CO$	−1446	[a]	90
	DMF	−1452	[a]	90
	CH_3CN	−1455	[a]	90
	DMSO	−1458	[a]	90
2,6-Me_2pip	CH_2Cl_2	−1524	10	36
2,2,6,6-Me_4pip	CH_2Cl_2	−1552	10	36
quin	CH_2Cl_2	−1523	20	36
pyr	CH_2Cl_2	−1470	40	36
py	$CDCl_3$	−1387 to −1396	70–76	47, 91
	CH_2Cl_2	−1397	50	92
	py	−1404	91	91
3-CN-py	CH_2Cl_2	−1366	122	92
4-CN-py	CH_2Cl_2	−1367	100	92
3-Cl-py	CH_2Cl_2	−1379	86	92
3-Br-py	CH_2Cl_2	−1380	98	92
4-C(O)Me-py	CH_2Cl_2	−1382	93	92
4-Ph-py	CH_2Cl_2	−1402	93	92
4-Bz-py	CH_2Cl_2	−1403	117	92
2-Me-py	CH_2Cl_2	−1403	60	92
4-Me-py	CH_2Cl_2	−1405	53	92
3-Me-py	CH_2Cl_2	−1406	70	92
4-Et-py	CH_2Cl_2	−1406	70	92
4-^{t}Bu-py	CH_2Cl_2	−1409	92	92
4-NMe_2-py	CH_2Cl_2	−1433	68	92

[a]Not reported.

Hammet parameters[92] and/or increasing ligand pK_a values.[90,92] Increased shielding also corresponds to decreased ν(CO) values for the *trans*-carbonyl ligands,[92,101] in complete accordance with *trans*-Mo–C bond strengthening via a synergistic mechanism. Chemical shifts observed for the mixed-ligand species, *cis*-[Mo(CO)$_4$(pip)(substituted-py)], are consistently shielded from expected positions calculated from averages of positions observed for *cis*- [Mo(CO)$_4$N$_2$] (N = pip or substituted-py),[90] thus reaffirming that pip is more shielding than py. Corresponding thermochemical data for

Table 8. ^{95}Mo NMR data for tetracarbonyl compounds containing nitrogen donor ligands.

N-donor Ligand	Geometry	Solvent	δ^{95}Mo (p.p.m.)	$\Delta\nu_{1/2}$ (Hz)	Ref.
$NCCH_3$	*cis*	CH_3CN	−1307	49	54
	cis	DMF	−1304	73	92
$NCCH_2CH_3$	*cis*	DMF	−1305	67	92
pn	*cis*	DMF	−1311	90	40
Et_3N	*cis*	CH_2Cl_2	−1152	20	70
	trans	CH_2Cl_2	−1327	30	70
pip	*cis*	CH_2Cl_2	−1075	[a]	90
	cis	$(CH_3)_2CO$	−1077	[a]	90
	cis	THF	−1064	[a]	90
	cis	DMF	−1093	90	70, 90
	cis	DMSO	−1097	[a]	70
2,6-Me_2-pip	*trans*	CH_2Cl_2	−1351	10	70
quin	*trans*	CH_2Cl_2	−1401	180	70
pyr	*cis*	CH_2Cl_2	−1140	60	70
	trans	DMF	−1155	60	70
py	*cis*	$CDCl_3$	−1037	104	91
	cis	CH_2Cl_2	−1046	80	70
	cis	py	−1051	130	91
	cis	DMF	−1060	140	90
4-Ph-py	*cis*	DMF	−1063	305	90
4-Bz-py	*cis*	DMF	−1070	300	90
3-Me-py	*cis*	DMF	−1062	154	90
4-Me-py	*cis*	DMF	−1074	115	90
4-Et-py	*cis*	DMF	−1071	139	90
4-^{t}Bu-py	*cis*	DMF	−1077	215	76, 90
4-NMe_2-py	*trans*	DMF	−1369	132	90
2,4,6-Me_3-py	*cis*	DMF	−1067	148	90
1-$MeIm_2$	*cis*	CH_2Cl_2	−1036	20	70
2-NH_2Et-py	*cis*	DMF	−1002	70	70
2-NH_2Me-py	*cis*	DMF	−978	90	70
pip/$NCCH_3$	*cis*	DMF	−1213	60	90
pip/$NCCH_2CH_3$	*cis*	DMF	−1213	61	90
pip/4-CN-py	*cis*	DMF	−1053	106	90
pip/3-Cl-py	*cis*	DMF	−1066	145	90
pip/3-Br-py	*cis*	DMF	−1062	180	90
pip/py	*cis*	DMF	−1079	120	90
pip/4-Ph-py	*cis*	DMF	−1079	147	90
pip/4-Bz-py	*cis*	DMF	−1083	137	90
pip/3-Me-py	*cis*	DMF	−1079	138	90
pip/4-Me-Py	*cis*	DMF	−1087	141	90

Table 8.–*cont.*

N-donor Ligand	Geometry	Solvent	δ^{95}Mo (p.p.m.)	$\Delta\nu_{1/2}$ (Hz)	Ref.
pip/4-Et-py	*cis*	DMF	−1084	123	90
pip/2,4,6-Me_3-py	*cis*	DMF	−1084	152	90
pip/4^{t}Bu-py	*cis*	DMF	−1090	320	90
pip/4-NMe_2-py	*cis*	DMF	−1120	143	90
pip/P(C_6H_4-*p*-Cl)$_3$[b]	*cis*	DMF	−1314	273	90
pip/P(Ph)$_3$[b]	*cis*	DMF	−1322	265	90
pip/P(C_6H_4-*p*-MeO)$_3$[b]	*cis*	DMF	−1327	475	90
pip/P(OMe)$_3$[c]	*cis*	CH_2Cl_2	−1421	70	70
pip/P(Et)$_3$[d]	*cis*	CH_2Cl_2	−1355	80	70
pip/P(O^{i}Pr)$_3$[e]	*cis*	CH_2Cl_2	−1396	210	54, 70
pip/P(OPh)$_3$[f]	*cis*	CH_2Cl_2	−1362	110	54, 70
phen	*cis*	CH_2Cl_2	−1175	35	69
bipy	*cis*	CH_2Cl_2	−1161 to −1167	55–90	37, 39, 69, 93
		DMF	−1189 to −1190	110–120	54, 90
bpym[g]	*cis*	CH_2Cl_2	−1162	64	93
bpm	*cis*	CH_2Cl_2	−1162	67	93
bpz	*cis*	CH_2Cl_2	−1112	41	93
bpdz	*cis*	CH_2Cl_2	−1102	28	93
bptz[h]	*cis*	CH_2Cl_2	−904	12	93
2-PAP	*cis*	CH_2Cl_2	−1030	10	39
TMEDA	*cis*	CH_2Cl_2	−1010	56	37
abpy	*cis*	CH_2Cl_2	−936	4	93

[a]Not reported.
[b]$^1J(^{95}Mo–^{31}P)$ not resolved.
[c]$^1J(^{95}Mo–^{31}P)$ = 220 Hz.
[d]$^1J(^{95}Mo–^{31}P)$ = 129 Hz.
[e]$^1J(^{95}Mo–^{31}P)$ = 208 Hz.
[f]$^1J(^{95}Mo–^{31}P)$ = 257 Hz.
[g][$Mo(CO)_4$]$_2$(bpym): δ^{95}Mo = −1162 p.p.m. and $\Delta\nu_{1/2}$ = 58 Hz in CH_2Cl_2, Ref. 93.
[h][$Mo(CO)_4$]$_2$(bptz): δ^{95}Mo = −847 p.p.m. and $\Delta\nu_{1/2}$ = 22 Hz in CH_2Cl_2, Ref 93.

[$Mo(CO)_{6-n}(N)_n$] (n = 1–3)[102–104] indicate that the Mo–N bond strength increases as N = py < pip < $NCCH_3$ implying that greater shielding indicates stronger Mo–N bonding.

The ligands, $NCCH_3$ and pip, have negligible π-acid properties. Pyridine, on the other hand, can potentially π back-bond via its π^*-orbitals[105] but this is considered unlikely.[81,106–108] Thus, for the monodentate nitrogen ligands, π-acceptor properties are not important but the balance of relative positions

Table 9. ^{95}Mo NMR data for tricarbonyl compounds containing nitrogen donor ligands.[a]

N-donor Ligand	Solvent	δ^{95}Mo (p.p.m.)	$\Delta\nu_{1/2}$ (Hz)	$^1J(^{95}Mo–^{31}P)$ (Hz)	Ref.
$NCCH_3$	CH_3CN	−1114	10	–	54
py	py	−800	7	–	91
dien	DMF	−1058	70	–	40
NH_3	NH_3[b]	−1162	60	–	94
$HB(3,5\text{-}Me_2pz)_3$	DMF	−1149	80	–	95
$Me_3[9]aneN_3$	DMSO	−1092	169	–	95
$[12]aneN_3$	CH_2Cl_2	−1001	10	–	95
$[9]aneN_3$	CH_2Cl_2	−886	20	–	95
2-PAP/$P(Ph)_3$	CH_2Cl_2	−763	180	150	39
bipy/$P(C_6H_4\text{-}p\text{-}Cl)_3$	CH_3CN	−1061	51	127	96
bipy/$P(C_6H_4\text{-}p\text{-}F)_3$	CH_3CN	−1060	30	132	96
bipy/$P(Ph)_3$	CH_3CN	−1063	18	127	96
bipy/$P(C_6H_4\text{-}p\text{-}Me)_3$	CH_3CN	−1064	32	128	96
bipy/$P(C_6H_4\text{-}p\text{-}MeO)_3$	CH_3CN	−1063	61	127	96
bipy/$P(C_6H_4\text{-}p\text{-}NMe_2)_3$	CH_3CN	−1066	43	129	96
bipy/$P(^nBu)_3$	CH_3CN	−1071	[c]	125	96
bipy/$P(Me)_3$	CH_3CN	−1077	[c]	130	96
bipy/$P(OMe)_3$	CH_3CN	−1113	31	221	92
bipy/$P(OEt)_3$	CH_3CN	−1109	32	209	92
	CH_2Cl_2	−1097	53	240	49
bipy/$P(O^iPr)_3$	CH_3CN	−1108	55	209	92
bipy/$P(OMe_2Ph)_3$	CH_3CN	−1097	35	176	92
bipy/$P(OMePh_2)_3$	CH_3CN	−1081	29	149	92
bipy/$P(OPh)_3$	CH_3CN	−1087	43	233	92

[a]All complexes have the fac-configuration.
[b]Measured at 225 K.
[c]Not reported.

in the spectrochemical and nephelauxetic series is important in determining δ^{95}Mo. This situation is almost reversed for the somewhat related α-diimine ligands (see Fig. 2). The latter are deemed poor σ-donors but strong π-acceptors, especially the diazenes which can effectively back-bond through their N=N π^* molecular orbitals. The shielding order observed, phen > bipy > bpym ≥ bpm > bpz > bpdz > 2-PAP > abpy > bptz, cannot readily be rationalized in terms of ground-state ligand basicities or MLCT absorption energies.[93] Correlations are observed, however, between δ^{95}Mo and the calculated LUMO coefficients at the chelating nitrogen centres, McLachlan π-spin populations, and ESR coupling constants for the anion radical complexes[93] showing that the amount of metal to ligand

Table 10. ^{95}Mo NMR data for dicarbonyl and higher substitution compounds containing nitrogen donor ligands.

Compound	Solvent	δ^{95}Mo (p.p.m)	$\Delta\nu_{1/2}$ (Hz)	Ref.
[([9]aneN$_3$)Mo(CO)$_2$(NO)][BF$_4$]	H_2O	−616	110[a]	95
[([12]ane N$_3$)Mo(CO)$_2$(NO)][ClO$_4$]	H_2O	−580	90	95
[(Me$_3$[9]aneN$_3$)Mo(CO)$_2$(NO)][PF$_6$]	CH_3CN	−437	80	95
cis-[Mo(CO)$_2$(2-PAP)$_2$]	CH_2Cl_2	+294	90	39
trans-[Mo(CO)(NCC$_6$H$_4$-*p*-MeO)(dppe)$_2$][b]	CH_2Cl_2	−1126	[c]	38
trans-[Mo(CO)(NCC$_6$H$_5$)(dppe)$_2$][b]	CH_2Cl_2	−1118	[c]	38
trans-[Mo(CO)(NCC$_6$H$_4$-*p*-C(O)Me)(dppe)$_2$][b]	CH_2Cl_2	−1089	[c]	38
[Mo(2-PAP)$_3$]	CH_2Cl_2	+1502	180	39
trans-[Mo(NCCH$_3$)(NO)(dppe)$_2$][BF$_4$][b]	CH_2Cl_2	−553	[c]	97
trans-[Mo(N$_3$)(NO)(dppe)$_2$][b]	CH_2Cl_2	−614	[c]	97
trans-[Mo(Br)(NO)(dppe)$_2$][b]	CH_2Cl_2	−514	[c]	97
trans-[Mo(N$_3$)(NNEt)(dppe)$_2$][b]	CH_2Cl_2	−180	[c]	38
trans-[Mo(NCCH$_3$)(NNEt)(dppe)$_2$][BPh$_4$][b]	CH_2Cl_2	−140	[c]	38
trans-[Mo(N$_3$)(NNHEt)(dppe)$_2$]Br[b]	CH_2Cl_2	+140	[c]	38
Mo(NO)$_2$Cl$_2$(PPh$_3$)$_2$	DMF	−500	530	98
Mo(NO)$_2$Cl$_2$(bipy)	DMF	−263	170	98

[a] $^1J(^{95}\text{Mo}–^{14}\text{N})$ = 39 Hz at 373 K.
[b] $^1J(^{95}\text{Mo}–^{31}\text{P})$ not reported.
[c] Not reported.

charge transfer is very important in determining the ^{95}Mo chemical shifts. The greater shielding observed for the bipy compound, relative to *cis*-[Mo(CO)$_4$(py)$_2$], is largely attributable to a chelate ring effect.[69] The chemical shift for [Mo(2-PAP)$_3$] is the most deshielded value thus far reported for a Mo(0) compound.[39] Merlic and Adams[37] have used ^{95}Mo to distinguish tri- and tetracarbonyl diamine and diimine complexes. The diastereomers tend to be 25–30 p.p.m. different in chemical shift.[5,37,109]

The line widths are reasonably narrow (< 150 Hz) except in the case of the mixed ligand species, *cis*-[Mo(CO)$_4$(pip)(PR$_3$)], for which scalar coupling between the Mo and P nuclei is not easily resolved. Coupling between ^{95}Mo and N-14 nuclei is not generally observed and is much smaller ($^1J(^{95}\text{Mo}–^{14}\text{N})$ = 32–45 Hz)[5,38,110] than $^1J(^{95}\text{Mo}–^{31}\text{P})$ values. The latter, for the mixed P/N-donor ligand species, are not significantly affected by the presence of the N-donor coligands, although the ^{95}Mo chemical shifts do tend to be deshielded. Generally, shielding of the Mo nucleus increases as the phosphine pK_a increases, concomitantly with increased shielding of the phosphorus nucleus.[92] For the species, fac-[Mo(CO)$_3$(bipy)(P(OMe$_{3-n}$Ph$_n$))], the molybdenum and phosphorus nuclei are each deshielded as n increases from 1 to 3.[92]

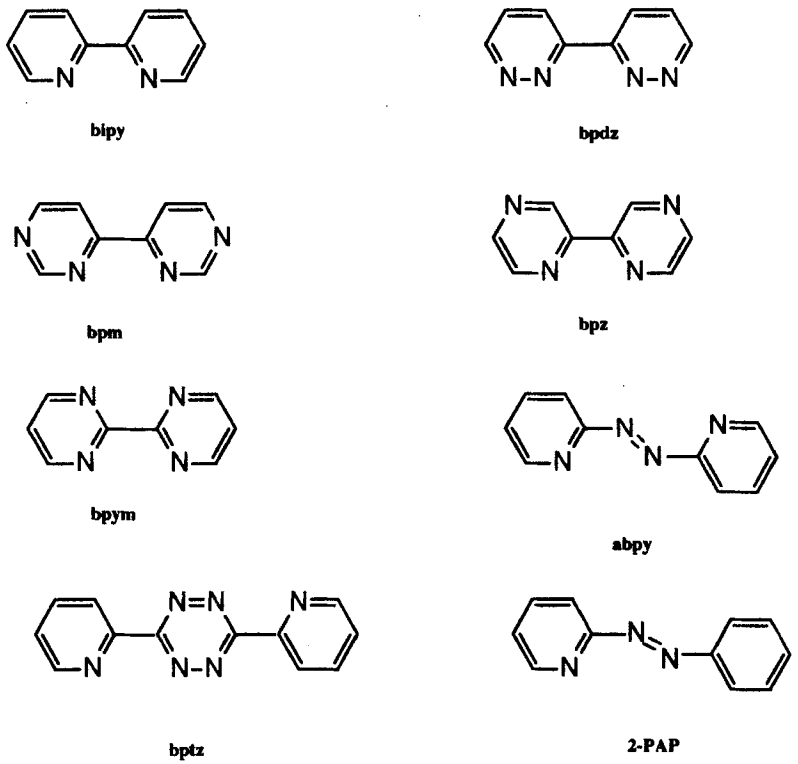

Fig. 2. Skeletal structures for some α-diimine ligands.

^{95}Mo NMR for some dinitrogen compounds are presented in Table 11 while data for nitrosyl species appear in Table 10. These data suggest the following overall shielding order; $CO > P(Alk)_3 > P(Ar)_3 > N_2 > N_3^- \geq NCR > NO^+ > N{=}NR^+ > N\text{-}NR_2^{2-}$. Clearly, all the terms in the Ramsey expression are important here.[23,38] Few new data for nitrosyl and thionitrosyl compounds have been reported since the last review.[5]

2.1.4. Sulphur donor ligands

Data for compounds containing sulphur donor ligands are presented in Table 12. The line widths are greater than 100 Hz in most cases and, in all cases, the chemical shifts are deshielded relative to $Mo(CO)_6$. Compounds with the anionic dithiocarbonato, xanthato and phosphorodithioato ligands show shifts in the range observed for comparable halide and pseudohalide species (see 2.1.2). Relative shielding of the molybdenum decreases as $S_2CNPh_2 > S_2CNMe_2 > S_2CNEt_2 > S_2CN(CH_2)_4 > S_2COEt$. The position for $S_2P(OEt)_2$ in this series depends upon its bonding mode, i.e.,

Table 11. ^{95}Mo NMR data for some dinitrogen Mo(0) compounds.[a]

Compound	δ^{95}Mo (p.p.m.)	$\Delta\nu_{1/2}$ (Hz)[e]	$^1J(^{95}Mo–^{31}P)$ (Hz)	Ref.
trans-[Mo(N_2)(CO)(dppe)$_2$]·toluene	−1167	[b]	[b]	38
[Mo($^{15}N_2$(P(Me)$_3$)$_5$][c]	−178	15	170	38
trans-[Mo(N_2)(NCC$_6$H$_4$-4-MeO)(dppe)$_2$]	−667	170	170	38
trans-[Mo(N_2)$_2$(depe)$_2$]	−1022	65	185	97
trans-[Mo(N_2)$_2$(depe)(dppe)]	−899	65	185	97
trans-[Mo(N_2)$_2$(dppe)$_2$]	−787	50	180	97
trans-[Mo(N_2)$_2$(dptpe)$_2$]	−793	50	175	97
	−776	85	205	49[d]
trans-[Mo(N_2)$_2$\{(C$_6$H$_4$-*p*-MeO)$_2$P(CH$_2$)$_2$P(C$_6$H$_4$-*p*-MeO)$_2$\}$_2$]	−798	(100)	190	97
trans-[Mo(N_2)$_2$\{(C$_6$H$_4$-*p*-Me)$_2$P(CH$_2$)$_2$P(C$_6$H$_4$-*p*-Me)$_2$\}$_2$]	−793	(100)	175	97
trans-[Mo(N_2)$_2$\{(C$_6$H$_4$-*m*-Me)$_2$P(CH$_2$)$_2$P(C$_6$H$_4$-*m*-Me)$_2$\}$_2$]	−795	(100)	165	97
trans-[Mo(N_2)$_2$\{(C$_6$H$_4$-*p*-Cl)$_2$P(CH$_2$)$_2$P(C$_6$H$_4$-*p*-Cl)$_2$\}$_2$]	−785	(100)	180	97
trans-[Mo(N_2)$_2$\{(C$_6$H$_4$-*p*-CF$_3$)$_2$P(CH$_2$)$_2$P(C$_6$H$_4$-*p*-CF$_3$)$_2$\}$_2$]	−774	(100)	180	97
trans-[Mo(N_2)$_2$(dppe)(P(Me$_2$Ph))$_2$]	−701	20	175	38
cis-[Mo(N_2)$_2$(P(Me)$_3$)$_4$]	−637	20	175	38
cis-[Mo(N_2)$_2$(P(MePh$_2$)$_4$]	−455	25	[b]	38
trans-[Mo(N_2)$_2$(P(MePh$_2$)$_4$]	−454	25	190	97
mer-[Mo(N_2)$_3$(P^{n}Pr$_2$Ph)$_3$]	−392	10	180	38

[a]All spectra recorded in THF.
[b]Not reported.
[c]$^1J(^{95}Mo–^{15}N)$ = 32 Hz.
[d]Spectrum measured at 328 K.
[e]Approximate values in brackets.

mono- versus bi-dentate bonding. The high deshielding observed for [Mo(CO)$_4$(S$_2$P(OEt)$_2$)]$^-$ may be due partially to steric effects. Young and Enemark[111] reported chemical shifts in the range +310 to −430 p.p.m. for the adduct species, [Mo(S$_2$CNEt$_2$)$_2$(CO)$_2$L] and [Mo(S$_2$CNEt$_2$)$_2$(CO)$_2$]$_2$-μ-L (L = various ligands). They rationalize the shielding observed, relative to the [Mo(S$_2$CNEt$_2$)$_2$(CO)$_2$] precursor, on the basis of a correlation of the chemical shift with both the π-acidity and stereochemistry of L.

For compounds of the chelating dithioethers, RSCH$_2$CH$_2$S*R*, shielding decreases as *R* = ^{t}Bu > ^{i}Pr > Et > Me. The chemical shift for *cis*-[Mo(CO)$_4$(MeSCH$_2$CH$_2$S^{t}Bu)] is the exact average of chemical shifts observed for the two species, *cis*-[Mo(CO)$_4$(RSCH$_2$CH$_2$S*R*)] (*R* = Me, ^{t}Bu),

Table 12. ^{95}Mo NMR data for Mo(0) compounds containing sulphur donor ligands.

Compound	Solvent	δ^{95}Mo (p.p.m.)	$\Delta\nu_{1/2}$ (Hz)	Ref.
$[NH_4][Mo(CO)_5\{S_2P(OEt)_2\}]$	DMSO	−1626	90	48, 112
$Na[Mo(CO)_5(S_2CNPh_2)]$	DMSO	−1596	50	48, 112
$Na[Mo(CO)_5(S_2CNMe_2)]$	DMSO	−1534	100	48, 112
$K[Mo(CO)_5(S_2COEt)]$	DMSO	−1417	170	112
$Na[Mo(CO)_4(S_2CNMe_2)]$	DMSO	−1414	270	112
$Na[Mo(CO)_4(S_2CNEt_2)]$	DMSO	−1409	170	112
$[NH_4][Mo(CO)_4\{S_2P(OEt)_2\}]$	DMSO	−1390	150	112
$K[Mo(CO)_4\{S_2CN(CH_2)_4\}]$	DMSO	−1388	250	112
$[NH_4][Mo(CO)_4\{S_2CN(CH_2)_4\}]$	NMP	−1380	270	112
$[Mo(CO)_4(cis\text{-}^tBuSCH{=}CHS^tBu)]$	$CDCl_3$	−1432	170	113
$cis\text{-}[Mo(CO)_4(^tBuSCH_2CH_2S^tBu)]$	$CDCl_3$	−1421	210	113
$cis\text{-}[Mo(CO)_4(^iPrSCH_2CH_2S^iPr)]$	$CDCl_3$	−1400	130	113
$cis\text{-}[Mo(CO)_4(EtSCH_2CH_2SEt)]$	$CDCl_3$	−1393	130	113
$cis\text{-}[Mo(CO)_4(MeSCH_2CH_2S^tBu)]$	$CDCl_3$	−1392	120	113
$cis\text{-}[Mo(CO)_4(MeSCH_2CH_2SMe)]$	$CDCl_3$	−1362	80	113
$[Mo(CO)_3([9]aneS_3)]$	$MeNO_2$	−1350	30	114

indicating that substituent effects at individual sulphur sites are additive. Dithioethers are expected to be poor π-acceptors and the observation that increased shielding corresponds to increased electron-donating ability for *R* is in accord with this expectation. However, as *R* becomes more electron-donating, it also becomes more sterically demanding. Abel *et al.*[113] rationalized the shielding order in terms of relative Mo–S bond strengths. That is, the chemical shifts correlate in a qualitative way with the pyramidal sulphur inversion barriers which are, in turn, dependent upon the ligand steric requirements. Increased shielding corresponds with decreases in the inversion barrier energies which are thought to parallel Mo–S bond weakening.

2.1.5. Carbon ligands[11–13]

^{95}Mo NMR data for compounds containing Mo–C bonds, formed with ligands other than CO, are presented in Table 13. Monosubstitution of an isocyanide, CNR, for a CO ligand leads to minor shielding which becomes progressively greater with each successive substitution, apparently independent of the steric and/or electronic nature of R. Deshielding of the Mo nucleus corresponds to a concomitant deshielding of the isocyanide carbons[115] and, in the higher substitution species, the isocyanide carbons *trans* to CO ligands are more

Table 13. ^{95}Mo NMR data for some organomolybdenum (0) compounds.

Compound	Solvent	δ^{95}Mo (p.p.m.)	$\Delta\nu_{1/2}$ (Hz)[a]	Ref.
$[Mo(CO)_5(CNCMe_2Ph)]$	$CDCl_3$	−1937	130	47
$[Mo(CO)_5(CNMe)]$	CH_2Cl_2	−1850	6	37
$[Mo(CO)_5(CN^tBu)]$	CH_2Cl_2	−1849 to −1850	7–10	37, 115
$[Mo(CO)_5(CN^iPr)]$	CH_2Cl_2	−1850	(10)	115
$[Mo(CO)_5(CNCy)]$	CH_2Cl_2	−1853	(10)	115
$[Mo(CO)_5(CN\text{-}2,6\text{-}Me_2\text{-}C_6H_3)]$	CH_2Cl_2	−1848	(10)	115
cis-$[Mo(CO)_4(CNMe)_2]$	CH_2Cl_2	−1829	4	37
cis-$[Mo(CO)_4(CN^tBu)_2]$	CH_2Cl_2	−1825	7–10	37,115
cis-$[Mo(CO)_4(CN^iPr)_2]$	CH_2Cl_2	−1825	(10)	114
cis-$[Mo(CO)_4(CNCy)_2]$	CH_2Cl_2	−1831	(10)	114
cis-$[Mo(Co)_4(CN\text{-}2,6\text{-}Me_2\text{-}C_6H_3)_2]$	CH_2Cl_2	−1825	(10)	114
$[Mo(CO)_4(norbornadiene)]$	$CDCl_2$	−1591	25	47
fac-$[Mo(CO)_3(CNMe)_3]$	CH_2Cl_2	−1786	4	37
fac-$[Mo(CO)_3(CN^nBu)_3]$	CH_2Cl_2	−1792	4	37
fac-$[Mo(CO)_3(CN^tBu)_3]$	CH_2Cl_2	−1782 to −1783	8–10	37, 115
fac-$[Mo(CO)_3(CN^iPr)_3]$	CH_2Cl_2	−1784	(10)	115
fac-$[Mo(CO)_3(CNCy)_3]$	CH_2Cl_2	−1793	(10)	115
fac-$[Mo(CO)_3(CN\text{-}2,6\text{-}Me_2\text{-}C_6H_3)_3]$	CH_2Cl_2	−1783 to −1786	2–10	37, 115
fac-$[Mo(CO)_3(CNPh)_3]$	CH_2Cl_2	−1772	[b]	37
$[(\eta^5\text{-}C_5H_5)Mo(CO)_3]$	$CHCl_3$	−1834	160	120, 121
$Na[(C_5H_5)Mo(CO)_3]$	CH_2Cl_2	−2123	20	118
$[(\eta^5\text{-}C_5H_5)Mo(CO)_3]HgCl$	$CHCl_3$	−1826	160	122
$[(\eta^5\text{-}C_5H_5)Mo(CO)_3]HgBr$	$CHCl_3$	−1815	180	122
$[(\eta^5\text{-}C_5H_5)Mo(CO)_3]HgI$	$CHCl_3$	−1795	120	122
$[(\eta^5\text{-}C_5H_4Me)Mo(CO)_3]$	$CHCl_3$	−1795	80	122
$[(\eta^5\text{-}C_5H_4Me)Mo(CO)_3]HgCl$	$CHCl_3$	−1793	50	122
$[(\eta^5\text{-}C_5H_4Me)Mo(CO)_3]HgBr$	$CHCl_3$	−1775	80	122
$[(\eta^5\text{-}C_5H_4Me)Mo(CO)_3]HgI$	$CHCl_3$	−1756	100	122
$[(\eta^5\text{-}C_5HMe_4)Mo(CO)_3]$	$CHCl_3$	−1666	140	122
$[(\eta^5\text{-}C_5HMe_4)Mo(CO)_3]HgCl$	$CHCl_3$	−1635	150	122
$[(\eta^5\text{-}C_5HMe_4)Mo(CO)_3]HgBr$	$CHCl_3$	−1615	130	122
$[(\eta^5\text{-}C_5HMe_4)Mo(CO)_3]HgI$	$CHCl_3$	−1600	100	122
$[(\eta^5\text{-}C_5Me_5)Mo(CO)_3]$	$CHCl_3$	−1631	140	122
$[(\eta^5\text{-}C_5Me_5)Mo(CO)_3]HgCl$	$CHCl_3$	−1567	80	122
$[(\eta^5\text{-}C_5Me_5)Mo(CO)_3]HgBr$	$CHCl_3$	−1551	160	122
$[(\eta^5\text{-}C_5Me_5)Mo(CO)_3]HgI$	$CHCl_3$	−1537	120	122
$[(\eta^5\text{-}C_5HPh_4)Mo(CO)_3]$	$CHCl_3$	−1547	150	122
$[(\eta^5\text{-}C_5HPh_4)Mo(CO)_3]HgCl$	$CHCl_3$	−1547	150	122
$[(\eta^5\text{-}C_5HPh_4)Mo(CO)_3]HgBr$	$CHCl_3$	−1536	270	122
$[(\eta^5\text{-}C_5HPh_4)Mo(CO)_3]HgI$	$CHCl_3$	−1539	150	122
$[(\eta^6\text{-}C_6H_6)Mo(CO)_3]$	CH_2Cl_2	−2095	[b]	119
$[(\eta^6\text{-}C_6H_5Me)Mo(CO)_3]$	CH_2Cl_2	−2034	<10	118
	$CDCl_3$	−2032	[b]	124
$[(\eta^6\text{-}o\text{-xylyl})Mo(CO)_3]$	CH_2Cl_2	−1988	<10	118
	$CDCl_3$	−1986	[b]	124
$[(\eta^6\text{-}p\text{-xylyl})Mo(CO)_3]$	CH_2Cl_2	−1979	10	118

Table 13.–*cont.*

Compound	Solvent	δ^{95}Mo (p.p.m.)	$\Delta\nu_{1/2}$ (Hz)[a]	Ref.
	$CDCl_3$	−1977	[b]	124
[η^6-*m*-xylyl)Mo(CO)$_3$]	CH_2Cl_2	−1971	10	118
	$CDCl_3$	−1967	[b]	124
[(η^6-*o*-mesityl)Mo(CO)$_3$]	CH_2Cl_2	−1907	10	118
	$CDCl_3$	−1903	[b]	124
[(η^6-C_6Me_6)Mo(CO)$_3$]	CH_2Cl_2	−1799	[b]	119
[(η^6-C_7H_8)Mo(CO)$_3$]	CH_2Cl_2	−1684	10	40, 118
	$CDCl_3$	−1675	20	47
cis-[Mo(CO)$_2$(CN^{n}Bu)$_4$]	CH_2Cl_2	−1731	4	37
cis-[Mo(CO)$_2$(CN^{t}Bu)$_4$]	CH_2Cl_2	−1714 to −1716	6–10	37, 115
cis-[Mo(CO)$_2$(CN^{i}Pr)$_4$]	CH_2Cl_2	−1726	(10)	115
cis-[Mo(CO)$_2$(CNCy)$_4$]	CH_2Cl_2	−1729	(10)	115
cis-[Mo(CO)$_2$(CN-2,6-Me_2-C_6H_3)$_4$]	CH_2Cl_2	−1711 to −1715	5–10	37, 115
cis-[Mo(CO)$_2$(CNPh)$_4$]	CH_2Cl_2	−1699	5	37
[(η^7-C_7H_7)Mo(CO)$_2$I]	$CDCl_3$	−1349	107	47
[(η^7-C_7H_7)Mo(CO)$_2$(dppe)][PF_6][c]	CD_2Cl_2	−1083	25	47
[Mo(CO)(CN-2,6-Me_2-C_6H_3)$_5$]	CH_2Cl_2	−1626	20	115
[Mo(CN-2,6-Me_2-C_6H_3)$_6$]	CH_2Cl_2	−1525	40	115
[Mo(η^5,-σ–$C_5H_4CMe_2$)(η^6-C_6H_6)]	C_6H_6/ Toluene	−1923	40	117
[Mo(η^5-σ–$C_5H_4CPh_2$)(η^6-C_6H_6)]	Toluene	−1922	300	117
[Mo(η^6-C_6H_6)$_2$]	Toluene	−1362	50	117
[Mo(η^6-C_6H_5Me)$_2$]	Toluene	−1270	55	117
[Mo(η^6-C_6H_6)(η^7-C_7H_7][PF_6]	CH_2Cl_2	−487	150	117
[Mo(η^5-C_7H_9)(η^7-C_7H_7)]	C_6H_6/ Toluene	−469	170	117
[Mo(η^6-C_6H_5Me)(η^7-C_7H_7)][PF_6]	CH_2Cl_2	−457	150	117
[Mo(η^6-C_7H_8)$_2$]	Toluene	+358	100	117

[a]Approximate values in brackets.
[b]Not reported.
[c]$^1J(^{95}Mo–^{31}P) = 160$ Hz.

shielded than those *trans* to other isocyanide carbons.[115] Given that CNR is deemed a better σ-donor but a poorer π-acceptor than CO, these observations lend credence to the idea of an active synergism in [$Mo(CO)_{6-n}(CNR)_n$]. Although there is no linear correlation between δ^{95}Mo and λ_{max}, an increase in n, from 1 to 6, corresponds to a colour change from white to orange-red. This suggests that deshielding corresponds with decreasing values for ΔE.[115]

Although the line widths observed for the isocyanide species are narrow

they are nonetheless about 10 times greater than theoretical values. A study of relaxation behaviour for $[Mo(CO)_{6-n}(CNR)_n]$ has indicated that the line widths observed are not due to coupling with the electric field gradient but to unresolved two-bond scalar coupling between ^{95}Mo and ^{14}N.[37] The magnitude for the unresolved coupling (on the order of less than 10 Hz) is thought to be inversely proportional to n.[37]

^{95}Mo NMR has been used to identify conformational isomers for the cyclopentadienyl molybdenum allyl complexes, $[CpMo(CO)_2(allyl)]$ and $[CpMo(NO)Y(allyl)]$ (Y = CO, I), which have chemical shifts in the range -790 to -1850 p.p.m.[116] It is concluded that the oxo isomer is invariably more shielded than the endo isomer. Green, Grieves and Mason[117] found that for sandwich complexes, shielding decreases with increase in ring size ($\eta^5 - C_5H_5 > \eta^6 - C_6H_5Me > \eta^6 - C_7H_8$) and in going from closed to open π-systems. They rationalized these observations with MO diagrams and related them to complex reactivity (i.e., increased deshielding corresponds to increased reactivity/decreased stability).

With the exception of $[Mo(CO)_4(norbornadiene)]$ and the isocyanide complexes, the compounds in Table 13 contain carbon ligands which occupy three coordination sites. The chemical shift observed for $Na[CpMo(CO)_3]$ is the most shielded value thus far reported for Mo(0) compounds. Generally, deshielding increases as electron-donating methyl groups are added successively to the arene ring, as the arene ring increases in size, and in going from closed to open π-systems. The overall shielding order is:

$$Cp^- > \eta^5\text{-}\sigma\text{-}C_5H_5CR_2\ (R = Me > Ph) > \eta^6\text{-}C_6H_6 > \eta^6\text{-}C_6H_5Me > \eta^6\text{-}o\text{-xylene} > \eta^6\text{-}p\text{-xylene} > \eta^6\text{-}m\text{-xylene} > \eta^6\text{-mesitylene} > \eta^6\text{-}C_6Me_6 > \eta^6\text{-}C_7H_8$$

Although the nature of the Mo–arene bond is still not fully understood, this order for shielding has been linked with increasing π-character in the bond and consequently, with increasing bond strength for both the piano-stool[118] and sandwich[119] compounds. In the early 1980s, Kubicki *et al.*[120,121] reported ^{95}Mo NMR data for a series of Mo–Hg complexes, $[Cp(CO)_2LMoHgX]$ (L = CO or $P(OMe)_3$; X = Cl, Br, I, S_2COEt, $S_2P(OEt)_2$ and $CpMo(CO)_3$), for which the chemical shifts ranged from -1706 to -1939 p.p.m. They have since extended their data set[122] by examining tricarbonyl species with substituted cyclopentadienyl ligands (see Table 13). The shielding observed follows the order:

$$C_5H_5 > C_5H_4Me > C_5HMe_4 > C_5Me_5 > C_5HPh_4$$

which indicates that substitution into the Cp ring leads to deshielding, in accordance with ^{95}Mo NMR spectra measured for other related species.[98,110,117,123,124] However, ESCA studies[125] indicate that substitution

of organo groups into the ring system should increase the electron density at Mo. Thus, the deshielding observed upon ring substitution might not be due to inductive effects but rather, to the paramagnetic contribution with a build-up of electron-density at the metal centre which is off-loaded via $d\pi$–$p\pi$ back-bonding.[122]

2.1.6. Oxygen donor ligands

Mo(0) exhibits very little chemistry with oxygen donor ligands; however, Beyerholm *et al.*[94] reported NMR data for a series of Mo clusters which are held together by bridging hydroxy groups (see Table 14). Other compounds with oxygen donors are discussed above (see Section 2.11).

2.1.7. Summary[9,10,38]

The known chemical shift range for Mo(0) compounds now spans 3625 p.p.m. from a most shielded value for Na[CpMo(CO)$_3$] (−2123 p.p.m.)[118] to a most deshielded value for [Mo(2-PAP)$_3$] (+1502 p.p.m.).[39] Thus, ^{95}Mo chemical shifts can be fairly selective for the study of structural and electronic variations within a series of closely related Mo(0) compounds. For a given ligand type, deshielding increases with n in Mo(CO)$_{6-n}$L$_n$ and subtle changes

Table 14. ^{95}Mo NMR data for Mo(0) compounds containing oxygen donor ligands.[a]

Compound	Solvent	δ^{95}Mo (p.p.m.)	$\Delta\nu_{1/2}$ (Hz)
$K_4[Mo_4(\mu_3\text{-}OH)_4(CO)_{12}].2H_2O$	H_2O	−870	90
	H_2O/EtOH	−867	250
	NH_3[b]	−889	140
	DMSO	−834	400
	DMF	−843	800
	DMF[c]	−857	*c.* 1000
$Cs_4[Mo_4(\mu_3\text{-}OH)_4(CO)_{12}].4H_2O$	H_2O	−870	90
	2M NaOH	−873	160
$(NEt_4)_4[Mo_4(\mu_3\text{-}OH)_4(CO)_{12}]$	H_2O	−869	100
	2M NaOH	−871	*c.* 60
	CH_3CN	−829	80
	DMF	−827	180
	DMSO	−828	230

[a]All data from ref. 94.
[b]Measured at 225 K.
[c]Measured at 273 K.

in the ligand steric and/or electronic parameters can also have significant effects upon the ^{95}Mo chemical shifts observed. The magnetochemical series for several different ligand types which take up one, two or three coordination sites at molybdenum are as follows:

$$H^- > CN^- > Sb(Ph)_3 > PF_3 > CO > CNR > P(OAlk)_3 > P(Alk)_3 > N_2 > P(OPh)_3 > P(Ph_2YR)\ (Y = O > NH > S) > As(Ph)_3 > P(Ar)_3 > I^- > S_2(P(OEt)_2) > NCY\ (Y = O > S > Se) > S_2CNR_2 > Br^- > PCl_3 \geq N_3^- \geq quin > NO_2^- > Cl^- > O_2CH^- > pyr > NCR > N{=}NR^+ > N\text{-}NR_2^{2-} > SeCN > OCH_3^- > NEt_3 > pip > S_2COEt > PBr_3 \geq py;$$

$$dpfe > diars > vpp > Ph_2P(CH_2)_nPPh_2\ (n > 2) > Ph_2PCH_2PR_2 > norbornadiene > O_2N^- > RSCH{=}CHSR > S_2CNR_2 > RSCH_2CH_2SR > S_2(P(OEt)_2) > S_2CN(CH_2)_4 > phen > bipy > \alpha\text{-diimine} > diazene > bptz;$$

$$Cp^- > \eta^5\text{-}\sigma\text{-}C_5H_5CR_2\ (R = Me > Ph) > \eta^6\text{-}C_6H_6 > \eta^6\text{-}C_6H_5Me > \eta^6\text{-}o\text{-xylene} > \eta^6\text{-}p\text{-xylene} > \eta^6\text{-}m\text{-xylene} > \eta^6\text{-mesitylene} > \eta^6\text{-}C_6Me_6 > triphos > \eta^6\text{-}C_7H_8 > [9]aneS_3 > dien.$$

In rationalizing these shielding orders, all three main terms in the Ramsey expression (see equation (2)) must be considered. Although the donor/acceptor properties and the steric requirements of a given ligand have significant effects, shielding of the molybdenum nucleus is usually promoted by high position in the optical spectrochemical series and by large nephelauxetic effects. For ligating atoms from the same row of the Periodic Table, shielding follows the ordering of the spectrochemical series and this effect is reinforced by the nephelauxetic effect (e.g., C > N > O). On descending in a column of the Periodic Table, however, there is a trade-off. The nephelauxetic effects tend to increase with increasing atom polarizability (increased shielding, e.g., Sb > As > P > N) while the ligand field splits tend to decrease in the same direction (decreased shielding). For the nitrogen family, however, the much more effective π-acceptor properties of the phosphorus ligands tend to make these ligands stronger bonders than their nitrogen counterparts. Generally, changes in ΔE correlate qualitatively with decreases in the amounts of Mo to ligand π-back donation so that good π-acceptor ligands enhance shielding by affecting all the terms in the Ramsey expression and the shielding orders observed agree with Horrocks' order for a π-bonding spectrochemical series.[126]

Temperature dependence is often observed for ^{95}Mo chemical shifts.[34,36,38,127] Typically, there is a deshielding with increase in temperature (*c.* 0.5 p.p.m. per degree) commonly ascribed to an increase in accessibility of ligand field excited states[15–17] so that a predominance of the energy term

in the Ramsey expression is indicated. Higher temperatures increase the LUMO-orbital populations thereby reducing ΔE[34,36,38] and/or cause Mo-ligating atom bond extensions.[127] Smaller temperature coefficients are observed for smaller more rigid molecules than for larger more flexible molecules.[127] Solvent effects are also indirectly related here. That is, increased solvent polarity enhances shielding and solvent dielectric constants normally decrease with increasing temperature.

Sterically demanding ligands enhance deshielding via the promotion of bond extensions and/or angular distortions which will increase the charge imbalance in the molecule. This, in turn, will lead to larger field gradients at the Mo nucleus and therefore, larger line widths. The line widths for *cis*- and fac-isomers are expected to be smaller than those for their *trans*- and mer-isomeric counterparts but often they are not owing to steric congestion in the coordination sphere. This leads to geometric distortions with consequential enhancement of the quadrupolar contribution to the line widths. In some cases, broadness may be partially attributable to unresolved scalar coupling to other quadrupolar nuclei (e.g., ^{14}N, ^{75}As, ^{121,123}Sb). Smaller ligands, lower solvent viscosities and higher sample temperatures all give rise to narrowing of the line widths. Point charge models have also been employed to explain the observed line widths for Mo(0) compounds[34] and T_1 measurements have been made for some complexes.[5,37]

Unfortunately, coupling to molybdenum is not very sensitive to subtle changes in the steric and electronic properties of coordinating ligands and does not correlate with corresponding chemical shifts. For the phosphorus ligands, however, $^1J(^{95}\text{Mo}–^{31}\text{P})$ values do increase as $P(Alk)_3 < P(Ar)_3 < P(Ph_2OC_6H_4\text{-}p\text{-}R) < P(OAlk)_3 < P(OPh)_3$ indicating that higher coupling may correspond to greater π-character in the Mo–P bonds. Nevertheless, this is not a general conclusion but a ligand-specific one as are some of the correlations observed for δ^{95}Mo. For example, for a series of closely related compounds for a given ligand type, increased shielding may imply bond strengthening (monodentate N-donors, PR_3) or bond weakening (dithioethers, arenes).

2.2. Other oxidation states for molybdenum

The treatment for Mo(0) above has been a detailed one relative to what follows below and there has been some overlap with previous reviews. The sections which follow for the oxidation states Mo(I) to Mo(VI) are meant to be supplementary to the very comprehensive treatment of Minelli *et al.*[5] The bulk of the new data presented here are for compounds of Mo(II) and Mo(VI). NMR investigations for the normally paramagnetic Mo(I) d^5, Mo(III) d^3 and Mo(V) d^1 metal centres have been somewhat restricted to diamagnetic spin-paired dimers and related extended species $(Mo_2)_n$. There

Table 15. ^{95}Mo NMR data for some Mo(I) species.

Compound	Solvent	δ^{95}Mo (p.p.m.)	$\Delta\nu_{1/2}$ (Hz)	Ref.
$(\eta^5\text{-}C_5H_5)_2Mo_2(CO)_6$	CH_2Cl_2	−1856	180	47. 123
$(\eta^5\text{-}C_5Me_5)_2Mo_2(CO)_6$	CH_2Cl_2	−1701	180	123
$(\eta^5\text{-}C_5H_5)_2Mo_2(CO)_4$	CH_2Cl_2	+182	160	123
$(\eta^5\text{-}C_5Me_5)_2Mo_2(CO)_4$	CH_2Cl_2	+133	150	123
$(\eta^5\text{-}C_5Me_5)_2Mo_2(CO)_3\{P(OMe)_3\}$	CH_2Cl_2	+373[a]	150	123
		+154	150	

[a]Doublet, $^1J(^{95}Mo\text{–}^{31}P) = 416$ Hz.

have been some quantitative reports in the Russian literature of magnetic susceptibility and spin-lattice relaxation rates for species such as Mo_3Y (Y = Si, Ge) and $SnMo_6Y_8$ (Y = S, Se) in both normal and superconducting states.[128–130]

2.2.1. *Mo(I)*

Prior to 1985 only one Mo(I) species, $Cp_2Mo_2(CO)_6$, had been observed by ^{95}Mo NMR.[47] Young *et al.*[123] extended this to include some related singly and triply Mo–Mo bonded dimers for which the ^{95}Mo chemical shift shows a huge sensitivity to Mo–Mo bond order (see Table 15). The triply bonded species are up to 1800 p.p.m. less shielded than their singly bonded counterparts. The $^1J(^{95}Mo\text{–}^{31}P)$ value of 416 Hz observed for $[Cp^*_2Mo_2(CO)_3\{P(OMe)_3\}]$ has the largest magnitude reported to date for an Mo–P coupling constant.

2.2.2. *Mo(II)*

A wide variety of organometallic, carbonyl, and isocyanide metal–metal bonded dimeric complexes of this oxidation state had been studied before 1985. The overall chemical shift range is the broadest for this particular oxidation state, spanning from the most shielded tricarbonyl species (−2100 p.p.m.) to the most deshielded quadruply bonded Mo(II)–Mo(II) dimer (+4150 p.p.m.).[5] Typically, the monomeric and dimeric species resonate at opposite ends of the chemical shift scale. Because many complexes had been observed by 1985, Table 16, which contains only one carbonyl and two cyclopentadienyl species, serves to supplement the large number of Mo(II) complexes discussed previously by Minelli *et al.*[5]

The more recent data include assignments made by Proust *et al.*[131,132] for mixed valence Mo(II)–Mo(VI) oxo nitrosyl complexes (see Tables 16 and 21). Young *et al.*[133] reported data for 17 mono-nitrosyl compounds of the type, $[Mo\{HB(Me_2pz)_3\}(NO)XY]$, for which they observed a very marked

Table 16. ^{95}Mo NMR data for some Mo(II) species.

Compound	Solvent	δ^{95}Mo (p.p.m.)	$\Delta\nu_{1/2}$ (Hz)	Ref.
$[Mo(\eta^6\text{-}C_6H_6)(\eta^5\text{-}C_5H_5)P(Me)_3](PF_6)$	Acetone	−2170	350	23
$[Mo(\eta^5\text{-}C_5H_5)_2CO]$	THF	−1964	150	23
$[Mo(\eta^6\text{-}C_6H_6)(^iPrCp)(MeCN](BF_4)$	Acetone	−1805	550	23
$[Mo(\eta^6\text{-}C_6H_6)(\eta^5\text{-}C_5H_5)Cl]$	Toluene	−1750	>600	23
$[Mo(CNCMe_3)_7](PF_6)_2$	Acetone	−960	35	134
$[Mo(CNC_6H_{11})_7](PF_6)_2$	Acetone	−970	70	134
$[Mo(CNCMe_3)_6Cl](PF_6)$	Acetone	−688	450	134
$[Mo(CNCMe_3)_6Br](PF_6)$	Acetone	−703	450	134
$[Mo(CNCMe_3)_6I](PF_6)$	Acetone	−795	500	134
$[Mo(CNCMe_3)_6(P^nBu_3)](PF_6)_2$	Acetone	−970	300	134
$[Mo(CNCMe_3)_6(py)](PF_6)_2$	Acetone	−508	600	134
$[Mo(CNCMe_3)_5(dppe)](PF_6)_2$	Acetone	−980	600	134
$[Mo(CNC_6H_{11})_5(dppe)](PF_6)_2$	Acetone	−1003	1100	134
$[Mo(CNCH_3)_5(bipy)](PF_6)_2$	Acetone	−19	130	134
$[Mo(CNCHMe_2)_5(bipy)](PF_6)_2$	Acetone	−64	120	134
$[Mo(CNCMe_3)_5(bipy)](PF_6)_2$	Acetone	−57	100	134
$[Mo(CNC_6H_{11})_5(bipy)](PF_6)_2$	Acetone	−68	200	134
$[Mo(CNCH_2Ph)_5(bipy)](PF_6)_2$	Acetone	−115	220	134
$[Mo(CNCMe_3)_5(Me_2bipy)](PF_6)_2$	Acetone	−86	140	134
$[Mo(CNCMe_3)_5(phen)](PF_6)_2$	Acetone	−78	130	134
$[Mo(CNC_6H_{11})_5(phen)](PF_6)_2$	Acetone	−98	260	134
$[\{Mo(CNCMe_3)_4(bipy)\}_2(\mu\text{-}CN)](PF_6)_3$	Acetone	+69	360	134
		−61	220	
$[\{Mo(CNCMe_3)_4(Me_2bipy)\}_2(\mu\text{-}CN)](PF_6)_3$	Acetone	+46	320	134
		−92	200	
$[\{Mo(CNCMe_3)_4(phen)\}_2(\mu\text{-}CN)](PF_6)_3$	CH_3CN	+55	200	134
		−85	100	
	Acetone	+50	400	134
		−79	170	
$[Mo\{HB(Me_2pz)_3\}(NO)I_2]$	CH_2Cl_2	+2272	1800	133
$[Mo\{HB(Me_2pz)_3\}(NO)Cl_2]$	CH_2Cl_2	+1811	1400	133
$[Mo\{HB\{Me_2pz)_3\}(NO)F_2]$	CH_2Cl_2	+1274	1490	133
$[Mo\{HB(Me_2pz)_3\}(NO)(SPh)_2]$	CH_2Cl_2	+990	1560	133
$[Mo\{HB(Me_2pz)_3\}(NO)(OPh)_2]$	CH_2Cl_2	+624	1600	133
$[Mo\{HB(Me_2pz)_3\}(NO)(OEt)_2]$	CH_2Cl_2	+464	800	133
$[Mo\{HB(Me_2pz)_3\}(NO)(NHPh)_2]$	CH_2Cl_2	+161	600	133
$[Mo\{HB(Me_2pz)_3\}(NO)Cl(SPh)]$	CH_2Cl_2	+1200	2340	133
$[Mo\{HB(Me_2pz)_3\}(NO)Cl(OPh)]$	CH_2Cl_2	+1050	1750	133
$[Mo\{HB(Me_2pz)_3\}(NO)Cl(OEt)]$	CH_2Cl_2	+910	1450	133
$[Mo\{HB(Me_2pz)_3\}(NO)Cl(NHC_6H_4\text{-}p\text{-}Br)]$	CH_2Cl_2	+539	1500	133
$[Mo\{HB(Me_2pz)_3\}(NO)Cl(NHC_6H_4\text{-}p\text{-}Me)]$	CH_2Cl_2	+523	1700	133
$[Mo\{HB(Me_2pz)_3\}(NO)Cl(NHEt)]$	CH_2Cl_2	+404	1000	133
$[Mo\{HB(Me_2pz)_3\}(NO)I(OPh)]$	CH_2Cl_2	+1179	1600	133
$[Mo\{HB(Me_2pz)_3\}(NO)I(NHC_6H_4\text{-}p\text{-}Me)]$	CH_2Cl_2	+568	1350	133
$[Mo\{HB(Me_2pz)_3\}(NO)I(NHEt)]$	CH_2Cl_2	+430	1200	133
$[Mo\{HB(Me_2pz)_3\}(NO)I(NHNMe_2)]$	CH_2Cl_2	+284	900	133
$[Mo(\eta^5\text{-}C_5H_5)(NO)(SPh)_2]$	$CDCl_3$	+144	580	133
$[\{Mo(\eta^5\text{-}C_5H_5)(NO)I_2\}_2]$	DMF	−26	750	133
$[Mo_2I_4(PMe_3)_4]$	Toluene	+2927	850	23
$[Mo_2Br_4(PMe_3)_4]$	Toluene	+2927	850	23

Table 16.–*cont.*

Compound	Solvent	δ^{95}Mo (p.p.m.)	$\Delta\nu_{1/2}$ (Hz)	Ref.
	Toluene	+3008	840	23
	THF	+2996	800	23
$[Mo_2Cl_4(PMe_3)_4]$	Toluene	+3008	800	23
	THF	+3021	800	23
$[Mo_2(O_2CMe)_4]$	THF	+3702[c]	520	135
	DMF	+3768[a]	670	135
$[Mo_2(O_2CCHCl_2)_4]$	DMF	+4006[a]	1070	135
$[Mo_2(O_2C^nBu)_4]$	THF	+3661[c]	1440	135
	DMF	+3746[a]	1390	135
$[Mo_2(O_2C^tBu)_4]$	THF	+3667	870	23
	THF	+3656[c]	1040	135
	DMF	+3696[a]	1130	135
$[Mo_2(O_2C^nPr)_4]$	DMF	+3730[a]	1400	23, 136
	THF	+3682[c]	1320	135
$[Mo_2(O_2C^iPr)_4]$	DMF	+3719[a]	1200	135
	THF	+3670[c]	950	135
$[Mo_2(O_2CH)_4]$	HCO_2H	+3768	670	23
$[Mo_2(O_2CCF_3)_4]$	$CDCl_3$	+3874	430	23
	THF	+4021	400	23, 135
	THF	+4026[b]	250	23, 130
	DMF	+4144	640	135
	DMF	+4148[a]	280	135
	CH_3CN	+4029	320	135
	CH_3CN	+4025[c]	220	135
$[Mo_2(O_2CCF_3)_4(py)_2]$	CH_2Cl_2	+4199	320	23
	py	+419	320	23
$[Mo_2]^{4+}$ (aq)	CF_3SO_3H[e]	+4056	430	135
$K_4[Mo_2(SO_4)_4 \cdot 2H_2O$	CF_3SO_3H[e]	+4090	990	135
$K_4[Mo_2Cl_8]$	1MHCl	+3816	1440	135
$Cs_4[Mo_2Br_8]$	DMF	+3227	510	135
$[MoO_{18}(WO)]^{2-c}$	CH_3CN	+65.2	[d]	131, 132
$[Mo_5O_{18}\{(W(NO)\}]^{3-c}$	CH_3CN	+614	90	131, 132
$[Mo_6O_{18}(NO)]^{3-c}$	CH_3CN	+878	600	131, 132
$[Mo_6O_{17}(OCH_3)(NO)]^{2-c}$	CH_3CN	+1107	600	131, 132
$[Mo_5O_{13}(OCH_3)_4(NO)]^{3-c}$	CH_3CN	+758	1800	131, 132

[a]Spectrum measured at 343 K.
[b]Spectrum measured at 328 K.
[c]Mixed valence species measured at 333 K, see Table 21 for Mo(VI) assignments.
[d]Not reported.
[e]1 M concentration at about 313 K.

inverse halogen dependence (see Table 16) and opposite shielding trends for the ^{95}Mo and ^{14}N (NO^+) nuclei. The apparent shielding order from shift data for $[Mo\{HB(Me_2pz)_3\}(NO)XY]$ is:

$$NHNMe_2 > NHEt > NHPh > NHC_6H_4\text{-p-Me} > NHC_6H_4\text{-}p\text{-Br} > OEt > OPh > SPh > F > Cl > I.$$

Table 17. ^{95}Mo NMR data for some Mo(III) species.

Compound	Solvent	δ^{95}Mo (p.p.m.)	$\Delta\nu_{1/2}$ (Hz)	Ref.
$Mo_2(CH_2CMe_3)_6$	Toluene	+3695	530	137
$Mo_2(CH_2SiMe_3)_6$	Toluene	+3624	530	123
$Mo_2(OCMe_3)_6$	Toluene	+2645	120	123
$Mo_2(OCH_2CMe_3)_6$	Toluene	+2447	600	123
$Mo_2(OCHMe_2)_6$	Toluene	+2444	350	123
$Mo_2(NMe_2)_6$	Toluene	+2430	1320	123
	Hexane	+2420	630	123
$Mo_2(OCHMe_2)_6(dmpe)$	Toluene	+2880	850	137
$Mo_2(OCHMe_2)_6(py)$	Toluene	+2725	1000	137
$Mo_2(OCHMe_2)_6(Me_2en)$	Toluene	+2720	950	137
$Mo_2(O_2CMe)_4(CH_2CMe_3)_2$	Toluene	+2040	1460	137
$(\eta^5\text{-}C_5H_5)_2Mo_2\{\mu\text{-}S_2C_2(CF_3)_2\}_2$	CH_2Cl_2	+2301	37	123
$(\eta^5\text{-}C_5H_5)_2Mo_2(CO)_2\{\mu\text{-}S_2C_2(CF_3)_2\}_2$	CH_2Cl_2	−789	190	123

Mason and Grieves[23] reported measurements for both mononuclear and dinuclear Mo(II) compounds. The chemical shifts for $[Mo_2X_4(PMe_3)_4]$ (X = Cl, Br, I) show a normal halogen dependence and, for all the dinuclear species, shielding increases with the Mo–Mo bond order as quadruple < triple < double < single bond, which they note is opposite to the sequence for ^{13}C NMR.

2.2.3. Mo(III)

Prior to 1985, Mo(III) complexes had not been studied by ^{95}Mo NMR but Enemark and coworkers[123,137] have since reported data for several triply bonded dinuclear Mo(III) species (see Table 17). The general shielding trends follow the orders:

$$NR_2 > 1°, 2°\ OR > 3°\ OR > RSi > R \text{ and } R_2en > py > dmpe$$

$$[Mo \equiv Mo]^{4+}\ (\sigma^2\pi^2\delta^2) < [Mo \equiv Mo]^{6+}\ (\sigma^2\pi^4) < [Mo \equiv Mo]^{6+}$$
$$(\pi^4\delta^2) \leq [Mo \equiv C]^{3+} < [M \equiv N]^{3+}$$

2.2.4. Mo(IV)

The data in Table 18 greatly augment those data which were available prior to 1985. They span a quite large chemical shift range of almost 5700 p.p.m. Prior to 1985 the total chemical shift range for this oxidation state was about

Table 18. ^{95}Mo NMR data for some Mo(IV) species.

Compound	Solvent	δ^{95}Mo (p.p.m.)	$\Delta\nu_{1/2}$ (Hz)	Ref.
$[MoH_4(dppe)_2]$	CH_2Cl_2	−1865	[a]	38[b]
$[MoH_2(\eta^5\text{-}C_5H_5)_2]$	Toluene	−2507	300	23
$[MoO(S_2CNEt_2)_2]$	CH_2Cl_2	+2400	2700	139[b]
$[MoO(S_2CN^nPr_2)_2]$	CH_2Cl_2	+2400	3900	139
$[MoO(S_2CN^nBu_2)_2]$	CH_2Cl_2	+2450	>5000	139
$[MoO(S_2P(OEt)_2)_2]$	CH_2Cl_2	+2230	5170	139
$K_2[MoO(SCH_2CH_2S)_2.2KOH$	H_2O	+1680	1450	139
$(PPh_4)[MoO(mnt)_2]$[c]	CH_2Cl_2	+1400	1220	139
$K_4[MoO(CN)_4]\cdot 6H_2O$	KOH(aq)	+1220	240	139
$K_4[MoO(OH)(CN)_4]$	H_2O[d]	+1444	240	139
$[MoO(S_2CNEt_2)_2(P(Me)_3)]$	CH_2Cl_2	+2300	1360	139
$[MoO(S_2CNEt_2)_2(P(Et)_3)]$	CH_2Cl_2	+2370	1800	139
$[MoO(S_2CNEt_2)_2(P(^nBu)_3)]$	CH_2Cl_2	+2400	2820	139
$[MoO(S_2CN^nPr_2)_2(P(Me)_3)]$	CH_2Cl_2	+2290	2120	139
$[MoO(S_2CN^nPr_2)_2(P(Et)_3)]$	CH_2Cl_2	+2340	2580	139
$[MoO(S_2CN^nPr_2)_2(P(^nBu)_3)]$	CH_2Cl_2	+2390	>5000	139
$[MoO(S_2CN^nBu_2)_2(P(Me)_3)]$	CH_2Cl_2	+2270	3160	139
$[MoO(S_2CN^nBu_2)_2(P(Et)_3)]$	CH_2Cl_2	+2330	3800	139
$[MoO(S_2P(OEt)_2)_2(P(Me)_3]$	CH_2Cl_2	+1610	1650	139
$[MoOCl_2(P(Me)_3]$	CH_2Cl_2	+1890	820	139
$[MoO(NCS)_2(P(Me)_3)_3]$	CH_2Cl_2	+1590	680	139
$[MoO(NCO)_2(P(Me)_3)_3]$	CH_2Cl_2	+1590	820	139
$[MoOCl_2(PMe_2Ph)_3]$[e]	CH_2Cl_2	+2020	1120	139
$[MoOBr_2(PMe_2Ph)_3]$	CH_2Cl_2	+2050	1100	139
$[MoOI_2(PMe_2Ph)_3]$	CH_2Cl_2	+2050	1100	139
$[MoO(NCS)_2(PMe_2Ph)_3]$	CH_2Cl_2	+1690	845	139
$[MoO(NCO)_2(PMe_2Ph)_3]$	CH_2Cl_2	+1690	890	139
$[MoOCl_2(PPh_2Me)_3]$	CH_2Cl_2	+2180	1210	139
$[MoOCl_2(PEt_2Ph)_3]$	CH_2Cl_2	+2200	1200	139
$[MoOCl_2(bipy)(PPh_2Me)_3]$	CH_2Cl_2	+3160	800	139
$[MoOCl_2(phen)(PPh_2Me)_3]$	CH_2Cl_2	+3180	800	139
$[MoOCl_2(ox)(PPh_2Me)_3]$	CH_2Cl_2	+2520	570	139
$[MoOCl(dppe)_2][BPh_4]$	CH_2Cl_2	+1260	1780	139
$[MoOCl(CNMe)_4]][BPh_4]$[f]	$MeNO_2$	+1035	330	139
$[MoOBr(CNMe)_4][BPh_4]$[f]	$MeNO_2$	+1050	530	139
$[(HB(Me_2pz)_3MoO(S_2CNMe_2)]$	CH_2Cl_2	+3000	2400	139
$[(HB(Me_2pz)_3MoO(S_2CNEt_2)]$	CH_2Cl_2	+3000	2400	139
$[(HB(Me_2pz)_3)MoO(S_2CN^nPr_2)]$	CH_2Cl_2	+3000	1850	139
$[(HB(Me_2pz)_3)MoO(S_2P(OEt)_2)]$	CH_2Cl_2	+2950	1750	139
$(\eta^5\text{-}C_5Me_5)_2Mo_2(\mu\text{-}S)_2(\mu\text{-}S_2)$	CH_2Cl_2	+440	110	123
$(\eta^5\text{-}C_5Me_5)_2Mo_2(\mu\text{-}S)_2(\mu\text{-}Se_2)$	CH_2Cl_2	+770	110	123
$(\eta^5\text{-}C_5Me_5)_2Mo_2(\mu\text{-}S)_2(\mu\text{-}SH)_2$	CH_2Cl_2	+714	40	123
		+728	50	
$(\eta^5\text{-}C_5Me_5)_2Mo_2(\mu\text{-}S)_2(\mu\text{-}SMe)_2$	CH_2Cl_2	+790	70	123
$[\eta^5\text{-}C_5Me_5)_2Mo_2(\mu\text{-}S)(\mu\text{-}SMe)(\mu\text{-}S_2)]I$	CH_2Cl_2	+382	110	123
$(\eta^5\text{-}C_5Me_5)_2Mo_2S_2(\mu\text{-}S_2)$	CH_2Cl_2	+756	20	123
$(\eta^5\text{-}C_5Me_5)_2Mo_2OS(\mu\text{-}S_2)$	CH_2Cl_2	−54	100	123
		+699	100	
$[Mo_3(\mu_3\text{-}O)(\mu\text{-}O)_3(OH_2)_9]^{4+}$	H_2O	+996	[a]	75
$[Mo_2W(\mu_3\text{-}O)(\mu\text{-}O)_3(OH_2)_9]^{4+}$	H_2O	+1189	[a]	75

[a] Not reported.
[b] $J(^{95}Mo\text{-}^{31}P)$ not reported.
[c] mnt = *cis*-1,2-dicyanoethenedithiolate.
[d] pH 12.5.
[e] Two isomers, blue and green, have the same chemical shift.
[f] Spectra measured at 343 K.

half as large, 2800 p.p.m., and based on observations for only seven compounds. The large extension into the shielded region is due to observation of two hydride species (see Table 18). It is interesting to compare the progression to more deshielded positions for the series, $K_4[Mo(CN)_8]$ (−1309 p.p.m.)[138] < $K_4[MoO(CN)_4]$ (+1220 p.p.m.) < $K_4[MoO(OH)(CN)_4]$ (+1444 p.p.m.) < $K_4[MoO_2(CN)_4]$ (+1452 p.p.m.).[5] Also, comparison of the chemical shifts for the last two entries in Table 18 shows, once again, that substitution of W for Mo leads to a significant deshielding of the latter (see Sections 2.1.1 and 3.2).

Examination of the species having the $[MoO]^{2+}$ core suggests the shielding orders:

$$CN^- > mnt > NCO^-,\ NCS^- > SCH_2CH_2S > S_2P(OEt)_2 > Cl^- > Br^- \geq I^- > S_2CN^nBu_2 \geq S_2CN^nPr_2 > S_2CNEt_2;$$

$$PR_3 > PR_2Ph > PRPh_2 > ox > bipy > phen$$

which shows an inverse halogen dependence. Addition of a phosphorus donor invariably leads to deshielding and the shielding order for the phosphorus donors appears to be:

$$PMe_3 > PMe_2Ph > PMePh_2 > PEt_3 > PEt_2Ph > P^nBu_3.$$

2.2.5. Mo(V)

Attempts[140] to observe the bimetallic Mo(V) imido species, $[(dtc)MoO(\mu\text{-}NC_6H_4S)]_2$, failed despite the fact that dioxo-bridged Mo(V) dimers had been observed previously.[5,141] This failure has been ascribed to very low solubilities and very fast relaxation times. However, Young *et al.*[123] have observed some spectra for singly bonded Mo–Mo dimers of the type, $[Cp^*Mo_2Y_2)(\mu\text{-}X)_2]$, that show the substitution of bridging versus terminal atoms can be readily distinguished (see Table 19). The shielding order for the bridging moieties observed for both Mo(IV) and Mo(V) species is as follows:

$$\mu - S_2^{2-} < \mu - SH < \mu - SMe < \mu - S < \mu - Se < \mu_3 - O < \mu_3 - S.$$

The chemical shifts observed for the Mo(V) species (−93 to +478 p.p.m.) extend the range previously known for syn- and anti-$[Mo_2O_2(\mu\text{-}X)_2]^{2+}$ (X = O, S) and the related syn- and anti-$[Mo_2O_2([9]aneN_3)_2]^{2+}$ compounds (+320 to +982 p.p.m.).[5,95] The two signals observed at ambient temperatures for syn-$[([12]aneN_3)Mo_2O_2(\mu\text{-}O)_2][ClO_4]$ coalesce at higher temperatures suggesting the coexistence of conformational isomers at ordinary

Table 19. ^{95}Mo NMR data for some Mo(V) species.

Compound	Solvent	δ^{95}Mo (p.p.m.)	$\Delta\nu_{1/2}$ (Hz)	Ref.
$(\eta^5\text{-}C_5Me_5)_2Mo_2O_2(\mu\text{-}S)_2$	CH_2Cl_2	−93	90	123
$(\eta^5\text{-}C_5Me_5)_2Mo_2S_2(\mu\text{-}S)_2$	CH_2Cl_2	+478	260	123
$(\eta^5\text{-}C_5Me_5)_2Mo_2O_2(\mu\text{-}Se)_2$	CH_2Cl_2	+131	90	123
anti-$[([12]aneN_3)_2Mo_2O_2(\mu\text{-}O)_2](PF_6)_2$	CH_3CN	+320	680	95
anti-$[([9]aneN_3)_2Mo_2O_2(\mu\text{-}O)_2]I_2$	H_2O	+342	250	95
syn-$[([12]aneN_3)_2Mo_2O_2(\mu\text{-}O)_2](ClO_4)_2$	H_2O	+548 +527	700	95
	CH_3CN	+547 +521	700	95
	CH_3CN[a]	+575	650	95
syn-$[([9]aneN_3)_2Mo_2O_2(\mu\text{-}O)_2]I_2$	H_2O	+586	250	95

[a]Spectrum measured at 353 K.

temperatures.[95] Other sulphur-bridging species observed include some homo- and heterometallic (Fe) cubane-like compounds which usually show magnetic nonequivalencies for the molybdenum atoms present.[123] The chemical shifts for the latter species appear in the −133 to −1619 p.p.m. region.

2.2.6. *Mo(VI)*

Unlike Mo(0), chemical shifts for Mo(VI) species can be very dependent upon measurement conditions. For example, ^{95}Mo NMR chemical shifts are usually reported relative to an external reference of aqueous alkaline (pH 11) 2M $[MoO_4]^{2-}$ set to 0.0 p.p.m. However, the chemical shift for molybdate is both solvent and pH dependent (see Table 20), as well as counter-cation/concentration dependent.[5,44,142] There is up to a 1000 p.p.m. variation in the solvent dependence of the chemical shift for $[MoS_4]^{2-}$,[143] but in general the polyoxomolybdates show only a narrow shift range.[144] The latter also appears to be true for mixed metal polyanions.[145]

In aqueous and acidic media, the ^{95}Mo NMR indicates the existence of $[Mo_2O_5(H_2O)_6]^{2+}$ (−63 p.p.m.) and $[MoO_2X_2(H_2O)_2]$ (X = Cl (+157 p.p.m.), Br (+217 p.p.m.), Cl/Br (+187 p.p.m.).[146] In any case, Mo(VI) is very stable in water which suggests very good potential for biological applications for ^{95}Mo NMR. Molybdate reacts with sugars and polyhydroxy organics[147,148] and dinuclear complexes of aditols in water show chemical shifts in the region, +21 to −34 p.p.m. ($\Delta\nu_{1/2}$ = 270–730 Hz).[147–149] Ramos *et al.*[150] have measured the spectra for Mo(VI) coordination complexes of D-galactaric (+32 to +107 p.p.m., $\Delta\nu_{1/2}$ = 218–878 Hz) and D-mamaric acids (+23 to +99 p.p.m., $\Delta\nu_{1/2}$ = 736–1627 Hz). For the latter

Table 20. Some ^{95}Mo NMR data for molybdate, Y_2MoO_4.[a]

Y	pH	Solvent	δ^{95}Mo (p.p.m.)	$\Delta\nu_{1/2}$ (Hz)
Na	11	H_2O	0.00	<1
K	11	H_2O	0.00	<1
Na	7	H_2O	−0.81	1
Na	7	Propylene Glycol	−11.71	36
Na	7	Propylene Glycol/H_2O[b]	−8.30	10
Na	9	Propylene Glycol	−10.33	33

[a]Reference 77.
[b]50% Vol/vol.

species, the number of signals observed indicates two different possible binuclear dimolybdate species with symmetrical (one signal) and asymmetrical (two signals) structures.

Interestingly, for Mo–Cu–S compounds of bidentate dialkyldithiocarbamate ligands only single-line spectra are observed (see Table 21) despite the solid-state evidence which suggests that the two molybdenum centres should be magnetically nonequivalent.[151] The broadness of the shielded lines observed, relative to the chemical shift and line width for $[MoS_4]^{2-}$, is most likely due to the presence of the rapidly relaxing quadrupolar copper.[152] Some earlier data for related thiomolybdate clusters[152–154] also show shielded single line spectra (δ^{95}Mo = +474 to +1921 p.p.m., $\Delta\nu_{1/2}$ = 15–1400 Hz).

^{95}Mo NMR has been gainfully employed in observing Mo(VI) complexes formed during the catalytic epoxidation of cyclohexene with organic hydroperoxides.[155] Similarly, data are reported for peroxomolybdic intermediates formed during the catalytic disproportionation of hydrogen peroxide by molybdate ions.[156,157] Assignments from the latter studies are not entirely clear as peak positions for species such as $[Mo(O_2)_4]^{2-}$, $[MoO(O_2)_3]^{2-}$, $[MoO(O_2)_3(H_2O)]^{2-}$ and $[Mo_2O_3(O_2)_4(H_2O)]^{2-}$ (−110 to −496 p.p.m., $\Delta\nu_{1/2}$ = 190–500 Hz) are very pH and peroxide concentration dependent. Talsi *et al.*[158] have used ^{95}Mo NMR to investigate the mechanism of alkene epoxidation with hydrogen peroxide in the presence of Mo(VI) species.

Unouva *et al.*[159] very recently reported correlations between the ^{95}Mo chemical shifts and the rate constants for oxygen atom transfer reactions for some $[MoO_2(R_2dtc)_2]$ species for R = Me, Et, ^{i}Pr, ^{t}Bu, Ph and Bz. The chemical shifts range from + 151 p.p.m. (Me) to +216 p.p.m. (^{i}Pr). For the

Table 21. ^{95}Mo NMR data for some Mo(VI) species.

Compound	Solvent	δ^{95}Mo (p.p.m.)	$\Delta\nu_{1/2}$ (Hz)	Ref.
$[Mo(\eta^5\text{-}C_5H_5)_2H_3]Cl$	HCl (aq)	−2953	300	23
$[Mo(NC_6H_4S)(OCH_3)(dtc)_2]$	CH_2Cl_2	+200	2100	140
$[Mo(NC_6H_4S)F(dtc)_2]$	CH_2Cl_2	−335	2100	140
$[Mo(NC_6H_4S)Cl(dtc)_2]$	CH_2Cl_2	+292	300	169
$[MoO(O_2)_2(ox)]^{2-}$	H_2O	−228.3	Sharp	170
$[MoO(O_2)_2(ox)(H_2O)]^{2-}$	H_2O	−229.7	Sharp	170
		+4.4		
$[MoO(O_2)_2(cit)]^{2-}$ [a]	H_2O	−247	Broad	170
$[Mo_2O_2(O_2)_4(tart)]^{4-}$ [a]	H_2O	−235.0	Sharp	170
$[MoO(O_2)_2(mal)]^{2-}$ [a]	H_2O	−233.0	Sharp	170
$[MoO(O_2)_2(tron)]^{2-}$ [a]	H_2O	−227.7	Sharp	170
$[MoO(O_2)_2(glyc)]^{2-}$ [a]	H_2O	−220.6	Sharp	170
$[MoO(O_2)_2(quin)]^{2-}$ [a]	H_2O	−245.0	Sharp	170
$[MoO(O_2)_2(tart)]^{2-}$ [a]	H_2O	−252.0	Sharp	170
		−231.7		
$[MoO_3(ox)]^{2-}$	H_2O	+5.1	Sharp	170
$[([9]aneN_3MO_3)_4Co_{11}](ClO_4)_2$	D_2O	+86	280	171
$[Me_3[9]aneN_3MO_3)_4Co_{11}(ClO_4)_2$	D_2O	+98	267	171
$[MoO_3)_2(edta)]^{4-}$	D_2O	+63	290	172
$[MoO_3(ida)]^{2-}$	D_2O	+66	130	172
$[MoO_3(nta)]^{3-}$	D_2O	+67	160	172
$[Mo(CSiMe_3)(CH_2SiMe_3)_3]$	Toluene	+1845	16	137
$[Mo(CCMe_3)(CH_2CMe_3)_3]$	Toluene	+1400	16	137
$[NEt_4]_2[Mo_2Cu_5S_8(Me_2NCS_2)_3]$	DMF	+995	800	151
$[NEt_4]_2[Mo_2Cu_5S_6O_2(Me_2NCS_2)_3]$	DMF	+830	600	151
$[PPh_4]_2[Mo_2Cu_5S_6O_2(Et_2NCS_2)_3]$	DMF	+830	600	151
$[NEt_4]_2[MoCu_3S_4(Et_2NCS_2)_3]$	DMF	+1296	800	151
$MoO(NO_2cat)(ONMe_2)_2$	CH_3CN	−55	200	160
$MoO(cat)(ONMe_2)_2$	CH_3CN	−20	320	160
$MoO(CH_3cat)(ONMe_2)_2$	CH_3CN	−4	130	160
$MoO(DTBcat)(ONMe_2)_2$ [b]	CH_3CN	+5	170	160
$MoO(NO_2cat)(ONEt_2)_2$	CH_3CN	−36	320	160
$MoO(cat)(ONEt_2)_2$	CH_3CN	0	290	160
$MoO(CH_3cat)(ONEt_2)_2$	CH_3CN	+12	310	160
$MoO(DTBcat)(ONEt_2)_2$	CH_3CN	+19	410	160
$[Mo_2O_7]^{2-}$	CD_2Cl_2	−5.8	10	160
$[Mo_6O_{19}]^{2-}$	DMF-d_7	+126	70	160
[c]	CH_3CN	+124	[f]	131
$[Mo_7O_{24}]^{6-}$	D_2O [d]	+210	550	145
		+33	300	
	D_2O [e]	+200	550	145
		+28	300	
$[Mo_8O_{26}]^{4-}$	CD_3CN	+24.2	41	144
		−4.2	463	
$[V_9MoO_{28}]^{5-}$	D_2O	+115	300	145
$[V_2Mo_4O_{19}]^{4-}$	D_2O	+130	200	145
$[V_2Mo_4O_{19}H]^{3-}$	D_2O	+126	[f]	145
	H_2O	+124	[f]	165[g]
$[V_5Mo_4O_{27}]^{5-}$	H_2O	0 to +50	[f]	165[h]

Table 21.–*cont.*

Compound	Solvent	δ^{95}Mo (p.p.m.)	$\Delta\nu_{1/2}$ (Hz)	Ref.
$[V_5Mo_4O_{27}H]^{4-}$	H_2O	0 to +50	*f*	165*h*
$[VMo_5O_{19}]^{3-}$	H_2O	+128	*f*	165
$[MoW(O)_2(\mu\text{-}O)_2(\mu\text{-edta})]^{2-}$	D_2O	+877	*f*	173
$[Mo_2(O)_2(\mu\text{-}O)_2(\mu\text{-edta})]^{2-}$	D_2O	+612	*f*	173
$[Mo_4O_{10}(OMe)_2(N_2Ph)_2]^{2-}$	CD_2Cl_2/	+26.3	300	144
	CH_3OH	−17.5	100	
$[Mo_4O_8(OMe)_2(N_4Ph)_4]^{2-}$	CD_2Cl_2	+35.1	100	144
$[Mo_4O_{10}(OMe)_2(N_2MePh)_2]^{2-}$	CD_2Cl_2/	+25.0	300	144
	CH_3OH	−16.0	100	
$[Mo_4O_{12}(hydralazine)]^{2-}$	CD_2Cl_2	+25.0	200	144
		−16.0	100	
$[Mo_8O_{16}(OMe)_6(N_2MePh)_6]^{2-}$	CD_2Cl_2/	+60.0	700	144
	CH_3OH			
$[Mo_6O_{18}(N_2Ph)]^{3-}$	CD_3CN	−57.9	100	144
		−23.9	500	144
$[Mo_8O_{20}(N_2Ph)_6]^{3-}$	CD_2Cl_2	−58.9	100	144
		−27.5	500	144
$[Mo_6O_{18}(NO)]^{3-}$ *c*	CH_3CN	+212	250	131
		+146	350	
$[Mo_6O_{17}(OCH_3)(NO)]^{2-}$ *c*	CH_3CN	+203	135	131
		+191	325	
		+182	140	
		+134	250	
$[Mo_5O_{13}(OCH_3)_4(NO)]^{3-}$ *c*	CH_3CN	+61	425	131
$[Mo_5O_{18}\{W(NO)\}]^{3-}$ *c*	CH_3CN	+228	180	131
		+150	230	

*a*cit = citrate, tart = tartrate, mal = malate, tron = tartronate, glyc = glycolate, quin = quinate.
*b*DTB = 3,5-ditertbutyl derivative.
*c*Mixed valence species measured at 323 K, see Table 16 for Mo(II) assignments.
*d*pH 6.
*e*pH 4.1.
*f*Not reported.
*g*The spectrum is slightly pH dependent.
*h*Unclear spectra with overlapping peaks, see text.

seven coordinate species, $MoO(cat)(ONR_2)_2$ (R = Me, Et, Bz) the chemical shift correlates linearly with the wavelength for the LMCT,[160] in accordance with the shielding theory as described above. There is also a rare comparison made to electrochemical data which shows a direct relationship between chemical shift and Mo-centred reduction potentials. For the aryldiazenido and organohydrazido molybdates the narrow shift range (< 100 p.p.m.)[144] makes it difficult to correlate chemical shift with chemical structure. Some

variable temperature studies and T_1 measurements are also reported in that work.[144]

In the case of $Mo_2O_5L_2$ ($L = Me_2NCH_2CH_2NHCH_2CH_2S^-$ or $Me_2NCH_2CH_2CMe_2S^-$) in DMF, δ^{95}Mo values can be used to easily distinguish between ligand bonding through the N (+125 p.p.m.) and S (+330 p.p.m.) donor atoms.[161] Several more species containing the $[Mo_2O_5]^{2+}$ core have been characterized by ^{95}Mo NMR.[162–164] In the case of molybdovanadate complexes,[165] however, the ^{95}Mo data are structurally inconclusive despite quite informative O-17 and V-51 NMR data for the same species. This is very unlike the case for the analogous tungsten species[166] wherein the ^{183}W NMR data are very clear.

Finally, ^{95}Mo NMR has been applied to the study of molybdate absorption on alumina[167,168] and silica[168] where it has proved to be a very sensitive *in situ* probe for the adsorption of $[MoO_4]^{2-}$, $[Mo_7O_{24}]^{6-}$, $[MoO_{26}]^{4-}$ and $[SiMo_{12}O_{40}]^{4-}$ species during interaction of heptamolybdate solutions with silica and alumina. The technique is a fairly selective one as only the unadsorbed species are observed for different initial concentrations and pH levels.[168]

3. CHROMIUM AND TUNGSTEN NMR

3.1. ^{53}Cr

The amount of data available for this nucleus is small due to several factors. ^{53}Cr ($I = 3/2$) has a relatively large quadrupolar moment, $-0.15(5) \times 10^{-28}$ m^2,[174] (but a value of 0.041×10^{-28} m^2 has also been suggested[5]) which leads to short relaxation times (T_1 and T_2) especially in those cases of low symmetry when the line widths are exceedingly large.[1] The natural abundance (9.55%) and the overall receptivity (0.49 relative to ^{13}C) are insufficient to offset the rather small magnetic moment which results in a low Larmor frequency (20.3 MHz at 8.4 *T*) which, in turn, leads to a low sensitivity.[1,2,11–13]

In some limited cases Cr shows chemistry similar to that of Mo and W but typically behaves very differently.[31–33] It is interesting to note, however, that for all three Group 6 nuclei, a 2M aqueous solution of the tetraoxide, $[MO_4]^{2-}$, at an apparent pH of 11 is used as the usual chemical shift reference material and that the chemical shift differences, $\delta[MO_4]^{2-}$–$\delta[M(CO)_6]$, are about 1800, 1857 and 3500 for Cr, Mo and W respectively.[5,9] In fact, prior to 1985, ^{53}Cr NMR data had been reported only for $[CrO_4]^{2-}$ (0.0 p.p.m., $\Delta\nu_{1/2} = 11$ Hz)[175] and for $Cr(CO)_6$ (+1795 p.p.m., $\Delta\nu_{1/2} = 17$ Hz).[176] As is the case for molybdate, the $[CrO_4]^{2-}$ resonance and line width are both sensitive to measurement conditions.[175,176]

Dove *et al.*[177] have since reported data for some Cr(0) and Cr(VI) (e.g.,

CrO_2ClF) compounds and have observed $^1J(^{53}Cr-^{31}P)$ values for the species, $Cr(PF_3)_6$ and fac-$Cr(CO)_3(PF_3)_3$. ^{53}Cr NMR data[178] have also been reported for 46 chromium–carbene complexes and three isonitrile complexes for which the chemical shifts (+20 to +303 p.p.m., relative to $Cr(CO)_6$ as external standard) correlate well with the donor–acceptor properties of the ligands and show some sensitivity to steric effects. The spectra, measured in THF at ambient temperatures, show line widths ranging from 50 to 3500 Hz ($\Delta\nu_{1/2}$ $Cr(CO)_6$ = 2–3 Hz). The narrowest lines are observed for the isonitrile compounds.

^{53}Cr NMR has also been used to study spin-reorientation in the chromates, $Ho_{0.07}Y_{0.93}CrO_3$[179] and $Li_{0.5}Fe_{2.5-x}Cr_xO_4$.[180] Spin-echo ^{53}Cr NMR has shown that the frequency dependence of the echo reflects the quadrupolar structure of the spectra for $CdCr_2S_4$[181,182] and $CdCr_2Se_4$[183] and the technique has been employed in the investigation of the indium doped spinel $CdCr_2Se_4$:In at 4.2 K.[184]

3.2. ^{183}W

^{183}W is a spin 1/2 nucleus of 14.4% natural abundance but it has a low magnetogyric ratio and its sensitivity relative to ^{13}C is only 0.06.[1,2] Technically, ^{183}W offers several measurement difficulties. This nucleus tends to have relatively long relaxation times which means a large number of scans are required for reasonable signal-to-noise ratios. Its low NMR frequency[1,2,5,185] is near the lower limit of many commercial instruments. Thus, ^{183}W NMR studies had been limited for several years relative to ^{95}Mo NMR despite its huge chemical shift range that exceeds 11 000 p.p.m.[5]

Minelli and Maley's[115] study of the species $M(CO)_{6-n}(CNR)_n$ for M = Mo referred to above included a parallel study of the analogous tungsten species by ^{183}W NMR. This has often been the case. That is, because of the similar chemistry that Mo and W undergo,[31–33,168,186] similar NMR studies have been carried out. For example, Roy and Wieghardt[171] reported some data for W(VI) complexes of 1,4,7-triazacyclononane in their parallel study of Mo and W species. Young and Enemark[111] found that a linear relationship exists between the ^{95}Mo and ^{183}W chemical shifts for analogous species in the series, $[M(S_2CNEt_2)_2(CO)_2L]$ and $[M(S_2CNEt_2)_2(CO)_2]_2$-μ-L (M = Mo, W; L = various ligands). The ratio $\delta^{183}W:\delta^{95}Mo$ has been reported for several similar sets of M(0) (1.7),[34] M(II) (1.3)[134] and M(VI) (1.7)[153] species.

Often, in mixed-metal compounds containing both Mo and W, ^{183}W NMR has tended to be used more for characterization, but not always.[131] It appears that ^{183}W is more effective than ^{95}Mo NMR for the study of molybdotungstates.[147,148] Andersson *et al.*[187] studied the substitution of Mo(VI) for W(VI) in $[W_7O_{24}]^{6-}$, α-$[H_2W_{12}O_{40}]^{6-}$ and $[H_2W_{12}O_{40}]^{6-}$. The mixed metal polyanionic complexes, α-$[H_2W_{11}VO_{40}]^{7-}$ and α-

$[H_2W_{11}MoO_{40}]^{7-}$, have also been studied by ^{183}W[188] as have the octadeca(molybdotungstovanado) diphosphates, α-1,2,3-$[P_2MM_2'W_{15}O_{62}]^{n-}$ (M/M' = Mo, V, W).[189] For mixed metal M_3 clusters, stepwise replacement of Mo by W leads to deshielding in Mo and shielding in W.[190] Similar behaviour was observed for the species $[HMoM(CO)_{10}]^-$ (M = Cr, W).[46] Generally, for mixed metal dinuclear and trinuclear clusters, Mo and W tend to show lower and higher formal oxidation states respectively,[5] implying a transfer of negative charge from W to Mo. Increased shielding at W, with increasing oxidation state upon replacement of W with Mo has been corroborated by measurements for valence orbital bonding energies.[190]

McDonnell *et al.*[191] measured the ^{183}W spectra for $WO_2(ONEt_2)_2$ and $WO_2(ONC_5H_{10})_2$. The chemical shifts for thioether-bridged face-sharing bioctahedral (FBO) systems, $[Cl_3W(\mu\text{-}X)_n(\mu\text{-}SR_2)_{3-n}WCl_3]^{n-}$ ($n = 0,1$; X = Cl, thiolate or thioether), increase as $\mu - Cl^- < \mu - SR^- < \mu - SR_2$.[192] Enemark and coworkers[123,137] reported data for several triply bonded dinuclear W(III) species. ^{183}W NMR has been used extensively in the delineation of Dawson-type structures[193–198] including the use of 2D NMR for Wells–Dawson structures.[199] 2D COSY has been used to study the heteropolyoxometalate species, α-$[SiMo_2W_9O_{39}]^{8-}$ and α-$[SiMo_{3-x}V_xW_9O_{40}]^{(4+x)-}$ ($x = 1, 2$).[200] For the latter, a correlation is observed for ^{51}V and ^{183}W line broadenings. Isomerism in the polyoxotungstates of the Dawson structure, $[X_2W_{18}O_{62}]^{6-}$ (X = P, As), has been studied by ^{183}W NMR[201] as have the organophosphonyl polyoxotungstates, $[PhP(O)]_2X^{n+}W_{11}O_{39}^{(8-n)-}$ ($X^{n+} = P^{5+}$, Si^{4+}).[202] ^{183}W NMR was used in conjunction with X-ray crystallography to identify the structure for $K_4H_2[P_2W_{21}O_{71}(H_2O)_3].28H_2O$.[203]

Recently, many ^{183}W NMR data for tungstates, especially dinuclear tungstate complexes of carbohydrates in aqueous media, have become available.[204–206] There have also been several reports for studies of W(IV) heteropoly tungstate anions[207–210] and some assignments for mixed W(III)/W(IV) valence species.[207–210] The 10-line ^{183}W spectra in tandem with 2D COSY plots have yielded good structural information for the heteropolyanions, $[WM_3(H_2O)_2(XW_9O_{34})_2]^{12-}$ (X = M = Zn, Co),[211] $[H_xSiW_9V_3O_{40}]^{x-7}$[212] and $[H_xP_2W_{15}V_3O_{62}]^{x-9}$.[212] 2D heteronuclear ^{183}W–^1H,[213,214] ^{31}P[214] NMR have been used to study a series of W(II) metallocycles[213] and W(IV)[214] compounds.

Templeton *et al.*[215] have reported ^{183}W–^1H long-range shift correlations for several W(II) hydrido-pyrazolylborate complexes and more recently, they have used inverse detection based on nonspecific long-range interactions for W(VI) imidoaryl and imidoalkyl complexes.[216] For the Fischer-type carbyne complexes, $[WX(CO)_2(dppf)(CR)]$ (X = Cl, Br; *R* = Me, Ph, thienyl, furyl and ferrocenyl), increased shielding of the tungsten centre corresponds to a decreased shielding of the carbyne carbon with increasing π-donicity of the carbyne substituents.[217] The ^{13}C and ^{31}P chemical shifts for the carbonyl

carbon and the dppf phosphorus, however, show no dependence on the nature of R.[217]

Spectra measured for the W(VI) oxotetraalkoxides, $WO(OR)_4$ (R = Me, Et, ^{i}Pr, Cy and ^{t}Bu)[218] show line widths in the range, 2–40 Hz, which are much broader than the <1 Hz line widths expected.[5] This line broadening is ascribed to fluxionality, as indicated by variable temperature ^{1}H NMR. Dobson and Holcomb[219] investigated the relaxation times (T_1 and T_2) for several sodium–tungsten bronzes, $Na_xTa_yW_{1-y}O_z$ ($0<x,y<1$), to probe the distribution of local electronic environments for these disordered materials.

4. SOLID-STATE NMR

There has not been much work reported for the solid-state NMR of the Group 6 metals and there was none at all reported before 1985. Several recent and general reviews about the technique[220–223] contain only very limited data for ^{95}Mo and ^{183}W nuclei and apparently none for ^{53}Cr. Some detailed ^{95}Mo solid-state studies have been carried out to examine reduced/sulfided MoO_3–Al_2O_3 catalysts and the effects due to the addition of CO, CS and K to these catalysts.[224,225] Hee Han *et al.*[226,227] have used solid-state ^{27}Al and ^{95}Mo NMR to investigate hydration effects for aluminium molybdate, $Al_2(MoO_4)_3$, in hydrotreating catalysts. Merwin and Sebalb[228] have only recently reported what they claim are the first CP-MAS spectra for ^{183}W; however, some earlier solid-state work[229] for the polytungstate species, $H_3[P(W_{12}O_{40})].nH_2O$, showed that the twelve tungsten atoms present are all magnetically nonequivalent.

5. CONCLUDING REMARKS

All known oxidation states for Mo, 0–VI, have been observed by ^{95}Mo NMR in solution. The resultant overall chemical shift range spans greater than 7200 p.p.m. but there is severe overlap for different oxidation states (see Fig. 3) contrary to the classical expectation that high shielding should be associated with low oxidation states and build-up of negative charge, and vice versa. Thus, ^{95}Mo is not an effective technique for the differentiation of compounds of Mo in different oxidation states.

Nevertheless, for a given oxidation state, the Mo chemical shift is sensitive to ligand environment and overall stereochemistry. The normal halogen dependence,[44] i.e., increased shielding in the order Cl < Br < I, P < As < Sb, or C < Sn, etc., tends to be true for the case of Mo(0) but does not hold in many instances for Mo(II),[23,133] Mo(IV),[139] and Mo(VI).[45,140,141] This phenomenon has been pursued in NMR studies of other transition metal

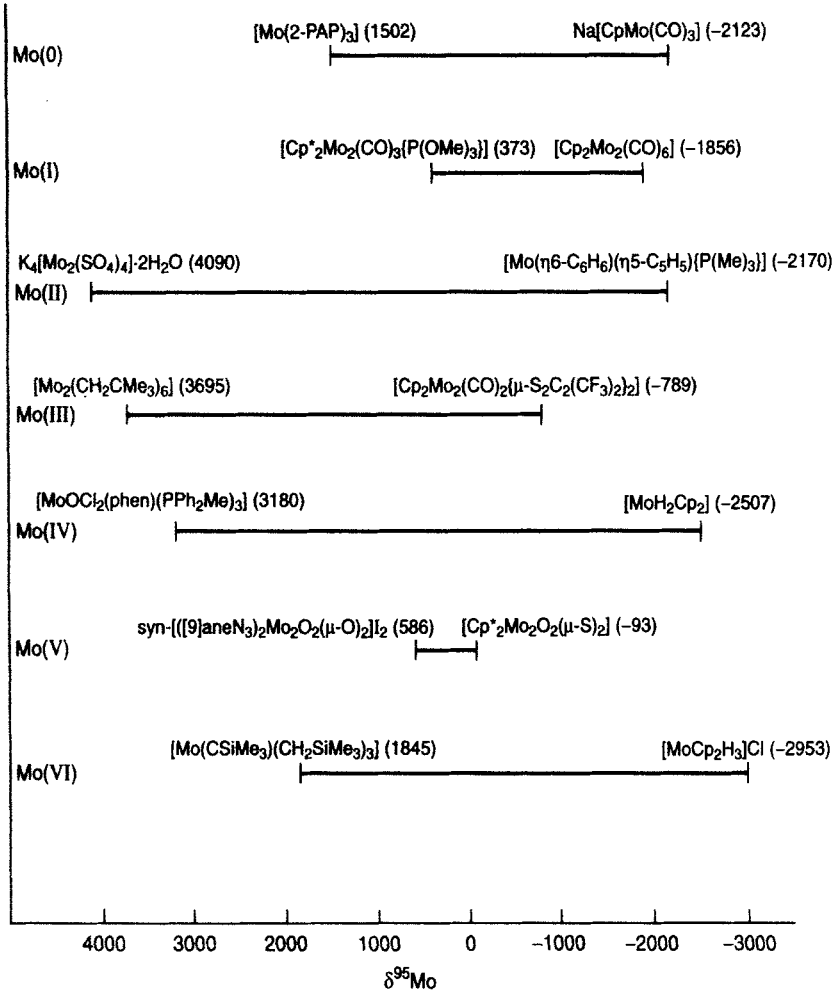

Fig. 3. The ^{95}Mo NMR chemical shift range by oxidation number.

nuclei.[6,8,10,60,89] Other orders for shielding, culled from all the data presented here, cannot be exact and must be taken from series of similar compounds for the same oxidation state. Nevertheless, some generally self-consistent orders might be summarized as follows:

$$\begin{aligned}&\text{PTA} > \text{PF}_3 > \text{P(OR)}_3 > \text{P(OCH}_2\text{C(Me)}_2\text{CH}_2\text{O)OR} \geq \text{P(Alk)}_3 > \\ &\text{P(OCH}_2)_2\text{CH(Me)O)OR} \geq \text{P(OCH}_2\text{C(Me)}_2\text{CH}_2\text{O)NHR} > \\ &\text{P(O(CH}_2)_2\text{CH(Me)O)NHR} > \text{P(OPh)}_3 > \text{PPh(OR)}_2 > \text{P(PH}_2\text{OR)} \geq \\ &\text{DBP} > \text{Ph}_2\text{P(CH}_2)_n\text{PPh}_2 > \text{P(Ph}_2\text{OC}_6\text{H}_4\text{-}p\text{-R)} > \text{P(OCH}_2\text{C(Me)}_2\text{CH}_2\text{O)X} >\end{aligned}$$

$$P(OCH_2C(Me)_2CH_2)SR > P(Ph_2NHR) > P(O(CH_2)_2CH(Me)SR > P(O(CH_2)_2CH(Me)O)Cl > P(AR)_3 > P(Ph_2SR) \geq P(Ph_2SC_6H_4\text{-}p\text{-}R) > P(Ph_2Cl) > P(PhCl_2) > PCl_3 \gg PBr_3;$$

$$H^- > CN^- > Sb(Ph)_3 > CO > CNR > P(OAlk)_3 > P(Alk)_3 > N_2 > P(OAr)_3 > P(Ph_2YR)\ (Y = O > NH > S) > As(Ph)_3 > P(Ar)_3 > I^- \geq S_2(P(OR)_2) > NCY\ (Y = O > S > Se) > S_2CNR_2 > Br^- > N_3^- \geq quin > NO_2^- > Cl^- > O_2CH^- > pyr > NCR > NO^+ > N{=}NR^+ > N\text{-}NR_2^{2-} > SeCN > OCH_3^- > NEt_3 > pip > S_2COEt > py;$$

$$dpfe > diars > vpp > Ar_2P(CH_2)_nPAr_2\ (n > 2) > Ar_2PCH_2PR_2 > norbornadiene > O_2N^- > RSCH{=}CHSR > S_2CNR_2 > RSCH_2CH_2SR > S_2(P(OR)_2) > S_2CN(CH_2)_4 > phen \geq bipy > \alpha\text{-diimine} > diazene > bptz;$$

$$Cp^- > \eta^5\text{-}\sigma\text{-}C_5H_5CR_2\ (R = Me > Ph) > \eta^6\text{-}C_6H_6 > \eta^6\text{-}C_6H_5Me > \eta^6\text{-}o\text{-xylene} > \eta^6\text{-}p\text{-xylene} > \eta^6\text{-}m\text{-xylene} > \eta^6\text{-mesitylene} > \eta^6\text{-}C_6Me_6 > triphos > \eta^6\text{-}C_7H_8 > [9]aneS_3 > dien.$$

In Mo–Mo, bonding increased shielding with increasing bond order, quadruple < triple < double < single bond, occurs over a range of greater than 6000 p.p.m.[23,47,138,230] and for multiple bonds:

$$[Mo \equiv Mo]^{4+}\ (\sigma^2\pi^2\delta^2) < [Mo \equiv Mo]^{6+}\ (\sigma^2\pi^4) < [Mo \equiv Mo]^{6+}\ (\pi^4\delta^2) \leq [Mo \equiv C]^{3+} < [M \equiv N]^{3+}$$

Correlations between ^{95}Mo NMR chemical shifts and chemical shifts for other NMR active nuclei, ^{13}C,[56,58,59,67,74,115] ^{31}P,[56,58–60,72,74] ^{17}O,[56,58,59,72,74] ^{14}N,[134] and ^{183}W,[34,135,154,191] have been observed as have correlations with ^{119}Sn Mössbauer isomer shifts,[231] and data from visible,[72,96,161] infrared,[92,93] and ESR spectroscopy.[93] ^{95}Mo NMR chemical shifts have also been related to solvent electrophilicity,[100] thermochemical data,[90] sulphur inversion barriers,[113] theoretical calculations,[28,117] reaction kinetics,[117,160] and electrochemical data.[161] In fact, it has been suggested that transition metal NMR is a generally more sensitive probe than optical spectroscopy for locating ligands in the spectrochemical series.[179,232] Finally, correlations to various ligand parameters such as Taft and Hammett parameters,[92] and pK_a[60] have also been investigated.

Line widths are of reasonable magnitudes for ^{95}Mo spectra, except in those extreme cases of high solvent viscosity, very large molecules or smaller molecules which suffer severe steric crowding and distortion, and unusually unsymmetrical electronic environments at the metal centre. Reasons given for broader than theoretically expected line widths have been based on short relaxation times, decreased electronic and complex symmetry, the

presence of neighbouring quadrupolar nuclei, unresolved scalar coupling, solvent viscosities and temperature effects. On average, the observed line widths for the seven Mo oxidation states increase approximately as Mo(0) < Mo(I) < Mo(III), Mo(V), Mo(VI) < Mo(II) < Mo(IV).

Spin–spin coupling constants between ^{95}Mo and ^{1}H, ^{13}C, ^{14,15}N, ^{17}O, ^{19}F and ^{31}P have been measured (see Tables). Except for the case of ^{31}P, the total amount of data is still not abundant.[5] The coupling constants observed tend to be small in magnitude (< 50 Hz for nuclei other than ^{31}P). In some cases, such as ^{19}F, they are of second order and very small in magnitude. Thus, the ^{n}J values measured are of questionable accuracy considering the inherent broadness of both the spectral lines and the spectral range in ^{95}Mo NMR. Furthermore, the coupling constants appear to be insensitive to subtle changes in the chemical environment of Mo, thereby being less informative than they tend to be for other transition metal nuclei.

REFERENCES

1. R. K. Harris and B. E. Mann, *NMR and the Periodic Table*. Academic Press, London, 1978.
2. W. Kemp, *NMR in Chemistry, A Multinuclear Introduction*. Macmillan, London, 1986.
3. W. Ertmer, U. Johann and R. Mosmann, *Z. Phys. A*, 1982, **309**, 1.
4. M. Dubke, W. Jitschin, G. Meisel and W. J. Childs, *Phys. Lett. A*, 1978, **65**, 109.
5. M. Minelli, J. H. Enemark, R. T. C. Brownlee, M. J. O'Connor and A. G. Wedd, *Coord. Chem. Rev.*, 1985, **68**, 169.
6. C. Brevard and P. S. Pregosin, Stud. *Inorg. Chem.*, 1991, **13**, 59.
7. X.-L. Xie, R. Cao, M.-C. Hong, B.-S. Kang, F.-L. Jiang and H.-Q. Liu, *Jiegou Huaxue*, 1994, **13**, 480 (CA: 122: 149611v).
8. D. J. Rehder, *Magn. Reson. Rev.*, 1984, **9** 125.
9. J. Mason, *Chem. Rev.*, 1987, **87**, 1299.
10. J. Mason (ed.), *Multinuclear NMR*. Plenum Press, New York, 1987.
11. M. Sugimoto and H. Nakatsuji, *Organomet. News*, 63 (1992).
12. R. Benn and A. Rufinska, *Angew. Chem., Int. Ed. Engl.*, 1986, **25**, 861.
13. P. Laszlo (ed.), *NMR of Newly Accessible Nuclei*. Academic Press, New York, 1983.
14. P. S. Pregosin, *Coord. Chem. Rev.*, 1982, **44**, 247.
15. N. F. Ramsey, *Phys. Rev.*, 1950, **77**, 567.
16. N. F. Ramsey, *Phys. Rev.*, 1950, **78**, 699.
17. J. S. Griffith and L. E. Orgel, *Trans. Faraday Soc.*, 1957, **53**, 60.
18. C. J. Jameson and H. S. Gutowsky, *J. Chem. Phys.*, 1964, **40**, 1714.
19. H. Nakatsuji, K. Kanda, E. Endo and T. Yonezawa, *J. Am. Chem. Soc.*, 1984, **106**, 4653.
20. N. Juranic, *Coord. Chem. Rev.*, 1989, **96**, 253.
21. K. Kanda, H. Nakatsuji and T. Yonezawa, *J. Am. Chem. Soc.*, 1984, **106**, 5888.
22. D. Rehder, *Bull. Magn. Reson.*, 1982, **4**, 33.
23. J. Mason and R. A. Grieves, *Polyhedron*, 1986, **5**, 415.
24. H. Nakatsuji and M. Sugimoto, *Inorg. Chem.*, 1990, **29**, 1221.
25. H. Nakatsuji, M. Sugimoto and S. Saito, *Inorg. Chem.*, 1990, **29**, 3095.
26. J. E. Combariza, J. H. Enemark, M. Barfield and J. C. Facelli, *J. Am. Chem. Soc.*, 1989, **111**, 7619.

27. J. E. Combariza, M. Barfield and J. H. Enemark, *J. Phys. Chem.*, 1990, **95**, 5463.
28. Y. Sun, L. Zhu, X. You and Y. Jiang, *Theor. Chim. Acta*, 1992, **82**, 213.
29. N. Juranic, *J. Chem. Phys.*, 1981, **74**, 3690.
30. J. J. Dechter, *Prog. Inorg. Chem.*, 1985, **33**, 393.
31. F. A. Cotton and G. Wilkinson, *Advanced Inorganic Chemistry*, 5th edn. John Wiley and Sons, New York, 1988.
32. G. Wilkinson (ed.), *Comprehensive Coordination Chemistry*, Vol. 3. Pergamon Press, Oxford, 1987.
33. E. R. Braithwaite and J. Haber (eds), *Molybdenum: An Outline of its Chemistry and Uses*, Chaps 2–8. Elsevier, Amsterdam, 1994.
34. G. T. Andrews, I. J. Colquhoun, W. McFarlane and S. O. Grim, *J. Chem. Soc., Dalton Trans.*, 1982, 2353.
35. O. Lutz, A. Nolle and P. Kroneck, *Z. Naturforsch., Teil A*, 1976, **31**, 454.
36. E. C. Alyea and A. Somogyvari, *Transition Met. Chem.*, 1987, **12**, 310.
37. C. A. Merlic and B. Adams, *J. Organomet. Chem.*, 1992, **431**, 313.
38. M. Hughes, J. Mason, G. J. Leigh and R. L. Richards, *J. Organomet. Chem.*, 1988, **341**, 381.
39. M. A. Ackerman, C. R. Barton, C. J. Deodene, E. M. Specht, S. C. Keill, W. E. Schreiber and H. Kim, *Inorg. Chem.*, 1989, **28**, 397.
40. A. F. Masters, R. T. C. Brownlee, M. J. O'Connor, A. G. Wedd and J. D. Cotton, *J. Organomet. Chem.*, 1980, **195**, C17.
41. S. Ozkar and Z. Ozer, *Z. Naturforsch., B: Chem. Sci.*, 1993, **48**, 1431.
42. R. T. C. Brownlee, M. J. O'Connor, B. P. Shehan and A. G. Wedd, *J. Magn. Reson.*, 1985, **61**, 22: 1985, **61**, 516.
43. R. T. C. Brownlee, B. P. Shehan and A. G. Wedd, *Aust. J. Chem.*, 1988, **41**, 1457.
44. R. G. Kidd, *Annu. Rep. NMR Spectrosc.*, 1980, **10**, 1.
45. M. Minelli, J. H. Enemark, K. Wieghardt and M. Hahn, *Inorg. Chem.*, 1983, **22**, 3953.
46. E. C. Alyea, A. Malek and J. Malito, *Inorg. Chim. Acta*, 1985, **101**, 147.
47. S. Dysart, I. Georgii and B. E. Mann, *J. Organomet. Chem.*, 1981, **213**, C10.
48. E. C. Alyea, A. Malek and J. Malito, *Polyhedron*, 1986, **5**, 403.
49. A. F. Masters, G. E. Bossard, T. A. George, R. T. C. Brownlee, M. J. O'Connor and A. G. Wedd, *Inorg. Chem.*, 1983, **22**, 908.
50. P. C. Ford, *Acc. Chem. Res.*, 1981, **14**, 31.
51. S. Attali, R. Mathieu and G. J. Leigh, *J. Mol. Catal.*, 1982, **14**, 293.
52. D. J. Darensbourg and A. Rokicki, *Organometallics*, 1982, **1**, 1685.
53. B. H. Weiller, J.-P. Liu and E. R. Grant, *J. Am. Chem. Soc.*, 1985, **107**, 1595.
54. E. C. Alyea, R. E. Lenkinski and A. Somogyvari, *Polyhedron*, 1982, **1**, 130.
55. G. M. Gray, *Inorg. Chim. Acta*, 1984, **81**, 157.
56. G. M. Gray, R. J. Gray and D. C. Berndt, *J. Magn. Reson.*, 1984, **57**, 347.
57. G. M. Gray and R. J. Gray, *Organometallics*, 1983, **2**, 1026.
58. G. M. Gray, J. E. Whitten and J. W. Box, *Inorg. Chim. Acta*, 1986, **21**, 116.
59. G. M. Gray, J. E. Whitten and J. W. Box, *Inorg. Chim. Acta*, 1986, **21**, 120.
60. E. C. Alyea, K. J. Fisher, S. Foo and B. Philip, *Polyhedron*, 1993, **12**, 489.
61. E. C. Alyea and S.-Q. Song, *Inorg. Chem.*, 1995, **34**, 3864.
62. J. T. Bailey, R. J. Clark and G. C. Levy, *Inorg. Chem.*, 1982, **21**, 2085.
63. S. Affandi, J. H. Nelson, N. W. Alcock, O. W. Howarth, E. C. Alyea and G. M. Sheldrick, *Organometallics*, 1988, **7**, 1724.
64. W. L. Wilson, N. W. Alcock, E. C. Alyea, S. Song and J. H. Nelson, *Bull. Soc. Chim. Fr.*, 1993, **130**, 673.
65. E. C. Alyea, G. Ferguson, K. J. Fisher, R. A. Gossage and M. C. Jennings, *Polyhedron*, 1990, **9**, 2393.

66. J. L. Bookham, W. McFarlane and I. J. Colquhoun, *J. Chem. Soc., Dalton Trans.*, 1988, 503.
67. B. Chaudret, B. Delavaux and R. Poilblanc, *Coord. Chem. Rev.*, 1988, **86**, 191 (and references therein).
68. T. S. A. Hor and H. S. O. Chan, *Inorg. Chim. Acta*, 1989, **160**, 53.
69. E. C. Alyea and A. Somogyvari, *Magn. Reson. Chem.*, 1986, **24**, 357.
70. E. C. Alyea and A. Somogyvari, *Can. J. Chem.*, 1988, **66**, 397.
71. E. C. Alyea, G. Ferguson, J. F. Gallagher and S.-Q. Song, *Acta Crystallogr., Sect. C: Cryst. Struct. Commun.*, 1994, **C50**, 1084.
72. G. M. Gray and C. S. Kraihanzel, *Inorg. Chem.*, 1983, **22**, 2959.
73. J. Jaitner and M. Wohlgenannt, *Montash. Chem.*, 1982, **113**, 699.
74. G. M. Gray and W. Watt, *J. Organomet. Chem.*, 1992, **434**, 181.
75. A. Patel, S. Shehla, D. T. Richens, M. E. Harman and M. B. Hursthouse, *J. Chem. Soc., Dalton Trans.*, 1993, 767.
76. E. C. Alyea, G. Ferguson and S.-Q. Song, *Acta Crystallogr., Sect. C: Cryst. Struct. Commun.*, 1995, **C51**, 2238.
77. John Malito, manuscript in preparation.
78. P. S. Pregosin, *Annu. Rep. NMR Spectrosc.*, 1986, **17**, 285.
79. L. H. Green, Y.-A. Park and D. W. Meek, *Inorg. Chem.*, 1988, **27**, 1658.
80. H. C. Clark and A. M. de P. Nichols, *Magn. Reson. Chem.*, 1990, **28**, 99.
81. D. S. Marynick, S. Askari and D. F. Nickerson, *Inorg. Chem.*, 1985, **24**, 868.
82. C. Daniel and A. Veillard, *Inorg. Chem.*, 1989, **28**, 1170.
83. P. E. Garrou, *Chem. Rev.*, 1981, **81**, 226.
84. P. S. Pregosin and R. W. Kunz, *NMR: Basic Prin. Prog.*, 1979, **16**, 133.
85. P. E. Garrou and D. Rehder, *J. Magn. Reson.*, 1980, **38**, 419.
86. C. J. Jameson in J. G. Verkade and L. D. Quin (eds), *^{31}P NMR Spectroscopy in Stereochemical Analysis*, Chap. 6. VCH, Weinheim, Germany, 1987.
87. J. R. Delerno, L. M. Trefonas, M. Y. Darensbourg and R. J. Majeste, *Inorg. Chem.*, 1976, **15**, 816.
88. F. A. Cotton, D. J. Darensbourg and W. H. Ilsley, *Inorg. Chem.*, 1981, **20**, 578.
89. J. Mason, *Adv. Inorg. Chem. Radiochem.*, 1979, **22**, 199.
90. J. Malito, E. C. Alyea and R. A. Gossage, *Spectrochim. Acta*, 1992, **48A**, 873.
91. R. T. C. Brownlee, M. J. O'Connor, B. P. Shehan and A. G. Wedd, *J. Magn. Reson.*, 1985, **64**, 142.
92. E. C. Alyea, K. J. Fisher and R. A. Gossage, *Spectrochim. Acta*, 1989, **45A**, 203.
93. E. C. Alyea, J. Malito, S. D. Ernst, W. Kaim and S. J. Kohlman, *Polyhedron*, 1989, **8**, 921.
94. A. Beyerholm, M. Brorson, M. Minelli and L. K. Skov, *Inorg. Chem.*, 1992, **31**, 3672.
95. K. Wieghardt, M. Guttmann, P. Chaudhuri, W. Gebert, M. Minelli, C. G. Young and J. H. Enemark, *Inorg. Chem.*, 1985, **24**, 3151.
96. E. C. Alyea, R. A. Gossage, J. Malito and Z. A. Munir, *Polyhedron*, 1990, **9**, 1059.
97. S. Donovan-Mtunzi, M. Hughes, G. J. Leigh, H. Modh. Ali, R. L. Richards and J. Mason, *J. Organomet. Chem.*, 1983, **246**, C1.
98. M. Minelli, J. L. Hubbard and J. H. Enemark, *Inorg. Chem.*, 1984, **23**, 970.
99. V. Gutmann, *Coord. Chem. Rev.*, 1976, **18**, 225.
100. C. D. Taz and N. Yutronic, *Polyhedron*, 1988, **7**, 673.
101. H. O. Desseyn, B. J. van der Veken, J. R. Moss, B. J. Smith, P. Verhoeven and D. A. Thornton, *Spectrochim. Acta*, 1984, **40A**, 467.
102. R. H. T. Bleijerveld and K. Vrieze, *Inorg. Chim. Acta*, 1976, **19**, 195.
103. H. Daamen, H. van der Poel, D. J. Stufkens and A. Oskam, *Thermochim. Acta*, 1979, **34**, 69.

104. K. J. Cavell, J. M. Ernsting and D. J. Stufkens, *Thermochim. Acta*, 1980, **42**, 343.
105. R. J. Dennenberg and D. J. Darensbourg, *Inorg. Chem.*, 1972, **11**, 72.
106. C. S. Kraihanzel and F. A. Cotton, *Inorg. Chem.*, 1963, **2**, 533.
107. R. C. Elder, *Inorg. Chem.*, 1968, **7**, 1117.
108. H. van Dam, G. Boxhoorn, D. J. Stufkens and A. Oskam. *Inorg. Chim. Acta*, 1981, **53**, L235.
109. H. Brunner, P. Beier, E. Frauendorfer, M. Muschiol, D. K. Rastogi, J. Wachter, M. Minelli and J. H. Enemark, *Inorg. Chim. Acta A*, 1985, **96**, L5.
110. M. Minelli, J. L. Hubbard, K. A. Christensen and J. H. Enemark, *Inorg. Chem.*, 1983, **22**, 2652.
111. C. G. Young and J. H. Enemark, *Aust. J. Chem.*, 1986, **39**, 997.
112. E. C. Alyea and A. Somogyvari, *Inorg. Chim. Acta*, 1984, **83**, L49.
113. E. W. Abel, D. E. Budgeon, I. Moss, K. G. Orrell and V. Sik, *J. Organomet. Chem.*, 1989, **362**, 105.
114. M. T. Ashby and D. L. Lichtenberger, *Inorg. Chem.*, 1985, **24**, 636.
115. M. Minelli and W. J. Maley, *Inorg. Chem.*, 1989, **28**, 2954.
116. J. W. Faller and B. C. Whitmore, *Organometallics*, 1986, **5**, 572.
117. J. C. Green, R. A. Grieves and J. Mason, *J. Chem. Soc., Dalton Trans.*, 1986, 1313.
118. A. F. Masters, R. T. C. Brownlee, M. J. O'Connor and A. G. Wedd, *Inorg. Chem.*, 1981, **20**, 4183.
119. M. J. Aroney, R. M. Clarkson, R. J. Klepetko, A. F. Masters and R. K. Pierens, *J. Organomet. Chem.*, 1990, **393**, 371.
120. J. Y. LeGall, M. M. Kubicki and F. Y. Petillon, *J. Organomet. Chem.*, 1981, **221**, 287.
121. M. M. Kubicki, R. Kergoat, J. Y. LeGall, J. E. Guerchais, J. Douglade and R. Mercier, *Aust. J. Chem.*, 1982, **35**, 1543.
122. M. M. Kubicki, J. Y. LeGall, R. Pichon, J. Y. Salaun, M. Cano and J. A. Campo, *J. Organomet. Chem.*, 1988, **348**, 349.
123. C. G. Young, M. Minelli, J. H. Enemark, G. Miessler, N. Janietz, H. Kauermann and J. Wachter, *Polyhedron*, 1986, **5**, 407.
124. R. T. C. Brownlee, M. J. O'Connor, B. P. Shehan and A. Wedd, *Aust. J. Chem.*, 1986, **39**, 931.
125. P. G. Gassman, D. W. Macomber and J. W. Hershbergen, *Organometallics*, 1983, **2**, 1470.
126. W. D. Horrocks and R. C. Taylor, *Inorg. Chem.*, 1963, **2**, 723.
127. D. Rehder and M. Hoch, *J. Am. Chem. Soc.*, 1987, **109**, 2589.
128. N. E. Alekseevskii, S. V. Verkhovskii, N. I. Lobachevskaya, K. N. Mikhalev, B. A. Aleksashin and E. G. Nikolaev, *Zh. Eksp. Teor. Fiz.*, 1988, **94**, 363 (CA: 108: 215050a).
129. N. E. Alekseevskii, K. N. Mikhalev, B. A. Aleksashin, S. V. Verkhovskii, E. G. Nikolaev and A. P. Stepanov, *Zh. Eksp. Teor. Fiz.*, 1986, **91**, 677 (CA: 105: 163640j).
130. B. A. Aleksashin, S. V. Verkhovskii, K. N. Mikhalev, A. P. Stepanov, V. E. Arkhipov and B. N. Goshchitskii, *Fiz. Met. Metalloved.*, 1986, **62**, 284 (CA: 105: 163676a).
131. A. Proust, R. Thouvenot, F. Robert and P. Gouzerh, *Inorg. Chem.*, 1993, **32**, 5299.
132. A. Proust, R. Thouvenot, S.-G. Roh, J.-K. Yoo and P. Gouzerh, *Inorg. Chem.*, 1995, **34**, 4106.
133. C. G. Young, M. Minelli, J. H. Enemark, W. Hussain, C. J. Jones and J. A. McCleverty, *J. Chem. Soc., Dalton Trans.*, 1987, 619.
134. M. Minelli, A. Bell, J. H. Enemark and A. R. Walton, *J. Organomet. Chem.*, 1985, **284**, 25.
135. P. B. Shehan, R. T. C. Brownlee, M. Kony, M. J. O'Connor and A. G. Wedd, *J. Magn. Reson.*, 1985, **63**, 343.

136. S. F. Gheller, T. W. Hambley, R. T. C. Brownlee, M. J. O'Connor, M. R. Snow and A. G. Wedd. *J. Am. Chem. Soc.*, 1983, **105**, 1527.
137. C. G. Young, E. M. Kober and J. H. Enemark, *Polyhedron*, 1987, **6**, 255.
138. O. Lutz, A. Nolle and P. Kroneck, *Z. Naturforsch., Teil A*, 1977, **32**, 505.
139. C. G. Young and J. H. Enemark, *Inorg. Chem.*, 1985, **24**, 4416.
140. M. Minelli, R. L. Kuhlman, S. J. Shaffer and M. Y. Chiang, *Inorg. Chem.*, 1992, **31**, 3891.
141. M. Minelli, K. Yamanouchi, J. H. Enemark, P. Subramanian, B. B. Kaul and J. T. Spence, *Inorg. Chem.*, 1984, **23**, 2554.
142. W. D. Kautt, H. Krüger, O. Lutz, H. Maier and A. Nolle, *Z. Naturforsch., Teil A*, 1976, **31**, 351.
143. S. F. Gheller, P. A. Gazzana, A. F. Masters, R. T. C. Brownlee, M. J. O'Connor, A. G. Wedd, J. R. Rodgers and M. R. Snow, *Inorg. Chim. Acta*, 1981, **54**, L131.
144. S. Bank, S. Liu, S. N. Shaikh, J. Zubieta and P. D. Ellis, *Inorg. Chem.*, 1988, **27**, 3535.
145. R. I. Maksimovskaya and N. N. Chumachenko, *Polyhedron*, 1987, **6**, 1813.
146. J. M. Coddington and M. J. Taylor, *J. Chem. Soc., Dalton Trans.*, 1990, 41.
147. S. Chapelle, J.-F. Verchère and J.-P. Sauvage, *Polyhedron*, 1990, **9**, 1225.
148. J.-F. Verchère and S. Chapelle, *Polyhedron*, 1989, **8**, 33.; M. Matulovà and V. Bílik, *Chem. Pap.*, 1990, **44**, 703.
149. S. Chapelle and J.-F. Verchère, *Carbohydr. Res.*, 1991, **9**, 1225.
150. M. L. Ramos, M. Caldeira, V. M. S. Gil, H. van Bekkum and J. A. Peters, *Polyhedron*, 1994, **13**, 1825.
151. H. Liu, R. Cao, X. Lei, D. Wu, G. Wei, Z. Huang, M. Hong and B. Kang, *J. Chem. Soc., Dalton Trans.*, 1990, 1023.
152. M. Minelli, J. H. Enemark, J. R. Nicholson and C. D. Garner, *Inorg. Chem.*, 1984, **23**, 4384.
153. S. F. Gheller, T. W. Hambley, J. R. Rodgers, R. T. C. Brownlee, M. J. O'Connor, M. R. Snow and A. G. Wedd, *Inorg. Chem.*, 1984, **23**, 2519.
154. S. R. Acott, C. D. Garner, J. R. Nicholson and W. Clegg, *J. Chem. Soc., Dalton Trans.*, 1983, 713.
155. E. P. Talsi, O. V. Klimov and K. I. Zamaraev, *J. Mol. Catal.*, 1993, **83**, 329.
156. V. Nardello, J. Marko, G. Vermmeersch and J. M. Aubry, *Inorg. Chem.*, 1995, **34**, 4950.
157. N. J. Campbell, A. C. Dengel, C. J. Edwards and W. P. Griffith, *J. Chem. Soc., Dalton Trans.*, 1989, 1203.
158. E. P. Talsi, K. V. Shalyaev and K. I. Zamaraev, *J. Mol. Catal.*, 1993, **83**, 347.
159. K. Unouva, P. Kikuchi, A. Nagasawa, Y. Kato and Y. Fukuda, *Inorg. Chim. Acta*, 1995, **228**, 89.
160. S. F. Gheller, W. E. Newton, L. Pabon de Majid, J. R. Bradbury and F. A. Schultz, *Inorg. Chem.*, 1988, **27**, 359.
161. M. B. Hursthouse, R. L. Short, B. Piggott, A. Tucker and S. F. Wong, *Polyhedron*, 1986, **5**, 2121.
162. B. Piggott, S. D. Thorpe and R. N. Shepard, *Inorg. Chim. Acta*, 1985, **103**, L1.
163. M. V. Capparalli, B. Piggott, S. D. Thorpe, S. F. Wong and R. N. Shepard, *Inorg. Chim. Acta.*, 1985, **106**, 19.
164. B. Piggott, S. F. Wong and R. N. Shepard, *Inorg. Chim. Acta.*, 1985, **107**, 97.
165. O. W. Howarth, L. Pettersson and I. Andersson, *J. Chem. Soc., Dalton Trans.*, 1991, 1799.
166. M. A. Leparulo-Loftus and M. T. Pope, *Inorg. Chem.*, 1989, **26**, 2112.
167. N. P. Luthra and W. C. Cheng, *J. Catal.*, 1987, **107**, 154.
168. P. Sarrazin, B. Mouchel and S. Kasztelan, *J. Phys. Chem.*, 1989, **93**, 904.

169. M. Minelli, M. R. Carson, D. W. Whisenhunt, Jr, W. Imhof and G. Huttner, *Inorg. Chem.*, 1990, **29**, 4801.
170. A. C. Dengel, W. P. Griffith, R. D. Powell and A. C. Skapski, *J. Chem. Soc., Dalton Trans.*, 1987, 991.
171. P. S. Roy and K. Wieghardt, *Inorg. Chem.*, 1987, **26**, 1885.
172. M. A. Freeman, F. A. Schultz and C. N. Reilley, *Inorg. Chem.*, 1982, **21**, 567.
173. S. Ikari, Y. Sasaki, A. Nagasawa, C. Kabuto and T. Ito, *Inorg. Chem.*, 1989, **28**, 1248.
174. R. G. Kidd, *J. Magn. Reson.*, 1981, **45**, 88.
175. Y. Egozy and A. Loewenstein, *J. Magn. Reson.*, 1969, **1**, 494.
176. B. W. Epperlein, H. Krüger, O. Lutz, A. Nolle and W. Mayr, *Z. Naturforsch., Teil A*, 1975, **30**, 1237.
177. M. F. A. Dove, E. M. L. Jones and R. L. Clark, *Magn. Reson. Chem.*, 1989, **27**, 973.
178. A. Hafner, L. S. Hegedus, G. de Weck, B. Hawkins and K. H. Dötz, *J. Am. Chem. Soc.*, 1988, **110**, 8413.
179. A. S. Kharanachev, M. M. Lukina, A. S. Moskvin and E. E. Solovyev, *Fiz. Tverd. Tela*, 1992, **34**, 3572 (CA: 118: 246108m).
180. G. N. Abelyashev, V. V. Mal'nev, V. N. Seleznev, N. A. Sergeev and Yu. V. Fedotov, *Fiz. Tverd. Tela*, 1991, **33**, 1884 (CA: 116: 267650f).
181. G. N. Abelyashev, V. N. Berzhanskii, N. A. Sergeev and Yu. V. Fedotov, *Phys. Lett. A*, 1988, **133**, 263.
182. T. G. Aminov, V. T. Kalinnikov, V. K. Prokopenko, G. G. Shabunina and A. A. Shemyakov, *Izv. Akad. Nauk. SSSR, Neorg. Mater.*, 1988, **24**, 1918.
183. G. N. Abelyashev, V. N. Berzhanskii, N. A. Sergeev and Yu. V. Fedotov, *Pis'ma Zh. Eksp. Teor. Fiz.*, 1988, **48**, 619 (CA: 110: 68353n).
184. G. N. Abelyashev, V. N. Berzhanskii and Yu. V. Fedotov, *Fiz. Tverd. Tela*, 1986, **28**, 2548 (CA: 105: 163643n).
185. J. Banck and A. Schwenk, *Z. Physik., Teil B*, 1975, **20**, 75.
186. R. Colton, *Coord. Chem. Rev.*, 1985, **62**, 145; J. M. Charnock, *ibid.*, 1987, **81**, 101; M. M. Minelli, *ibid.*, 1987, **81**, 1; R. Fereday, *ibid.*, 1987, **81**, 51.
187. I. Andersson, J. J. Hastings, O. W. Howarth and L. Pettersson, *J. Chem. Soc., Dalton Trans.*, 1994, 1061.
188. J. J. Hastings and O. W. Howarth, *Polyhedron*, 1993, **12**, 847.
189. M. Abbessi, R. Contant, R. Thouvenot and G. Hervé, *Inorg. Chem.*, 1991, **30**, 1695.
190. A. Nagasawa, Y. Sasaki, B. Wang, S. Ikari and T. Ito, *Chem. Lett.*, 1987, 1271.
191. A. McDonnell, S. Vasudevan, M. J. O'Connor and A. G. Wedd, *Aust. J. Chem.*, 1985, **38**, 1017.
192. H.-B. Kraatz, J. M. Aramini, X. Gao, P. M. Boorman and H. J. Vogel, *Inorg. Chem.*, 1993, **32**, 3976.
193. R. Thouvenot, A. Tézé, R. Contant and G. Hervé, *Inorg. Chem.*, 1988, **27**, 524.
194. J. Canny, R. Thouvenot, A. Tézé, G. Hervé, M. Leparulo-Loftus and M. T. Pope, *Inorg. Chem.*, 1991, **30**, 976.
195. R. Contant and R. Thouvenot, *Can. J. Chem.*, 1991, **69**, 1498.
196. X. Wu and A. Jiang, *Gaodeng Xuexiao Huaxue Xuebao*, 1992, **13**, 429 (CA: 118: 93151t).
197. J. Gong, L. Qu, Y. Chen and B. Li Wuji, *Huaxue Xuebao*, 1995, **11**, 102 (CA: 123: 186393s).
198. M. Kozik, C. F. Hammer and L. C. W. Baker, *J. Am. Chem. Soc.*, 1986, **108**, 2748.
199. M. Kozik, R. Acerete, C. F. Hammer and L. C. W. Baker, *Inorg. Chem.*, 1991, **30**, 4429.
200. E. Cadot, R. Thouvenot, A. Tézé and G. Hervé, *Inorg. Chem.*, 1992, **31**, 4128.

201. R. Contant and R. Thouvenot, *Inorg. Chim. Acta*, 1993, **212**, 41.
202. G.-S. Kim, K. S. Hagen and C. L. Hill, *Inorg. Chem.*, 1992, **31**, 5316.
203. C. M. Tourné, G. F. Tourné and T. J. R. Weakley, *J. Chem. Soc., Dalton Trans.*, 1986, 2237.
204. S. Chapelle, J.-P. Sauvage, P. Köll and J.-F. Verchère, *Inorg. Chem.*, 1995, **34**, 918.
205. S. Chapelle, J.-P. Sauvage and J.-F. Verchère, *Inorg. Chem.*, 1994, **33**, 1966.
206. S. Chapelle and J.-F. Verchère, *Inorg. Chem.*, 1992, **31**, 648.
207. C. Rong and M. T. Pope, *J. Am. Chem. Soc.*, 1992, **114**, 2932.
208. J. Liu, F. Ortéga, P. Sethuraman, D. E. Katsoulis, C. E. Costello and M. T. Pope, *J. Chem. Soc., Dalton Trans.*, 1992, 1901.
209. K. Piepgrass and M. T. Pope, *J. Am. Chem. Soc.*, 1987, **109**, 1586.
210. A. Patel, M. R. McMahon and D. T. Richens, *Inorg. Chim. Acta*, 1989, **163**, 73.
211. C. M. Tourné, G. F. Tourné and F. Zonnevijlle, *J. Chem. Soc., Dalton Trans.*, 1991, 143.
212. R. G. Finke, B. Rapko, R. J. Saxton and P. J. Domaille, *J. Amer. Chem. Soc.*, 1986, **108**, 2947.
213. R. Benn, A. Rufinska, M. A. King, C. E. Osterberg and T. G. Richmond, *J. Organomet. Chem.*, 1989, **376**, 359.
214. R. Benn and A. Rufinska, *Magn. Reson. Chem.*, 1988, **26**, 895.
215. J. L. Templeton, C. C. Phillipp, P. S. Pregosin and H. Ruegger, *Magn. Reson. Chem.*, 1993, **31**, 58.
216. A. Macchioni, P. S. Pregosin, H. Ruegger, G. van Koten, P. A. van der Schaaf and R. A. T. M. Abbenhuis, *Magn. Reson. Chem.*, 1994, **32**, 235.
217. M. Sekino, M. Sato, A. Nagasawa and K. Kikuchi, *Organometallics*, 1994, **13**, 1451.
218. W. Clegg, R. J. Errington, P. Kraxner and C. Redshaw, *J. Chem. Soc., Dalton Trans.*, 1992, 1431.
219. M. A. Dobson and D. F. Holcomb, *Phys. Rev. B: Condens. Matter*, 1986, **34**, 25.
220. F. Tautelle, *Nato ASI Ser., Ser. C.*, 1990, **322**, 293.
221. R. A. Wind, *Pract. Spectrosc.*, 1991, **11**, 53.
222. J. L. Dye, A. S. Ellaboudy and J. Kim, *Pract. Spectrosc.*, 1991, **11**, 217.
223. J. Haase and H. Pfeifer, *J. Magn. Reson.*, 1990, **86**, 217.
224. John Christian Edwards, *Diss. Abstr. Int. B*, 1991, **51**, 5887.
225. J. C. Edwards and P. D. Ellis, *Langmuir*, 1991, **7**, 2117.
226. Oc. Hee Han, C. Y. Lin and G. Haller, *Catal. Lett.*, 1992, **14**, 1.
227. Oc. Hee Han, C. Y. Lin and G. Haller, *Prepr. -Am. Chem. Soc., Div. Pet. Chem.*, 1992, **37**, 988.
228. L. H. Merwin and A. Sebalb, *Solid State Nucl. Reson.*, 1992, **1**, 45.
229. C. T. G. Knight, G. L. Turner, R. J. Kirkpatrick and E. Oldfield, *J. Am. Chem. Soc.*, 1986, **108**, 7426.
230. M. Green, N. C. Norman, A. G. Orpen and C. J. Schaverien, *J. Chem. Soc., Dalton Trans.*, 1984, 2455.
231. L. Linteng and X. You, *Chin. Sci. Bull.*, 1993, **38**, 1358.
232. K. I. Hagen, C. M. Schwab, J. O. Edwards and D. A. Sweigart, *Inorg. Chem.*, 1986, **25**, 978.

APPENDIX

Abbreviations

acac	2,4-pentanedione
Alk	alkyl group

[9]aneN$_3$	1,4,7-triazacyclononane
[12]aneN$_3$	1,5,9-triazacyclododecane
[9]aneS$_3$	1,4,7-trithiacyclononane
Ar	aryl group
bipy	2,2′-bipyridine
Bu	butyl group
^{i}Bu	isobutyl group
^{n}Bu	normal butyl group
^{s}Bu	secondary butyl group
^{t}Bu	tertiary butyl group
Bz	benzyl group
cat	catechol
cht	cycloheptatriene
Cp	cyclopentadienide, C$_5$H$_5$
Cp*	pentamethylcyclopentadienide, C$_5$Me$_5$
Cy	cyclohexyl group
DBP	5-phenyldibenzophosphole
depe	1,2-bis(diethylphosphino)ethane
diars	1,2-phenylenebis(dimethylarsine)
dien	diethylenetriamine
DMF	*N*,*N*-dimethylformamide (HCONMe$_2$)
dmpe	1,2-bis(dimethylphosphino)ethane
DMSO	dimethylsulphoxide
dppm	bis(diphenylphosphino)methane
dppe	1,2-bis(diphenylphosphino)ethane
dppf	1,1′-bis(diphenylphosphino)ferrocene
dppp	1,3-bis(diphenylphosphino)propane
dppb	1,4-bis(diphenylphosphino)butane
dppent	1,5-bis(diphenylphosphino)pentane
dpph	1,6-bis(diphenylphosphino)hexane
dptpe	1,2-bis(di-p-tolylphosphino)ethane
dtc	dithiocarbamate
en	1,2-diaminoethane
Et	ethyl group
Et$_2$dtc	diethyldithiocarbamate
HB(3,5-Me$_2$Pz)$_3$	hydrotris(3,5-dimethyl-1-pyrazolyl)borate
ida	iminodiacetate
Me	methyl group
Me$_2$dtc	dimethyldithiocarbamate
Me$_3$[9]aneN$_3$	*N*, *N*′, *N*″-trimethyl-1,4,7-triazacyclononane
mes	mesitylene
NMP	*N*-methylpyrrole
nta	nitrilotriacetate
ox	oxalate

2-PAP	2-(phenylazo)pyridine
Ph	phenyl group
phen	1,10-phenanthroline
pip	piperidine
pn	1,2-diaminopropane
Pr	propyl group
^{i}Pr	isopropyl group
^{n}Pr	normal propyl group
PTA	1,3.5-triaza-7-phosphaadamantane
py	pyridine
pyr	pyrrole
pz	pyrazine
quin	quinoline
R	organic group
sae	dianion of 2-(salicylideneamino)ethanol
THF	tetrahydrofuran
TMEDA	*N*, *N*, *N'*, *N'*-tetramethylethylenediamine
tppe	1,1,2-tris(diphenylphosphino)ethane
triphos	bis(*o*-diphenylphosphinophenyl)phenylphosphine

Applications of Solid-state NMR in Oil Shale Research

FRANCIS P. MIKNIS

Western Research Institute, 365 North Ninth Street, Laramie, WY 82070, USA

1. INTRODUCTION

An oil shale can be defined as a compact rock of sedimentary origin with an ash content of more than 33% and containing organic matter that yields oil when destructively distilled, but not appreciably when extracted with ordinary solvents.[1] This is an operational definition. There is no geological, or chemical definition of an oil shale. The term is used mostly in an economic sense so that any shallow rock that yields a commercial amount of oil upon pyrolysis may be considered an oil shale. The key words are "commercial amount" because petroleum source rocks, which often contain only 1% organic matter, can produce commercial amounts of oil over geologic times. Conversely, oil shales must have a large enough fraction of organic matter to be of economic interest. The organic matter content of an oil shale should be *c.* 2.5 wt%, just to provide the calorific requirements necessary to heat

ANNUAL REPORTS ON NMR SPECTROSCOPY
VOLUME 33 ISBN 0-12-505333-9

the rock to *c.* 500°C in order to produce shale oils by thermal decomposition of the organic matter.[2] Below this amount of organic matter the rock cannot be a source of energy because it requires more energy to heat the rock than can be derived from the shale oil produced. A lower limit of 5% organic matter is sometimes used to define a commercial deposit,[2] although such a limit is subject to change, depending on prevailing economic conditions. An oil shale can be a petroleum source rock, if subjected to the proper burial conditions over geologic times, but a petroleum source rock at shallow depths is not an oil shale because of the requirement of organic matter richness.

Oil shales occur worldwide, span geologic time from Cambrian to present, and were deposited principally in large freshwater lakes (lacustrine environment), shallow seas and continental shelves (marine environment), and in small lakes, bogs and lagoons associated with coal-producing swamps (paludal environment).[3] Oil shale deposits occur in at least 50 countries and the estimated world supply of potential oil from shale is 5×10^{12} barrels. Shale oil industries in Scotland, Australia, France, Russia and China have been active since about 1860.[4] In Australia, France and Scotland oil shales have been the source of products similar to that obtained from petroleum. However, the discovery of petroleum in the United States in 1859, and elsewhere soon after, sounded the death knell for the economic production of shale oil and the situation remains much the same today. Limited, but continued use of oil shale as an energy resource has been made since about 1909 in China and 1916 in Russia. In Brazil, a pilot plant has been in operation since 1982 and has produced over a million barrels of shale oil. Oil shale is used for some power generation in Israel, and in Australia a new oil shale demonstration plant has been scheduled for construction in the near future.

In the United States, which has the most attractive oil shale reserves, interest in oil shale development has waxed and waned. This is partly because the richest oil shale reserves, the Green River Formation in Colorado, Utah and Wyoming, are on lands owned mostly by the US government and therefore are not available for commercial development. Tracts of oil shale lands in the Green River Formation were leased for commercial development in 1974 and the decade between 1974 and 1984 represented the greatest activity ever in oil shale research in the USA. Since then, interest has diminished and hardly any oil shale research is presently being conducted. Understandably, the plentiful supply and low cost of petroleum has suppressed the commercialization of oil shale and other fossil fuel conversion processes (tar sand processing and coal liquefaction).

There are two fractions of organic matter in oil shale: (1) *bitumen*, which is that fraction that is soluble in organic solvents; and (2) *kerogen*, which is that portion of the organic matter that is insoluble in common organic solvents. Generally, kerogen constitutes the major portion of the organic matter (around 90% or greater), and its insolubility is one reason why an

oil shale must be heated to produce liquid products. Because of the insolubility of kerogen, it has been very difficult to obtain information about its chemical structure and composition. Compositional data can be acquired after first carrying out laborious and time-consuming procedures to remove mineral and prepare kerogen concentrates.[5] For an introduction to oil shales and kerogen, the reader is referred to the various books and reviews that are available.[2,4–10]

The development of solid-state NMR techniques of cross-polarization (CP) and magic-angle spinning (MAS), *c.* 1976, was a great advance in characterizing and understanding the chemical nature of oil shales. With solid-state NMR, information is obtained about the carbon structure of the kerogen in oil shale without the need for preparation of kerogen concentrates. It is interesting that some of the first published CP/MAS ^{13}C NMR spectra were of coals[11,12] and oil shales,[13,14] materials that are largely insoluble and for which few good techniques existed at the time to probe the carbon structure of these fossil fuels. The main parameter obtained by CP/MAS is a measurement of the carbon aromaticity, i.e., the fraction of total carbon that is in aromatic (sp^2) carbon structures.

In this chapter, an introduction to solid-state NMR and its applications to the study of oil shales are presented. Emphasis is on applications of ^{13}C NMR, but for completeness some ^{1}H NMR studies are included. Examples from oil shale studies are used to illustrate these concepts. However, because most solid-state NMR studies of fossil fuels are of coals, some examples taken from the coal literature are used to illustrate some of the concepts. A number of books,[15–17] conferences and symposia proceedings,[18–20] and reviews[21–24] have been written about the use of solid-state NMR in fossil fuel and related research, to which the reader is referred for additional information.

2. ^{13}C NMR IN SOLIDS

In most forms of spectroscopy, sensitivity and resolution are primary concerns. This is particularly true for the observation of ^{13}C NMR spectra in solids such as oil shales. Because the ^{13}C isotope is about 1% naturally abundant, NMR sensitivity is already low. Coupled with the fact that a "rich" oil shale might contain only 10–15 wt% organic matter, the remaining being mineral matter, it becomes evident that signal averaging must be employed in order to observe an NMR signal. There are also other factors that must be considered for observation of NMR in solids: these are described in the next sections.

There are three major problems that must be overcome in order to acquire NMR spectra that provide useful information about the carbon structure of the organic matter in oil shales. These are: (1) the ^{1}H–^{13}C dipole–dipole interaction, (2) the chemical shift anisotropy, and (3) the long-spin lattice

relaxation times in solids. Problems (1) and (2) must be overcome to improve spectral resolution, (3) must be overcome to improve sensitivity.

The pursuit of sensitivity and resolution in the solid state has led to the variety of NMR techniques that are now available to the oil shale researcher. The development of these techniques is attributable to the development of ^{1}H–^{13}C cross-polarization,[25] coupled with magic-angle sample spinning.[26] The combination of these techniques solved a number of the problems associated with sensitivity and resolution of ^{13}C NMR in solids. Cross-polarization overcomes some of the problems associated with sensitivity while magic-angle spinning overcomes some problems of resolution.

2.1. High-power decoupling

In solids, the major source of line broadening for ^{13}C is the dipole–dipole interaction between a nearby proton, ^{1}H, and the ^{13}C nucleus. The interaction is of the form

$$H_{loc} \alpha \mu_h (1 - 3\cos^2\phi)/r^3 \quad (1)$$

where μ_h is the magnetic moment of the proton, r is the internuclear distance between the proton and the ^{13}C nucleus, and ϕ is the angle between r and the applied magnetic, H_0. Because of the dipolar interaction, the ^{13}C nucleus experiences a local magnetic field, H_{loc}, given by equation (1) that adds to or subtracts from the main field, H_0. The strength of the interaction depends on the third power of the separation between the nuclei, so that carbons that have protons attached feel a strong dipolar interaction. The net result of this interaction is a ^{13}C NMR spectrum that is very broad and featureless because of the large number of protons that would be strongly coupled to the carbons in a solid.

The line broadening caused by ^{1}H–^{13}C interactions is largely eliminated by irradiating the ^{1}H nuclei with a strong radio-frequency field at their Larmor (resonance) frequency. This induces rapid transitions between the proton energy levels, i.e., spin flips, so that the protons cannot interact strongly with the ^{13}C nucleus. Thus, the ^{13}C nuclei do not feel the strong dipolar interaction because they have been decoupled from the protons. Hence the term high-power decoupling.

2.2. Magic-angle spinning

While high-power proton (^{1}H) decoupling removes the dipolar line-broadening, the ^{13}C NMR spectra of solids are still much broader than those of corresponding solution spectra. This residual broadening is due to chemical

shift anisotropy (CSA), and without its removal the spectral lines exhibit anisotropic line shapes that prevent resolution of carbon types useful for structural studies.

The chemical shift anisotropy arises from the nonspherical electron density around the ^{13}C nuclei, and is particularly prominent for aromatic and carbonyl (C=O) carbon types. These carbon types experience different shieldings of the magnetic field depending on whether the bond axes are parallel or perpendicular to the external magnetic field. For polycrystalline or amorphous materials all orientations are possible, including these two extremes.

The CSA is removed by spinning the sample at an angle of 54.7° with the external magnetic field. In the theoretical description of chemical shift anisotropy, the broadening is proportional to a term, $3\cos^2\phi$-1. The angle, 54.7°, makes this term zero, hence removing the broadening from chemical shift anisotropy. However, simply orienting the sample at this angle in the magnetic field is not sufficient. The sample must be rotated about this axis at a rate comparable to the magnitude of the CSA broadening, which for aromatic and carbonyl carbons can be the entire width of the chemical shift range, i.e. *c.* 200 p.p.m. This has important consequences on the strength of the magnetic field used to observe ^{13}C signals in solids such as oil shales. For example, for a magnetic field strength of 2.3 *T*, equivalent to a ^{13}C NMR frequency of 25 MHz, 200 p.p.m. corresponds to 5000 Hz. This means that to remove the CSA the sample must be spun about the magic-angle axis at the rate of 5000 revolutions per second. For a field strength twice this (50 MHz ^{13}C frequency), the spinning rate would have to be twice as great, i.e., 10 000 Hz. Although such rates are achievable, most CP/MAS ^{13}C NMR spectra of oil shales and coals have been acquired using field strengths of 1.4–2.3 *T* and spinning rates of *c.* 3–4 kHz. Increases in sensitivity that might be gained at higher fields are offset by the use of large-volume spinners at the lower fields.[27,28]

The effect of magic-angle spinning on the ^{13}C NMR spectra of oil shales is shown in Fig. 1. The improvement in resolution is clearly evident, particularly for shales that have a sizable aromatic component. This is because aromatic carbons have a larger chemical shift anisotropy than the aliphatic carbons. In the absence of spinning, the aromatic carbons yield broad anisotropic line shapes. Note also that for the spinning spectra, the maximum intensity of the aromatic band shifts to the isotropic value, which lies between the perpendicular and parallel components of the chemical shift tensor.

If the sample rotation is not fast enough to remove the chemical shift anisotropy artefacts, known as spinning sidebands, are introduced in the spectra which can interfere with the measurements of the carbon signal intensities. An example of the effect of sidebands on CP/MAS spectra of a coal for different field strengths is shown in Fig. 2.[29] All spectra were

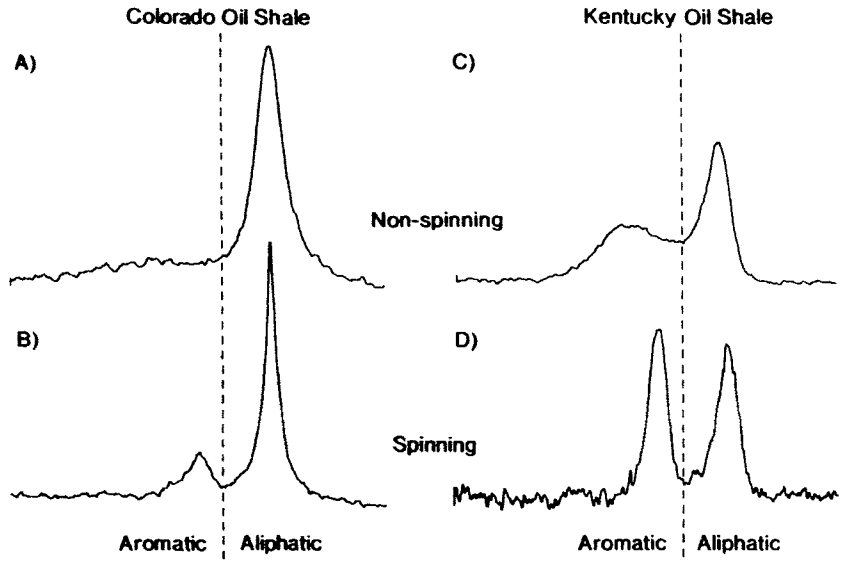

Fig. 1. Effect of magic-angle spinning on the ^{13}C NMR spectra of oil shales. (A) Colorado oil shale non-spinning; (B) Colorado oil shale spinning; (C) Kentucky oil shale non-spinning; (D) Kentucky oil shale spinning.

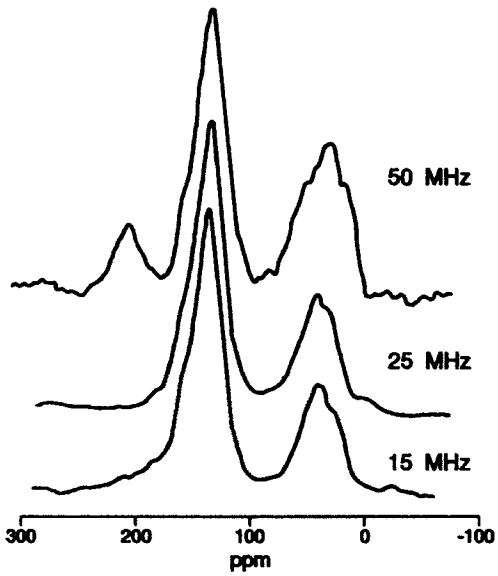

Fig. 2. Comparison of NMR spectra of Powhatan coal obtained at 15.1, 24.1 and 50.3 MHz. (Reprinted with permission of Sullivan and Maciel,[29] © 1982, American Chemical Society.)

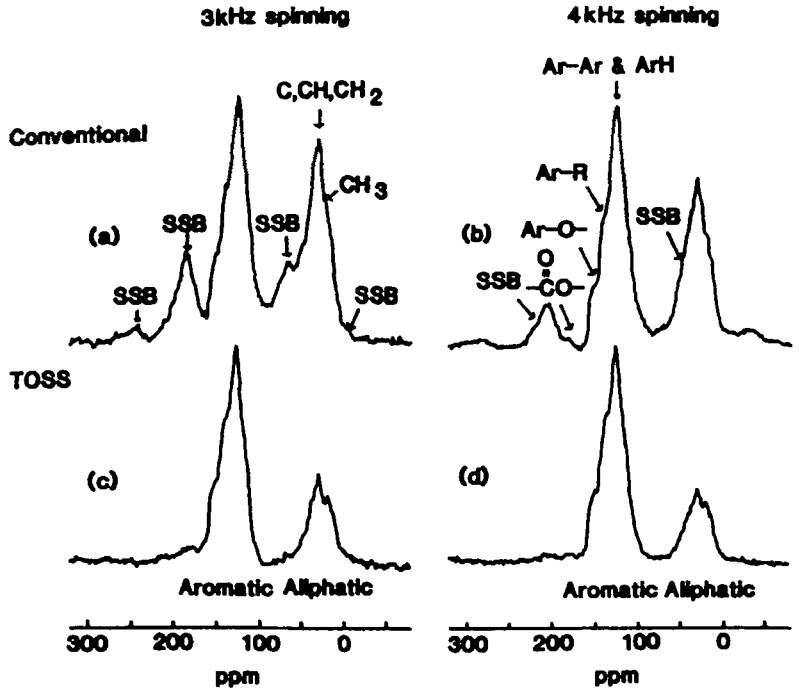

Fig. 3. Use of TOSS to suppress sidebands in Illinois No. 6 coal. (a) 3 kHz spinning without TOSS, (b) 4 kHz spinning without TOSS, (c) 3 kHz spinning without TOSS, (d) 4 kHz spinning with TOSS. (Reprinted with permission of Adachi and Nakazimo,[31] American Chemical Society © 1993.)

recorded at a spinning rate of 4.2 kHz. The aromatic carbon sidebands occur at ≈300 and ≈−30 p.p.m. in the 15 MHz spectrum, and do not interfere with the aliphatic signal intensity. At 25 MHz the high-field sideband appears as a shoulder in the aliphatic carbon region near 0 p.p.m. However, at 50 MHz, the high-field sideband is under the aliphatic carbon envelope, and thus gives a nonrepresentative aliphatic carbon resonance. The sidebands are symmetrical about the respective aromatic carbons giving rise to the signal, so that the position of the interfering sideband under the aliphatic envelope can be inferred from the position of the low-field sideband. The low-field sideband is the prominent band slightly above 200 p.p.m.

A number of ingenious pulse techniques have been devised to eliminate sidebands from high-field spectra so that "normal" CP/MAS spectra are generated.[30] These are referred to as PASS (Phase Alternated Sideband Suppression) and TOSS (TOtal Sideband Suppression) techniques. An example of the use of TOSS to suppress sidebands from the aromatic carbons in Illinois No. 6 coal is shown in Fig. 3.[31] Two different spinning rates were

used to acquire the CP/MAS spectra. The spectra were recorded at 50 MHz so that a 10 kHz spinning speed would be required to obtain CP/MAS spectra free of spinning sidebands. The apparent advantages of using TOSS to suppress sidebands is evident. However, the spectra are misleading because of the quantitative reliability of the carbon intensities in these spectra.[15,27,32] Advantages and disadvantages of the sideband removal pulse sequences have been discussed elsewhere.[15]

The main reason for acquiring NMR spectra of oil shales and coals at higher magnetic fields is that, in principle, greater resolution and sensitivity should be achievable at the higher fields. In practice, this need not be the case, as demonstrated in Fig. 2, which shows comparable resolution for 15 MHz and 50 MHz spectra, respectively. Oil shale spectra, especially those of raw shales, typically yield only broad aliphatic and aromatic components so that higher fields may not provide any benefits in resolution. There is a gain in sensitivity in going to higher fields,[29] but this is partly offset by the fact that smaller sample sizes must be used to achieve the higher spinning rates needed to remove the sidebands. The use of large-volume spinners[27,33,34] at lower fields compensates for the gains in sensitivity at higher fields. The use of large-volume spinners is increasing, mainly because single-pulse spectra can be acquired in reasonable times using these spinners. For quantitative work, single-pulse measurements have been recommended over CP/MAS measurements.[27,35,36]

2.3. Cross-polarization of the ^{1}H–^{13}C spin system

Because ^{13}C has a low natural abundance, NMR measurements on this nucleus require signal averaging. The spin lattice relaxation time, T_1, determines how rapidly a single-pulse ^{13}C NMR experiment can be repeated. The rule of thumb is to repeat the experiment every $3T_1$ to $5T_1$ so that >95% of the equilibrium signal intensity is established between pulses. If we suppose that the T_1 of a ^{13}C nucleus is 2 min, the single-pulse experiment would be repeated every 6 to 10 min. If 1000 signals must be accumulated to obtain a reasonable signal-to-noise (S/N) ratio, the total experiment time would be between 100 and 167 h. Fortunately, cross-polarization overcomes the problems of the long T_1s and consequent limited sensitivity.

Cross-polarization NMR relies on the presence of an abundant spin system (^{1}H) to enhance the observation of a signal from a dilute spin system (^{13}C). The idea is to transfer polarization (hence signal intensity) from the abundant ^{1}H spins to the dilute ^{13}C spins. The CP experiment consists of four basic timed sequences of radio-frequency (r.f.) pulses (Fig. 4). The left portions of Fig. 4 represent the experimental timing sequence and the right portions depict what happens to the nuclei in the sample under the action of the pulses. The four-part procedure consists of (1) polarization of the ^{1}H spin system,

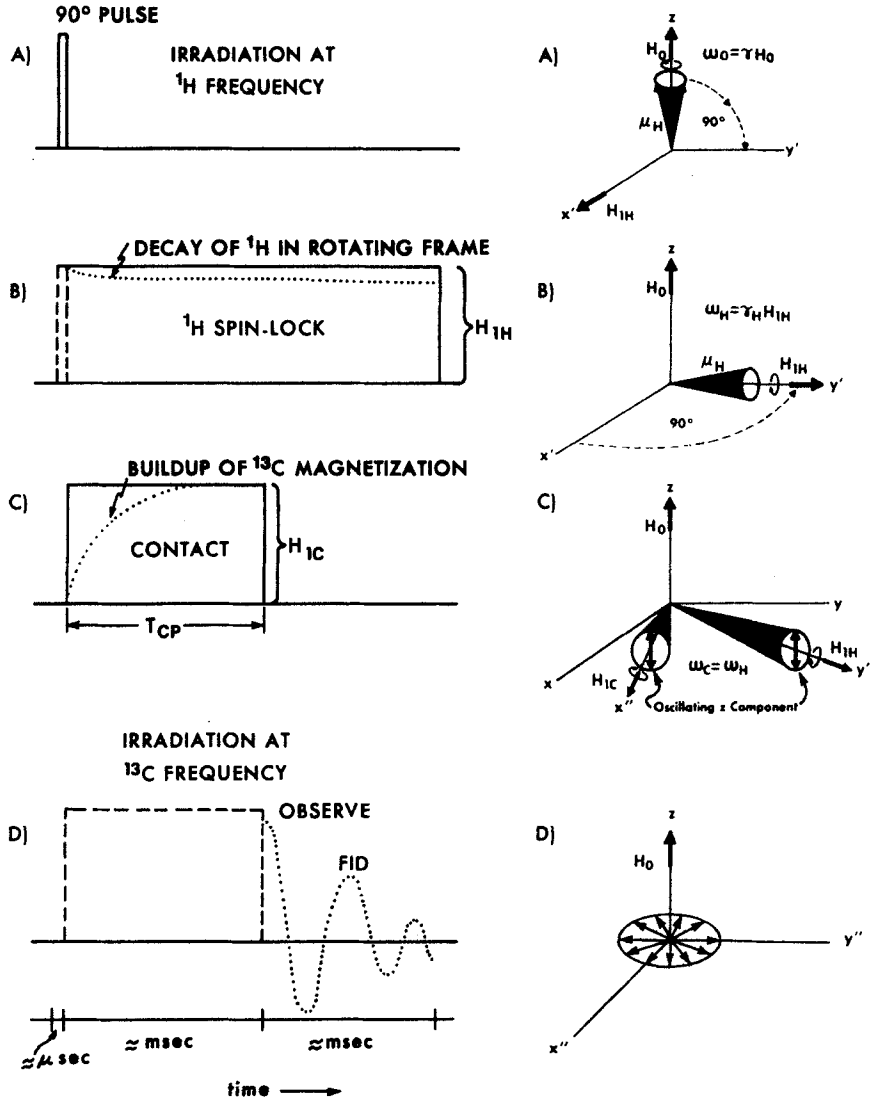

Fig. 4. Timing sequence of cross-polarization experiment: (a) polarization of ^{1}H in rotating frame; (b) spin locking of ^{1}H in rotating frame; (c) ^{13}C–^{1}H contact under Hartmann–Hahn conditions; and (d) observation of ^{13}C free induction decay. Left: timing sequence of CP experiment. Right: behaviour of nuclear spins. (Reprinted with permission from Miknis[23], © 1995, Kluwer Academic Publishers.)

(2) spin-locking in the rotating frame, (3) establishment of ^{13}C–^{1}H contact, and (4) observation of the ^{13}C free induction decay (FID).

The sample is "prepared" by applying a 90° pulse of intensity H_{1H} at the ^{1}H resonance frequency. The action of this pulse rotates the magnetization 90° into the $x'y'$ plane, along y'. Immediately after the 90° pulse, a 90° phase shift is applied to the field, H_{1H} to bring it colinear with the ^{1}H magnetization. This causes the protons to precess about H_{1H} at a frequency, $\omega_H = \gamma_H H_{1H}$. During the proton spin-lock, a second radio-frequency field, H_{1C} is applied at the ^{13}C resonance frequency. Although there may not be substantial ^{13}C magnetization initially, the ^{13}C nuclei in the sample will precess about H_{1C} at a frequency, $\omega_c = \gamma_C H_{1C}$. By adjusting the power levels so that $\gamma_H H_{1H} = \gamma_C H_{1C}$, then the frequencies of the oscillating components will be the same, i.e., $\omega_C = \omega_H$. By making $\omega_C = \omega_H$, a means is established to transfer efficiently magnetization from the abundant ^{1}H spins to the dilute ^{13}C spin system. This transfer is called cross-polarization. The Hartman–Hahn condition is maintained for a time, τ_{cp}, the contact time so that a significant build-up in ^{13}C magnetization (Fig. 4c, dotted line) is available for detection as a ^{13}C free induction decay (Fig. 4d, dotted line). The fourth part of the CP experiment is to terminate the ^{13}C pulse and observe the free induction decay, while maintaining the ^{1}H field for decoupling (Fig. 4d). The entire four-part procedure is repeated many times until a suitable signal-to-noise ratio for ^{13}C is obtained. The resultant FID is then Fourier transformed to give the more common frequency-domain spectrum. For solids, cross-polarization is far more efficient than ^{13}C spin-lattice relaxation, and a CP experiment can be repeated at intervals shorter than $3–5T_1$. For oil shales pulse repetition rates of 1 s and contact times of 1 ms are typical.

2.4. Dipolar dephasing

Solid-state ^{13}C NMR spectra of oil shales, obtained by CP/MAS with high-power decoupling are broad because of the multitude of resonances from the different carbon types found in these complex materials. A number of approaches have been taken to improve the resolution of solid-state NMR of fossil fuels.[15,22,24,29,37,38] Such techniques include variable temperature studies, variable frequency studies, mathematical enhancements and deconvolution techniques, and relaxation rate methods. The most popular method of enhancing solid-state NMR spectra is a relaxation rate method called dipolar dephasing (DD),[39] which is sometimes referred to as interrupted decoupling.[37,40] The exploitation of relaxation methods in CP NMR of fossil fuels has been reviewed elsewhere.[38]

Dipolar dephasing is a variation of cross-polarization; the timing sequence is shown in Fig. 5. The variation is the switching off of the ^{1}H decoupler for a time, t_1, after the cross-polarization contact time. During t_1, the signals

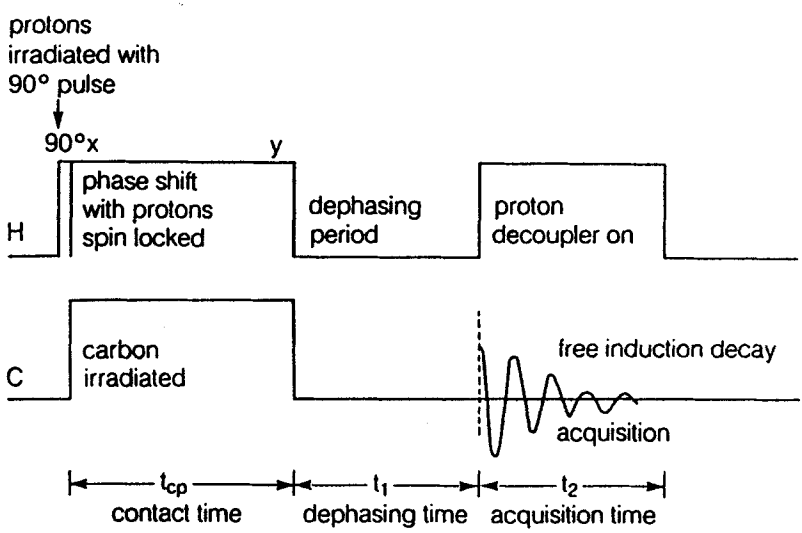

Fig. 5. Timing sequence for dipolar dephasing experiment.

from different carbon types decay at different rates depending on the strength of the ^1H–^{13}C dipolar interaction. The characteristic time for this decay is T_2, the spin–spin relaxation time. Carbons that are attached directly to hydrogen (primary, secondary, and tertiary carbons) experience strong ^1H–^{13}C interactions and decay more rapidly than carbons without attached hydrogen (quaternary carbons). When the decoupler is switched on after a time, t_1, the resultant signal is due primarily to quaternary (nonprotonated) carbons. However, methyl groups (CH_3) are not completely suppressed because of their rapid rotation in the solid state and appear in the aliphatic carbon signal. These carbons can be distinguished from the other quaternary aliphatic carbons on the basis of chemical shifts.

In the DD experiment, signals are recorded for a series of dephasing times, t_1, in order to establish the relaxation behaviour of the system. Generally, the signal decay is characterized by two components, a rapid and a slow relaxing component. The rapid decay is best characterized by a Gaussian or second-order exponential function, and the slow decay best fits with a Lorentzian or first-order exponential function (Fig. 6).[39]

In order to determine the amounts of protonated and nonprotonated carbons, the intensities of the various carbons must be extrapolated to zero dephasing time, $t_1 = 0$. The mathematical expression describing the signal decay is given by,

$$I(t_1) = I_g^0 \exp\ (-0.5(t_1/T_{2g})^2) + I_{l0} \exp\ (-t_1/T_{2l}) \qquad (2)$$

where the subscripts g and l refer to Gaussian and Lorentzian components,

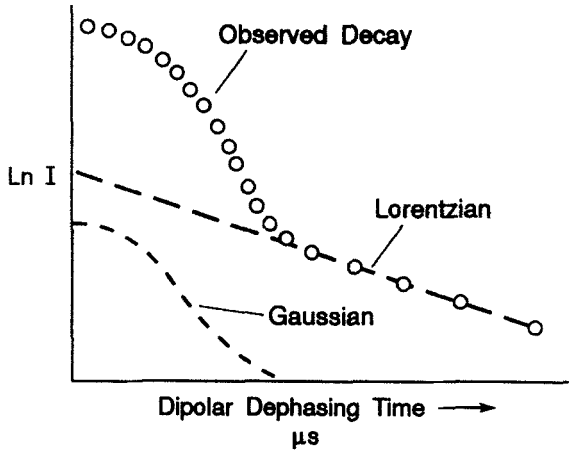

Fig. 6. Schematic representation of the Gaussian–Lorentzian two-component decay in a dipolar dephasing experiment.

respectively. At $t_1 = 0$, $I(0) = I_g^0 + I_l$, which is the signal intensity for a normal CP spectrum.

For a sufficiently long t_1 (>40 μs) the observed signal results from the Lorentzian component, so that equation (2) reduces to

$$I(t_1) \simeq \mathrm{I}_{10} \exp\ (-t_1/T_{2l}) \tag{3}$$

By extrapolating this curve to zero time, the contribution of nonprotonated carbons, I_l^0, to the total signal is obtained. The contribution of protonated carbons is obtained by difference,

$$I_g^0 = I\ (t_1 = 0) - I_l^0 \tag{4}$$

Some applications of dipolar dephasing to oil shales are discussed in the section 4.

3. QUANTIFICATION

3.1. Cross-polarization

The problem of quantification in cross-polarization has been recognized from the beginning of its application to fossil fuels,[12,13,15,24,41–48] has been debated,[49] and is still a concern in solid-state NMR.[27,35,36] The main concerns are whether all carbons are observed equally in the CP experiment, and whether the fraction of carbons observed at true signal intensity is a faithful

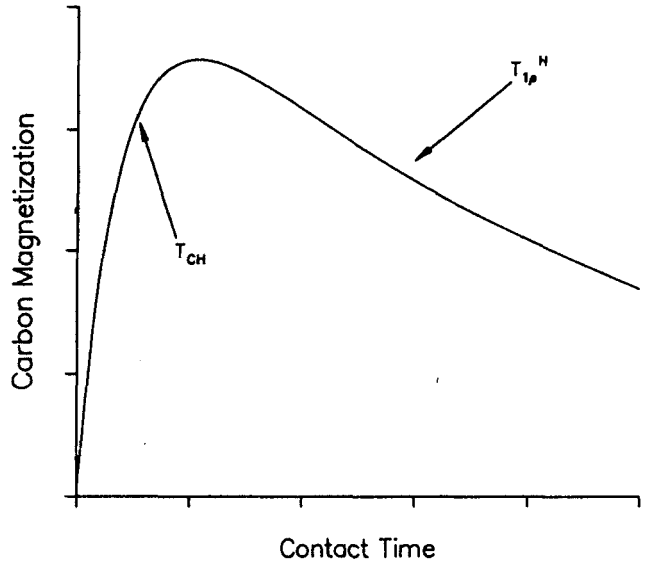

Fig. 7. Idealized behaviour of the carbon magnetization as a function of the experimental contact time in the cross-polarization experiment.

enough representation that the small loss of signal from unobserved carbons can be ignored. Other concerns relate to sample heterogeneity, spinning sidebands, unpaired electrons, magic-angle spinning, and the pulse repetition rate. The problems associated with quantification of ^{13}C NMR in carbonaceous solids have recently been reviewed.[27]

The build-up of signal during cross-polarization depends on two relaxation processes (Fig. 7), the cross-polarization transfer time, T_{CH}, and the proton spin-lattice relaxation time in the rotating frame, $T_{1\rho}^{H}$. Figure 7 shows that the ^{13}C signal intensity builds exponentially at a rate characteristic of T_{CH}, while at the same time the signal is being truncated by another exponential function, $T_{1\rho}^{H}$. The analytic form of the curve in Fig. 7 is,

$$M_t = M_0 \exp(-\tau_{CP}/T_{1\rho}^{H})(1 - \exp(b\tau_{CP}/T_{CH})) \quad (5)$$

where $b = 1 - T_{CH}/T_{1\rho}^{H}$. The condition $T_{CH} << \tau_{CP} << T_{1\rho}^{H}$ would be the ideal situation. On the instrument, the contact time, τ_{CP}, should be set at the time that corresponds to the maximum in the signal intensity.

Questions of quantification arise because different carbon types have different T_{CH}s and $T_{1\rho}^{H}$s. Generally, T_{CH} depends on the number of protons attached to the carbons. Thus, aliphatic carbons, aromatic carbons, and carboxylate carbons, for example, should all have different T_{CH}s. By observing the signal at a single contact time, the maximum signal intensity of all the carbon types may not be observed, in which case, nonrepresentative carbon

distributions would be measured. To overcome this problem, CP/MAS spectra should be recorded at different contact times in order to construct curves, such as in Fig. 7, for each carbon type.[41] By extrapolating the $T_{1\rho}^{H}$ curves to zero time, the correct signal intensity of each carbon type is obtained, from which the true carbon type distributions can be obtained.

In practice, generating carbon magnetization curves at different contact times can be time consuming. However, carbon aromaticities for source rocks from the Brent group (North Sea), acquired at a 1 ms contact time, have been compared with aromaticities obtained by varying the contact between 10 μs and 8 ms, and calculating the intensities by curve-fitting.[50] In seven out of eight cases, there was excellent agreement between aromaticities determined by the two methods. This led to the conclusion that a contact time of 1 ms can be used with confidence for source rock studies.

A variety of compounds have been mixed with oil shale and coals as internal standards to determine the percentage of carbons observed in CP and single-pulse NMR measurements.[41,42,51–55] In some cases, the spinner material, Delrin, has been used as an internal standard.[42] An excellent reference material is tetrakis (trimethyl silyl) silane (TKS).[52,53] Furthermore, treatment with samarium (II) iodide selectively reduces the free radical content which can lead to an increase in the percentage of observable carbon.[56] For example, treatment of Wyodak sub-bituminous coal with samarium (II) iodide has been shown to increase the percentage of observable carbons by 27%, leading to an increase in the carbon aromaticity of around 10% from 0.66 to 0.73.

3.2. Single-pulse excitation

Single-pulse excitation (SPE), also referred to as Bloch decay, can be employed as an independent verification of the quantitative reliability of CP/MAS aromaticity measurements. In SPE experiments, the NMR signal is observed after a 90° pulse using magic-angle spinning and high-power decoupling. The signals from SPE arise from relaxation mechanisms that differ from those in the CP experiment. Therefore, agreement between aromaticities from the two measurements indicates that both measurements are observing the same types and amounts of carbon. The SPE experiments do not have the sensitivity advantage of cross-polarization and, consequently, they require much longer times to record a spectrum of suitable quality. For example, a typical single-pulse dipolar dephasing experiment using 10 delays, 1000 scans, and a 20-s pulse repetition rate takes about 56 h.[36] However, the use of a large-volume sample spinner can offset much of this disadvantage.[33,42,57]

SPE experiments, as checks on the reliability of CP measurements of coals and oil shales, have been employed for some time.[58,59] However, such

Table 1. Carbon aromaticities and percentage of carbon observed in single-pulse and cross-polarization experiments.[a]

	Aromaticity		% Carbon Observed	
Sample	CP	SP	CP	SP
Resinite	0.16	0.15	105	100
Sporinite	0.56	0.57	90	90
Vitrinite (Illinois)	0.70	0.73	38	59
Fusinite	0.82	0.92	26	43
Lignite	0.55	0.58	55	65
Illinois hvC bituminous	0.67	0.67	56	73
Oklahoma mv bituminous	0.81	0.84	40	70

[a]Source: modified from Wilson *et al.*[41]

measurements were made without the use of spin counting techniques for quantifying the amounts of carbon observed in a CP and SPE experiments. Recent work[35,36,41–43] has demonstrated that generally more carbon is observed in SPE than in CP experiments on coals. The main reason is that paramagnetic centres cause the $T_{1\rho}^{H}$ of the protons to relax too quickly for efficient cross-polarization to be achieved. This is usually more of a problem with aromatic carbons. However, the relationship between aromaticities and observable carbon is not straightforward (Table 1). For example, SPE measurements detect more carbon and generally give higher aromaticities than CP measurements. However, the aromaticities observed by CP agree fairly well with SPE values, even though considerably less carbon is observed in the CP experiment. Greater discrepancies appear in the aromaticities of low-rank coals.[35] SPE measurements combined with dipolar dephasing also give higher values for nonprotonated aromatic carbons than CP with dipolar dephasing.[36]

Quantitative comparisons between CP and SPE experiments on oil shales have recently been made.[60] SPE and CP spectra (1 ms contact time) are shown in Fig. 8 for an oil shale from the Göynük deposit in Turkey, and an oil shale kerogen from the Kimmeridge deposit in the United Kingdom. The intense, narrow peak at 3.2 p.p.m. is TKS, the internal standard. Quantitative data are given in Table 2. The difference between sp^2 carbons is not that great for SPE and CP measurements for the more aromatic Kimmeridge kerogen; however, the differences are significant for Göynük oil shale. Because oil shales are generally aliphatic materials, one would expect aromaticity values that are more in agreement with those from SPE measurements because of better cross-polarization efficiency of the aliphatic carbons. Carbon aromaticities of most oil shales should probably lie between the resinite and sporinite values in Table 1. However, the data in Table 2 indicate that this is not the case, and care must be exercised when quantitative

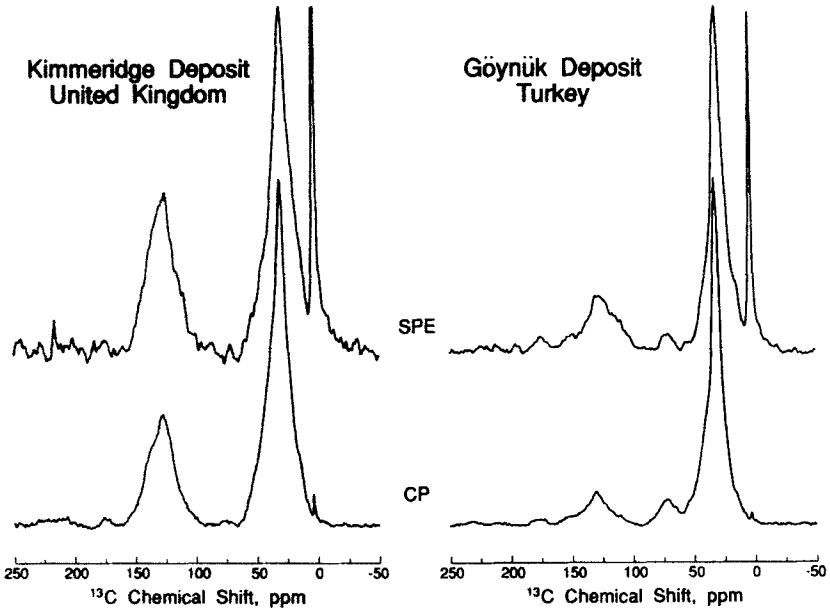

Fig. 8. Single-pulse excitation (SPE) and cross-polarization (CP) spectra of oil shales. (Reproduced, courtesy of C. E. Snape.)

Table 2. Single-pulse excitation (SPE) ^{13}C NMR spectra of oil shales.[a]

	Göynük		Kimmeridge	
	CP	SPE	CP	SPE
Aromaticity	0.14	0.24	0.30	0.37
Carboxyl/carbonyl	0.01	0.03	0.01	0.01
Total sp^2 carbon	0.15	0.27	0.31	0.38

[a]Source: C. E. Snape, personal communication.

measurements are required in oil shale studies. There is also a noticeable difference in the width of the aliphatic band for the CP versus the SPE spectra.

4. APPLICATIONS OF ^{13}C NMR

4.1. Oil shale resource evaluation

Probably the single most important item of information about an oil shale is its potential to produce oil during heating. The Fischer assay (American

Society for Testing Materials Method D3904-80) is the traditional method for determining the oil potential of an oil shale. The Fischer assay (FA) consists of heating a 100-g sample of −8 mesh (2.38 mm) particle size oil shale to 500°C at 12°C min^{-1} and maintaining this temperature for 40 min. During this heating cycle, hydrocarbon vapours are distilled from the rock and condense to form a shale oil. The material is collected and its volume, weight and specific gravity are recorded. From these measurements, the oil potential is reported in gallons (or litres) of oil per ton of shale: The greater the FA oil yield, the greater the commercial viability of the deposit.

The Fischer assay is strictly a specification test. It does not provide any information about the quality of the organic matter in the oil shale. Indirectly, it provides information about the quantity of organic matter in the shale. Nevertheless, it is the benchmark for evaluating an oil shale deposit, and also for determining the efficiencies of oil shale retorting processes. For issues involving exchange or leasing agreements of public oil shale lands in the western United States, the Fischer assay is the only accepted method to determine the value of the lands in question. Methods for analysing oil shale have been reviewed elsewhere.[61]

4.1.1. Oil shale assay methods

Because the Fischer assay does not provide information about what chemical properties of oil shales are important for producing liquids, a number of attempts have been made to correlate various chemical and physical property measurements with oil yields determined by the Fischer assay. The assay procedure has been modified for different types of oil shale, or to more closely resemble a certain type of retorting process.[62,63]

A summary of some methods for correlating oil shale properties with Fischer assay oil yields is given in Table 3. Except for the CP measurements, these assay schemes have one thing in common: they all measure, or attempt to measure, some parameter that can be related to the amount (quantity) of organic matter in an oil shale. While these methods might provide reasonably good correlations with oil yields, they are generally valid only for a specific deposit, and if the type of organic matter, or its composition does not vary significantly throughout the deposit. They do not provide much insight into what chemical structures are important for producing shale liquids during pyrolysis of oil shales.

4.1.2. Solid-state ^{13}C NMR measurements

As discussed above, CP/MAS measurements on coals[11,12] and oil shales[13,14] were among some of the first published applications of the techniques to solids. The main impetus for this was that the CP/MAS techniques provided information about the organic carbon structure in intractable solids such as

Table 3. Summary of methods of correlating kerogen properties with Fischer assay oil yields.[a]

Method	Property measured	Ref.
Elemental analysis	Organic carbon, total hydrogen	110, 111
Nuclear magnetic resonance (NMR)		
Pulsed NMR	Total hydrogen	88, 112, 113
Cross-polarization (CP)	Aliphatic/aromatic carbon distribution	64
CP with magic-angle spinning	Aliphatic/aromatic carbon distribution	51, 58, 65, 66, 75, 114
Electron spin resonance (ESR)	Unpaired electron concentration	115, 116
Laser pyrolysis	Acetylene yield	117, 118
Thermal analysis	Weight loss and evolved gases upon heating	119–120
Densimetric	Oil shale density	121, 122, 123
Thermophysical	Thermal conductivity, thermal diffusivity, relative dielectric constant	124–127
Fourier transform infrared spectroscopy	Aliphatic hydrogen	128

[a]Source: Miknis.[61]

coals and oil shales. In addition, the measurements are direct and nondestructive, and can be applied to whole rock samples without the need to prepare organic concentrates.

The importance of kerogen structure on the conversion behaviour of oil shales has been known for a long time.[6] However, it has only been since the development of solid-state ^{13}C nuclear magnetic resonance (NMR) techniques, that direct information about the carbon structure could be obtained. This is nicely illustrated by the CP/MAS ^{13}C NMR spectra shown in Fig. 9. Included in the figure are the Fischer assay oil yields and carbon conversion data. The CP/MAS ^{13}C NMR spectra provide a simple explanation for the conversion data. To produce liquids by pyrolysis, a source of hydrogen must be available to cap radicals and reduce the molecular weights of the fragments. (Colorado oil shale is highly aliphatic, therefore hydrogen rich, and produces higher oil yields; Kentucky oil shale has less aliphatic carbon and correspondingly has a lower conversion; Wyoming coal is the most aromatic (hydrogen deficient) and produces the least amount of conversion to liquid products.) This is a major reason why hydrogen must be added during coal liquefaction to produce liquids.

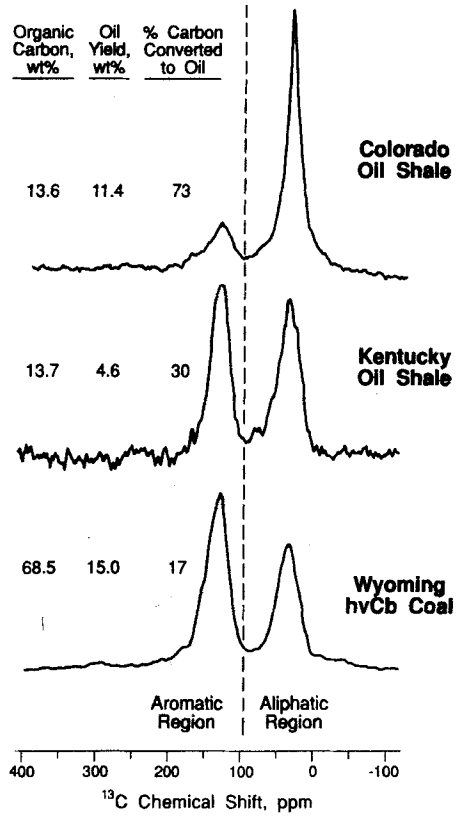

Fig. 9. CP/MAS ^{13}C NMR spectra of oil shales and coal, Fischer assay oil yield and per cent conversion of organic carbon to oil.

The implications of the data in Fig. 9 are that the aliphatic carbon moiety is largely responsible for producing liquids during heating of an oil shale. A number of studies have shown that the aliphatic carbon content of an oil shale correlates with the potential oil yield determined by the Fischer assay.[51,58,64–67] These correlations can be extended to include coals by substituting volatile matter for oil yields. A correlation between aliphatic carbon and volatile matter carbon is shown in Fig. 10a. For oil shales, volatile matter is the sum of the oil and the gas yields determined by Fischer assay. For the coals, volatile matter is obtained from the proximate analyses. Although the oil shale data are obtained at 500°C, and the coal volatile matter at 950°C, the correlation is very good, considering the extreme variations in carbon structure and carbon contents of the sample set. Coals of rank lignite to anthracite and oil shales (Fig. 10, filled circles) from different depositional environments and geologic ages are included in the sample set (Fig. 11).[65]

The scatter in the data around 20% aliphatic carbon is attributed to low-rank coals which evolve substantial amounts of CO_2 during heating. These carbons would not be expected to correlate with aliphatic carbons because the source of the CO_2 carbon is probably carboxylate carbons. It is obvious that there is no correlation between total organic carbon (quantity of organic matter) and volatile matter yields (Fig. 10b). It is also significant that, despite the range of organic matter types from widely different source materials and depositional environments, different aspects of the overall thermal decomposition of fossil fuels can be described by a single correlation based largely on NMR measurements. By using an internal standard the aliphatic carbon content can be correlated with oil yield without the need to determine organic carbon of the raw oil shale.[51]

Intuitively, one might expect that residue carbon should correlate with the aromatic carbons in the starting material because aromatic carbons are hydrogen deficient and are not prone to producing oil and gas during pyrolysis. This is indeed the case and the aromatic carbon content has also been shown to correlate with the carbon remaining on the residue after pyrolysis.[65,67–69] The correlation between residue and aromatic carbons is shown in Fig. 12a. For the oil shales, the residue carbon is that remaining on the spent shale after Fischer assay; for the coals, residue carbon is the fixed carbon obtained from proximate analysis. The data clearly show that aromatic carbons in either oil shales or coals prefer to remain in the residue during pyrolysis. The data also clearly show a poorer correlation between residue carbon and total carbon.

4.2. Oil shale conversion

The overall thermal decomposition of the organic matter (kerogen) in an oil shale can be expressed as a general process described by equation (6),

$$\text{Kerogen} \xrightarrow[\text{heat}]{} x\ \text{oil} + y\ \text{gas} + z\ \text{residue} \qquad (6)$$

where x, y, and z represent the stoichiometric amounts of their respective products that result from thermal decomposition of a unit mass of oil shale. For oil shale processing the objective is to optimize the amount of liquids formed and to minimize the amount of residue product. These amounts depend on process parameters such as temperature, residence times, heating atmosphere, particle size, etc., and also on the chemical structure of the

Fig. 10. Correlation between aliphatic carbon and volatile matter for oil shales (•) and coals (○, △) and vitrinite concentrates (+). (a) Volatile Matter vs Aliphatic Carbon, (b) Volatile Matter vs Total Organic Carbon.

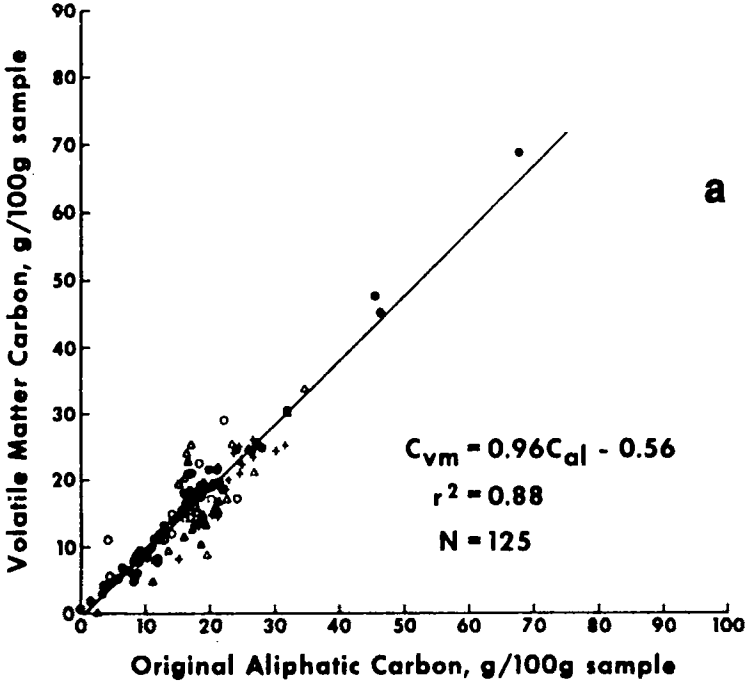
Volatile Matter Carbon, g/100g sample
Original Aliphatic Carbon, g/100g sample
$C_{vm} = 0.96C_{al} - 0.56$
$r^2 = 0.88$
N = 125
a

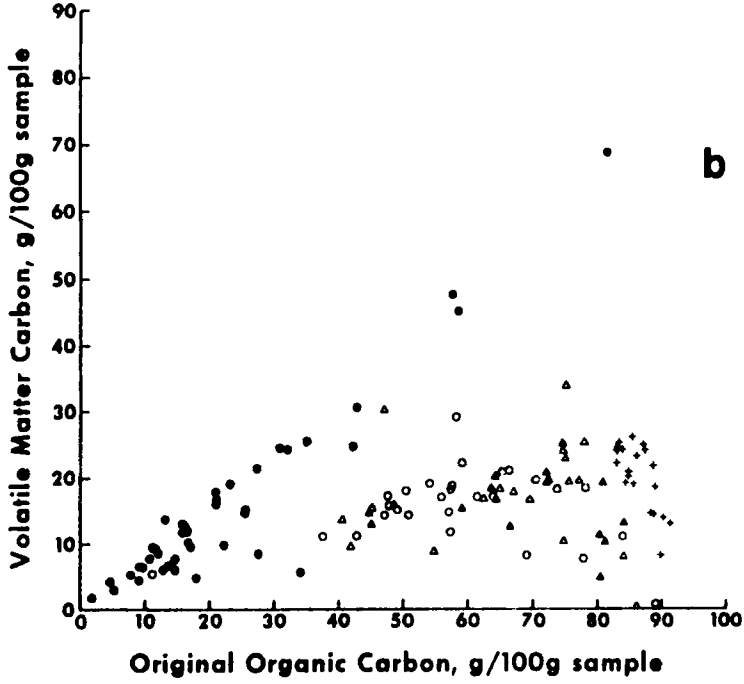
Volatile Matter Carbon, g/100g sample
Original Organic Carbon, g/100g sample
b

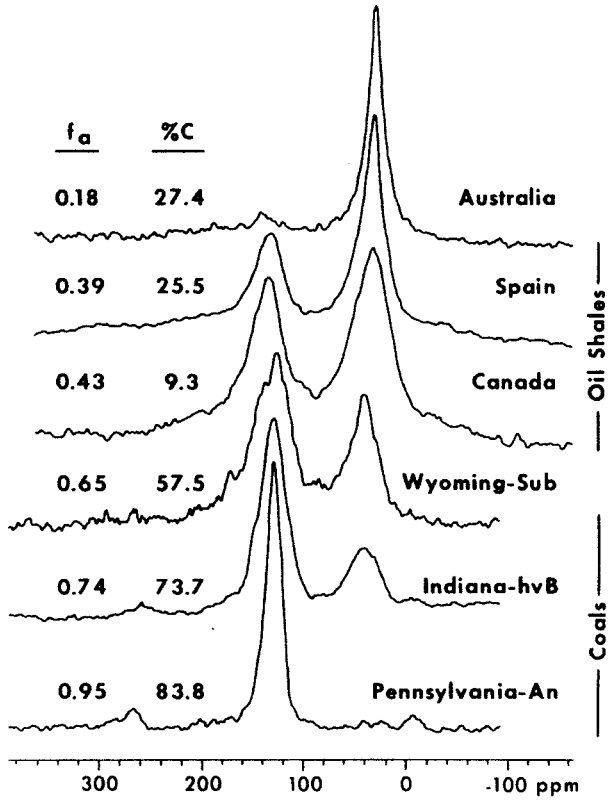

Fig. 11. CP/MAS ^{13}C NMR spectra of oil shales and coals illustrating variations in organic carbon structure: f_a, carbon aromaticity, %C as received organic carbon content. (Reprinted from Miknis and Conn[65] © 1986, with kind permission from Elsevier Science Ltd.)

kerogen as shown by the correlations in Figs 10 and 12. Solid-state NMR measurements provide insight into what happens when oil shales are heated to produce liquids. An example is shown in Fig. 13 for a Colorado oil shale heated for 24 h at the temperatures shown.[70] The decrease in the aliphatic carbon fraction relative to aromatic carbon fractions during oil and gas generation is clearly shown. The carbon remaining on the spent shale is almost exclusively aromatic carbon. The spectra in Fig. 13 are not normalized for weight loss and so the spectral intensities at the different temperatures

---

Fig. 12. Correlation between aromatic carbon and residue carbon for oil shales (•) and coals (○, △) and vitrinate concentrates (+). (a) Residue Carbon vs Aromatic Carbon; (b) Residue Carbon vs Total Organic Carbon. (Reprinted from Miknis and Conn[65], © 1986, with kind permission from Elsevier Science Ltd).

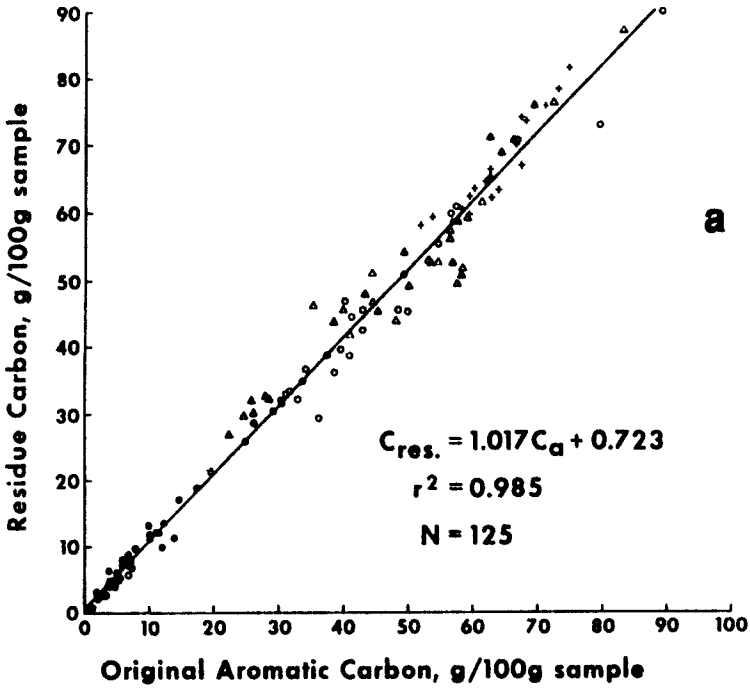
Residue Carbon, g/100g sample
Original Aromatic Carbon, g/100g sample
$C_{res.} = 1.017 C_a + 0.723$
$r^2 = 0.985$
N = 125
a
0
10
20
30
40
50
60
70
80
90
100

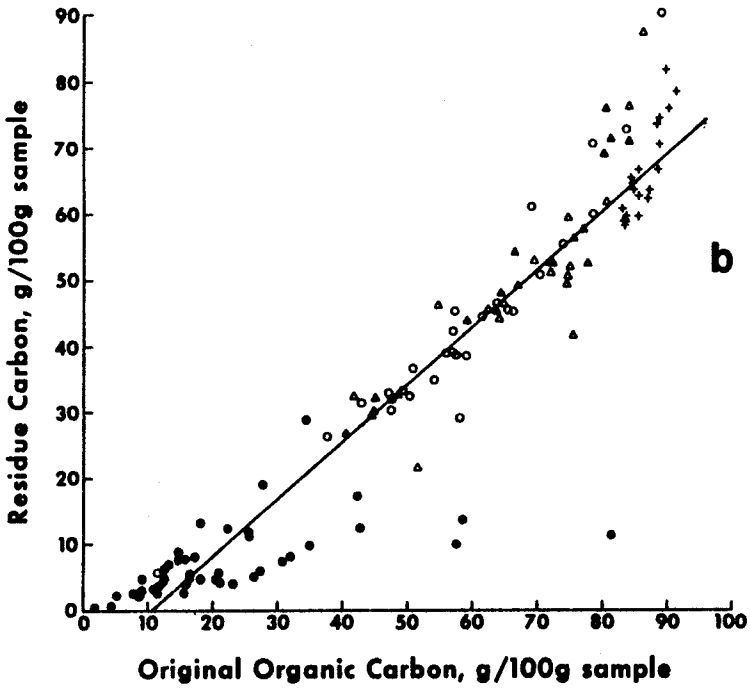
Residue Carbon, g/100g sample
Original Organic Carbon, g/100g sample
b
0
10
20
30
40
50
60
70
80
90
100

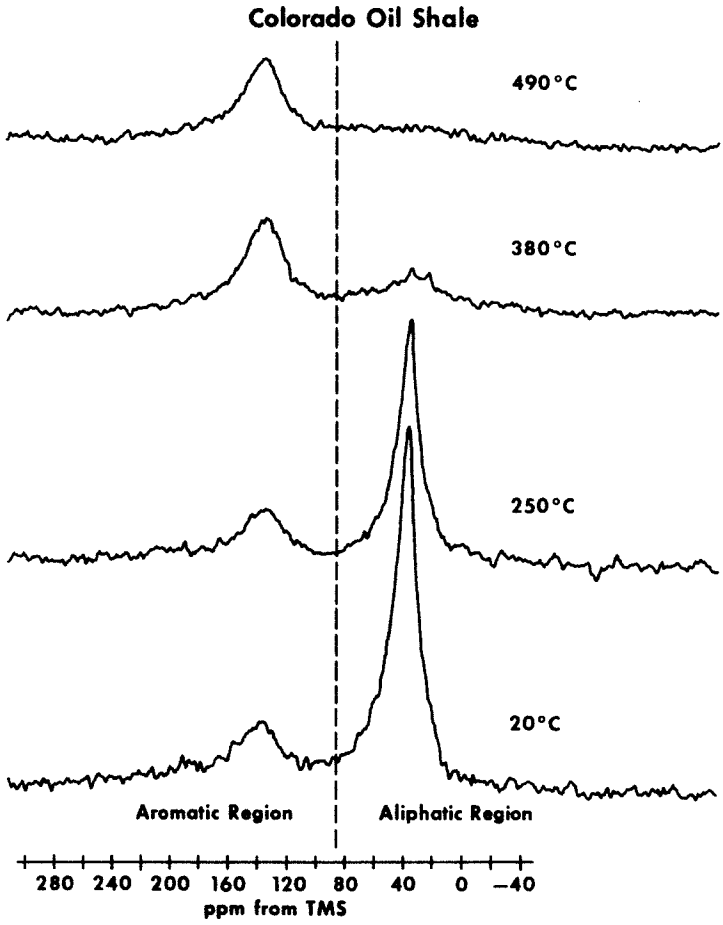

Fig. 13. CP/MAS ^{13}C NMR spectra of a Colorado oil shale heated to different temperatures for 24 h. (Reprinted from Miknis *et al.*[70], © 1982, with kind permission from Elsevier Sci. Ltd.)

cannot be compared quantitatively with that of the starting material. Therefore, how much of the aromatic carbon in the spent shale originated from aromatic carbon in the starting material and how much originated from aromatization of aliphatic carbon in the starting material cannot be determined without mass balance data.

By combining solid- and liquid-state ^{13}C NMR with elemental analyses and mass balance data, insight into some of the chemistry that occurs during oil shale conversion can be gained, which has practical applications in fossil fuel conversion processes. For example, during pyrolysis there is an increase in the amount of aromatic carbon in the products (oil plus residue) over that in the original shale.[71–73] This increase is produced at the expense of aliphatic carbon

moieties, which produce aromatic carbon either by dehydrogenation of hydroaromatic structures or by ring closure of alkyl groups followed by dehydrogenation.[74] Aromatization reactions are precursors to coke formation. Whether the aromatization reactions are initiated predominantly from the starting material or from a reaction intermediate affects the conversion behaviour of a fossil fuel, particularly for liquid generation. If the aliphatic carbons convert to aromatic carbons and remain in the solid residue, then this represents a loss mechanism for oil and gas generation. However, because the aromatic carbon in the oils can originate from either aromatic or aliphatic carbons in the starting material, there is no way to partition the aliphatic carbon that aromatizes between the oil and the residue. Nevertheless, measurement of the extent of aromatization of aliphatic carbons during processing can provide important information for understanding oil-generation processes and for process optimization. The number of aliphatic carbons that aromatize (C_a^{al}) is obtained by subtracting the total aliphatic carbon in the products (C_{al}^{P}) from the aliphatic carbon in the starting material (C_{al}^{0}),

$$C_a^{al} = C_{al}^{0} - \Sigma C_{al}^{P} \tag{7}$$

The aliphatic carbon in the products includes aliphatic carbon in gases (C_1–C_4 hydrocarbons), determined by gas chromatography (GC), and aliphatic carbon in the liquid and residue determined by liquid- and solid-state NMR, respectively.

NMR measurements have been combined with elemental and mass balance data to determine the extent of aromatization during pyrolysis.[71–73,75,76] Hershkowitz *et al.*[71] were the first to quantify the increase in the aromatic carbon formed during pyrolysis of Colorado oil shale. Their experiments were conducted at a slow heating rate, under high pressure (2600 kPa) N_2 or H_2 atmospheres, at temperatures up to 600°C, followed by a 10 min soak period at this temperature. In an N_2 atmosphere, the total aromatic carbon in the products increased by 83% over that in the raw shale. In H_2 the increase was only 17%. In addition, 87% of the raw shale carbon was recovered in the oil when heated under H_2, compared with 67% under N_2. An increase in aromatic carbon of about 83% has been observed in pyrolysis studies of Green River oil shale at heating rates of 1–720°C h^{-1} to 500°C.[72]

The aromatization of aliphatic carbon in oil shale and coal has been measured during isothermal pyrolysis at 425°C (Fig. 14).[73] As noted previously, the greater the number of aliphatic carbons in the starting material, the greater the total carbon conversion to oil and gas, and the fewer the number of aliphatic carbons that aromatize. During oil and gas generation free radicals that are formed by cracking reactions are capped by hydrogen atoms from the aliphatic carbon moieties, which results in some aromatization of the aliphatic carbons. In the absence of a hydrogen donor the oil shale or coal must supply its own hydrogen to form stable hydrocarbon liquids and

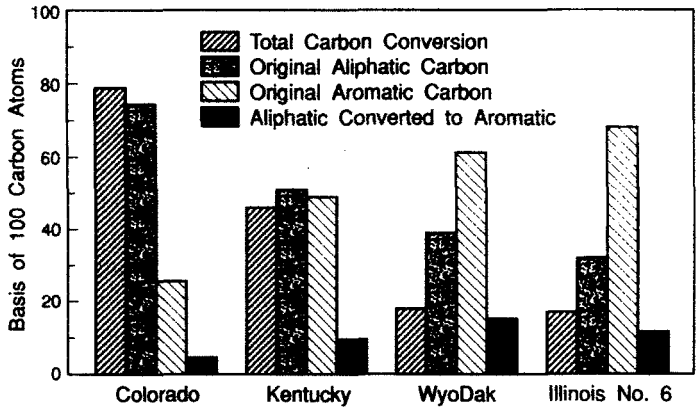

Fig. 14. Carbon conversion and aromatization of oil shales and coals during isothermal pyrolysis at 425°C for 60 min.

gases. For the Colorado oil shale the liquids produced are highly aliphatic and so therefore fewer hydrogen atoms per carbon removed are needed to cap radicals and to form stable products when long chain alkyl constituents are cleaved from the aromatic rings.

In coals, the alkyl sidechains are short, as are the bridges between rings and so there is less opportunity to form long-chain paraffinic products. Instead, more hydrogen atoms per carbon are required to cap radicals and to remove a smaller number of carbons in the gas and liquid products. The net effect is an inefficient use of hydrogen that results in aromatization of a significant fraction of the aliphatic carbons.

The effect of carbon structure on the conversion behaviour of oil shales has been described for a set of 10 oil shales from different deposits around the world.[75] For oil shales, with carbon aromaticities ranging from 16 to 49%, the amount of aliphatic carbon that aromatizes ranges from 0 to 42%. Shales with the lowest conversions to oil had the greatest extent of aromatization. Overall, between 10 and 20% of the aliphatic carbon ends up as aliphatic carbon in the residue, regardless of the carbon structure of the starting material. Although these carbons are not involved in coking reactions, they represent a loss in oil potential. These carbons are most likely short-chain aliphatic carbons (methyl, ethyl groups) attached to aromatic rings.

4.3. Structure studies

CP/MAS ^{13}C NMR spectra provide information about the carbon functionalities in oil shales. However, oil shales contain mostly mineral matter (>*c.* 85%) and the spectra usually consist mostly of a broad aliphatic

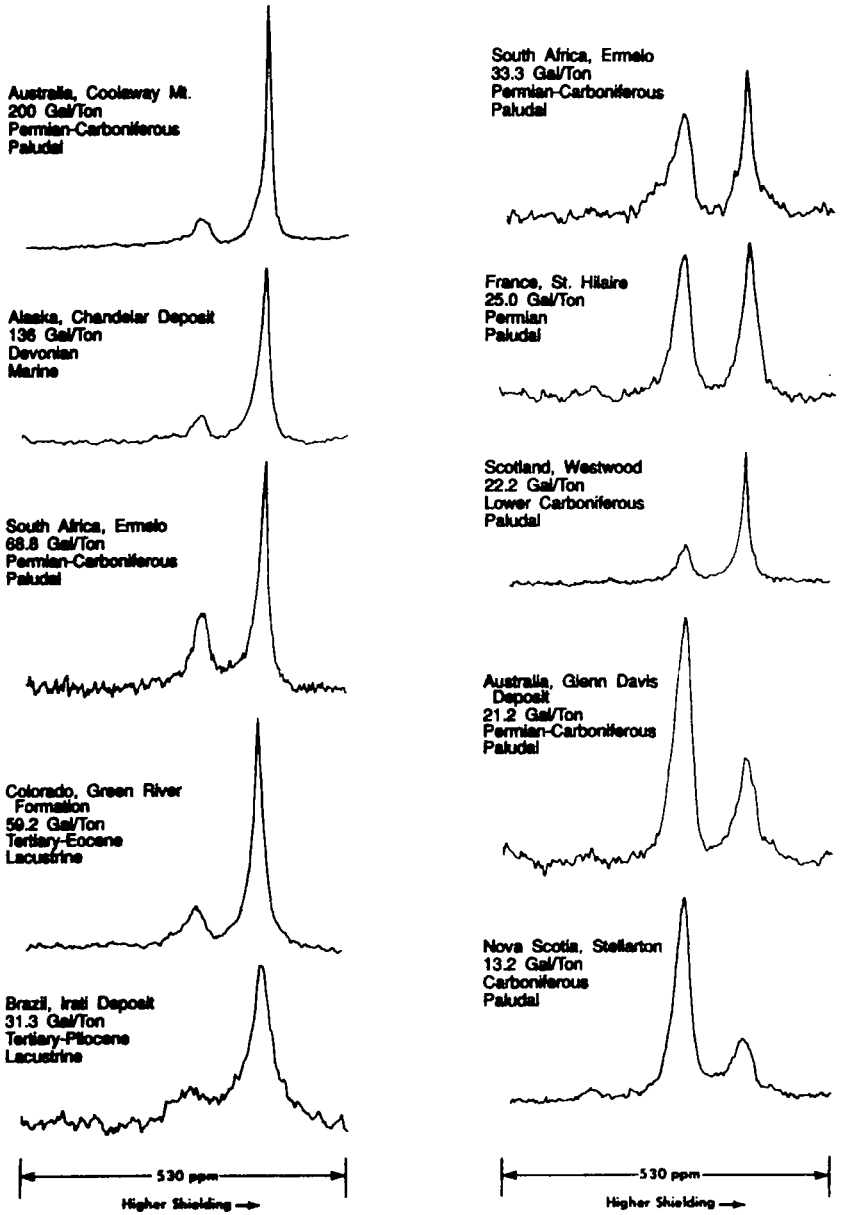

Fig. 15. CP/MAS ^{13}C NMR spectra of oil shales of different richness from different world deposits, depositional environments and geologic ages. (Reprinted from Miknis *et al.*,[59] © 1979, with kind permission from Elsevier Science Ltd.)

and a broad aromatic band. This is illustrated by the CP/MAS ^{13}C NMR spectra of oil shales from different worldwide deposits, geologic ages and depositional environments shown in Fig. 15. These spectra are typical of what is usually obtained for oil shales.

For more detailed studies of carbon structure, NMR spectra should be acquired on kerogen concentrates which are prepared by washing the sample with HCl/HF to remove the mineral matter[5]: carbonate minerals, if present, are removed by washing with HCl, silicates by treatment with HF. The effects of acid treatment on the NMR spectra of oil shales are shown in Fig. 16.[77] Spectra of kerogen concentrates are always sharper than those of raw shales. Even simple washing with HCl improves the quality of the spectra of oil shales,[34] particularly spent shales.[75] The sharper appearance of the spectra of the kerogen concentrates is mostly due to removal of paramagnetic impurities which, if present, generally broaden NMR signals.

As noted in Section 2.4 there are a number of ways to improve resolution in the NMR spectra of fossil fuels and to obtain additional structural parameters. Of these, the technique of dipolar dephasing has received the most attention. Dipolar dephasing provides information about the amounts of protonated and nonprotonated aromatic and aliphatic carbons in the sample, from which other structural parameters can be derived. Dipolar dephasing measurements have been made on raw oil shales[78] and kerogens[79–83] to elicit aspects of the carbon structure of these materials. The type of structural information that can be obtained is illustrated in Table 4. That the structural parameters for Tennessee and Kentucky oil shales are more similar to those of Wyodak coal is not too surprising, given the high aromaticities of these shales.

Curve fitting and dipolar dephasing techniques have been used to determine the amount and types of carbons in oil shale kerogens from different deposits and depositional environments.[80–83] Distinct differences were observed in the distribution of oxygen-containing, aromatic and aliphatic functionalities depending on the type of organic matter contributing to the sediment (algal/bacterial or terrestrial) and the depositional setting.[83] Although terrestrially derived kerogens had higher aromaticities than lacustrine or marine kerogens, the aromatic structure was less condensed. The aliphatic carbon distributions were basically the same for all kerogens, except for a sample of torbanite. NMR analyses have shown that Green River Formation oil shale kerogen is composed of long-chain aliphatic structures and polycondensed saturated ring structures, which although known from other measurements, have not been quantifiable without the use of solid-state NMR.[80] Similar results have been obtained for an oil shale kerogen from the Aleksinac deposit in Serbia.[82]

Normal CP/MAS, variable contact time and dipolar dephasing NMR measurements have been used to derive a set of 12 parameters related to the carbon skeletal structure of carbonaceous materials.[84] From the structural

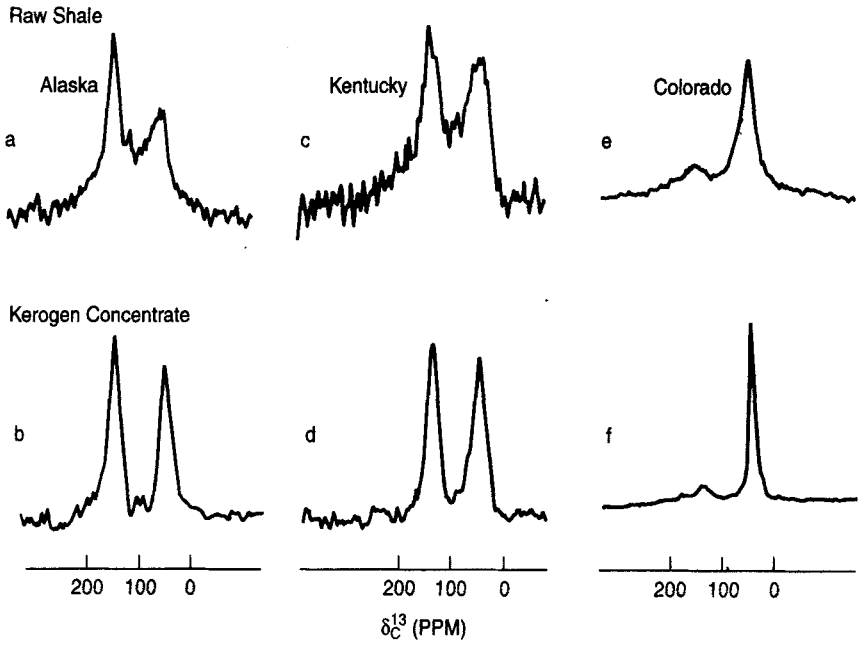

Fig. 16. The effects of acid treatment on the NMR spectra of oil shales. (Reprinted from Maciel and Dennis[77], © 1979, with kind permission from Elsevier Science Ltd.)

Table 4. NMR data and calculated results for coal and shale samples.[a]

	Wyodak coal	Green River shale	Chattanooga shale	New Albany shale
NMR data (relative areas)				
Total aromatic C	65	16	43	43
Quaternary aromatic C	46	12	32	28
Methyl plus quaternary aliphatic C	12	34	26	17
Carbon centre (mole fractions)				
Methyl	16	13	11	25
Aliphatic CH and CH_2	21	59	38	34
Quaternary aliphatic	0	11	7.8	0
Aromatic CH	19	4.2	11	14
Quaternary aromatic	45	12	32	27
Methyls per aromatic ring	1.5	4.9	1.6	3.7
Quaternary aromatics per ring	4.2	4.4	4.5	3.9
Minimum aliphatic chain length	2.2	7.0	5.1	2.2
Aliphatic chain length per methyl	2.4	6.3	5.1	2.2

[a]Source: Schmidt and Sheppard[78]

parameters, additional lattice parameters have been derived, including the mole fraction of bridgehead carbons in aromatic rings, the number of aromatic carbons per cluster, the number of attachments per cluster, the number of bridges and loops per cluster and the average molecular weight per cluster. Such structural and lattice parameter information makes NMR a useful tool in assessing fossil fuel conversion processes. The procedure has been used to characterize the structure of coals of different rank in the Argonne Premium Coal Sample Bank[84] and to monitor char structure evolution during rapid pyrolysis of coals.[85] The same procedure is applicable to oil shale, although it has yet to be applied.

The organic matter in a Rundle Ramsey Crossing oil shale from Queensland, Australia and a Green River Formation oil shale from Colorado, United States has been characterized in detail using a combination of NMR and chemical analyses.[86] Selective, nondestructive chemical derivatization with isotopic labelling followed by solid-state ^{13}C and ^{29}Si NMR were used to quantify the hydrocarbon, nitrogen and oxygen functionalities in these materials. From these analyses, molecular models of the kerogen structure were constructed (Fig. 17). The models agree well with experimental values for elemental composition, carbon aromaticity, distribution of chain lengths and ring system sizes, and hydrocarbon and heteroatom functionalities. The molecular models represent good examples of how NMR and chemical analyses can be combined to tackle complex structural problems for materials that are insoluble and largely intractable. The molecular models can be used to calculate other parameters. For example, solubility parameters calculated using the model of Green River kerogen agree closely with those determined experimentally from solvent-swelling studies.[87]

5. APPLICATIONS OF ^1H NMR STUDIES

5.1. Pulsed NMR assay

As noted in Table 2, the amount of organic hydrogen in an oil shale should be an indicator of the potential oil yield of an oil shale because the amount of available hydrogen is a key factor in producing liquids by pyrolysis. The amplitude of the NMR free induction decay, sampled after a 90° pulse, is proportional to the amount of hydrogen in the sample. By normalizing this signal for unit weight, oil yield correlations can be obtained.[88,89] A comparison between a Fischer assay oil yield histogram and a pulsed NMR hydrogen response histogram is shown in Fig. 18.[61] The NMR response, which is in arbitrary units, mimics quite faithfully the Fischer assay histogram. Some advantages of the NMR method are that it is rapid, nondestructive, and can be automated. It could be used for rapid screening of an oil shale deposit in the field. Disadvantages are the small sample sizes used, and

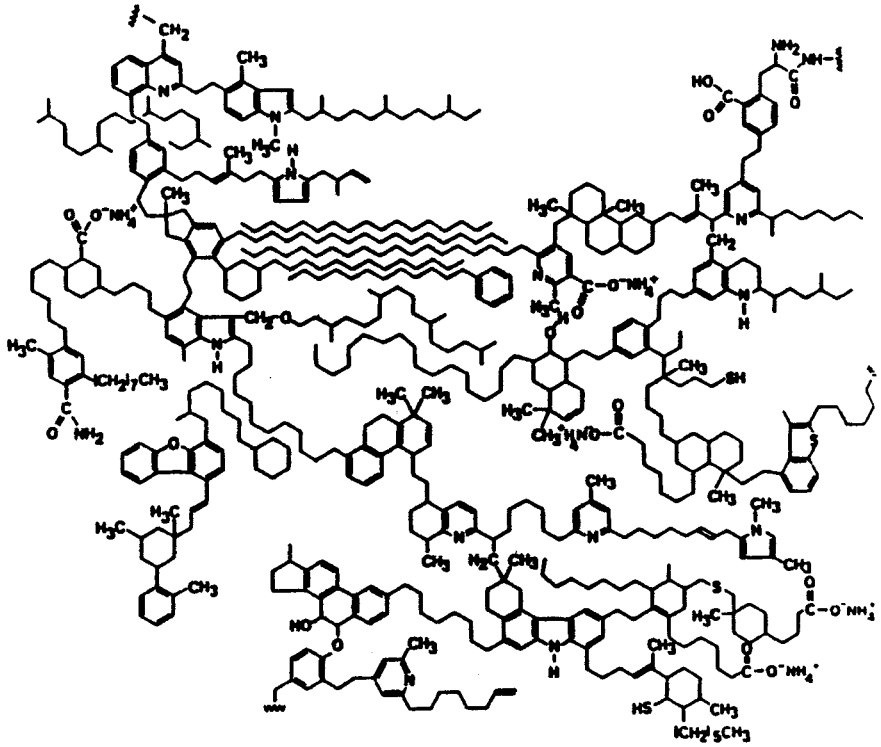

Fig. 17. Model of representative organic matter in Green River Formation oil shale. (Reprinted with permission from Siskin *et al.*,[86] ©1995, Kluwer Academic Publishers.)

interferences caused by water and other sources of inorganic protons such as clays and minerals. Because no structural information is obtained, calibrations must be obtained for each oil shale deposit.

5.2. Oil shale pyrolysis

Pulsed ^{1}H NMR measurements have been made as a function of temperature to study the pyrolysis behaviour of oil shales.[90–93] The method is sometimes referred to as ^{1}H NMR Thermal Scanning. To overcome receiver dead time, a 90–τ–90_{90} pulse sequence is used to form the "solid echo". The echo signal is then decomposed into a rigid (short relaxation time) and a mobile (longer relaxation time) component. These data are then related to various properties of the system. Parameters that can be extracted from the NMR data relate to the hydrogen content, phase structure, molecular mobility, and free radical content. By measuring the temperature dependence of these parameters

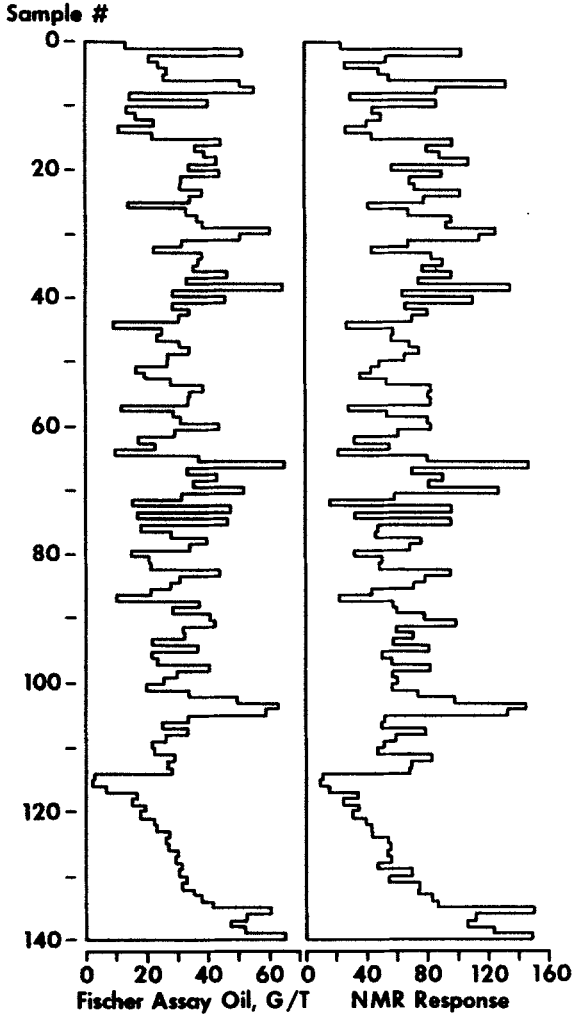

Fig. 18. Comparison of histograms of Fischer assay oil yields and pulsed NMR response for a set of 141 Colorado oil shales. (Reprinted with permission from Miknis,[61] © 1995, Kluwer Academic Publishers.)

some insight into the chemical and physical transformations that occur upon heating can be obtained.

A simple model of two parallel independent first-order reactions was found to closely describe the decomposition of an oil shale kerogen from the Rundle deposit in Australia.[92] The model was based on the fractions of mobile and rigid components in the kerogen, inferred from the ^{1}H NMR data. A major aspect of the model was that the macromolecular material in the oil shale kerogen had a bimodal distribution of cross-link density. During heating, a

broad glass-to-rubber transition occurs from room temperature to around 500 K, resulting in segmental mobility of the low cross-link density kerogen. Mobilization of the high cross-link density kerogen occurs between 600 and 800 K, also as a result of a glass-type transition, which overlaps with the thermal decomposition of the bulk kerogen. The ^{1}H NMR Thermal Scanning method has been applied to study the pyrolysis behaviour of oil shales from different Australian deposits and a Green River Formation kerogen.[93] A good account of high-temperature ESR and NMR methods applied to fossil fuels has been written.[94]

5.3. Multiple-pulse ^{1}H NMR

The most sensitive nucleus for detection by NMR is the proton or hydrogen nucleus, ^{1}H. However, obtaining "high resolution" ^{1}H NMR spectra of solids has been a formidable challenge, even though the use of ^{1}H NMR predates that of ^{13}C NMR. This is because the dominant line-broadening interaction is the homonuclear dipolar interaction between the ^{1}Hs themselves. Therefore, high-power decoupling cannot be used to remove this broadening mechanism. Magic-angle spinning could be used to average the dipolar interactions, but the spinning rates would have to be on the order of 27 kHz, a value in excess of what is currently available.[95] Instead, different NMR techniques have been developed to obtain "high"-resolution ^{1}H NMR spectra of solids. These techniques are referred to as multiple-pulse techniques.[96–100]

The basic principle behind the multiple-pulse NMR techniques to achieve line narrowing (i.e., eliminate the ^{1}H–^{1}H dipolar interaction) is to manipulate the ^{1}H spin system with r.f. pulses rather than by motion of the whole system, as is done with MAS. This manipulation is performed by using a series of well-timed r.f. pulses such that the average Hamiltonian over the entire period of the pulse sequence does not include the homonuclear dipolar interaction, but still maintains a scaled-down chemical shift effect. Because of the strict requirements on r.f. pulse widths, shapes, phasing and timing, the multiple-pulse techniques represent some of the most difficult solid-state NMR techniques to implement on a routine basis. The most popular multiple-pulse techniques are currently the eight-pulse MREV-8[97] and the 24-pulse BR-24 sequence.[98]

Although the multiple-pulse techniques eliminate the major ^{1}H line-broadening interaction, the ^{1}H–^{1}H dipolar interaction, the ^{1}H spectral lines still exhibit a residual line-broadening caused by the ^{1}H chemical shift anisotropy. For carbonaceous materials such as coals, this can be *c.* 16 p.p.m. This interaction can be eliminated by magic-angle spinning, and the combination of multiple-pulse techniques with magic-angle spinning is called CRAMPS (combined rotation and multiple-pulse spectroscopy).[99]

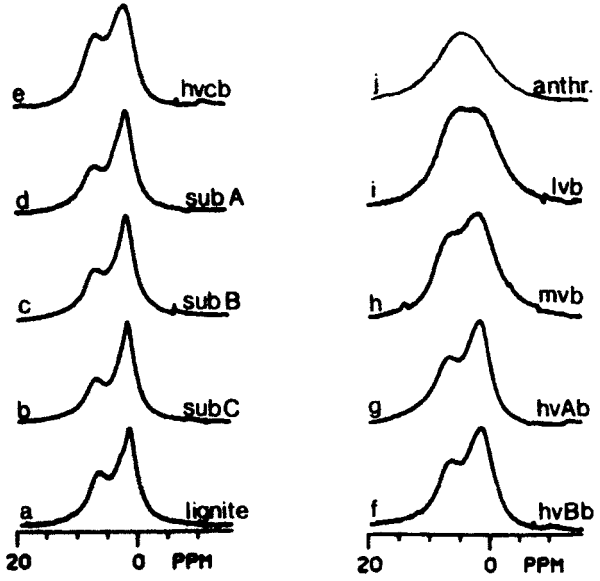

Fig. 19. ^{1}H CRAMPS spectra of coals of various rank; sub: subbituminous; hvb: high volatile bituminous; mvb: medium volatile bituminous; lvb: low volatile bituminous; anthr.: anthracite. (Reprinted from Bronniman and Maciel,[101] © 1989, with kind permission from Elsevier Science Ltd.)

In general, the CRAMPS ^{1}H NMR spectra of fossil fuel materials do not exhibit a high degree of resolution; this is because of the overlap of the multitude of resonances from the different ^{1}H types in these complex materials. ^{1}H CRAMPS spectra of 10 coals ranging in rank from lignite to anthracite are shown in Fig. 19.[101] These spectra illustrate the resolution typically obtained for carbonaceous materials. Estimates of the aliphatic and aromatic hydrogen contents can be obtained, but generally require computer-aided spectral deconvolution.

Some improvement in the resolution of CRAMPS spectra of coals has been achieved by saturating the coals with perdeuteropyridine.[28,43,55,95,102–105] The reasons for the improved resolution are not clear, but are thought to be due to some degree of susceptibility averaging when the pyridine molecules fill the voids in the coal structure and partially mobilize locally anisotropic moieties. However, the increase in resolution is not the same for all coals and generally decreases with increasing rank, i.e., the treatment is less effective with higher-rank coals.

CRAMPS dipolar dephasing experiments have also been carried out on coals.[105–107] The technique is more effective when combined with perdeuteropyridine saturation. By fitting the dephasing curves to Gaussian and

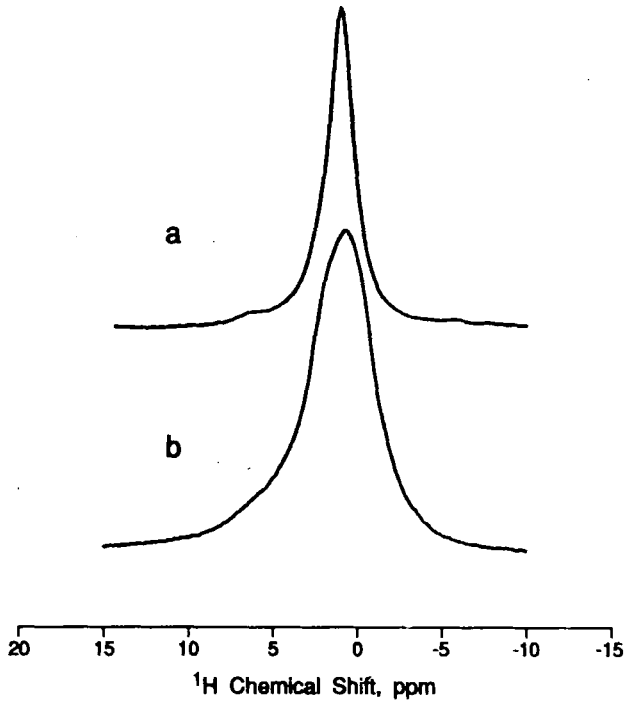

Fig. 20. ^{1}H CRAMPS spectra of (a) kerogen concentrate of Colorado oil shale, (b) Colorado oil shale. (Reprinted with permission from Maciel *et al.*,[95] © 1993, American Chemical Society.)

Lorentzian components, information about the mobilities and extractabilities of the molecular and macromolecular phases in coal was obtained.[104] The Gaussian component corresponded to the rigid macromolecular domain and the Lorentzian components corresponded to the more mobile components.

Other CRAMPS studies on fossil fuels have included the effects of thermal and chemical treatment on CRAMPS spectra of tar sands,[108] determination of the hydrogen distribution in coal macerals,[107] effects of water on CRAMPS spectra of coals,[109] and a comparison of proton aromaticities in coals and macerals determined by ^{1}H CRAMPS and ^{13}C dipolar dephasing methods.

With oil shales, the application of the CRAMPS technique is virtually nonexistent. To the author's knowledge, the only published CRAMPS spectra of an oil shale and its kerogen concentrate are shown in Fig. 20.[95] The ^{1}H spectra of the kerogen concentrate exhibit a narrower line width than the raw oil shale, analogous to that observed in the ^{13}C spectra (Fig. 16).

CONCLUDING REMARKS

Solid-state ^{13}C NMR techniques provide a powerful means by which to obtain information about the carbon structure of fossil fuel materials. Indeed, CP/MAS measurements have been applied to coals and oil shales almost from their inception around 1976. Solid-state NMR measurements are now made routinely in fossil fuel research, particularly in coal structure studies. For oil shales, solid-state NMR methods are particularly useful because the measurements can be made on raw shale, without the need to remove the mineral matter, which generally accounts for >85 wt% of the rock. However, because of the reduced emphasis in developing oil shale deposits commercially, applications of NMR in oil shale research are now not as common as in the past. Nevertheless, NMR measurements have provided valuable information about various aspects of oil shales. For example, the extent of aromatization of aliphatic carbon moieties during conversion can be obtained by combining solid- and liquid-state NMR measurements with mass balance data. Such information is difficult to obtain by other methods and provides insight into the chemical processes associated with fossil fuel conversion.

REFERENCES

1. J. M. Hunt, *Petroleum Geochemistry and Geology*, W. H. Freeman Co., San Francisco, 1979.
2. B. P. Tissot and D. H. Welte, *Petroleum Formation and Occurrence*, 2nd edition, Springer, Berlin, 1984.
3. D. C. Duncan, in *Oil Shale* (eds T. F. Yen and G. V. Chilingarian), pp. 13–26. Elsevier, New York, 1976.
4. P. L. Russell, *Oil Shales of the World: Their Occurrence and Exploitation*. Pergamon Press, New York, 1990.
5. B. Durand (ed.), *Kerogen*. Editions Technip, Paris, 1980.
6. T. F. Yen and G. V. Chilingarian (ed.), *Oil Shale*. Elsevier, New York, 1976.
7. I. A. Breger, *Organic Geochemistry*. Pergamon Press, London, 1963.
8. G. Eglinton and M. T. J. Murphy, *Organic Geochemistry*. Springer-Verlag, New York, 1969.
9. R. Pelet, in *Magnetic Resonance, Introduction, Advanced Methods, and Applications to Fossil Energy, NATO ASI Series C* (eds L. Petrakis and J. P. Fraissard), pp. 219–233. D. Reidel Pub. Co., Dordrecht, The Netherlands, 1984.
10. A. C. Hutton, in *Composition, Geochemistry and Conversion of Oil Shales, NATO ASI Series C* (ed. C. Snape), pp. 17–33. Kluwer Academic Publishers, Dordrecht, 1995.
11. D. L. vanderHart and H. L. Retcofsky, *Fuel*, 1976, **55**, 202.
12. V. J. Bartuska, G. E. Maciel, J. Schaefer and E. O. Stejskal, *Fuel*, 1977, **56**, 354.
13. H. A. Resing, A. N. Garroway and R. N. Hazlett, *Fuel*, 1978, **57**, 450.
14. F. P. Miknis and D. A. Netzel, in *Magnetic Resonance in Colloid and Interface Science, Symposium Series* (eds H. A. Resing and C. G. Wade), pp. 182–188. Am. Chem. Soc., Washington, DC, 1976.
15. D. E. Axelson, *Solid State Nuclear Magnetic Resonance of Solid Fossil Fuels*. Multiscience Publications Ltd. CANMET and Canadian Government Publishing Centre, Montreal, 1985.

16. C. A. Fyfe, *Solid State NMR For Chemists*. CFC Press, Guelph, Ontario, 1983.
17. M. A. Wilson, *NMR Techniques and Applications in Geochemistry and Soil Chemistry*, Pergamon Press, New York, 1987.
18. L. Petrakis and J. P. Fraissard (eds), *Magnetic Resonance, Introduction, Advanced Methods, and Applications to Fossil Energ., NATO ASI Series C., Vol. 124*. D. Reidel Pub. Co., Dordrecht, 1984.
19. R. L. Wershaw and M. A. Mikita (eds), *NMR of Humic Substances and Coal*. Lewis Publishers, Chelsea, MI, 1987.
20. R. E. Botto and Y. Sanada (eds), *Magnetic Resonance of Carbonaceous Solids, Adv. Chem. Ser. Vol. 229*. Am. Chem. Soc., Washington, DC, 1993.
21. F. P. Miknis, *Magnetic Reson. Reviews*, 1982, **7**, 87.
22. F. P. Miknis, in *New Trends in Coal Science, NATO ASI Series C* (ed. Y. Yürüm), pp. 117–158. Kluwer Academic Publishers, Dordrecht, 1988.
23. F. P. Miknis, in *Composition, Geochemistry, and Conversion of Oil Shales, NATO ASI Series C* (ed. C. Snape), pp. 69–91. Kluwer Academic Publishers, Dordrecht, 1995.
24. R. M. Davidson, *Report No. ICTIS/TR32*. IEA Coal Research, London, 1986.
25. A. Pines, M. G. Gibby and J. S. Waugh, *J. Chem. Phys.*, 1973, **54**, 569.
26. J. Schaefer and E. O. Stejskal, *J. Am. Chem. Soc.*, 1976, **98**, 569.
27. R. A. Wind, G. E. Maciel and R. E. Botto, in *Magnetic Resonance of Carbonaceous Solids, Adv. Chem. Ser.* (eds R. E. Botto and Y. Sanada), pp. 3–26. Am. Chem. Soc., Washington, DC, 1993.
28. G. E. Maciel and O. Erbatur, in *Nuclear Magnetic Resonance in Modern Technology, NATO ASI Ser. C*, pp. 165–224. Kluwer Scientific Publishers, Dordrecht, 1994.
29. M. J. Sullivan and G. E. Maciel, *Anal. Chem.*, 1982, **54**, 1615.
30. W. T. Dixon, *J. Magn. Reson.*, 1981, **44**, 220.
31. Y. Adachi and M. Nakamizo, in *Magnetic Resonance of Carbonaceous Solids, Adv. Chem. Series* (eds R. E. Botto and Y. Sanada), pp. 269–279. Am. Chem. Soc., Washington, DC, 1993.
32. M. J. Sullivan, in *Magnetic Resonance, Introduction, Advanced Methods, and Applications to Fossil Energy, NATO ASI Series C* (eds L. Petrakis and J. P. Fraissard), pp. 525–533. D. Reidel Pub. Co., Dordrecht, 1984.
33. M. Zhang and G. E. Maciel, *J. Magn. Reson.*, 1989, **25**, 156.
34. F. P. Miknis, Z.-S. Jiao, D. B. MacGowan and R. C. Surdam, *Org. Geochem.*, 1993, **20**, 339.
35. J. A. Franz and J. C. Linehan, in *Magnetic Resonance of Carbonaceous Solids, Adv. Chem. Ser* (eds R. E. Botto and Y. Sanada), pp. 377–400. Am. Chem. Soc., Washington, DC, 1993.
36. G. D. Love, R. V. Law and C. E. Snape, *Energy Fuels*, 1993, **7**, 639.
37. M. J. Sullivan and G. E. Maciel, *Anal. Chem.*, 1982, **54**, 1606.
38. M. A. Wilson, A. M. Vassallo and N. J. Russell, *Org. Geochem.*, 1983, **5**, 35.
39. P. D. Murphy, T. J. Cassady and B. C. Gerstein, *Fuel*, 1982, **61**, 1233.
40. S. J. Opella and M. H. Frey, *J. Am. Chem. Soc.*, 1979, **101**, 5854.
41. R. E. Botto, R. Wilson and R. E. Winans, *Energy Fuels*, 1987, **1**, 173.
42. M. Zhang and G. E. Maciel, *Fuel*, 1990, **69**, 557.
43. G. E. Maciel, C. E. Bronnimann, A. Jurkiewicz, R. A. Wind and V. H. Pan, *Fuel*, 1991, **70**, 925.
44. F. P. Miknis, M. J. Sullivan, V. J. Bartuska and G. E. Maciel, *Org. Geochem.*, 1981, **3**, 19.
45. R. L. Dudley and C. A. Fyfe, *Fuel*, 1982, **61**, 651.
46. K. J. Packer, R. K. Harris, A. M. Kenwright and C. E. Snape, *Fuel*, 1983, **62**, 999.
47. M. A. Wilson, P. J. Collin, R. J. Pugmire and D. M. Grant, *Fuel*, 1982, **61**, 959.
48. M. A. Wilson, A. M. Vassallo, P. J. Collin and H. Rottendorf, *Anal. Chem.*, 1984, **56**, 433.

49. C. E. Snape, D. E. Axelson, R. E. Botto, J. J. Delpeuch, P. Tekely, B. C. Gerstein, M. Pruski, G. E. Maciel and M. A. Wilson, *Fuel*, 1989, **68**, 547.
50. M. A. Wilson, A. Vassallo, D. Gizachew and E. Lafargue, *Org. Geochem*, 1991, **17**, 107.
51. E. W. Hagaman, F. M. Schell and D. C. Cronauer, *Fuel*, 1984, **63**, 915.
52. L. M. Stock, J. V. Muntean and R. E. Botto, in *New Trends in Coal Science, NATO ASI Series C* (ed. Y. Yurum), pp. 159–167. Kluwer Academic Publishers, Boston, 1988.
53. J. V. Muntean, L. M. Stock and R. E. Botto, *J. Magn. Reson.*, 1988, **76**, 540.
54. J. A. Franz, R. Garcia, J. C. Linehan, G. D. Love and C. E. Snape, *Energy Fuels*, 1992, **6**, 598.
55. A. Jurkiewicz, C. E. Bronnimann and G. E. Maciel, *Fuel*, 1994, **73**, 823.
56. J. V. Muntean, L. M. Stock and R. E. Botto, *Energy Fuels*, 1988, **2**, 108.
57. V. H. Pan and G. E. Maciel, *Fuel*, 1993, **72**, 451.
58. G. E. Maciel, V. J. Bartuska and F. P. Miknis, *Fuel*, 1979, **58**, 391.
59. F. P. Miknis, V. J. Bartuska and G. E. Maciel, *Org. Geochem.*, 1979, **1**, 169.
60. M. M. Maroto-Valer, G. D. Love and C. E. Snape, Conf. Presentation, Symp. on Recent Developments in the Characterization of Geomacromolecules, Amer. Chem. Soc. National Meeting, Orlando, FL, Aug. 25–29, 1996.
61. F. P. Miknis, in *Composition, Geochemistry, and Conversion of Oil Shales, NATO ASI Series C* (ed. C. Snape), pp. 191–209. Kluwer Academic Publishers, Dordrecht, 1995.
62. C. A. Audeh, in *Proc. of 1990 Eastern Oil Shale Symposium*, pp. 263–267. Inst. Mining Metallurgical Res., Lexington, KY, 1990.
63. J. R. Dyni, D. E. Anders and R. Rex, in *Proc. of 1989 Eastern Oil Shale Symp.*, p. 270. Inst. Mining Metallurgical Res., Lexington, KY, 1989.
64. G. E. Maciel, V. J. Bartuska and F. P. Miknis, *Fuel*, 1978, **57**, 505.
65. F. P. Miknis and P. J. Conn, *Fuel*, 1986, **65**, 248.
66. E. Evans, B. Batts and N. Cant, *Fuel*, 1987, **66**, 326.
67. K. Qin, D. Chen and Z. Li, *Org. Geochem.*, 1991, **17**, 856.
68. S. Sato, M. Enomoto and S. Takahashi, *Fuel Proc. Technol.*, 1988, **18**, 305.
69. F. P. Miknis, N. M. Szeverenyi and G. E. Maciel, *Fuel*, 1982, **61**, 341.
70. F. P. Miknis, D. A. Netzel, J. W. Smith, M. A. Mast and G. E. Maciel, *Geochim. Cosmochim. Acta.*, 1982, **46**, 977.
71. F. Hershkowitz, W. N. Olmstead, R. P. Rhodes and K. D. Rose, in *Geochemistry and Chemistry of Oil Shales, ACS Symp. Series* (eds F. P. Miknis and J. F. McKay), pp. 301–316. Am. Chem. Soc., Washington, DC, 1983.
72. A. K. Burnham and J. A. Happe, *Fuel*, 1984, **63**, 1353.
73. F. P. Miknis, D. A. Netzel and R. C. Surdam, *Energy Fuels*, 1996, **10**, 3.
74. A. M. Vassallo, M. A. Wilson and J. H. Edwards, *Fuel*, 1987, **66**, 622.
75. F. P. Miknis, *Fuel*, 1992, **71**, 731.
76. F. P. Miknis, T. F. Turner, L. W. Ennen and D. A. Netzel, *Fuel*, 1988, **67**, 1568.
77. G. E. Maciel and L. W. Dennis, *Org. Geochem.*, 1982, **3**, 105.
78. K. D. Schmitt and E. W. Sheppard, *Fuel*, 1984, **63**, 1241.
79. F. P. Miknis, A. W. Lindner, A. J. Gannon, M. F. Davis and G. E. Maciel, *Org. Geochem.*, 1984, **7**, 239.
80. M. J. Trewhella, I. J. F. Poplet and A. Grint, *Fuel*, 1986, **65**, 541.
81. R. L. Patience, A. L. Mann and I. J. F. Poplett, *Geochim. Cosmochim. Acta*, 1992, **56**, 2725.
82. Z. Zujovic, R. Srejic, D. Vucelic, D. Vitorovic and B. Jovancicevic, *Fuel*, 1995, **74**, 1903.
83. A. L. Mann, R. L. Patience and I. J. F. Poplett, *Geochim. Cosmochim. Acta*, 1991, **55**, 2259.
84. M. S. Solum, R. J. Pugmire and D. M. Grant, *Energy Fuels*, 1989, **3**, 187.

85. R. J. Pugmire, M. S. Solum, D. M. Grant, S. Critchfield and T. H. Fletcher, *Fuel*, 1991, **70**, 414.
86. M. Siskin, C. G. Scouten, K. D. Rose, T. Aczel, S. G. Colgrove and R. E. Pabst, in *Composition, Geochemistry and Conversion of Oil Shales, NATO ASI Series C* (ed. C. Snape), pp. 143–158. Kluwer Academic Publishers, The Netherlands, 1995.
87. J. W. Larsen and S. Li, *Energy Fuels*, 1994, **8**, 932.
88. F. P. Miknis, A. W. Decora and G. L. Cook, in *Recent Advances in the Science and Technology of Oil Shale* (ed. T. F. Yen), pp. 35–45. Ann Arbor Science Publishers, Ann Arbor, MI, 1976.
89. R. D. Sydansk, *Fuel*, 1978, **57**, 66.
90. L. Lynch and D. S. Webster, in *Geochemistry and Chemistry of Oil Shales, Symposium Series* (eds F. P. Miknis and J. F. McKay), pp. 353–369. Am. Chem. Soc., Washington, DC, 1983.
91. L. J. Lynch, D. S. Webster, N. A. Bacon and W. A. Barton, in *Magnetic Resonance. Introduction, Advanced Topics and Applications to Fossil Energy, NATO ASI Series C* (eds L. Petrakis and J. P. Fraissard), pp. 617–628. D. Reidel Pub. Co., Dordrecht, 1984.
92. T. J. Parks, L. J. Lynch and D. S. Webster, *Fuel*, 1987, **66**, 338.
93. T. J. Parks, L. J. Lynch, D. S. Webster and D. Barrett, *Energy Fuels*, 1988, **2**, 185.
94. Y. Sanada and L. J. Lynch, in *Magnetic Resonance of Carbonaceous Materials, Advances in Chemistry* (eds R. E. Botto and Y. Sanada), pp. 139–172. Am. Chem. Soc., Washington, DC, 1993.
95. G. E. Maciel, C. E. Bronnimann and C. F. Ridenour, in *Magnetic Resonance of Carbonaceous Solids*, Adv. Chem. Series (eds R. E. Botto and Y. Sanada), pp. 27–44. Am. Chem. Soc., Washington, DC, 1993.
96. J. S. Waugh, L. M. Huber and U. Haeberlin, *Phys. Rev. Lett.*, 1968, **20**, 180.
97. W.-K. Rhim, D. D. Elleman and R. W. Vaughan, *J. Chem. Phys.*, 1972, **58**, 1772.
98. D. P. Burum and W. K. Rhim, *J. Chem. Phys.*, 1979, **71**, 944.
99. B. C. Gerstein, R. G. Pembleton, R. C. Wilson and L. Ryan, *J. Chem. Phys.*, 1977, **66**, 361.
100. B. C. Gerstein, *Phil. Trans. Roy. Soc. Lond.*, 1981, **A229**, 521.
101. C. E. Bronnimann and G. E. Maciel, *Org. Geochem.*, 1989, **14**, 189.
102. M. F. Davis, G. R. Quinting, C. E. Bronnimann and G. E. Maciel, *Fuel*, 1989, **68**, 763.
103. A. Jurkiewicz, C. F. Bronnimann and G. E. Maciel, *Fuel*, 1989, **68**, 872.
104. A. Jurkiewicz, C. F. Bronnimann and G. E. Maciel, *Fuel*, 1990, **69**, 804.
105. A. Jurkiewicz, C. E. Bronnimann and G. E. Maciel, in *Magnetic Resonance of Carbonaceous Solids, Advances in Chemistry* (eds R. E. Botto and Y. Sanada), pp. 401–418. Am. Chem. Soc., Washington, DC, 1993.
106. J. V. Hanna, A. M. Vassallo and M. A. Wilson, *Energy Fuels*, 1992, **6**, 28.
107. M. A. Wilson, J. V. Hanna, K. B. Anderson and R. E. Botto, *Org. Geochem.*, 1993, **20**, 985.
108. D. A. Netzel, P. T. Coover and C. F. Bronnimann, *Fuel*, 1990, **69**, 429.
109. P. Panek, G. Scheler and N. J. Neiser, *Fuel*, 1990, **69**, 813.
110. E. W. Cook, *Fuel*, 1974, **53**, 16.
111. T. L. Robl, A. E. Bland, D. W. Koppenaal and L. S. Barron, in *Geochemistry and Chemistry of Oil Shales, ACS Symp. Series* (eds F. P. Miknis and J. F. McKay), pp. 159–180. Am. Chem. Soc., Washington, DC, 1983.
112. F. P. Miknis, A. W. Decora and G. L. Cook, *Rept. of Investig. 7984*. US Bureau of Mines, Laramie, WY, 1974.
113. D. Vitorovic, D. Vucelic, M. J. Gasic, M. Juranic and S. Macura, *Org. Geochem.*, 1979, **1**, 89.
114. F. P. Miknis and G. E. Maciel, in *Magnetic Resonance, Introduction, Advanced Methods,*

and Applications to Fossil Energy, NATO ASI Series C (eds L. Petrakis and J. P. Fraissard), pp. 545–555. D. Reidel Pub. Co., Dordrecht, 1984.
115. B. L. Sidewell, L. E. McKinney, M. F. Bozeman, P. C. Egbujor, G. R. Eaton, S. S. Eaton, and D. A. Netzel, *Geochim. Cosmochim. Acta*, 1979, **43**, 1337.
116. M. Choudhury, K. F. Rheams and J. W. Harrell, *Fuel*, 1986, **65**, 1028.
117. J. P. Biscar, *J. Chromatogr.*, 1971, **56**, 348.
118. R. L. Hanson, N. E. Vandenborgh and D. G. Brookins, *Anal. Chem.*, 1975, **47**, 335.
119. C. W. Schultz and J. B. Bates, in *Proc. of 1989 Eastern Oil Shale Symp.*, pp. 533–538. Institute for Mining, Minerals Res., Lexington, KY, 1989.
120. P. R. Reed and P. R. Warren, *Quart. Colo. Sch. Mines*, 1974, **69**, 221.
121. D. R. Johnson, N. B. Young and J. W. Smith, *Rept. Investig. 7716*. Laramie Energy Technology Center, Laramie, WY, 1977.
122. J. W. Smith, *Rept. Investig. 7248*, US Bureau of Mines, Laramie, WY, 1969, 14 pp.
123. K. P. Chong, A. I. Leskinen and F. P. Miknis, in *Proc. of 1987 Eastern Oil Shale Symp.*, pp. 119–123. Kentucky Energy Cabinet Lab., Lexington, KY, 1987.
124. A. Judzis and B. Williams, in *Proc. of 10th Oil Shale Symp.*, pp. 207–212. Colorado School of Mines, Golden, CO, 1977.
125. J. DuBow, R. Nottenburg, K. Rajeshwar and Y. Wang, in *Proc. of 11th Oil Shale Symp.*, pp. 350–631. Golden, CO, 1978.
126. K. Rajeshwar and J. D. Bow, in *Proc. of IGT Symposium on Synthetic Fuels From Oil Shale*, pp. 305–321. Inst. Gas Technol. Publ., Atlanta, GA, 1976.
127. K. Rajeshwar and R. Inguva, *Fuel*, 1985, **64**, 931.
128. P. R. Solomon and F. P. Miknis, *Fuel*, 1980, **59**, 893.

INDEX